1-1-1999

Synthesis and characterization of blends of poly(ethylene-B-(atactic)propylene) with polyethylene.

Andrew A. Bushelman
University of Massachusetts Amherst

SYNTHESIS AND CHARACTERIZATION OF BLENDS OF POLY(ETHYLENE-*B*-(ATACTIC)PROPYLENE) WITH POLYETHYLENE

A Dissertation Presented

by

ANDREW A. BUSHELMAN

Submitted to the Graduate School of the
University of Massachusetts Amherst in partial fulfillment
of the requirements for the degree of

DOCTOR OF PHILOSOPHY

May 1999

Polymer Science and Engineering

SYNTHESIS AND CHARACTERIZATION OF BLENDS OF POLY(ETHYLENE-*B*-(ATACTIC)PROPYLENE) WITH POLYETHYLENE

A Dissertation Presented

by

ANDREW A. BUSHELMAN

Approved as to style and content by:

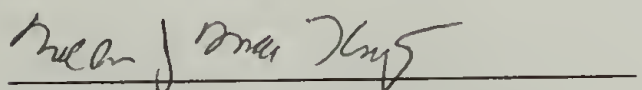

William J. MacKnight, Chair

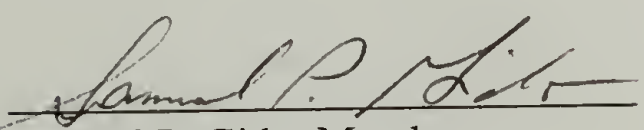

Samuel P. Gido, Member

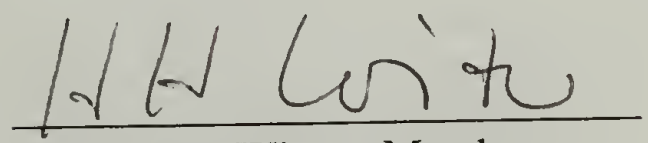

H. Henning Winter, Member

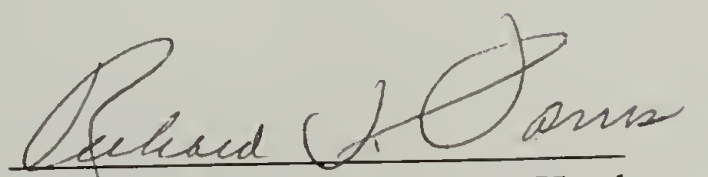

Richard J. Farris, Department Head
Polymer Science and Engineering

ACKNOWLEDGMENTS

First and foremost, I would like to thank my parents for their patience and support during my time in graduate school. I would like to thank Dr. William MacKnight for the opportunity to perform research in his group and to Exxon Research and Engineering for important experience in performing living anionic synthesis. Without their help, this research would not have been possible. I would like to thank the Materials Research Science, and Engineering Center at UMass for financial support of my research.

I would also like to extend my appreciation to my committee. To Dr. David Lohse for his continuing guidance and interest in my work. Much of the improvements to this text were made with his help. To Profs. S. P. Gido and H. H. Winter for their support and feedback during the course of my graduate studies.

To Julia Higgins, one of the finest academic scientists with whom I had the pleasure of collaborating. Her insight and experience, not to mention her warm sense of humor, were assets which made her indispensable to the neutron reflection (NR) aspect of this research. Another partner to the NR portion of my research which I would like to thank was Dr. David G. Bucknall, an expert in not only the experimental technique but also in the underlying science. Best of luck in your new academic forays.

A special thanks goes to Dr. Simon Butler and his girlfriend Dr. Allison Dunning, who have become good friends of mine through the NR collaboration. Simon and Allison are both dedicated scientists and I wish them all the best in their scientific and personal endeavors...And may Simon never have to eat the "food" served at the RAL ever again...

To Dr. Donald N. Schulz, who has always been helpful in questions on polymerization and a myriad of other topics. To Dr. Lewis J. Fetters and Prof. Thomas P. Russell—the former of which is a guru in living anionic polymerizations, while the latter is an expert in neutron scattering and refection. Thank you to both of you for helpful conversations which aided my work.

To Joe Sissano, who showed tremendous patience in teaching me the living anionic technique and to Pam Wright, who developed the spreadsheet which I used to determine molecular weights. To Enock Berluche, his wife, Ines, and his family. They are testaments to what hard word, family love, and living their faith can bring to life. May they never lose their hope and happiness.

To the Great Secretaries of PSE: Nancy, Eileen, Eleanor, and Sophie—THANKS!

To my "old friends" at Umass: Greg S., Susan, Heather, and the crew at the Newman Grad Group for keeping me sane while "commuting" between UMass and New Joisey. I would also like to thank Bin Hu for always giving me something to smile about.

To my "new friends" at UMass: Gary, Georgia and Jim, Amy, Sue, Ji Ho, Reg, Greg M., Uli, Stephan, and Dennis, for lunchtime entertainment and Friday beers.

To all my friends who have become scattered across the US. They have shown that friendship knows no bounds of time or space.

To Nicole, with whom I spent the early years of my graduate "career". With her love and friendship I learned much about myself. I hope our friendship never ends.

And finally to Corinne, I cannot say enough...I love you. You have made the last months at school the happiest ever. May this relationship blossom into something great.

ABSTRACT

SYNTHESIS AND CHARACTERIZATION OF BLENDS OF POLY(ETHYLENE-*B*-(ATACTIC)PROPYLENE) WITH POLYETHYLENE

MAY 1999

ANDREW A. BUSHELMAN, B.S. MAT. ENG., UNIVERSITY OF CINCINNATI

M.S., UNIVERSITY OF MASSACHUSETTS AMHERST

Ph.D., UNIVERSITY OF MASSACHUSETTS AMHERST

Directed by: Professor William J. MacKnight

Polymer blends involving a semi-crystalline/amorphous diblock copolymer and the corresponding semi-crystalline homopolymers were prepared and investigated to increase the understanding of the effect that crystallizability has on the phenomenon of microphase separation. Monodisperse symmetric diblock copolymers of poly(butadiene-*b*-2-methyl-pentadiene) and corresponding homopolymers of polybutadiene and poly(methylpentadiene) were synthesized by living anionic polymerization and characterized by GPC and NMR. These polymers were hydrogenated to form the saturated crystalline-amorphous diblock (DEP) and crystalline (PE) and amorphous (APP) homopolymers.

Blends were prepared using solution routes and physical mixing (the latter for DSC measurements only). A problem of spherulite formation arose due to the route of solution blending which was employed. Melt pressing and melt-annealing for several days was found to return the sample to the microphase separated state and to enhance the long-range order that was reduced by pressing. Blends were quenched in liquid nitrogen

and their thermal properties measured by TG and DSC. The change in the crystallization peak which had been in previous studies seen by DSC for the blends with the APP was no longer present. It is proposed that the mechanism which was previously responsible for the change in crystallization peak (the continuity of the PE phase) was no longer applicable and that the cooling rate (10°C/min) was insufficient to prevent spherulite formation (possibly due to the solution casting technique used). TEM showed the latter to be true and that the morphology was directed by the increased driving force for crystallization, even upon rapid cooling from the melt using liquid nitrogen.

Neutron reflectometry (NR) was used to investigate the interfacial behavior and miscibility of a diblock copolymer of *deuterated*-PE and APP when blended or in contact with polyethylenes and atactic polypropylene homopolymers while in the melt. A study on the effect of the amount of short chain (ethyl) branching on miscibility at the PE/APP interface determined that the combination of molecular weight, polydispersity, and the presence of additives had more of an effect on miscibility than did branch content, as an HDPE sample was found to have a wider interface than did an ethylene-1-butene (EB) copolymers. The form (as a film or in a blend) and location of the labeled diblock were found to have a large effect on the mobility and diffusion behavior. When blended with the amorphous homopolymer, simulations indicated that migration of the diblock to the free surface occurred, possibly due to surface free energy effects. Substantiation of this interpretation is studied using AFM. When placed as a film, the diblock appears to dissolve into either one or both of the homopolymers as micelles or as individual chains.

TABLE OF CONTENTS

LIST OF TABLES

LIST OF FIGURES

CHAPTER 1

INTRODUCTION

1.1 General Introduction

Polymer blends are pervasive in society today. Items ranging from plastic milk bottles to fabrics for apparel to components for automobiles can and often are made of polymer blends. Since very few systems in and of themselves are miscible or compatible, the desire to improve the combined properties of the blend necessitates the introduction of small amounts of diblock copolymer into the system. Two major functions of diblock copolymers are to serve as interfacial adhesion promoters and as agents by which the domain sizes of the individual polymer components can be reduced. Because the chapters of this dissertation are fairly independent of each other, this chapter will only cover the general topics of diblock copolymers, copolymer blends, and crystallization in polymers as relevant to this work.

Interest in the phase behavior of diblock copolymers has been a major driving force behind the intensive academic research of diblock copolymers. Neat diblock copolymers show a variety of microstructures which depend on the symmetry of the two blocks. The effect of block symmetry on the volume fraction of each component is the key to the phase behavior of linear diblock copolymers. Symmetric diblock copolymers display a morphology which is usually described as alternating planes of the essentially pure component blocks, called lamellae. As one moves toward increasing block asymmetry, the microstructure changes to a "bicontinuous"[1] or "modulated lamellae"[2] morphology, then to discrete cylinders arranged on a hexagonal lattice, on to spheres on a

base-centered cubic lattice, and finally to disordered micelles consisting of the shorter block microphase. Figure 1-1 illustrates these morphologies. This behavior is described in more detail in the second section of this chapter.

The focus of industrial research has traditionally been the blending of two homopolymers with small amounts (typically 1-5 wt.%) of diblock copolymer in order both to reduce phase size and also to increase the interfacial strength between the two homopolymer phases. This combination has been found to increase the physical properties (strength, modulus, or toughness) of the blend. Most polymers are immiscible with each other, and the physical properties of immiscible blends are usually lower that those of the component polymers. Inclusion of the diblock copolymer in the blend is beneficial because it is able to reduce the domain sizes of the homopolymers and increase interfacial strength across the interface between the homopolymer phases. Figure 1-2 illustrates how the diblock copolymer accomplishes this favorable change. When added to the homopolymer blend, the diblock copolymer is preferentially located at the interface between the two homopolymers with each block extending into its respective like phase. By bridging the interface in this way, the diblock serves to reduce unfavorable contacts between the homopolymers, thereby lowering the interfacial energy of the system. This results in smaller homopolymer domains. The interfacial strength is increased because the individual blocks are able to interdigitate with the respective homopolymer chains and form physical entanglements which serve to better increase the adhesion between the two phases. The role of the diblock copolymer in modifying the interface of homopolymers and the converse—of the individual homopolymer acting as an agent to "increase" block

asymmetry when blended with the neat diblock copolymer—is discussed in the third section of this chapter.

Crystallization is an important part of the research of polymers and their blends, especially since its presence increases the driving force for macrophase separation in homopolymer blends.[3] Because several commercially important polymers are semi-crystalline, it is important to understand how crystallinity affects physical and thermal properties. Control of microstructure would allow the aforementioned properties to be tailored to suit the final application. From the scientific standpoint, knowledge of the path dependence of crystallization allows the interrelation of results from different techniques and aids in the interpretation of sometimes confusing results.[4] Diblock copolymers containing a crystallizable block have been investigated both to look at the effect that an amorphous chain connected to the crystalline block has on crystallization kinetics and conversely, the effect of the crystallizable block on phase behavior as compared to that of the well-studied amorphous-amorphous diblock copolymer systems. The majority of work involving crystallization and the systems relevant to this dissertation have concentrated on studies of crystallization kinetics and morphological development of neat crystalline-amorphous diblock copolymer systems.[5-7] The phenomenon of crystallization in homopolymers, diblocks copolymers, and blends is discussed in the fourth section of this chapter, while the results from the pertinent studies of asymmetric crystalline-amorphous copolymers and blends of a crystalline-amorphous diblock copolymer with amorphous homopolymers are presented in the fifth section.

This chapter ends with a statement of the objectives of this study and an overview of the organization of the rest of this dissertation.

1.2 Diblock Copolymers

From the early predictions of Ziegler in the 1930s[8] to the present plethora of architectures and variety of choices of monomers,[9-13] the study of block copolymers has evolved into a wide field of endeavor. This area has attracted much attention not only from academic circles because of the unusual behavior of the materials, but also from industry due to its versatile applications. These range from interfacial strength promoters and compatibilizing agents to thermoplastic elastomers, adhesives, and coatings.[14-16]

It should be first acknowledged that the study of diblock copolymers could have only been made possible by the chemistry technique known as "living anionic synthesis". Although this method was originally proven possible by Szwarc and coworkers,[17,18] it was the work of Fetters and Morton[19-21] which perfected the high vacuum version of this technique that is the method of choice for producing these polymers today. Living anionic synthesis (combined with coupling chemistry)[22] allows preparation of model polymers with well-defined molecular weight, controlled microstructure and block lengths, and novel architectures.[23] It is these characteristics that allow the use of model copolymers to be produced which enable systematic investigations into the effects in which variation of one or more of the afore-mentioned parameters has on phase behavior and physical properties to be made possible. In addition to control over molecular variables, the inclusion of deuterated monomers or saturation of dienic copolymers with deuterium allows the labeling of individual blocks, or in the case of blends, whole chains for the study of structure/property relationships using neutrons as probes.

The phase behavior of pure diblock copolymers is primarily dependent on the relative volume fractions of the individual blocks and to a lesser degree dependent on the

difference in the stiffness of the component polymer chains. As the diblock becomes increasingly asymmetric, the combination of relative block volume fraction, the connectedness of the two blocks, and the driving force to maintain constant density throughout the polymer causes the morphology to change, as is shown schematically in Figure 1-3.

The theoretical work of Helfand,[24] Leibler,[25] and others[26-32] provide an excellent framework from which the phenomena of blending and microphase separation may be understood. According to Helfand,[24] the criterion for miscibility of two polymers depends on the product of χ, the Flory interaction parameter, and N, the degree of polymerization of the two polymers. For the case of two homopolymers, phase separation will occur for any system in which $(\chi N)_c$ is greater that two. Leibler[25] predicted that the boundary for microphase separation exists at a value of $(\chi N)_c$ of 10.5 for diblock copolymers. He predicted that several morphologies could be obtained merely by varying the relative volume fractions of each block: "microphase separation". An example of this phase diagram is shown in Figure 1-4. The point where the two blocks are chemically bonded together, the "junction point", is responsible for the increase in the critical value for χ over homopolymer blends. The ordering which occurs on the microscopic scale arises from a competition between minimization of free energy by reducing interactions between unlike polymer segments and the presence of a junction point in diblock copolymers which constrains the ability of the chains to completely phase separate.

Early studies of diblock copolymers centered on linear amorphous-amorphous diblock copolymers, since they were easily synthesized and the lack of crystallization or

specific interactions in these systems also made sample preparation simple—solutions and bulk samples could be prepared at room temperature with routine laboratory solvents (such as toluene).[33-37] The proper choice of blocks also allows wide separations in glass transition temperatures, which make determination of homogeneity (such as the order-disorder transition, or ODT) of the neat diblock straightforward.[38] Increasingly, the focus of diblock copolymer research is shifting from the study of linear amorphous-amorphous diblock copolymer[33-37] to linear diblock containing a crystallizable block[39-42] or blocks with highly different segment length, (such as random coil-rigid rod) or block copolymers with novel architectures (like "H", "pi", or star copolymers).[43-45]

1.3 Diblock Copolymer/Homopolymer Blends

It was stated in the first section of this chapter that the major industrial use for diblock copolymers is as "interfacial compatibilizers" or as "emulsifying agents".[46,47] It is advantageous that only a small amount of diblock copolymer is necessary to produce large changes in the phase size of the homopolymers, as making diblock copolymers with the desired block symmetry and molecular weight can be challenging and time-consuming.

Most academic research to date has focused on blending the diblock copolymer, which will be termed "b-AB", with one or the other homopolymer component, termed "h-A" and "h-B", of a blend system. Hereafter blends of this sort will be termed "b-AB/h-A" or "b-AB/h-B" blends, depending on the designation of blocks "A" and "B" in the copolymer. The majority of this research has dealt with entirely amorphous systems.[33-37] Increased attention is now being directed toward systems in which one block of the

copolymer is crystallizable.[38-42] However, very little work has been performed where the added homopolymer is also semicrystalline.

For blends of a symmetric diblock copolymer with a corresponding homopolymer, the morphology depends on the ratio of the molecular weight of the homopolymer to the molecular weight of the like block in the copolymer. If the molecular weight of the homopolymer is denoted $M_{h\text{-}A}$, and that of the like block of the copolymer is $M_{b\text{-}A}$, then the three possible blending cases are possible. These cases are illustrated in Figure 1-5. For Case 1, microphase separation will generally be observed, with the morphology varying from lamellar at low concentrations of homopolymer, to a bicontinuous network at somewhat higher amounts of homopolymer, to discrete cylinders at intermediate homopolymer concentrations, and finally to spheres and disordered micelles at high concentrations of homopolymer. (see Figure 1-1) It has been reported using SANS that the homopolymer chains diffuse to the center of the domain of the like block, due to the high concentration of chain ends (from the copolymer chains) in this region.[48] In doing so, the effective volume fraction occupied by the (now) majority component has increased, and the diblock behaves like an asymmetric copolymer. This induced asymmetry causes morphological transitions as they would occur in a neat diblock copolymer with blocks of different lengths. When the relative molecular weight of the homopolymer increases, as in Case 2, the ability of the block copolymer to mix with the larger chains of homopolymer decreases, so that only a small amount of homopolymer is able to enter into the microdomain morphology before the driving force to macrophase separate dominates. These changes result from the ability of the homopolymer chain to be "solubilized" by the larger chains of the block of the copolymer containing similar

repeat units and actually mix with the diblock. As one moves toward Case 3, the diblock copolymer is unable to accommodate the homopolymer and only macrophase separation occurs.

Recently, a morphological phase diagram was constructed by Winey et al.[49] which takes into account the effect of relative molecular weight as described above. The graphic in Figure 1-6 demonstrates that this method of plotting blend data is extremely useful for displaying the effect of composition and relative molecular weight on the resulting morphology of the blends.

1.4 Crystallization in Polymers

An accurate understanding of crystallization is critical to comprehending its effects on phase separation in polymer blends. The very fact that polyethylenes of slightly different branch contents will phase separate into macroscopic domains[50] is an excellent reason to study polyolefin blends.

The normal ways to determine crystallinity are DSC, dilatometry, and SAXS. DSC uses the ratio of the area under the crystallization peak to the heat of fusion for a perfect polyethylene (no branches) crystal to determine the degree of crystallinity. Dilatometry uses the difference in density between the sample and the extrapolated value for pure polyethylene. SAXS uses the ratio of the area under the crystalline peak to the sum of the areas under the crystalline and amorphous peaks to calculate the degree of crystallinity.[51]

Several theories of crystallization exist. A relevant theory to this work is that of Helfand and Lauritzen,[24] which is concerned with copolymer crystallization. The limiting

case of low concentrations of non-crystallizable units is very similar to what would be expected for hydrogenated 1,4-polybutadiene (LLDPE), where roughly 7% of the chain are ethyl branches. They predict that the combination of low impurity concentrations, large undercoolings (like room temperature), and high molecular weight will lead to an increase in the driving force to crystallize and include the impurity units in the crystallite. For the case of LLDPE this would result in an increase in the driving force to form spherulites.

Mandelkern and coworkers[52,53] applied Avrami theory to the phenomenon of crystallization in polymers using dilatometry. Originally devised to describe the kinetics of phase transformations with time, Avrami used an Arrhenius-type equation to describe a characteristic time, τ, which is a function of the geometry, number of germ nuclei, and the kinetics of the transformation process.[54] Recently, this theory has been applied to the crystallization in polymers using the equation:

$$\% \text{ crystallinity} = 1 - \phi = \exp(-kt^n) \qquad (1)$$

where ϕ is volume fraction, k is a rate constant and n is the Avrami exponent, which combines the type of nucleation process (simultaneous or sequential) with the dimensionality of the crystal growth. They found that crystallization in polymers is nucleation-controlled and is influenced by molecular weight, the number of germ nuclei, and the kinetics of the transformation process. Avrami theory is only applicable at the early stages of transformation. Beyond the early times, polymer crystallization deviates from theoretical predictions.[52] Also polymers have a strong molecular weight dependence, with the higher the molecular weight the earlier the crystallization begins to deviate from theory.

1.5 Relevant Studies

Previously in the MacKnight research group, investigations into the crystallization kinetics and microdomain morphologies of the blend system poly(ethylene-*at*-propylene) (DEP) and atactic polypropylene homopolymer (APP) were performed.[56-58] Since this was a new system, there were several interesting findings. First and foremost, the crystallization kinetics of the b-PE could be linked to the morphology of the blend (reflected in the location of the major crystallization peak which was dependent on the continuity of the b-PE phase). The physical interpretation for this observation is that as the PE morphology changes from a continuous (lamellar/CNC) phase to a discontinuous phase (discrete cylinders/spheres), a change could be observed by DSC in the dominant crystallization peak while cooling at 10°C/min. The change was related to morphology via a change in the Avrami component, n, and was confirmed by TEM. It was observed by SANS that a microphase separated state was present in the melt; and the melt microstructure could be preserved by quenching the molten blend using liquid nitrogen to room temperature, where crystallization of the b-PE occurred in the confines of the microdomains. In addition, the quenched morphology of DEP + APP blends was determined to qualitatively follow the morphological diagram for amorphous-amorphous systems.[49]

The crystallization kinetics and morphology of asymmetric amorphous-crystallizable diblocks have recently been studied in order to understand the effect of crystalline block symmetry on the ability of polymer chains to form microdomains.[55] A combination of Avrami theory and microstructural techniques (SANS, SAXS, TEM) were employed in order to determine Avrami exponents and morphology. For neat

diblocks in which the amorphous block was the larger block, normal order-order transitions were found. On the opposite extreme, crystallization was determined to has a profound effect on the morphology, changing cylinders in the melt to lamellae upon quenching and delaying order-order transitions to higher block asymmetries than would be observed in completely amorphous systems. It was also found that block symmetry did not affect the crystallization kinetics of the polyethylene component (namely, $n = 3$) because spherulites were formed upon slow cooling and order-order transitions were suppressed.

1.6 Objectives and Organization

The objectives of this research were to compare the results of blending PE homopolymer and DEP with the results using APP as the blended homopolymer to complete the study of blending a crystalline-amorphous diblock copolymer with either homopolymer, and to determine whether the morphological behavior was more similar to the amorphous homopolymer case or the case of a neat asymmetric diblock. Another aim was to investigate the effect of increasing the driving force of crystallization on the ability to retain the microphase separated state upon rapid cooling from the melt without the formation of spherulites. If this was possible, the next question to be answered was whether the resulting morphology would be affected by the additional crystallizable component. The final goal was to determine the miscibility of polyolefin blends containing both crystalline and amorphous polymers. NR was used to determine miscibility in polyolefin blends as a function of branch content (between polyethylenes and atactic polypropylene) and the effect of the manner of placement of a labeled diblock

copolymer into a immiscible homopolymer blend, while DSC and TEM were used to investigate the effects of relative chain length and overall composition on miscibility in solution blended samples.

In the second chapter of this dissertation, the synthesis and molecular characterization (microstructure and molecular weight) of the polymers produced for this research are described. All of the polymers synthesized for this research had narrow polydispersities and high 1,4-addition microstructures. The diblock copolymer was determined to be roughly symmetric at 45wt%PE/55wt%APP. The results from the saturation of the polydiene precursors are also presented in Chapter 2. The third chapter describes the various blending techniques which were used to prepare blend samples. The fourth chapter discusses the thermal characterization of these blends and compares the use of PE as the homopolymer versus APP. It is speculated in Chapter 4 that the data show that the addition of h-PE to b-PE causes an increase in the driving force for macroscopic crystallization and that a split in the heating peak at high h-PE loadings (lowest molecular weight h-PE) was due to the difference in the crystallization temperatures of the h-PE and the b-PE. In Chapter 5, TEM proves that this observation was due to the demixing of the homopolymer with the like block of the copolymer, and that behavior similar to that seen for the asymmetric diblock copolymers occurs.

In a different vein, Chapter 6 covers the results from neutron reflectometry experiments the interfacial and miscibility behavior of a diblock copolymer of deuterated-DEP and in contact with PE and APP homopolymers while in the melt. NR was used to determine the effect of the form (film or in a blend) and location of the labeled species has in its mobility and diffusion to the interface between two homopolymers at

equilibrium in the melt. Results indicated that a combination of effects come into play depending on whether the diblock copolymer is added to the homopolymers as part of a blend or as a discrete film and on the interfacial width between APP and PEs of different branch content.

1.7 References

1. Winey, K. I.; Thomas, E. L.; and Fetters, L. J. *J. Chem. Phys.* **1991**, *95*, 9367.

2. Hamley, I. W.; Koppi, K. A.; Rosendale, J. H.; Bates, F. S.; Almdal, K.; Mortensen, K. *Macromolecules* **1993**, *26*, 5959.

3. Cohen, R. E.; Torradas, J. M. *Macromolecules* **1984**, *17*, 1101.

4. Strobl, G. *Acta Polymerica* **1997**, *48*, 562.

5. Cohen, R. E.; Wilfong, D. E. *Macromolecules* **1982**, *15*, 370.

6. Douzinas, K. C.; Cohen, R. E.; Halasa, A. F. *Macromolecules* **1991**, *24*, 4457.

7. Rangaragan, P.; Register, R. A.; Fetters, L. J. *Macromolecules* **1995**, *28*, 4932.

8. Zeigler, A. *Angew. Chem.* **1936**, *49*, 499.

9. Iatrou, H.; Hadjichristidis, N. *Macromolecules* **1993**, *26*, 2479.

10. Avgeropoulos, A.; Poulos, Y.; Hadjichristidis, N.; Roovers, J. *Macromolecules* **1996**, *29*, 6076.

11. Gido, S. P.; Lee, C.; Pochan, D. J.; Pispas, S.; Mays, J. W.; Hadjichristidis, N. *Macromolecules* **1996**, *29*, 7022.

12. Pispas, S.; Hadjichristidis, N.; Mays, J. W. *Macromolecules* **1996**, *29*, 7378.

13. Stocker, W.; Stadler, R. *Macromolecules*, **1996**, *29*, 7502.

14. Allport, D. C.; Barker, C.; Chapman, J. F., in Developments in Block Polymers—1, Goodman, I., ed., Elsevier Applied Science Publishers: London, 1982.

15. Widmaier, J. M.; Meyer, G. C., in Developments in Block Polymers—2, Goodman, I., ed., Elsevier Applied Science Publishers: London, 1985.

16. Washiyama, J.; Kramer, E. A.; Hui, C.-Y. *Macromolecules* **1994**, *27*, 6011.

17. Szwarc, M. *Nature* **1956**, *178*, 1108.

18. Szwarc, M.; Levy, M.; and Milkovich, R. *J. Am. Chem. Soc.* **1956**, *78*, 2656.

19. Fetters, L. J. *J. Polym. Sci.: Part C* **1969**, *26*, 1.

20. Morton, M.; Fetters, L. J. *Rubber Rev.* **1975**, *48*, 359.

21. Morton, M. Anionic Polymerization: Principles and Practice, Academic Press: New York, 1983.

22. Morton, M.; Helminiak, T. E.; Gadkary, S. D.; Bueche, F. *J. Polym. Sci.* **1962**, *57*, 471.

23. Hsieh, H. L.; Quirk, R. P. Anionic Polymerization: Principles and Practical Applications, Marcel Dekker: New York, 1996.

24. Examples include Helfand, E.; Tagami, Y. *J. Chem. Phys.* **1972**, *56*, 3592. Helfand, E.; Lauritzen, J. I., Jr. *Macromolecules* **1973**, *6*, 631. Helfand, E. *Macromolecules* **1975**, *8*, 552. Helfand, E. *J. Chem. Phys.* **1975**, *62*, 999. Fredrickson, G. H.; Helfand, E. *J. Chem. Phys.*, **1987**, *87*, 697.

25. Examples include Leibler, L. *Macromolecules*, **1980**, *13*, 1602. Leibler, L. *Macromolecules*, **1982**, *15*, 1283. Ferreira, P. G.; Leibler, L. *J. Chem. Phys.*, **1996**, 105, 9362.

26. Cahn, J. W.; Hilliard, J. E. *J. Chem. Phys.* **1958**, *28*, 258.

27. Meier, D. J. *J. Polym. Sci.; Part C* **1969**, *26*, 81.

28. DiMarzio, E. A.; Guttman, C. M.; Hoffman, J. D. *Macromolecules* **1980**, *13*, 1194.

29. Hong, K. M.; Noolandi, J. *Macromolecules* **1983**, *16*, 1083.

30. Whitmore, M. D.; Noolandi, J. *Macromolecules* **1985**, *18*, 657.

31. Whitmore, M. D.; Noolandi, J. *Macromolecules* **1988**, *21*, 1482.

32. Semenov, A. N. *Macromolecules* **1993**, *26*, 6617.

33. Hashimoto, T.; Nagatoshi, K.; Todo, A.; Hasegawa, H.; Kawai, H. *Macromolecules* **1974**, *7*, 364.

34. Hashimoto, T.; Shibayama, M.; Kawai, H. *Macromolecules* **1977**, *10*, 377.

35. Handlin, Jr., D. L.; Thomas, E. L. *Macromolecules* **1983**, *16*, 1514.

36. Kinning, D. J.; Thomas, E. L.; Fetters, L. J. *J. Chem. Phys.* **1989**, *90*, 5806.

37. Bates, F. S.; Cohen, R. E.; Berney, C. V. *Macromolecules* **1982**, *15*, 589.

38. Bates, F. S.; Bair, H. E.; Hartney, M. A. *Macromolecules* **1984**, *17*, 2607.

39. Rangarajan, P.; Register, R. A.; Fetters, L. J. *Macromolecules* **1993**, *26*, 4640.

40. Kofinas, P.; Cohen, R. E. *Macromolecules* **1994**, *27*, 3002.

41. Sakurai, K., Ph.D. Thesis, Osaka University, Japan, 1995.

42. Jeon, H. S.; Lee, J. H.; Balsara, N. P. *Macromolecules* **1998**, *31*, 3228.

43. Hadjichristidis, N.; Iatrou, H.; Behal, S. K.; Chludzinski, J. J.; Disko, M. M.; Gardner, R. T.; Liang, K. S.; Lohse, D. J.; Milner, S. T. *Macromolecules* **1993**, *26*, 5812.

44. D. J. Pochan, Ph.D. Dissertation, University of Massachusetts, Amherst, 1997.

45. Beyer, F. L.; Gido, S. P.; Poulos, Y.; Hadjichristidis, N. *Macromolecules* **1997**, *30*, 2373.

46. Datta, S.; Lohse, D. J. Polymer compatibilizers: uses and benefits in polymer blends, Hanser/Gardner Publications, Inc.: Cincinnati, OH, 1996.

47. Dai, C.-A.; Kramer, E. J.; Washiyama, J.; Hui, C.-Y. *Macromolecules* **1996**, *29*, 7536.

48. Mastushita, Y.; Naoya, T.; Mogi, Y.; Noda, I.; Han, C. C. *Macromolecules* **1993**, *26*, 6346.

49. Winey, K. I.; Thomas, E. L.; Fetters, L.J. *Macromolecules*, **1992**, *25*, 2645.

50. Alamo, R. G.; Graessley, W. W.; Krishnamoorti, R.; Lohse, D. J.; Mandelkern, L.; Londono, D. L.; Wignall, G. D. *Macromolecules* **1996**, *29*, 3920.

51. Balta-Calleja, F. J.,; Vonk, C. G. X-ray scattering of synthetic polymers, Elsevier: London, 1989.

52. Ergoz, E.; Fatou, J. G.; Mandelkern, L. *Macromolecules* **1972**, *5*, 147.

53. Alamo, R. G.; Mandelkern, L. *Macromolecules* **1991** *24*, 6480.

54. Avrami, M. *J. Chem. Phys.* **1939**, *7*, 1103; **1941**, *9*, 177.

55. Ryan, A. J.; Hamley, I. W.; Bras, W.; Bates, F. S. *Macromolecules* **1995**, *28*, 3860.

56. Sakurai, K.; MacKnight, W. J.; Lohse, D. J.; Schulz, D. N.; Sissano, J. A. *Macromolecules* **1993**, *26*, 3236.

57. Sakurai, K.; MacKnight, W. J.; Lohse, D. J.; Schulz, D. N.; Sissano, J. A. *Macromolecules* **1994**, *27*, 4941.

58. Sakurai, K.; MacKnight, W. J.; Lohse, D. J.; Schulz, D. N.; Sissano, J. A.; Lin, J.-S.; Agamalyan, M. *Polymer* **1996**, *37*, 4443.

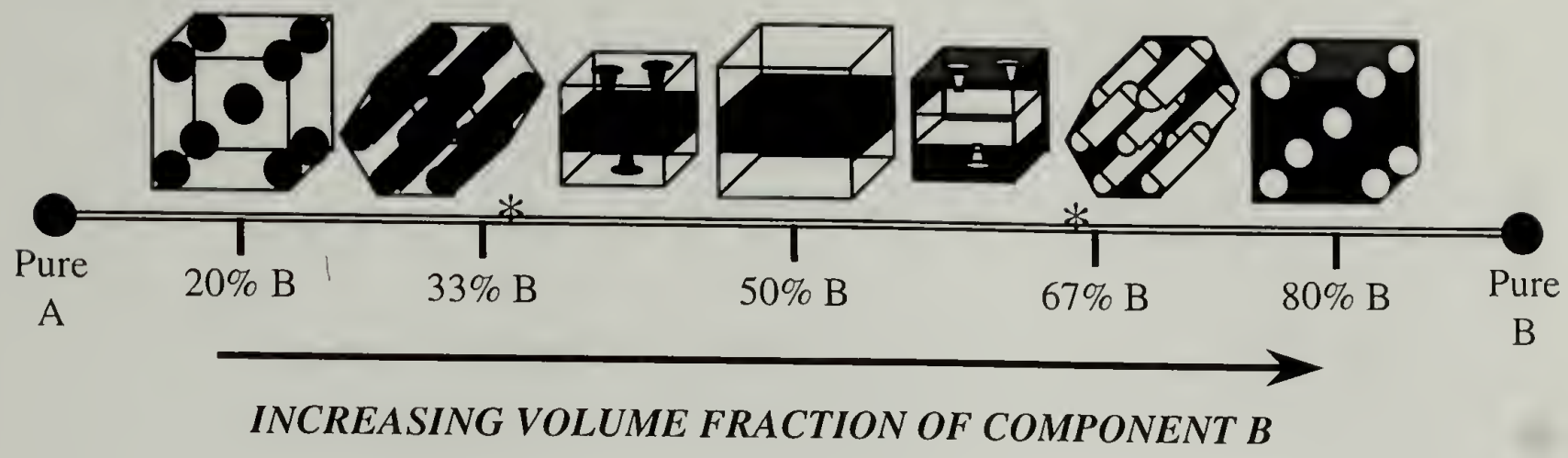

Figure 1.1 Ordered Morphologies in Neat Diblock Copolymers. (Astericks (*) denote approximate compositions of Bicontinuous Morphology.)

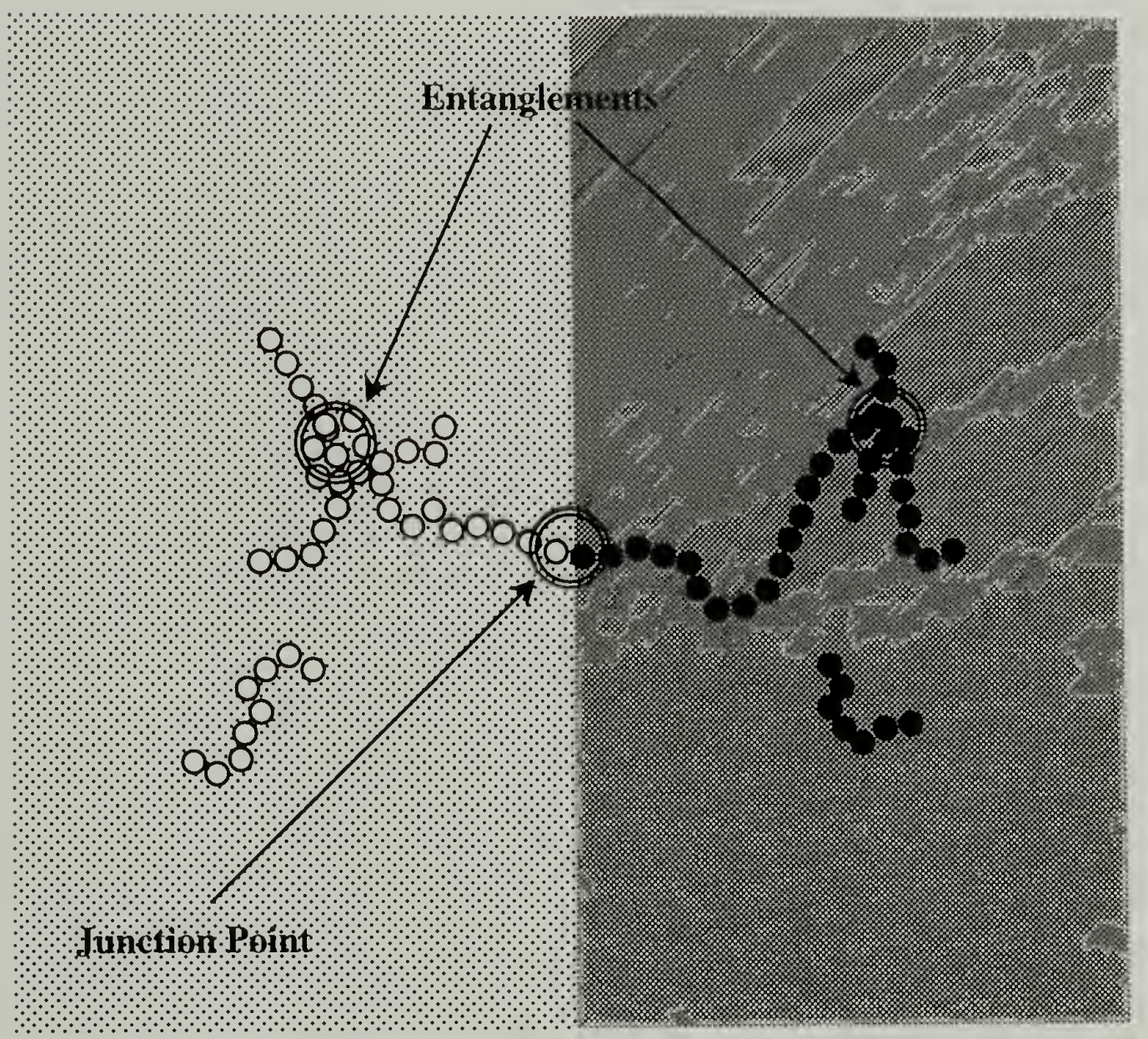

Figure 1.2 Drawing of Diblock Copolymer Bridging Two Immiscible Homopolymers.

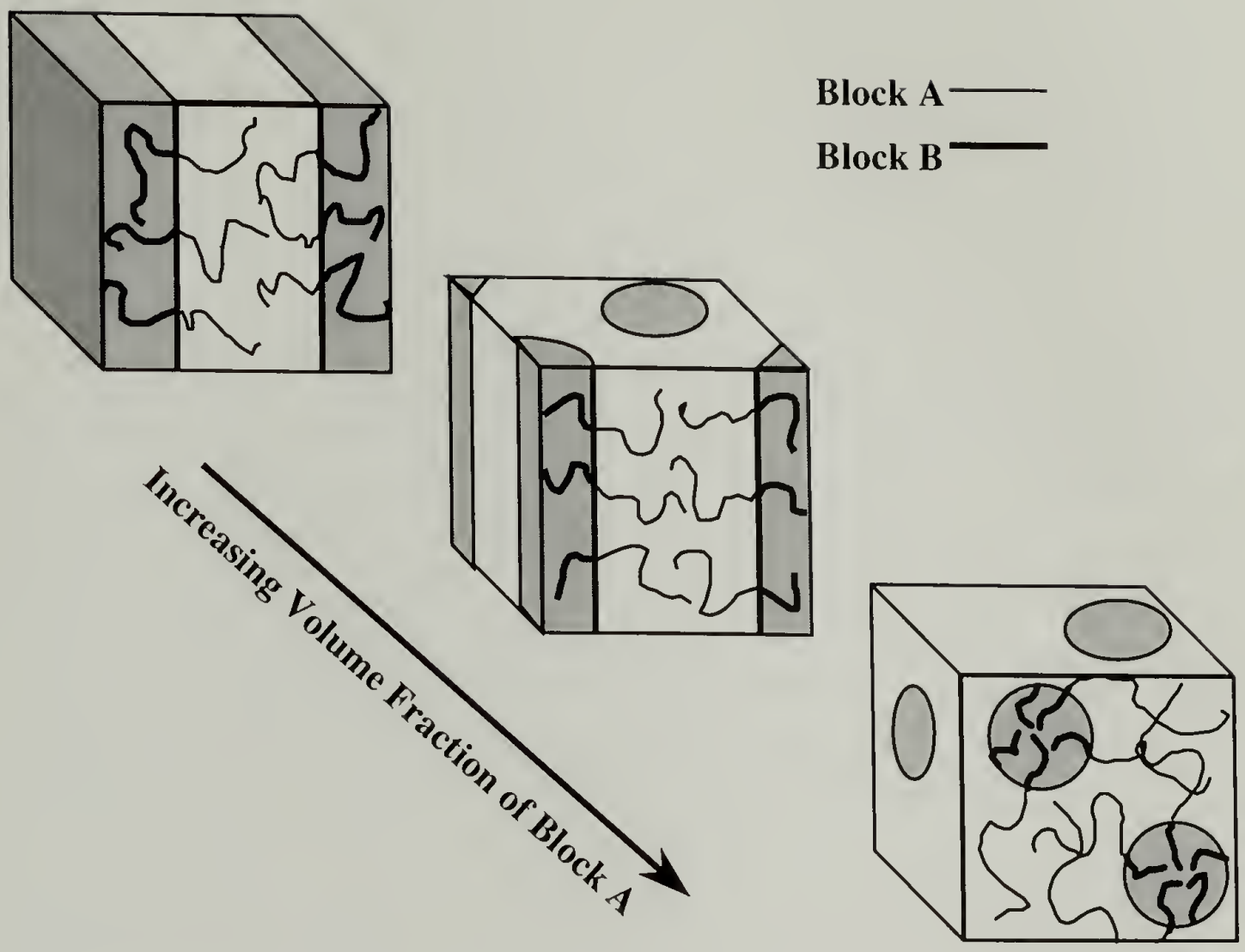

Figure 1.3 Schematic of the Effect of Block Asymmetry on the Morphology of a Diblock Copolymer.

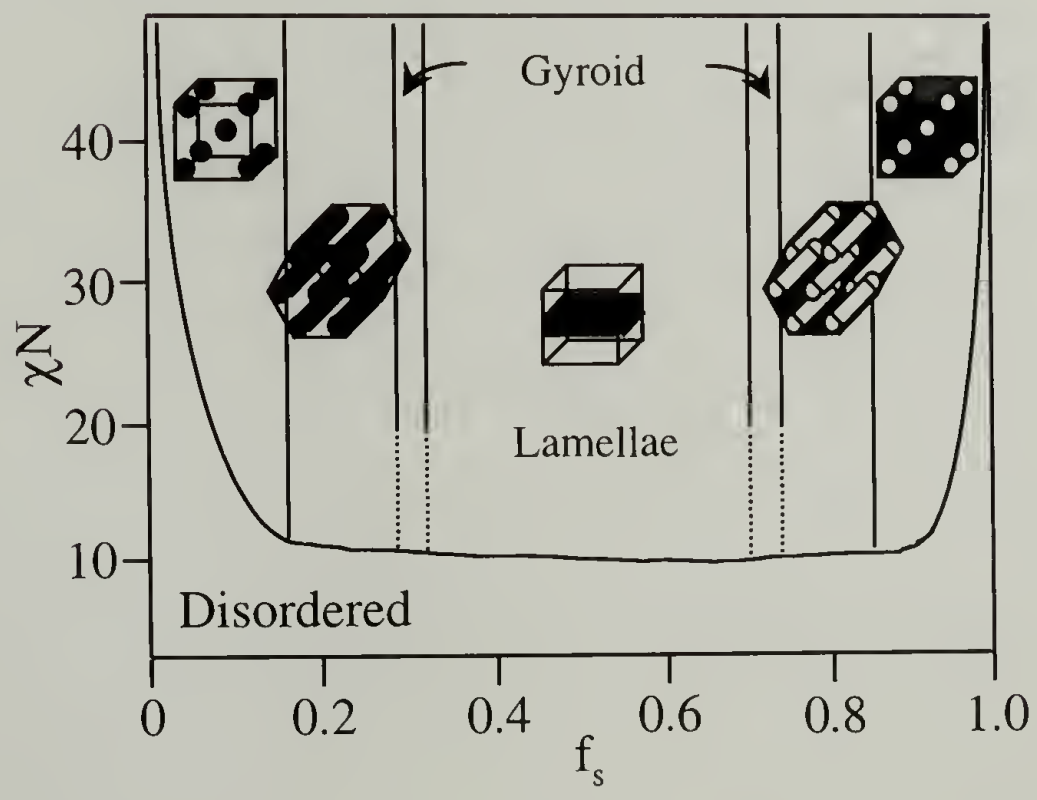

Figure 1.4 χN versus Composition (Vol. Fraction) Phase Diagram for Neat Diblock Copolymers.[25]

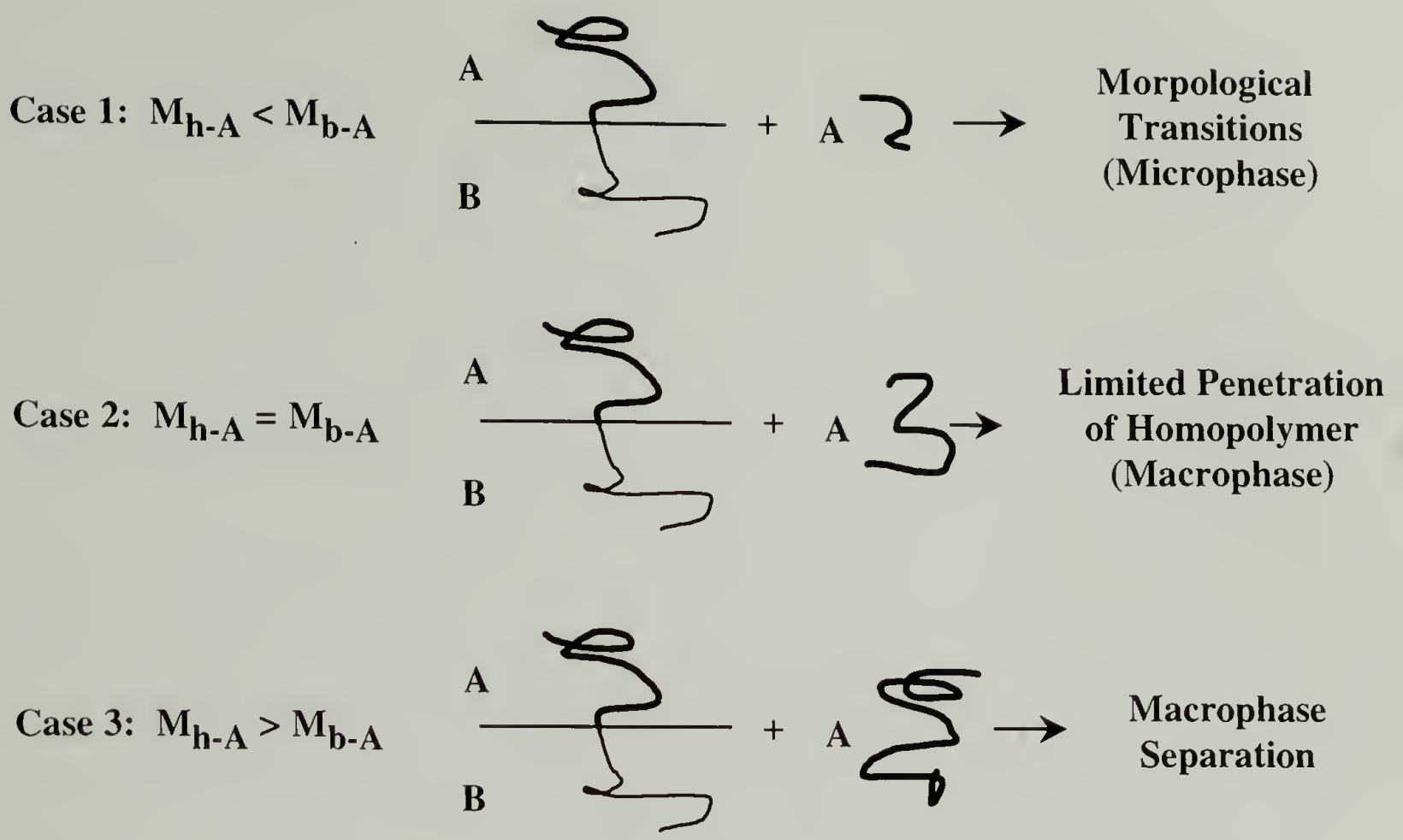

Figure 1.5 Schematic of the Three Cases for Blends of Diblock Copolymer and Homopolymer.

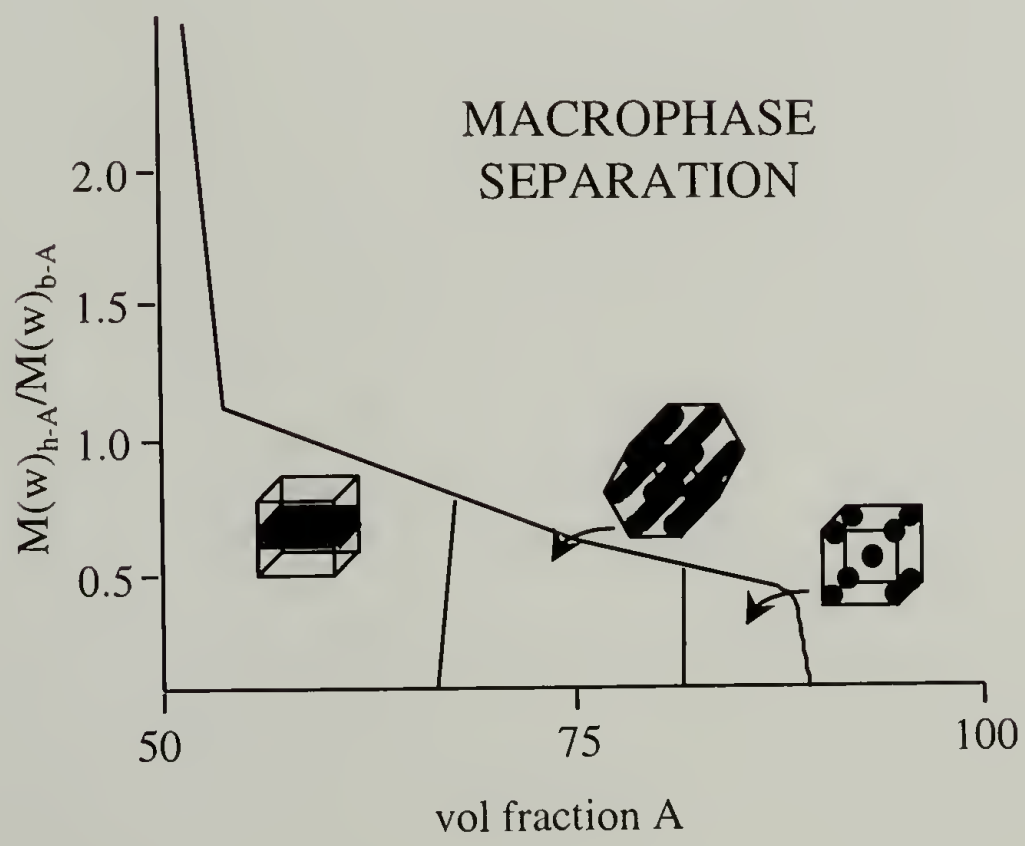

Figure 1.6 Morphological Diagram for Diblock Copolymer/Homopolymer Blends.[49]

CHAPTER 2

SYNTHESIS AND MOLECULAR CHARACTERIZATION OF MODEL POLYMERS AND COPOLYMERS

2.1 Introduction

Studies of model systems in polymers are useful for investigating phenomena such as phase separation while minimizing the effects of such variables as molecular weight distribution and microstructure (e.g. in polyolefins, branch content and length variation from chain to chain). These parameters introduce variability into the results, causing observed events or behavior to be clouded with conjecture as to what does or does not contribute to an individual observation. For this reason, a synthetic method which allows for control over length of individual chains, distribution of these chain lengths, and the architecture of the chain is necessary. This is where living anionic polymerizations excel.

The possibility of living anionic chain synthesis was first suggested by Ziegler in 1936.[1] In this paper it was proposed that butadiene and styrene could be polymerized by an organic alkali (lithium phenyl) to completion; and if impurities could be minimized to such an extent that they did not introduce termination to the active centers, a chain end could be kept "alive" indefinitely. The mechanism put forth by Ziegler is, in fact, the accepted mechanism today.[1] In present terminology where I is the initiator, C is the counterion, and M is the monomer,

Initiation Step	$I^-C^+ + M \rightarrow I\text{-}M^-\ C^+$	(1)
Propagation Step	$I\text{-}M^-\ C^+ + M \rightarrow I\text{-}M\text{-}M^-\ C^+$	(2)

The reaction scheme for this research is shown in Figure 2-1.

There is still debate, though, in the details of the reaction and its transition states. Szwarc[2] stated that he believes the transition states are actually an equilibrium between associated teramers, dimers, and "unimers" (see Figure 2-2), where unimers are the active species that allow monomer addition to the chain end. More recent work by Fetters et al.[3] interpret the data from neutron (SANS) and x-ray (SAXS) scattering experiments for living anionic systems as being devoid of tetramers, but instead containing a small percentage of long, train-like associated active chain ends in equilibrium with dimers and "unimers" as shown in Figure 2-3. An independent confirmation of either mechanism has not been published to date. It is the author's opinion that the main truth to be derived from these studies is that in reality, the mechanism of this polymerization is not as simple as it seems.

The actual term "living anionic polymerization" is attributed to M. Szwarc[4], and his group was the first to demonstrate that "living" conditions, which will be described in more detail below, could be created. Sodium naphthalane was used as the initiator and styrene as the monomer in THF to produce polystyryl anion (deep red color) from the sodium naphthalene (intense green color).[5] The basic conditions for defining a polymerization as "living" were described by Szwarc[4,5] as having no termination or transfer reactions, such as those oxygen or water could cause, and an increase in viscosity (now interpreted as molecular weight) with added monomer once the original amount of monomer had been consumed. It is now known that the increase in molecular weight

should be linear with time. Szwarc[5] went on further to propose that the living anionic method should be well suited to the synthesis of block polymers, which is definitely the case. Szwarc also believed that the reaction of the carbanionic chain end with water and reaction with oxygen would give quite different results.[4] Reaction with water would cause termination by abstraction of a proton from water and result in a dead polymer chain, ending in a hydrogen plus a hydroxyl anion.[4] (see Figure 2-4) Oxygen, on the other hand, was expected to abstract an electron from the anionic site, leading to the transformation of the chain end from anionic to a radical active center which would then undergo dimerization.[4] (see Figure 2-5) It was also speculated that the dimer formation process would involve oxygen bridges from the action of the other oxygen molecules. Unfortunately, this low concentration of oxygen (as an ether linkage) would not be detectable by either NMR or IR, except for very low degrees of polymerization.

The major criteria for living anionic polymerizations are a lack of termination or side reactions, an increase in molecular weight with added monomer once the original supply has been consumed, an initiation step which is substantially faster than the propagation step (which leads to narrow molecular weight distributions. The degree of polymerization can be determined by the relation DP = [M]/[I].[6] In many instances, the ability to control the microstructure of the resulting copolymer can be achieved by controlling the way in which the monomers add to the growing chain by the use of polar solvents or very low temperatures.

These factors allow for substantial control over molecular weight, polydispersity, and chain architecture. This ability to predict major variables of the final product (molecular weight, a narrow, monomodal molecular weight distribution, mode of

addition) is the reason why anionic polymerization is the method of choice in polymerizing dienic and styrenic monomers. An added advantage is the ability to preferentially stain diene polymers with heavy metals (via OsO_4 or RuO_4) to enhance contrast for TEM studies. For our work, a different route was utilized to create mass density contrast between dissimilar polymer segments: hydrogenation. In doing so, 1,4-polybutadiene becomes "polyethylene" and 1,4-poly(2-methylpentadiene) becomes "atactic polypropylene", and mass density contrast is produced through crystallization of the "polyethylene" segments of the diblock and homopolymer (since atactic polypropylene is amorphous). Hydrogenation also serves to increase the thermal stability of these polymers. Crystallinity is created by saturation of high 1,4-content polybutadiene. The saturation process allows the introduction of deuterium needed to label polymer chains for SANS/NR experiments. This will be discussed later in Section 2.7.

Previously in the MacKnight research group, blending of the diblock copolymer poly(ethylene-*at*-propylene) (DEP) with atactic polypropylene (APP) has been studied.[7-10] These polymers were synthesized at Exxon Research & Engineering Company (ER&E—Annandale, NJ) using the same techniques as was used by the author with one exception: methylpentadiene was originally bottled under an inert gas, thus it was more "pure" in the sense that it had less dissolved air and water vapor in it. This alleviated the need for the two-step drying as explained in Section 2.4 of this chapter (Monomer Preparation). ER&E has substantial resources and experience in living anionic synthesis techniques (to which the author is deeply indebted), which is why all polymerization work was performed there.

Finally, the objectives of the work presented in this chapter are as follow: the preparation of a model, symmetric diblock copolymer of the monomers 1,3-butadiene and 2-methyl-1,3-pentadiene; the preparation of three (3) model polybutadienes (PBDs) of high 1,4-content for the purpose of blending with the afore-mentioned diblock copolymer; the preparation of hydrogenated and deuterated high molecular weight PBD and PMPD and moderate molecular weight deuterated PBD-PMPD for neutron reflectivity studies; characterization of molecular weight and microstructure by GPC (SEC) and proton and ^{13}C NMR, respectively; hydrogenation (or deuteration, where required) of diene polymers to polyolefins to create crystallinity of the polymers; and characterization of the extent of saturation of the "polyolefins" by proton NMR. Included in this chapter will be information on attempts to synthesize and fractionate diblock copolymers based on the monomers 1,3-butadiene and 2,3-dimethyl-1,3-butadiene and termination of a PMPD with a hydroxyl group (to improve film adhesion with silicon wafers) both which proved unsucessful.

This chapter begins with a description of the glassware and its cleaning. Then the materials used in the polymerizations/hydrogenations and their preparation for use are explained, followed by the general synthetic method for diblock copolymers and homopolymers. Hydrogenation and characterization techniques are reported in the next two sections. A results and discussion section follows, and a summary is presented at the end of the chapter.

2.2 Description and Preparation of Glassware

All glassware was made by D. Nicholas of ER&E's glass shop to the specifications of J. Sissano. The glassware which was used for this research was of the modified Schlenk tube-type. A diagram of a typical reaction flask is shown in Figure 2-6.

The rationale for this design stems from the following considerations: fairly large quantities of polymer will be made (up to 100g); living anionic sythesis requires fairly dilute solutions (10-15% w/v); the ability to pull a high vacuum on the contents of the flask while also being able to isolate the flask from the vacuum and outside environment; the inclusion of a PTFE-coated stir bar to mix the solution; and relative ease of cleaning. As can be seen, two of the major design features are also sources of problems. Unlike the glassblowing technique of L. Fetters, where glass completely encases the reaction mixture, the PTFE-gasketed stopcocks allow the potential for air/water vapor leakage if the seals are not seated properly or the stopcock is not closed. (On the other hand, the presence of a flame in the vicinity of flammable materials is eliminated.) As in all reactions involving glass vessels, the possibility for star cracks or breaks exist, so proper care must be taken while handling the glassware.

All reaction glassware was cleaned by first filling the flask to the top with THF and allowing it to stir for 2-3 hours at room temperature to dissolve any residual polymer that might be left in the flask or neck from the previous reaction and then placing them in a KOH/IPA bath overnight. KOH etches the glass, which provides a clean surface for running reactions. For this same reason, glass syringes were not put in the KOH bath. After the KOH/IPA was drained from the flask, the flask was rinsed with dilute HCl to eliminate residual KOH. The glassware was inspected at this point for foreign matter or

cracks in the glass (from being in the base bath). Flasks were rinsed repeatedly with hot tap water. A couple rinses with acetone were used to eliminate the water from the glassware. Finally, all glassware was placed in a drying oven until needed for a reaction.

Prior to initiating a living anionic polymerization, steps must be taken to ensure that all traces of air and water have been removed from the reaction flask. (Syringes are covered at the end of this section.) Once the flask has been removed from the drying oven and cooled under a nitrogen stream, a small amount of vacuum grease (Apiezon-UK) was wiped around the male half of the 18/9 joint, and the flask was clamped to the vacuum rack. A vacuum was applied to the arm of the flask first to check whether the seal of the 18/9 joint was sound. After degassing the arm to under ten microns of mercury (10μm Hg) vacuum, the stopcock on the flask was opened, and the body of the flask evacuated. When the needle on the vacuum gauge had stopped moving, the flask was flamed with a propane torch to eliminate the layer of water molecules on the surface of the glass. Then glassware was allowed to cool under vacuum. The cooled flask was inspected for leaks using a tesla coil, and the stopcocks to the flask and the vacuum rack were closed. The flask was removed from the rack and placed in the antechamber of a glove box to degas before bringing it into the glove box.

Contaminated syringes (which might contain trace amounts of *t*-BuLi) were first rinsed while in the glove box with the waste hexane used for cleaning the reaction flask. After removal from the glove box, syringes were rinsed with IPA (or MeOH) to neutralize the butyllithium, and then with water and finally acetone before being stored in a drying oven until needed.

2.3 Materials List

The following is a list of materials that were used during the course of the synthetic work which was performed at ER&E:

1,3-Butadiene	(BD)
1,3-Butadiene-d_6	(*d*-BD)
2-Methyl-1,3-pentadiene	(MPD)
2,3-Dimethyl-1,3-butadiene	(DMBD)
Hexane	
Cyclohexane	
tert-Butyllithium	(*t*-BuLi)
Triethylaluminum	(TEAL)
Isopropanol	(IPA)
Methanol	(MeOH)
Acetone	
Ethylene Oxide	(EtO)
Paladium on barium sulfate	($Pd/BaSO_4$)
Wilkinson's catalyst	
Hydrogen	(H_2)
Deuterium	(D_2)

All liquid monomers and initiators/drying agents were obtained from Aldrich while all solvents and nonsolvents were obtained from J. T. Baker. 1,3-Butadiene and hydrogen were obtained from Matheson Gases, and the deuterated butadiene and deuterium were obtained from Cambridge Isotopes.

T-BuLi, TEAL, MeOH, IPA, $Pd/BaSO_4$, and Wilkinson's catalyst were used as received. The other chemicals were purified/degassed prior to use, as discussed below.

2.4 Preparation of Monomers

1,3-Butadiene (BD) was prepared by condensing the vapor over 3ml *t*-BuLi in a graduated trap (see Figure 2-7) which was cooled by a dry ice/isopropanol bath, and allowing it to stir for at least one hour (to give time for unwanted species—most notably

oxygen and water vapor—to react with the *t*-BuLi). Enough butadiene was condensed in the cooled trap to allow for a spare 5-10ml of butadiene in the trap after the transfer to the reaction flask was complete. This served the roles of keeping contaminants in the trap, keeping the level of butadiene above the 10ml gradation mark on the trap, and giving leeway if, for some reason, the bath ran low on dry ice and some butadiene evaporated into the space above the liquid (so one would not have to go back through the process of condensing more butadiene). Due to a higher level of impurities, deuterated butadiene (*d*-BD) was dried over 0.75mol *t*-BuLi for a minimum of two (2) hours using the same procedure as stated above.

Occasionally, if the supply of *t*-BuLi was running low or if many reactions were to be run involving butadiene, TEAL was used instead of butyllithium as the drying agent for butadiene. Using butyllithium as the drying agent had the major advantage of creating reaction conditions ("what the monomer would see in the reaction flask") before it is actually transferred into the reaction flask, whereas TEAL had the distinct benefits that the butadiene trap could be used several times before more drying agent would have to be added to the trap and many times before the trap contents would have to be neutralized and the glassware cleaned.

Liquid monomers (MPD and DMBD) were purified using a combination of drying with TEAL and butyllithium. DMBD was prepared for polymerization by degassing the (frozen) contents and allowing it to stir over *t*-BuLi for at least three (3) hours at room temperature prior to transferring it to the reaction flask. MPD was found to have the best polymerization results when purified using a two step procedure. First, the monomer was added to 5ml TEAL (93%), frozen in liquid nitrogen, degassed, and then allowed to stir

overnight in an ice/water bath. The next day, the monomer flask was removed from the ice/water bath, frozen, degassed, thawed, and distilled into a second (frozen) flask containing 0.45-0.75mol *t*-BuLi. The new monomer flask was warmed to room temperature and allowed to stir for at least three (3) hours prior to polymerization.

2.5 Preparation of Solvents

Hexane was dried over styryllithium anion prior to use. The styryllithium anion was generated by adding 2-3ml styrene monomer (0.02-0.03mol) to 1.5-3.0mol *sec*- or *tert*-BuLi which had been already introduced to the hexane. The styryllithium turned the mixture a ruddy orange color as an indication of dryness. The solvent flask degassed several times to eliminate air introduced by the addition of *t*-BuLi and styrene. Prior to a polymerization, the solvent flask was allowed to stir overnight and degassed several more times to eliminate any spurrious gases which may have seeped into the system.

The solvent flasks were degassed by the following procedure: The flask was frozen in liquid nitrogen and degassed to below 10 microns mercury; the stopcock to the flask was closed; and the glassware warmed by submerging the flask in warm water to room temperature. After stirring for several minutes at room temperature, the flask was immersed in liquid nitrogen and the process repeated.

Cyclohexane was dried in a manner analogous to hexane. However, there is a necessary precaution which must be taken in thawing frozen cyclohexane. Frozen cyclohexane has a proclivity to bumping violently in a flask if it is warmed too quickly. This leaves the possibility for glassware breakage, and therefore it should be warmed slowly.

2.6 Preparation of Terminating Agents

Isopropanol and methanol were used during the course of this research to terminate reactions and as nonsolvents. Both were added to clean, flamed modified-Schlenk flasks and repeatedly frozen with liquid nitrogen and degassed on a high-vacuum line. The terminating materials were considered ready for use when the needle on an attached vacuum gauge did not exceed 10 microns upon opening a frozen flask to the vacuum line. The methanol was used primarily with DMBD reactions, as it was thought to decrease side ("coupling") reactions that occurred during termination. Isopropanol was used to end all other reactions and as a nonsolvent for precipitating polymers. For one reaction ethylene oxide was used to prepare a hydroxy-terminated polymer which was to act as an adhesion promoter in NR studies. The ethylene oxide was dried over calcium hydride and degassed prior to use. This reaction was only performed once, and the polymer produced was hydrogenated to eliminate unsaturation. The reaction proved to be unsuccessful as the hydrogenation catalyst (Pd) became bound to the polymer chains and could not be removed.

2.7 Synthetic Method[11]

The first part of this section describes the general technique for synthesizing polybutadiene (PBD) homopolymer. The second contains the procedure for producing high molecular weight homopolymer from liquid monomers. The third portion of this chapter describes the attempt to terminate poly(methylpentadienyl) anion with ethylene oxide to form a hydroxy-terminated polymer. In the fourth section, the differences between deuterous and hydrogenous monomers as applied to living anionic

polymerizations are detailed. As a reminder to what was stated in the Introduction of this chapter, this is a high-vacuum technique involving modified Schlenk-type glassware, not high vacuum with blown glass and not Schlenk tube chemistry using inert gas atmospheres.

2.7.1 General Procedures for Living Anionic Polymerizations of Butadiene

The rinse flask and reaction flask were removed from the drying oven and cooled under a nitrogen stream. When cooled, the rinse flask was attached to the vacuum rack, (Figure 2-8) degassed, and flamed with a propane torch. The flask was then resealed, frozen in liquid nitrogen, and the stopcock to the upper rack was closed. 50-60ml of solvent was distilled into the frozen rinse flask, which was then degassed, sealed from the rack, warmed, and removed. Once sealed, the reaction flask was removed from the vacuum rack and placed in the antechamber of a glovebox. Along with the reaction flask and rinse flask, a 1cc syringe, a 5cc syringe, a 5ml glass pipet, and two small glass bottles were also placed in the antechamber, which was then closed and allowed to pump down for 15-20 minutes.

After the antechamber had been backfilled with argon and the contents brought into the box, 1cc of *t*-BuLi and 5ml of hexane (or cyclohexane) from the rinse flask were syringed into the reaction flask and swirled to scavenge remaining contaminants. The mixture was pipetted out of the reaction flask and into one of the small bottles. This solution was swirled around the first bottle and poured into the second. This process was repeated 3-4 times with solvent only. Then the initiation solution was prepared in the first bottle. by combining 0.5cc of *t*-BuLi solution (0.15M) and 20cc of hexane or

cyclohexane. The calculation to determine the amount of initiator solution needed to obtain the desired molecular weight is as follows:

$$\text{Moles of initiator needed} = \frac{\text{weight of monomer}}{\text{final molecular weight}} \quad (3)$$

$$\text{Molarity of initiator solution} = \frac{\text{molarity of initiator} * \text{cc of initiator}}{\text{cc of total solution}} \quad (4)$$

$$\text{cc of initiator solution needed} = \frac{\text{moles of initiator needed}}{\text{molarity of initiator solution}} \quad (5)$$

with weight in grams, molecular weight in g/mol, and molarity in mol/g. After the solution was prepared, the calculated amount was syringed into the reaction flask, which was then sealed. Everything was placed in the antechamber and removed from the glove box.

The reaction flask was reattached to the vacuum line, frozen, and degassed to under 10 microns Hg. Enough solvent was distilled into the flask to make a ~10% (by volume) solution with the monomer. The reaction flask was then closed, refrozen, and again degassed (to below 10 microns Hg). The seal on the reaction flask and those to the butadiene trap were closed; and the line to the butadiene trap was attached to the vacuum rack and degassed for ten (10) minutes, minimum. The butadiene trap was opened slightly to the vacuum to draw off gases/vapors trapped within the head space or dissolved in the condensed butadiene. Once the butadiene liquid started to bump, the stopcock was closed and the transfer line again degassed for 5-10 minutes. Then the frozen reaction flask was opened and checked for loss of vacuum (an indication of cracks or pinholes). The stopcock to the upper rack was closed, and the dry ice bath was removed from under the butadiene trap and replaced with acetone at room temperature.

Once the butadiene showed bubble formation, the stopcock to the transfer line was opened; and the desired amount of butadiene was allowed to distill into the frozen reaction flask. When finished transferring the butadiene, the graduated trap was resealed, transfer lines changed, and the trap opened to the argon flow which exited through the bubbler. This allowed the vapor to vent into the hood and prevented the possibility of explosion due to pressure buildup.

The reaction flask was completely frozen, degassed to under 10 microns mercury, resealed, and thawed in warm water. It was then moved to an oil bath at 40°C and allowed to stir overnight before termination. For diblock copolymer synthesis, the butadiene block was always performed first since it reacted faster than either of the liquid monomers used.

2.7.2 General Procedures for Living Anionic Polymerizations of Liquid Monomers

For liquid monomers, after drying/purification (see "Preparation of Monomers"), the monomer was frozen in liquid nitrogen and warmed with water to above room temperature, while the reaction flask was frozen and degassed. The lower vacuum rack was then isolated from the vacuum pump and the stopcock to the monomer flask opened to allow the monomer to distill into the frozen reaction flask. Once the bubbling in the monomer flask had ceased, this flask was sealed, as was the reaction flask. After degassing the frozen reaction flask for 5-10 minutes, it was resealed, thawed in warm water, and placed in an oil bath at 35°C. For reactions involving DMBD, the duration of the polymerization was four (4) days; for MPD, five (5), days as these reaction times were

found to be the best compromise between conversion and the final polymer molecular weight distribution.

The termination of reactions was accomplished by distilling 1-2ml of purified MeOH or IPA into the frozen reaction flask, degassing the reaction flask, and then thawing to cause the actual termination. (The reaction involving ethylene oxide is discussed below.)

2.7.3 Termination of Poly(methylpentadienyl) Anion with Ethylene Oxide

Ethylene oxide was purchased from MG Industries in the form of a lecture bottle and was condensed into a flask containing calcium hydride which was immersed in a dry ice/IPA bath. EtO was degassed and allowed to stir for 30 minutes prior to use. EtO was evaporated by replacing the dry ice bath with cool water and distilled into the frozen reaction flask to terminate the MPD reaction.

2.7.4 Differences between Hydrogenous and Deuterous Monomers

There were two major differences which were taken into account when working with deuterated 1,3-butadiene (*d*-BD). Cleaning of the condensed vapor of *d*-BD took longer than hydrogenous BD because the deuterated version is actually synthesized by a different route than the hydrogenous version and has more byproducts to be eliminated. Also the reaction times for *d*-BD were slightly longer than *h*-BD. Since all reactions were allowed to run overnight, both types of BD went to completion.

2.8 Characterization

Two techniques were used to characterize the homopolymers and diblock copolymers: gel permeation chromatography (GPC) and nuclear resonance spectroscopy (NMR).

2.8.1 Gel Permeation Chromatography (GPC)

GPC was used as a first pass technique to obtain a weight-average molecular weight (M_w) and polydispersity index (PDI) for polymers immediately after termination. For this purpose, a Waters GPC (Model 150) with an attached differential refractometer was used. Calibration of columns was accomplished using PBD standards (American Polymer Standards) ranging in molecular weights from 10^2 to 10^6 g/mol. Because the reported molecular weights are based on PBD standards and not on light scattering results, any polymer composed PMPD will have a molecular weight which is roughly 20-30% larger than reported. This arises from the presence of methyl branches which alter the hydrodynamic volume relative to the calibration curve and results in the ratio of the molecular weights of the homopolymers to the copolymer block being 10-15% off the value reported in the subsequent chapters. Since this did not appear to affect the results from the previous work whose molecular weights were also based on PBD standards, this custom was continued. Tetrahydrofuran (THF) was used as the solvent at a flow rate of 1ml/min. For some of the runs, elution columns (Waters-Millipore) with average pore diameters of 10^5, 10^4, and 10^3 angstroms were used, while for other samples, mixed pore size columns were used (with the pore size range being the same). Analyses were performed with either a DEC personal computer using Waters proprietary software or by

using an analog chart recorder, measuring the heights of slices of the peak, and calculating molecular weight values using an Excel (Microsoft) spreadsheet developed by P. Wright at Exxon. GPC/Light Scattering was performed on the hydrogenous diblock copolymer using a Waters 150 GPC with a Dana Instruments light scattering detector. The mobile phase and flow rate were the same as before. The change in refractive index with concentration was measured for the light scattering detector using a Photal Model RM-102 (Okutsu Electronics) differential refractometer for five solutions of polymer in THF.

2.8.2 Nuclear Magnetic Resonance Spectroscopy (NMR)

Once GPC had determined that the molecular weight and molecular weight distribution were acceptable, solution NMR was used to determine copolymer composition and microstructure in precursor diblocks as well as the level of unsaturation from diblocks and homopolymers that had been hydrogenated or deuterated.

NMR was performed by either M. Garcia or D. Sysyn of ER&E using the 300MHz Varian NMR on samples prepared by the author. For spectra to be performed on precursor (co)polymers, deuterated chloroform was used as the solvent and spectra were recorded at 30°C. For saturated materials, deuterated *ortho*-dichlorobenzene was used as the solvent, and spectra were recorded at 125°C. In both cases, tetramethylsilane was used as the internal reference. Carbon-13 (^{13}C) NMR was utilized to determine precursor copolymer composition and microstructure. Proton (^{1}H) NMR was used to evaluate microstructure in precursor homopolymers and the extent of saturation in hydrogenated homopolymers and diblocks and deuterated homopoly(methylpentadiene)

(which used hydrogenous-MPD as the monomer). Deuterium (^2D) NMR was performed on the deuterated precursor copolymer that had been saturated using deuterium instead of hydrogen in the "hydrogenation" process. Calculations of composition, microstructure (cis vs. trans, 1,2- vs. 1,4-addition) and level of residual unsaturation were performed.

2.9 Hydrogenation

Polymers which were identified as candidates for blending studies or neutron work (i.e. the appropriate molecular weight range and molecular composition) were hydrogenated or deuterated depending on their use. All polymers were saturated at ER&E.

First, polymers were dissolved in pentane to make up a 10% (w/v) solution. This solution was added to a two (2) liter Parr reactor with palladium on barium sulfate (1:1 ratio of polymer to catalyst, by weight). Hydrogenations were performed at 80°C and at hydrogen pressures of 2900-3200kPa. The reaction was allowed to proceed overnight. For the instances in which large quantities of polymer (i.e. over 15g) were to be hydrogenated, polymers were saturated in batches.

After the hydrogenated solution was drained and filtered, it was allowed to cool to room temperature. The polymer was precipitated using a 50/50 mixture (v/v) of acetone and methanol. The precipitated mixture was vacuum filtered using the methanol/acetone (1:1 ratio, by volume) since the mixture of acetone and methanol was a good solvent for the residual catalyst as well as a non-solvent for the polymers. The polymers were rinsed with the methanol/acetone mixture until no color remained in the filtrate.

Polymers were dried at room temperature overnight in a vacuum oven. A small sample was removed for proton NMR analysis. If the proton NMR results showed the hydrogenation process to be reasonably complete (over 98%), the polymer was dried at 50°C for several hours to assure that no solvent remained. If color returned to the sample with the initial drying, the polymer was rinsed several times again with acetone/methanol and dried in a vacuum oven at room temperature. If color again returned, this process was repeated until a white polymer was obtained after drying.

If proton NMR revealed an unsatisfactory level of saturation, the polymer was redissolved and sent through the hydrogenation process from the start. Palladium on barium sulfate was used on all samples, regardless of the type of polymers involved. For high molecular weight PBD, a mixture of $Pd/BaSO_4$ and Wilkinson's catalyst was used to increase the efficiency of the hydrogenation reaction.

2.10 Results and Discussion

Living anionic polymerizations are undoubtedly the method of choice for making diblock copolymers and homopolymers of well-defined microstructure and narrow polydispersity. This is a direct result of the ability to control important parameters such as molecular weight, molecular weight distribution, block length, and mode of addition (e.g. in the case of butadiene, 1,2- vs. 1,4-addition). Control is accomplished through the appropriate choices of solvents, initiators, monomers, and reaction temperature.

As can be seen in Table 2-1, the polydispersity in all cases was below 1.1—except for the atactic polypropylene used for neutron reflectometry. This was due to the "livingness" of the system. One of the major criteria for the term "living" is that the

initiation reaction is much faster than that of the propagation. Additionally, side reactions and termination reactions must be absent. An ideal state can only be approached through scrupulous cleaning of glassware, drying/purification of all chemicals, and the use of either dry inert gases or a vacuum in which the reactions are performed. This near absence of termination reactions allows different monomers to be added sequentially to the active chain end once the supply of original monomer has been exhausted. Another possibility is the use of modifying agents (polar solvents, for example) to create multiblock polymers of the same monomer but differing in architecture. An example of this is a diblock copolymer consisting of butadiene which has primarily 1,4-addition units in the first block and primarily 1,2-addition units in the second. The control over block length and microstructure is illustrated by the NMR data in Table 2-2. As can be seen, the diblock copolymers are close to being symmetric (50/50 by weight) and 1,2-addition in the butadiene homopolymers have been minimized.

The amount of effort that must go into cleaning glassware is a drawback to the living anionic technique. Another disadvantage is the relatively minuscule quantity of air or water that is required to ruin a reaction. A problem with monomers such as DMBD or MPD is that slow propagation of the chain allows for the termination of active chain ends and leads to a broadening of the molecular weight distribution.

A major difficulty in using DMBD for copolymerizations is that it couples upon termination more easily than BD or MPD. This was predicted by Swzarc[5] in 1956 when he proposed that oxygen has the potential cause a doubling of polymer molecular weight. (see Figure 2-5) It is possible that the increase in coupling was due to long reaction times, but this peak was not as pronounced in PMPD. It was originally thought that for

model studies, one must eliminate the coupled copolymer as it would affect the phase behavior in blends with homopolymer.[12] Therefore, fractionation was pursued to remove this high molecular weight shoulder. But there was a complication arising from the fact that PDMBD is semi-crystalline, possessing a melting temperature of roughly 40°C (by DSC). Fractionation entailed dissolving the copolymer in toluene at 50°C to make a 1-1.25% (w/v) solution. This was allowed to stir overnight, and the next day ethanol was added to the cloud point. The solution was then heated while stirring to 65-70°C, by which time the solution should have cleared. The mixture was added to a preheated separatory funnel and the filled separatory funnel was placed into a stirred water bath, also at 65-70°C. The temperature of the water bath was slowly lowered to 43-45°C, which caused the mixture to separate into lower and higher (and more dense) molecular weight fractions. Unfortunately, this procedure tended to either pull some of the "good" copolymer into the lower phase, lowering the yield, or there was no separation at all. As many as six passes were performed on diblocks containing coupled species before success was achieved in significantly reducing the "triblock" peak (as analyzed by GPC). After the sixth pass, only 1.5g of "clean" diblock remained out of roughly 7g at the start. This was unacceptable, and a new search for MPD was begun, since MPD was in fact the original comonomer used in studies of b-PE-APP/h-APP.[7-10] (The previous source, Wiley, discontinued making it.)

Another advantage of MPD over DMBD besides the reduction in the coupling peak is a lack of 1,2-addition.[13] Although one might initially think this would lead to crystallizability akin to that found in DMBD, it does not due to the fact that PMPD contains a high percentage of cis 1,4-addition segments.[14] A definite benefit insofar as

compositional analysis of copolymers is concerned is the lack of overlap of the major NMR peaks of PBD and PMPD, which allows for easier integration of peaks and simplifies calculations.

One disadvantage which should be discussed is the amount of waste inherent in using MPD, DMBD, or any other monomer which could be classified as a "slow polymerizer". MPD was usually terminated after five (5) days, at which time, the extent of reaction was 55-60%; for DMBD, it was 70-75% after four (4) days. Beyond these times, the active chain ends tended to become inactive, leading to increasingly broader molecular weight distributions. An example of a PDMBD is shown in Figure 2-9. This polymer was terminated after five days and had a polydispersity of 1.285 by GPC. If this reaction had been terminated after four days, the molecular weight distribution would most probably been under 1.1, as was evidenced by other PDMBDs. However, by shortening the times in order to achieve lower polydispersities, more waste is generated.

Degassing time was determined to be a very important variable for obtaining good polymers due to the leakage in the teflon seals on stopcocks which were used on essentially all glassware involved in the reactions. This variable was found to be relevant during the termination step of alcohol addition to the living polymer chains. If a sufficient duration of time was given for the frozen reaction flask to be degassed after the alcohol had been distilled into it, the coupling peak of the polymer could be minimized. This phenomenon was discovered in conjunction with problems that had been occurring with PDMBD-containing polymers and copolymers. Up to roughly ten (10) minutes of degassing time was found to reduce the height of the coupling peak as seen by GPC. Fifteen minutes of degassing time was observed to the reduce the size of the peak more,

but by a substantially lesser amount than in going from five to ten minutes. Therefore, the optimum degassing time (post-termination, pre-thawing) was determined to be ten (10) minutes. Another important point for degassing was when the transfer line for performing reactions with butadiene was attached to the vacuum rack. After a conversation with J. Sissano,[16] a change was made to the polymerization route: While pumping down the antechamber to the glove box, the transfer line to the cooled butadiene trap was attached to the vacuum rack and a vacuum was applied. It was found that this change helped to narrow the molecular weight distributions in PBD homopolymers.

An area which was not described in detail in the previous sections of the chapter was a 2-3 gram reaction of poly(methylpentadienyl) anion which was terminated with ethylene oxide (EtO). This reaction was intended to introduce a hydroxyl end-group to the PMPD, which would then be hydrogenated to APP-OH. The goal of the EtO-terminated reaction was 2-3g of PMPD-OH with an M_w of 10-15,000 g/mol. This hydrophilic end group would then be used as an adhesion promoter in NR experiments.[17] The need for a low molecular weight APP-OH arose from problems with cast films adhering properly to silicon substrates, especially when aged at room temperature. This loss of adhesion was a result of the incompatibility of the hydrophobic polymer film with the hydrophilic oxide layer on the surface of the silicon wafer. Two routes were identified as potential remedies to the adhesion stability problem: The first was the use of a hydrogen fluoride (HF) etch to dissolve the oxide layer and expose the less hydrophilic silicon underneath; while the second was the use of a small amount, a monolayer if possible, of hydroxy-terminated polymer to bridge the gap between the oxide layer and

the cast polymer films. Both routes were attempted; the description of the polymerization was described above. (The HF etch technique will be discussed in Chapter 6.)

A problem arose immediately when ethylene oxide was discussed as being used in the lab at ER&E: EtO has been listed as a Particularly Hazardous Chemical by the US-EPA. Unfortunately, the classification of EtO delayed the termination, so some premature termination of the "living" anion chains must have occurred in the weeks between the start and finish of the reaction. During most of this time, the reaction flask was attached to the house vacuum and placed in a dry ice/IPA bath to prolong the lifetime of the active chain ends. GPC (Figure 2-10) showed a surprisingly narrow polydispersity, but NMR was unable to detect whether any -OH groups were present on the chain ends. Due to time constraints, FT-IR was not performed to determine whether -OH groups were formed by the termination reaction with EtO. Hydrogenation with $Pd/BaSO_4$ was successful (by ^1H NMR), however the author was unable to remove the catalyst residue from the polymer. This was anticipated as a potential problem with the system which proved to be the case. Since the polymer would see several heating cycles and possibly degrade, it was not used for NR experiments. As discussed in the chapter on interfacial behavior, the HF etch proved to be the more successful of the two methods for preparing silicon wafers for NR.

GPC was performed on several instruments throughout the course of this research. With the exception of the GPC with an attached Light Scattering detector of the Novak research group at UMass, all molecular weight determinations via GPC were performed at ER&E. The majority of work was accomplished on a Waters GPC Model 150 with an attached microcomputer running Waters proprietary analysis software. Fractionation

analysis was performed on the Waters GPC Model 150 in the lab of J. Olkusz. All reported GPC chromatograms on the polymers used for this work were run on the Waters GPC Model 150 in the lab of L. Fetters. An Excel (Microsoft) spreadsheet was used which was based upon the measured heights of sections of the peak(s) using the following equations:[12]

$$M_n = \sum n_i M_i / \sum n_i \quad (6)$$

$$M_w = \sum n_i M_i^2 / \sum n_i M_i \quad (7)$$

$$M_z = \sum n_i M_i^3 / \sum n_i M_i^2 \quad (8)$$

where n is the peak height and M_i is the calibrated molecular weight at the time. The M_w values in Table 2-1 and the chromatograms in Figures 2-11 through 2-14 were tabulated from the strip chart data of L. Fetters' equipment. Measurements performed on the GPC with attached light scattering equipment (not shown) displayed similar results to those using GPC/RI detector.

^{13}C NMR was used for the analysis of microstructure for the diblock copolymers, whereas ^{1}H NMR was used for the homopolymers. For the diblock copolymers, PBD-*b*-PMPD, the resonances at 114.2 and 142.7 ppm were used for 1,2-addition in PBD, 129.6 ppm and 130.1 ppm for cis 1,4-PBD and trans 1,4-PBD,[18] and the resonances at 131.9 ppm and 133.1 ppm for cis 1,4-PMPD and trans 1,4-PMPD.[19] PMPD does not add in the 1,2-mode, thus simplifying the microstructure analysis.[19] For diblock copolymers containing PDMBD, proton NMR was used. Unfortunately, the methyl resonances at 1.73 ppm (cis 1,4-PDMBD) and 1.77 ppm (trans 1,4-PDMBD) and the methylene resonances at 2.16 ppm (trans 1,4-PDMBD) and 2.24 ppm (cis 1,4-PDMBD) overlapped

with the 1,4-PBD resonances and complicated calculations.[20] To determine the amount of 1,2-addition in PDMBD, the doublet at 4.85/4.90 ppm was used. PMPD, as can be observed from the above NMR assignments, did not overlap with the PBD resonances due to the combination of the protons from methyl groups (which were in the head-to-tail configuration) and the presence of the adjacent double bonds which created a chemical environment which was different than the PBD protons (and also led to a larger chemical shift in the PMPD protons relative to those of PBD). Figures 2-15 to 2-18 show NMR spectra for the polymers used in this research, while Figures 2-19 and 2-20 show NMR data for polymers containing PBD-*b*-PDMBD.

Hydrogenation was carried out using palladium supported on a substrate of barium sulfate ($Pd/BaSO_4$). A clear solution with a tint of gray (or if Wilkinson's catalyst was used, a tint of orange) indicated that the hydrogenation was at least partially successful. A cloudy solution indicated that the catalyst had partially attached itself to the polymer, while a black mixture meant that the polymer was a complete loss as the catalyst had firmly bound itself to the polymer backbone and one had to start over. The results of Graessley et al.[21] showed palladium to be the optimum catalyst for the hydrogenation of diene homopolymers and copolymers. The other hydrogenating agents, such as the diimide catalyst shown in Figure 2-21, proved to be too harsh on the polymer backbone and resulted in chain scission and a broadening in molecular weight distribution; while the homogeneous catalyst in Figure 2-22 did not add hydrogen efficiently across the double bond and resulted in incomplete saturation. Essentially, palladium attacks any bond that is not a C-H bond. It also causes proton exchange, which can be detrimental when hydrogenating polymers composed of deuterated monomers, such as *d*-PBD. For

butadiene homopolymers only, Wilkinson's catalyst (Figure 2-23) could be added to increase the efficiency of the saturation reaction while reducing hydrogen exchange (or deuterium exchange for deuterated polymers). Unfortunately, Wilkenson's catalyst binds to amorphous polymers strongly, and only with extreme effort can it be removed from the polymer.

^{1}H NMR was used to evaluate the saturation of olefin bonds in the diene precursors. NMR resonances in the range of 4.85-6.0 ppm were from double bonds in the backbone and in "ethyl" branches of the h-PBDs and copolymers. These are compared with C-C single bonds, which exist in the range of 1.0-3.0 ppm. The following expressions were used to calculate the residual unsaturation in the polymer after hydrogenation:

$$h_{C=C}/2 = \#\text{ hydrogens per C=C bonds} \qquad (9a)$$

$$h_{C-C}/4 = \#\text{ hydrogens per C—C bonds} \qquad (9b)$$

$$(h_{C=C}/2)/(h_{C-C}/4) \times 100\% = \%\text{ residual double bonds} \qquad (10)$$

where $h_{C=C}$ is the height of the integral for the resonance for double bonds, and h_{C-C} is that for single bonds. For the hydrogenated homopolymers (Table 2-2), the Pd/$BaSO_4$ proved to be adequate. The hydrogenous precursor diblock, DEP100, was not as fully saturated after the process as were the homopolymers, as is illustrated in Figure 2-24. This was due to the presence of tertiary carbons which reduced the ability of the Pd to access and change the C=C bonds to C-C bonds.

Major factors which affected the amount of residual double bonds after saturation were the age of the polymer to be hydrogenated and whether the polymer contained

deuterium or was to be saturated with deuterium. An example of the results from a polymer that was not hydrogenated immediately after termination was PBD20, which was saturated approximately three weeks after the polymerization had been ended. This polymer showed a large number of residual olefin bonds after the first time through the autoclave. Therefore, it had to be sent through the process a second time, which is quite severe to impose on the polymer chain. The origin of the problem was most likely from light cross-linking of the unsaturated polymers due to free-radical formation. It is advisable that all homopolymers and copolymers be hydrogenated as soon as possible to prevent this problem. On the other hand, the presence of deuterium appears to make the saturation process less effective. This effect is either due to deuterium preventing the Pd from efficiently attacking the double bond—a steric effect—or some electronic phenomena. In either case, the result is a lower level of saturation.

The diblock copolymer prepared for the blend work was close to the same composition as the diblock used previously for the blends involving atactic-PP (48wt% PE versus 52wt% APP). Therefore the blend results should be similar, with minor corrections for the differences in block and homopolymer molecular weights. The h-APP polymers which were used for the former study had M_ws of 15,000; 39,000; and 190,000. These give b-APP/h-APP ratios of 0.26, 0.67, and 3.2, respectively. By comparison, the h-PE polymers of this study had M_ws of 20,000; 48,000; and 107,000, which have h-PE/b-PE ratios of 0.45, 1.03, and 2.3, respectively. The latter ratios are slightly more amenable to direct comparison of microdomain structure with respect to the morphological diagram (Figure 1-6) described in first chapter than those of the previous study. On one hand, it is important to have polymers in different studies which give

similar molecular weight ratios so that results can be related more directly. On the other hand, it is also beneficial to use polymers which simulate the "ideal cases"—such as ratios of ½, 1, and 2, as mentioned above. These aspects must be considered when designing experiments and preparing polymers.

2.11 Summary

Living anionic polymerizations successfully yielded diblock copolymers and homopolymers based on butadiene and modified dienes. A list of those used for the research can be found in Table 2-1. The advantage of using the anionic synthesis technique is good control of molecular weight, polydispersity, block lengths, and microstructure. Proton and ^{13}C NMR and GPC were used to characterize these polymers with respect to the afore-mentioned parameters. Hydrogenation was used successfully to saturate diene copolymers and homopolymers. Once saturated, proton NMR was again performed to determine the amount of residual double bonds in each of the polyolefins. This data is also presented in Table 2-2. Polymerizations involving DMBD were not successfully fractionated from coupled precursors, and therefore were not used in later work. Changing to MPD reduced the coupling problem and resulted in cleaner polymer samples.

2.12 References and Notes

1. Zeigler, A. *Angew. Chem.* **1936**, *49*, 499.

2. Szwarc, M. *Adv. Polym. Sci.* **1983**, *49*, 1.

3. Fetters, L. J.; Balsara, N. P.; Huang, J. S.; Jeon, H. S.; Almdal, K.; Lin, M. Y. *Macromolecules* **1995**, *28*, 4996.

4. Szwarc, M. *Nature* **1956**, *178*, 1108.

5. Szwarc, M.; Levy, M.; and Milkovich, R. *J. Am. Chem. Soc.* **1956**, *78*, 2656.

6. Morton, M., Anionic Polymerization: Principles and Practice, Academic Press: New York, 1983.

7. Sakurai, K.; MacKnight, W. J.; Lohse, D. J.; Schulz, D. N.; Sissano, J. A. *Macromolecules* **1993**, *26*, 3236.

8. Sakurai, K.; MacKnight, W. J.; Lohse, D. J.; Schulz, D. N.; Sissano, J. A. *Macromolecules* **1994**, *27*, 4941.

9. Sakurai, K.; MacKnight, W. J.; Lohse, D. J.; Schulz, D. N.; Sissano, J. A.; Lin, J.-S.; Agamalyan, M. *Polymer* **1996**, *37*, 4443.

10. Sakurai, K.; MacKnight, W. J.; Lohse, D. J.; Schulz, D. N.; Sissano, J. A.; Wedler, W.; Winter, H. H. *Polymer* **1996**, *37*, 5159.

11. Fetters, L. J. *J. Polym. Sci.: Part C* **1969**, *26*, 1. Morton, M.; Fetters, L. J. *J. Rubber Chem. Technol.* **1975**, *48*, 145.

12. Thomas, E. L.; Fetters, L. J., in Model Polymers for Materials Science, 1992.

13. The Sadtler Standard Spectra of Carbon-13 NMR, Sadtler Research Labs, Inc.; Philadelphia, PA, 1988.

14. R. A. Register, private communication.

15. Aldrich Chemical Catalog, 1997.

16. J. A. Sissano, private communication.

17. T. P. Russell, private communication.

18. Zhonde, X.; Mays, J.; Xuexin, C.; Hadjichristidis, N.; Schilling, F. C.; Bair, H. E.; Fetters, L. J. *Macromolecules*, **1985**, *18*, 1211.

19. Schue, F.; Ortlieb, C.; Maillard, A,; Deluzarche, A. *Bull. Soc. Chim. Fr.* **1965**, *#178*, 982.

20. Blondin, D.; Regis, J.; Prud'homme, J. *Macromolecules* **1974**, *7*, 187.

21. Rachapudy, H.; Smith, G. G.; Radu, V. P.; Graessley, W. W. *J. Polym. Sci.; Polym. Phys. Ed.* **1979**, *17*, 1211.

Table 2.1 GPC Data and Nomenclature for Synthesized Polymers.

Name	Polymer Type	$M_n/10^3$ g/mol	$M_w/10^3$ g/mol	Mw/Mn
DEP100	(h) PBD-*b*-PMPD	95	100	1.06
PE20	(h) PBD	19	20	1.03
PE47	" "	45	47	1.05
PE107	" "	104	107	1.03

M(n), M(w), PDI by GPC; PBD standards.
GPC performed on polydiene precursor polymers.
For DEP100, estimated uncouple PBD < 5% (by peak height).

Table 2.2 NMR Data for Synthesized Polymers.

	PBD			PMPD		Copolymer	Saturation[c]
Name	1,2 (%)	cis 1,4 (%)	trans 1,4 (%)	cis 1,4 (%)	trans 1,4 (%)	wt%/vol%	%olefins
DEP100[a]	7	40	53	65	35	45/47 PBD	<1
PE20[b]	7	39	54	--	--	--	<1
PE47[b]	7	40	53	--	--	--	<1
PE107[b]	7	39	54	--	--	--	<1

a.) ^{13}C NMR was performed on precursor copolymer to determine composition and block symmetry.
b.) ^{1}H NMR was performed on precursor homopolymers to determine branch content.
c.) ^{1}H NMR was performed on saturated polymers to determine degree of residual unsaturation.

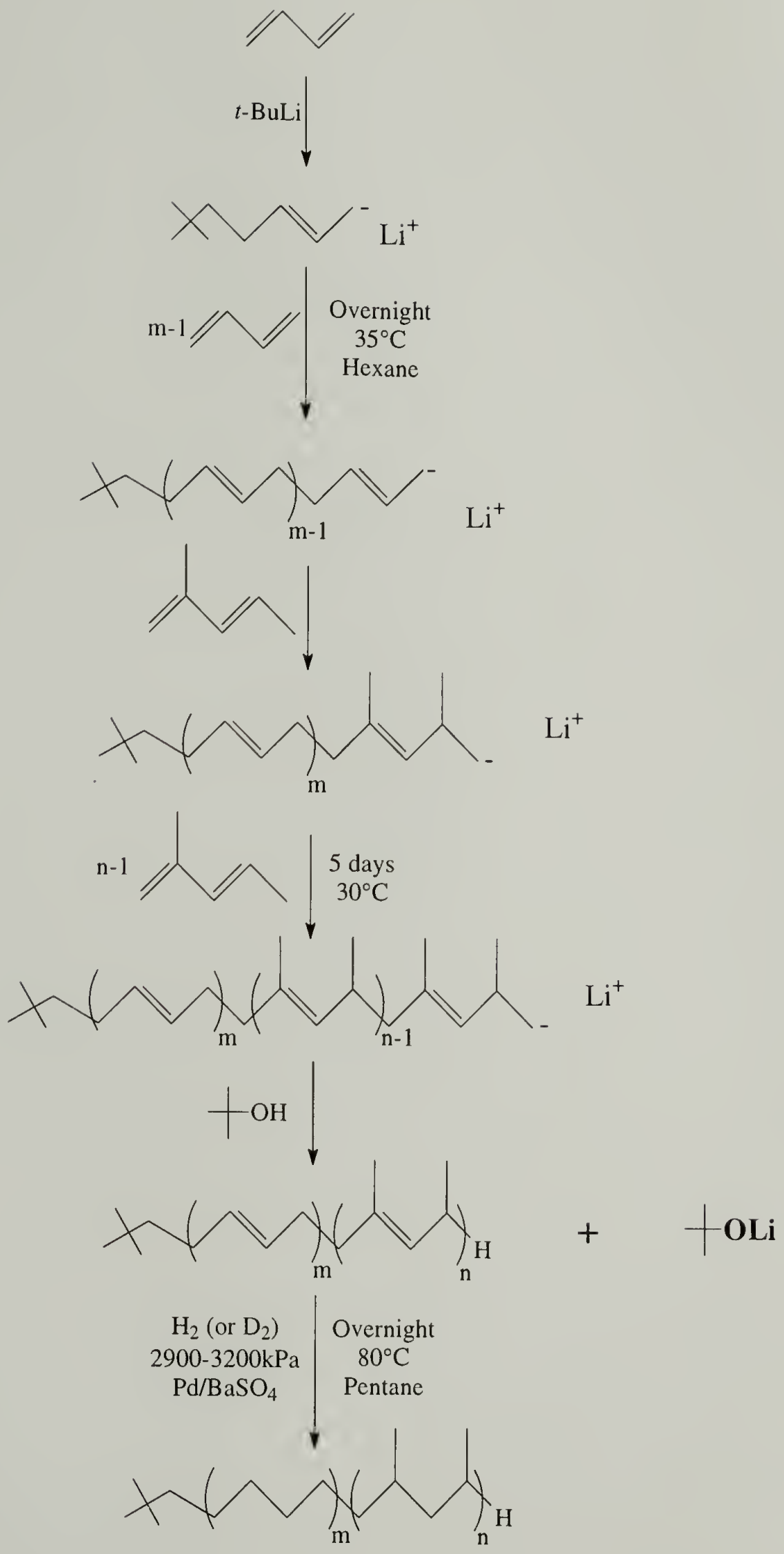

Figure 2.1 Reaction Scheme for Living Anionic Synthesis.

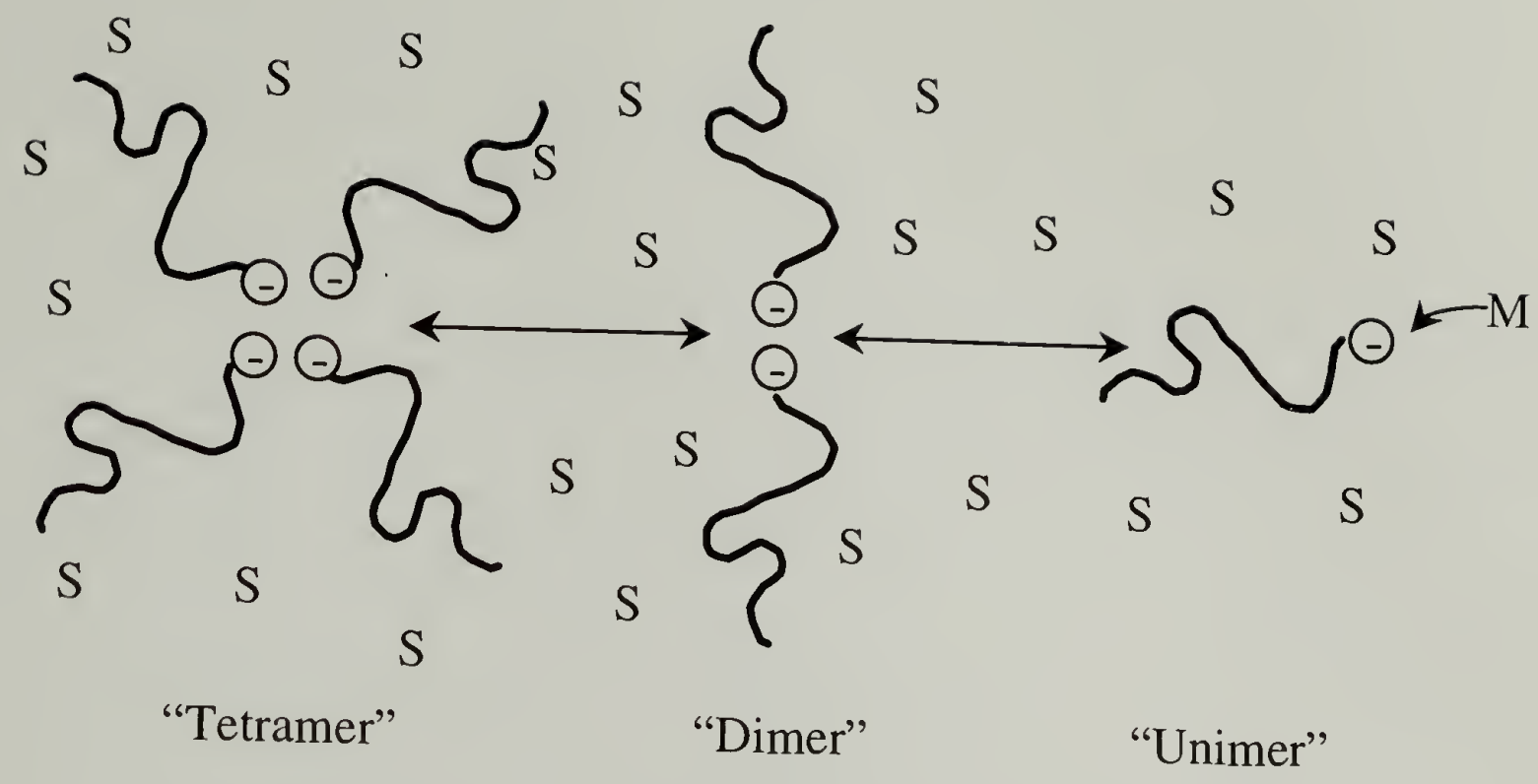

Figure 2.2 Schematic of Equilibrium Structures Proposed by Szwarc.[2]

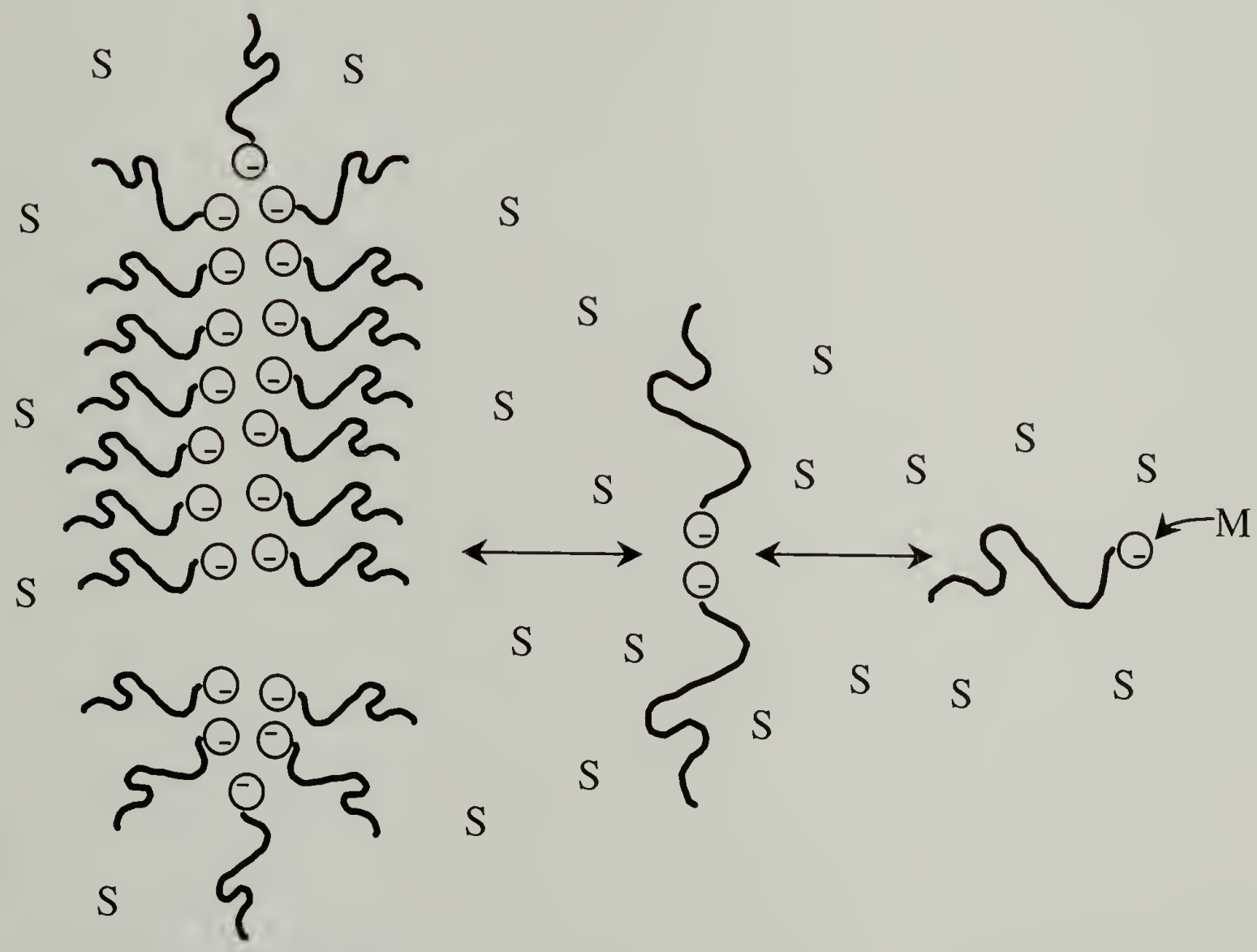

Figure 2.3 Schematic of Equilibrium Structures Proposed by Fetters et al.[3]

Figure 2.4 Reaction of Living Chain End with Water.[4]

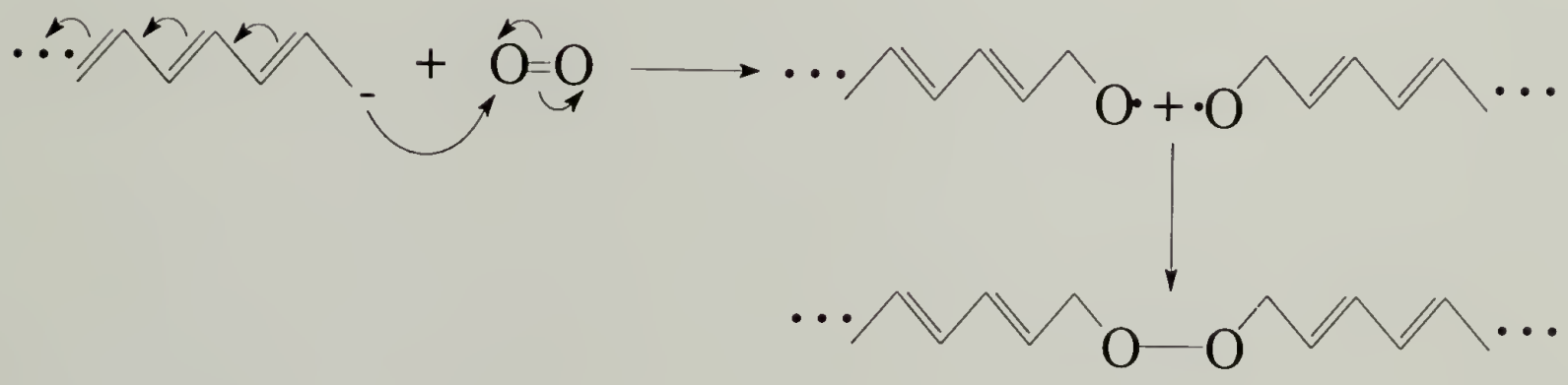

Figure 2.5 Reaction of Living Chain End with Oxygen.[4]

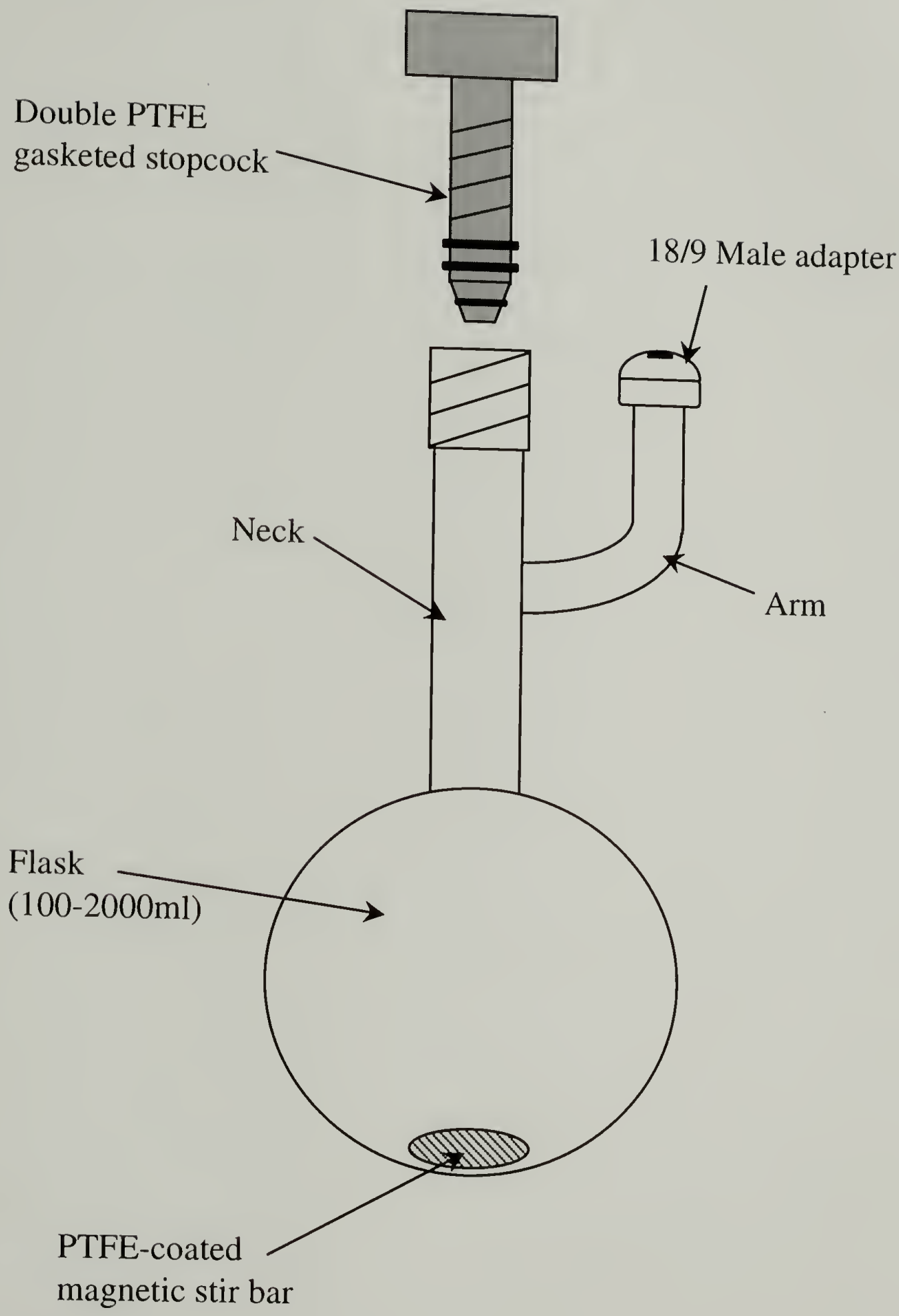

Figure 2.6 Drawing of Modified Schlenk-type Reaction Flask.

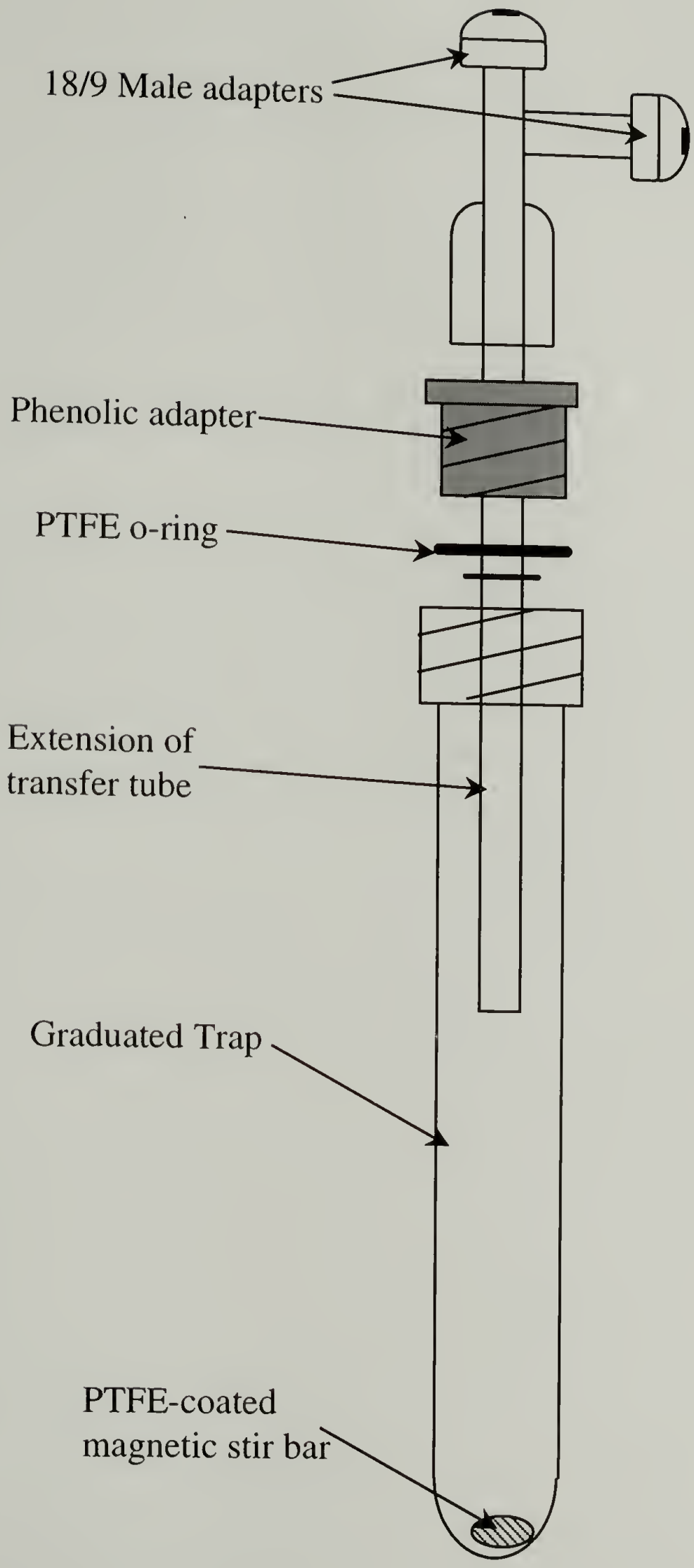

Figure 2.7 Drawing of Graduated Trap for Preparing Butadiene.

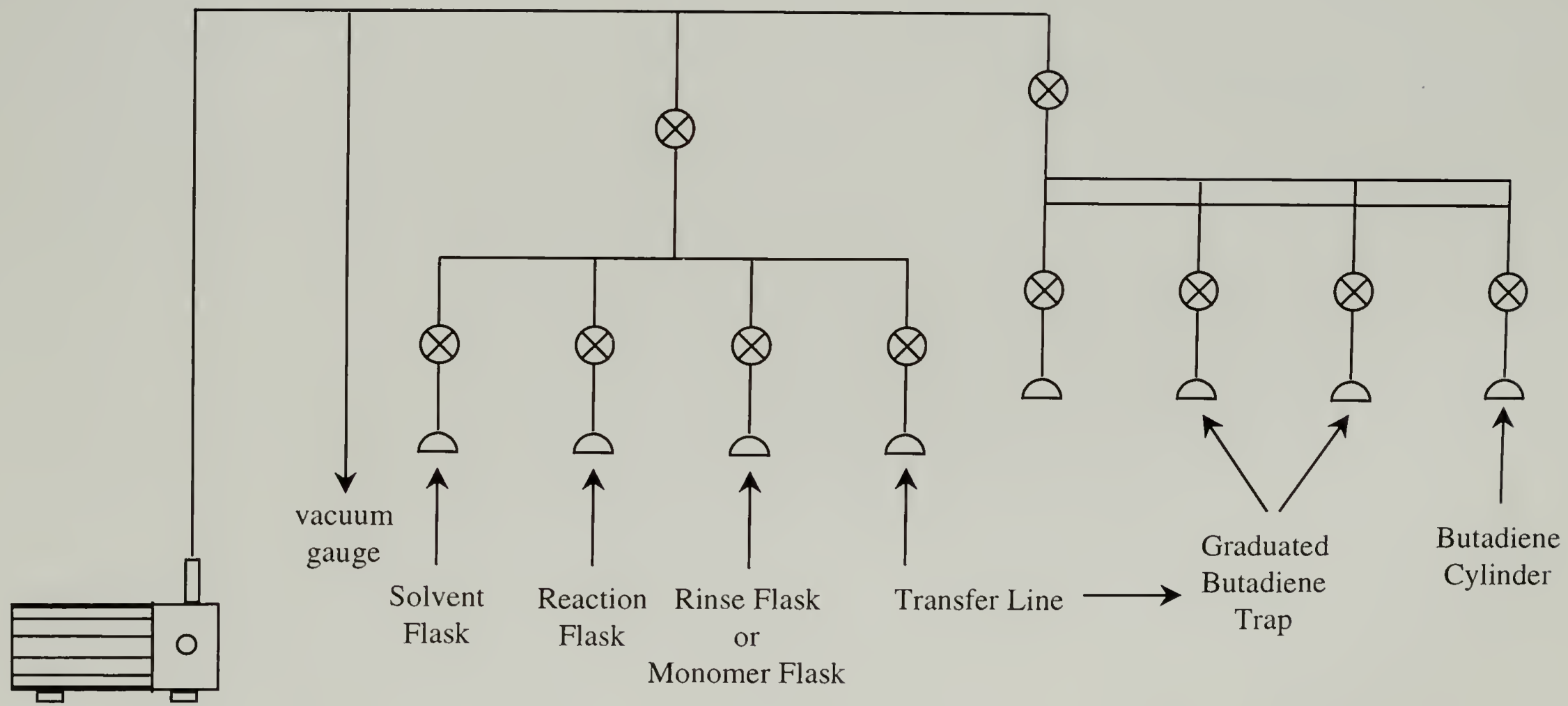

Figure 2.8 Drawing of Vacuum Manifold Set-up for Living Anionic Synthesis.

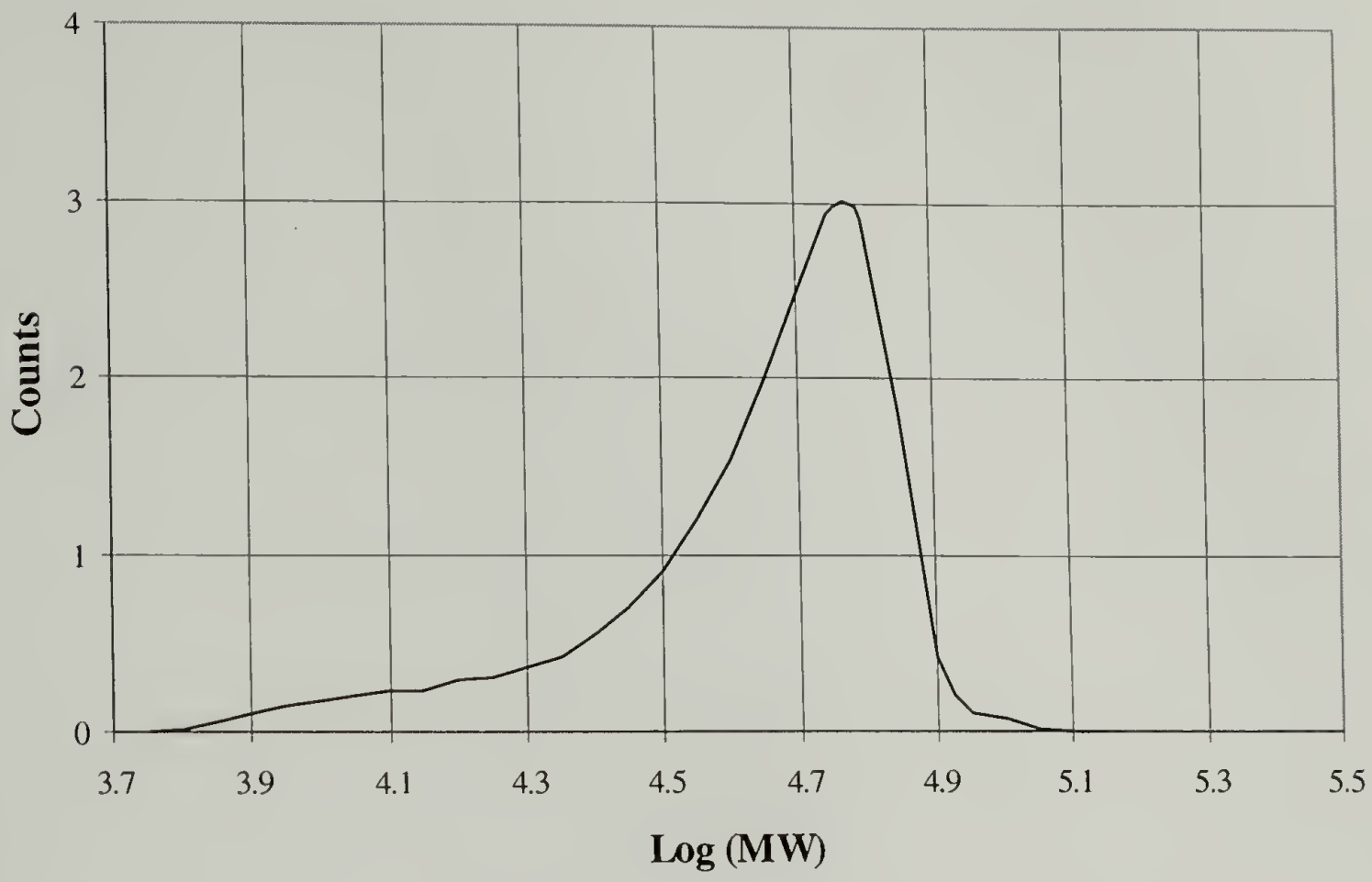

Figure 2.9 GPC Chromatogram of a PDMBD.

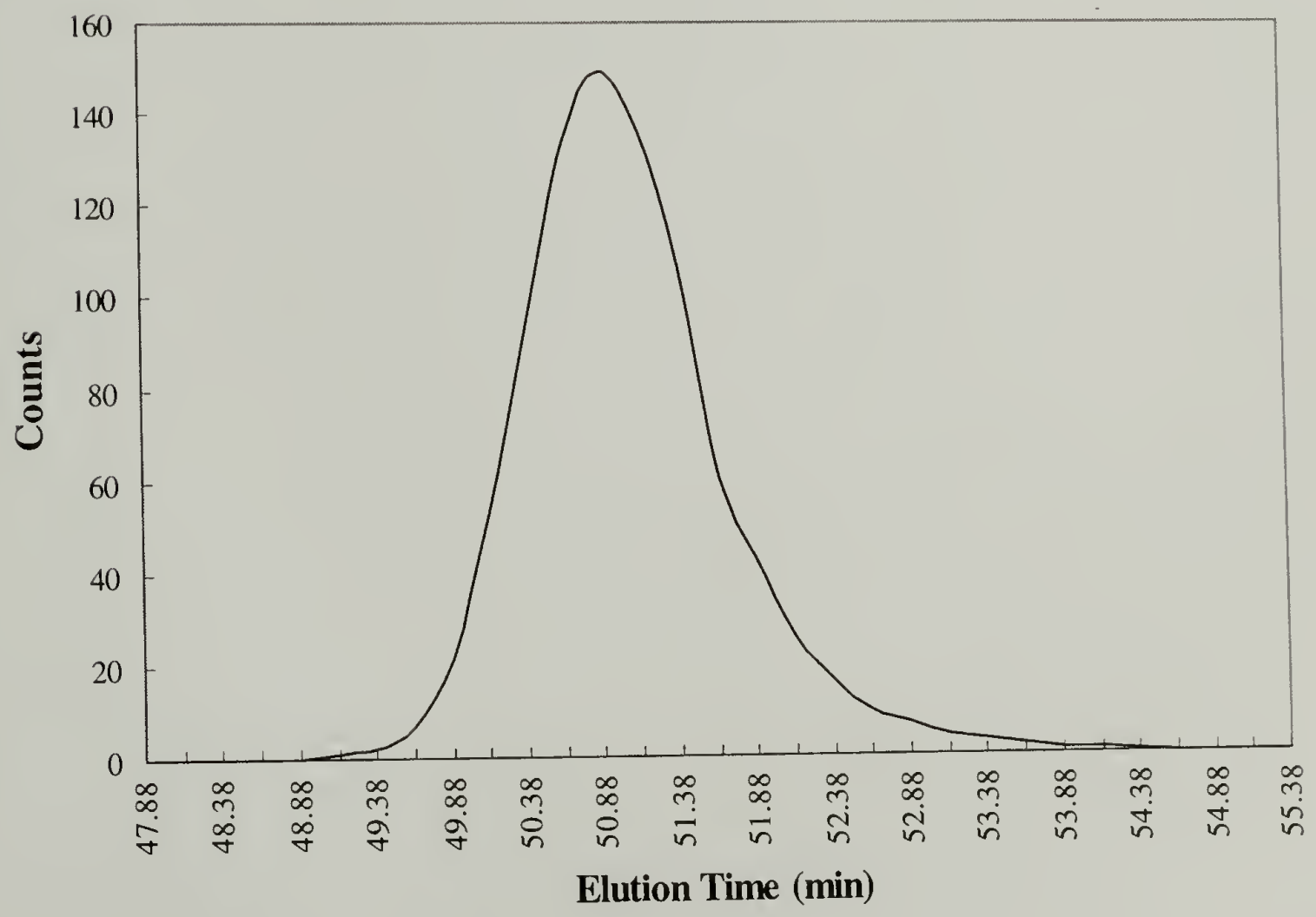

Figure 2.10 GPC Chromatogram EtO-Terminated PMPD.

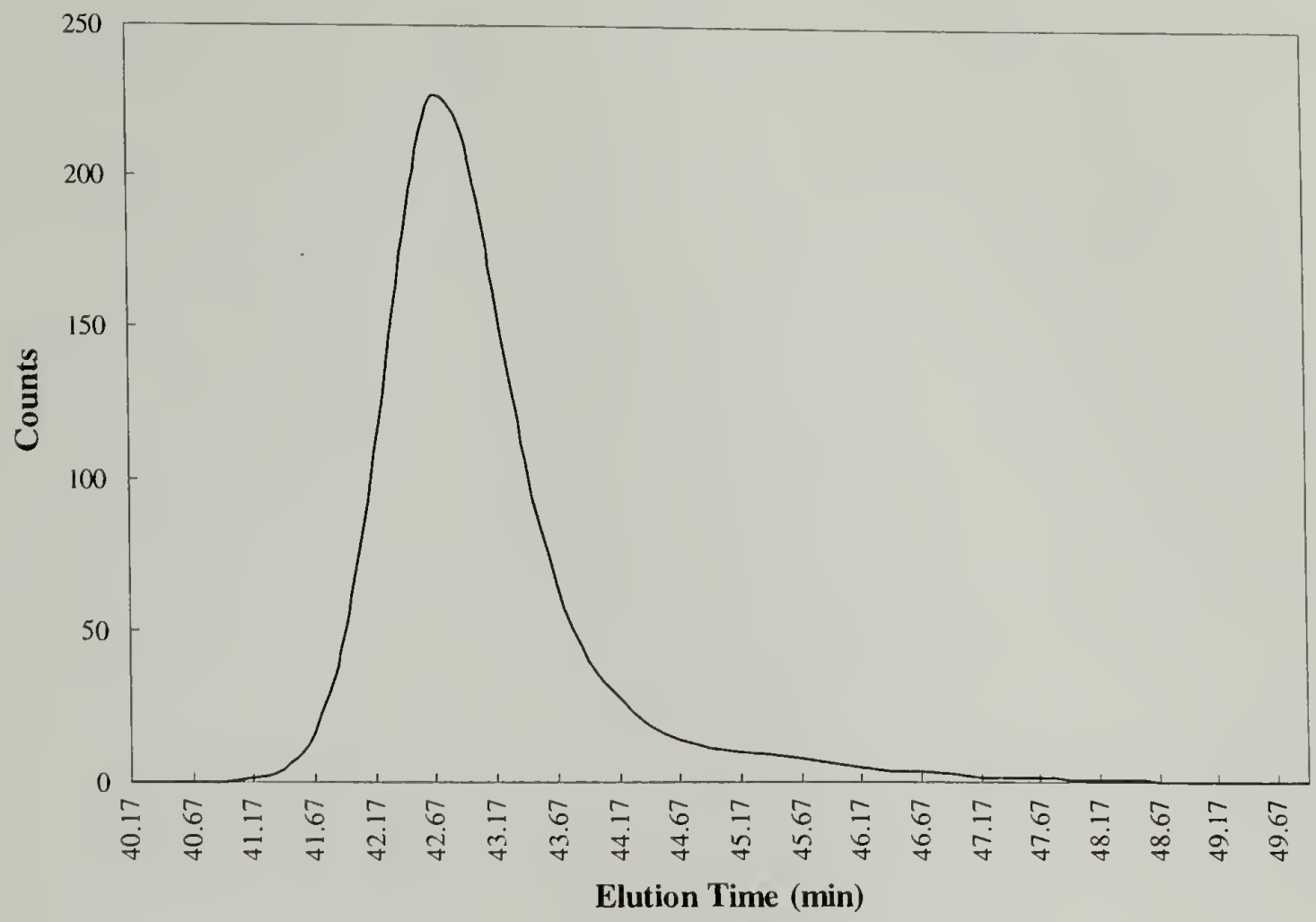

Figure 2.11 GPC Chromatogram of DEP100.

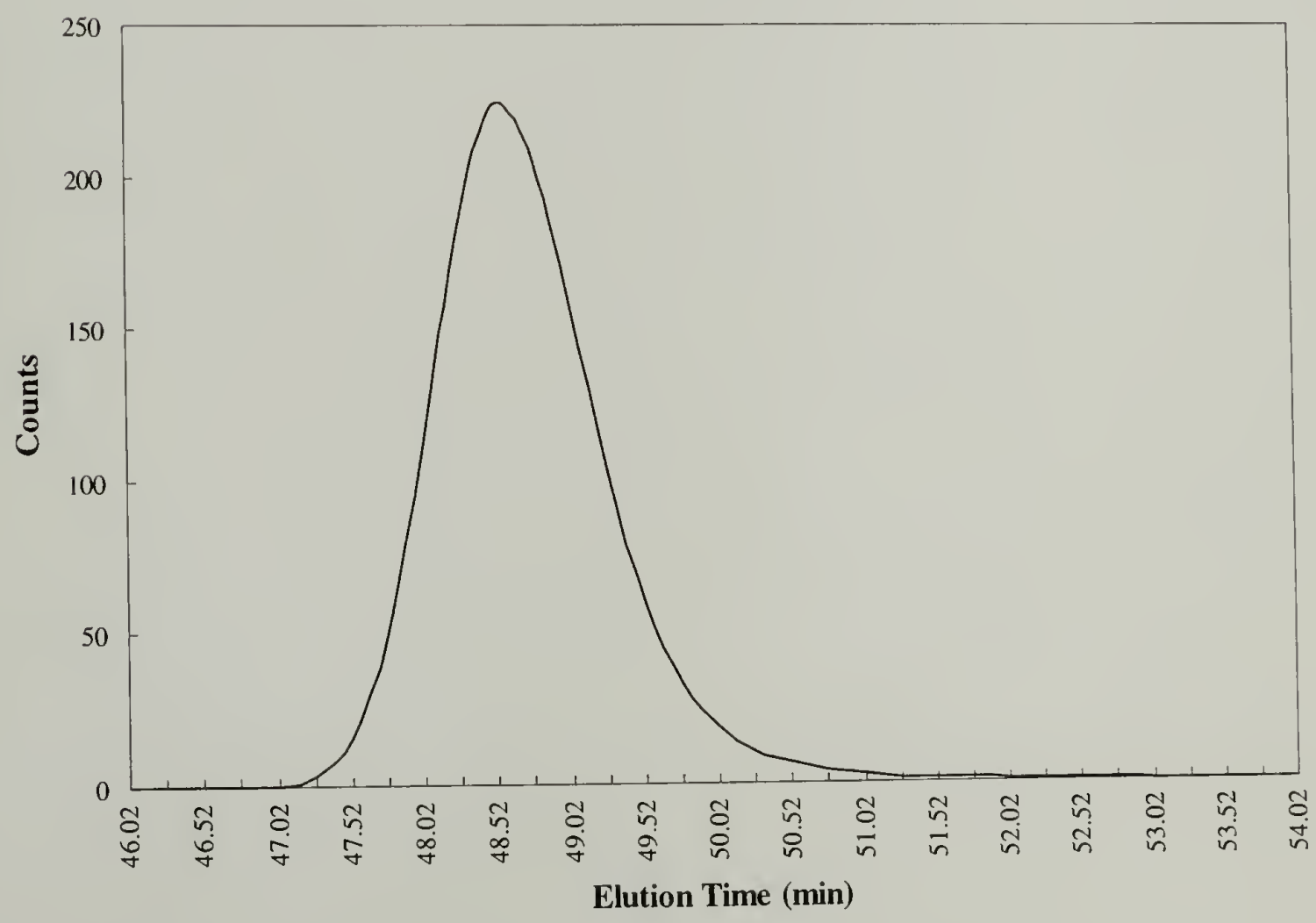

Figure 2.12 GPC Chromatogram of PE20.

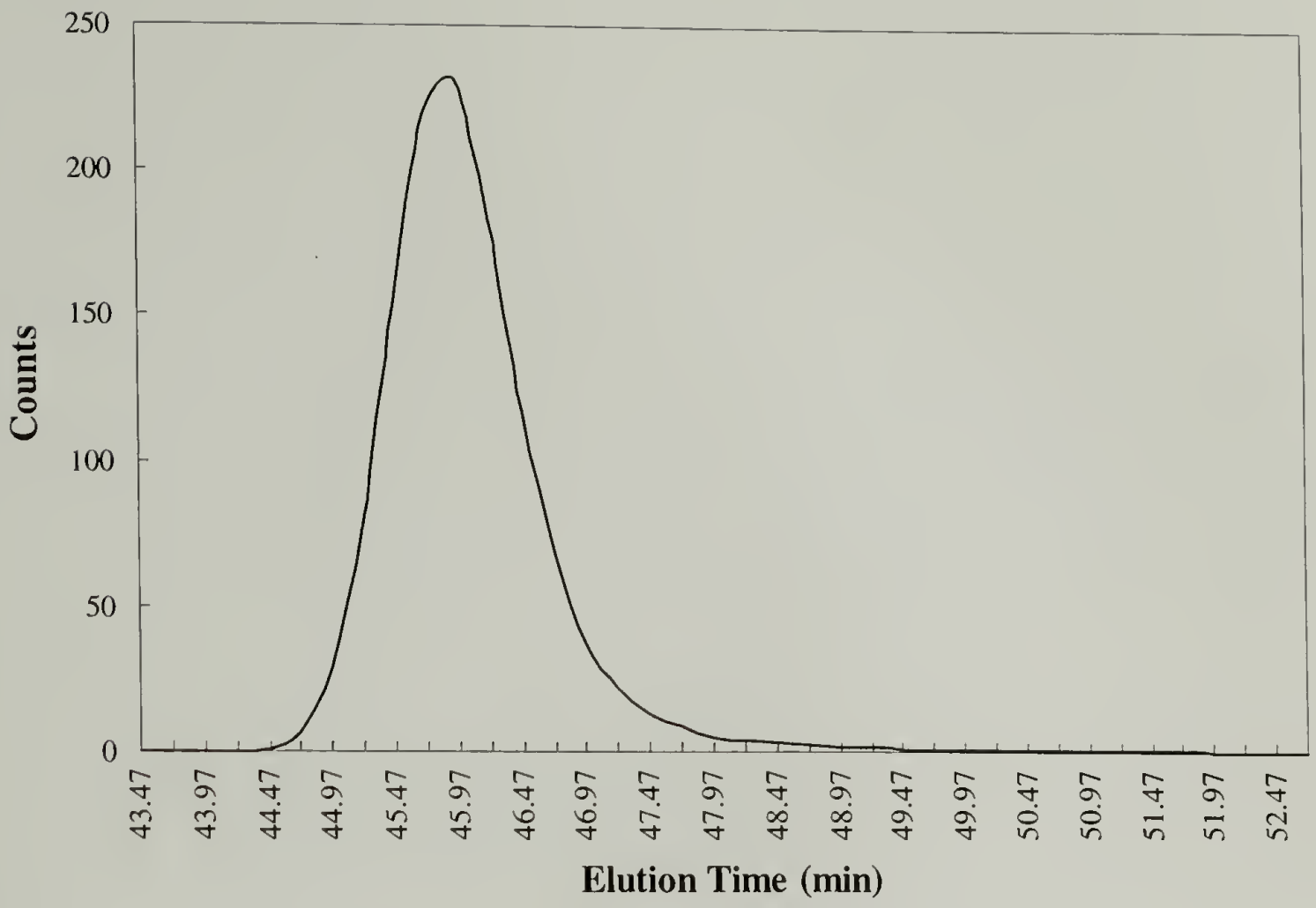

Figure 2.13 GPC Chromatogram of PE47.

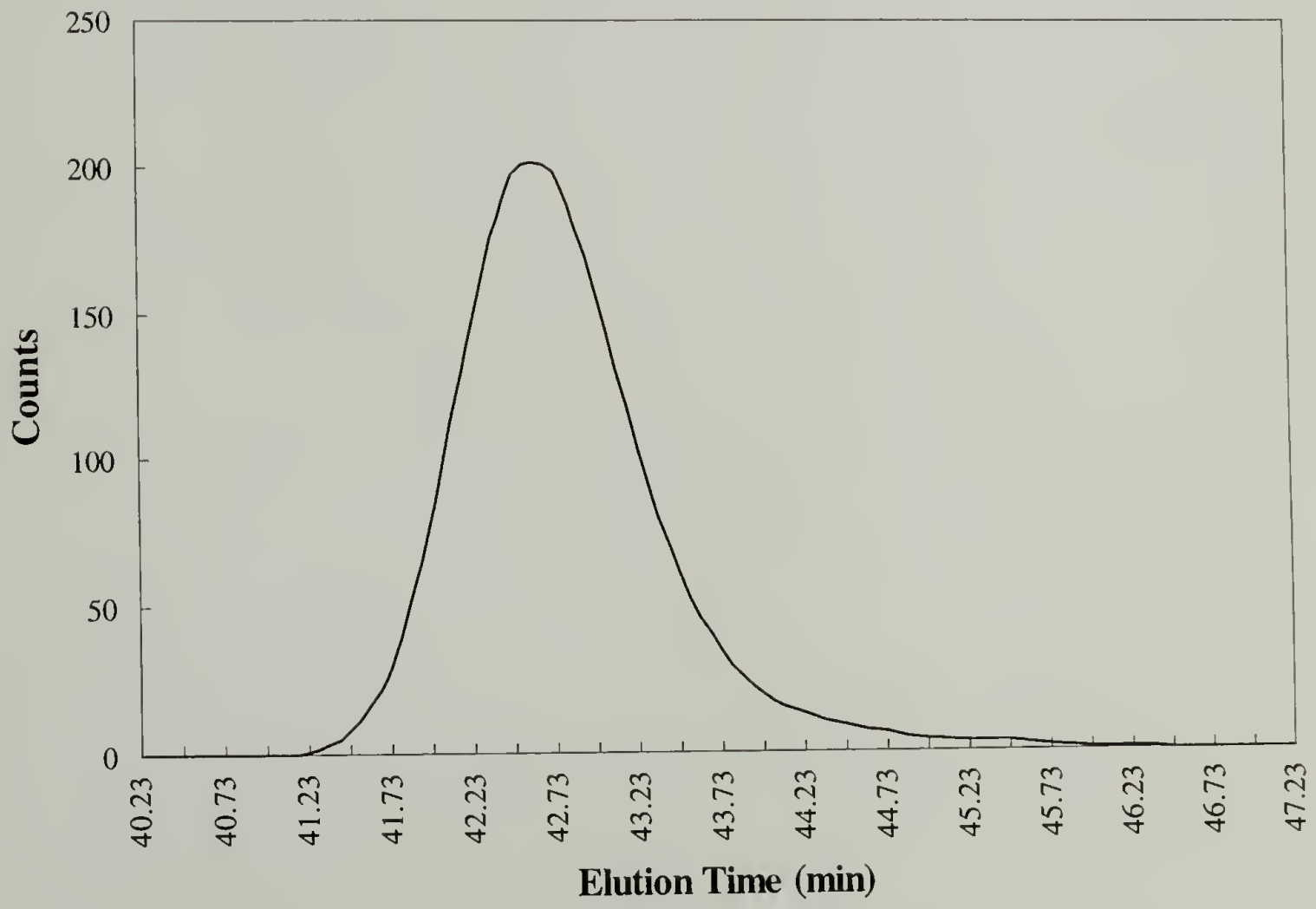

Figure 2.14 GPC Chromatogram of PE107.

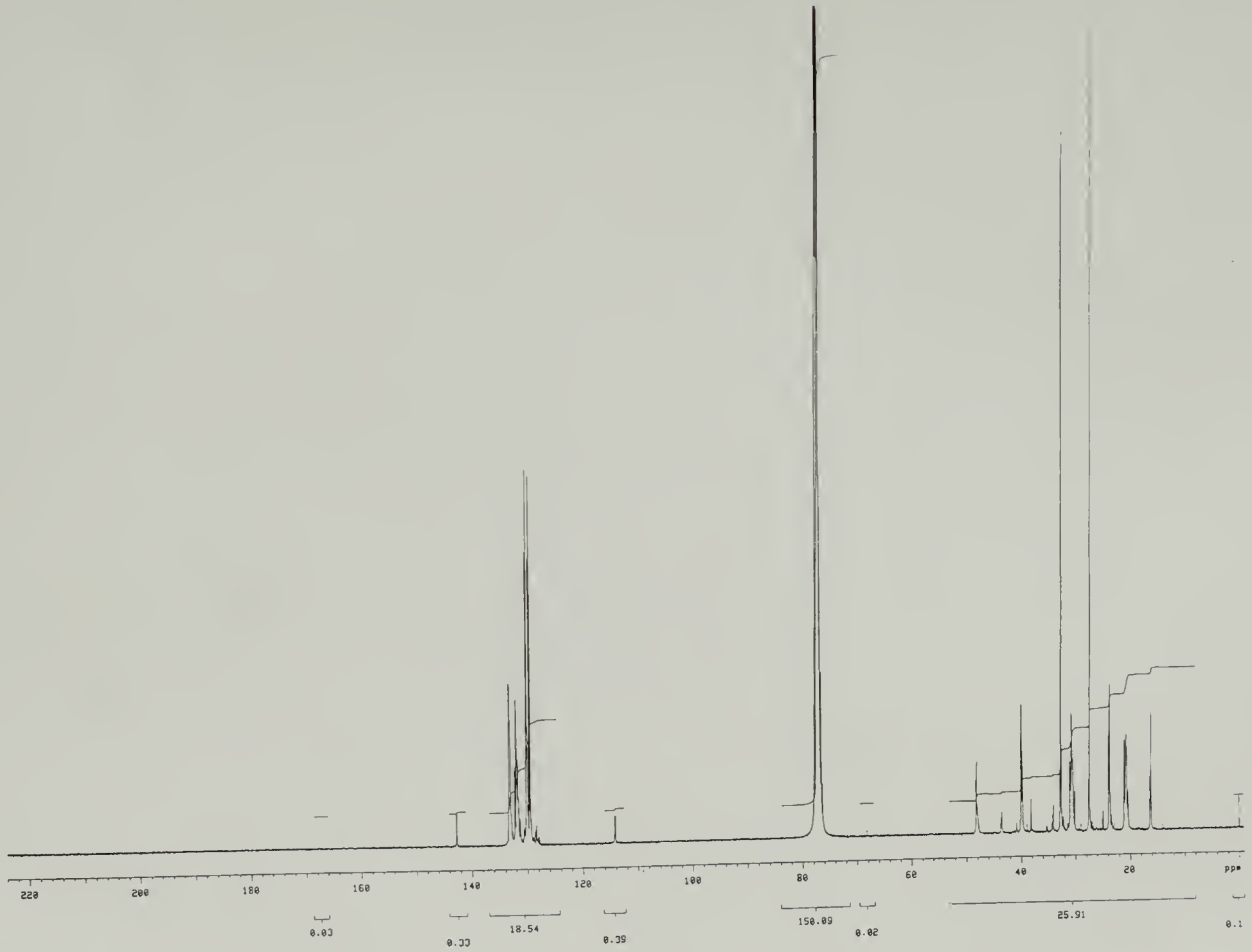

Figure 2.15 ^{13}C NMR Spectrum of DEP100.

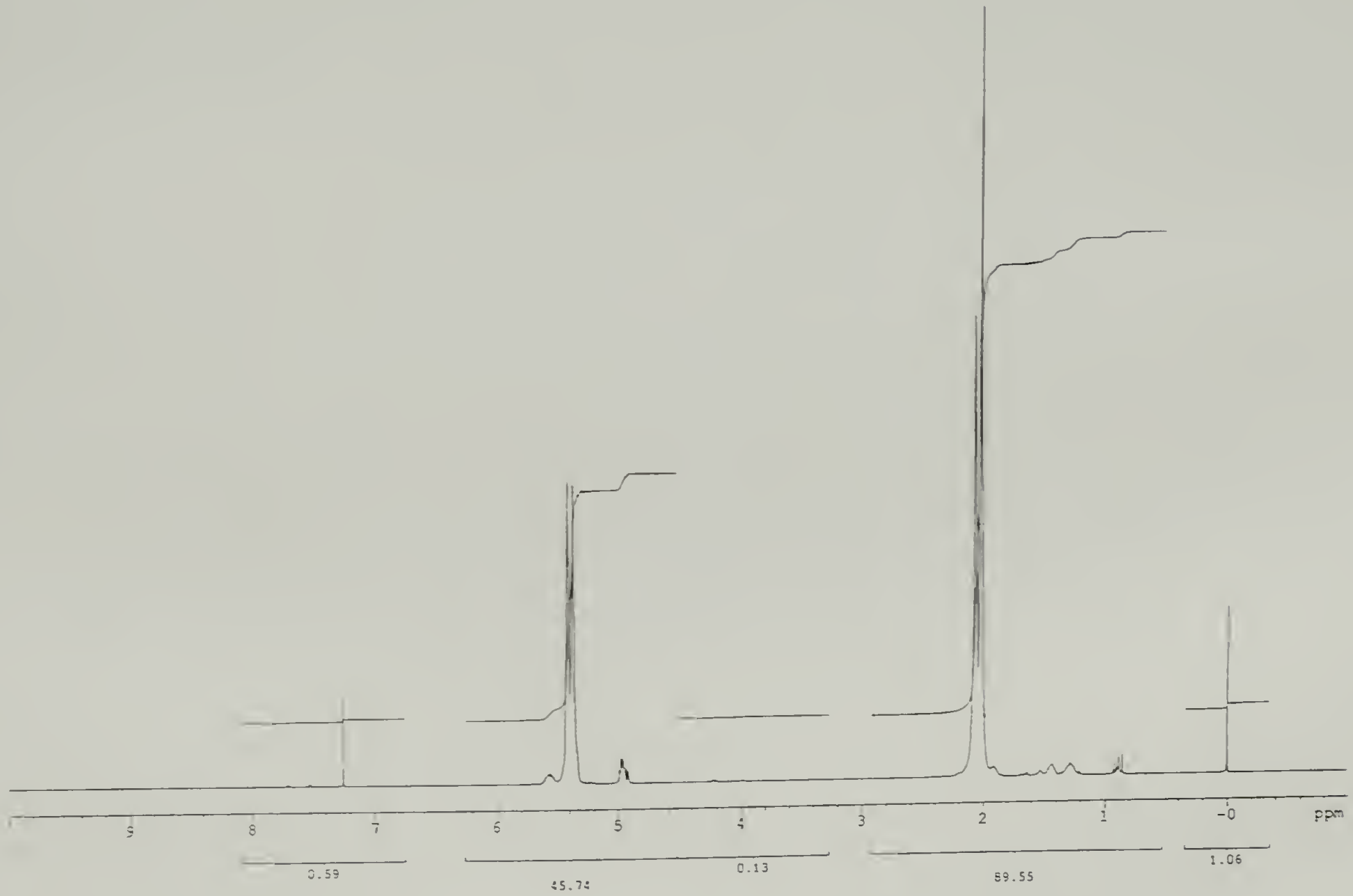

Figure 2.16 ^{1}H NMR Spectrum of PE20.

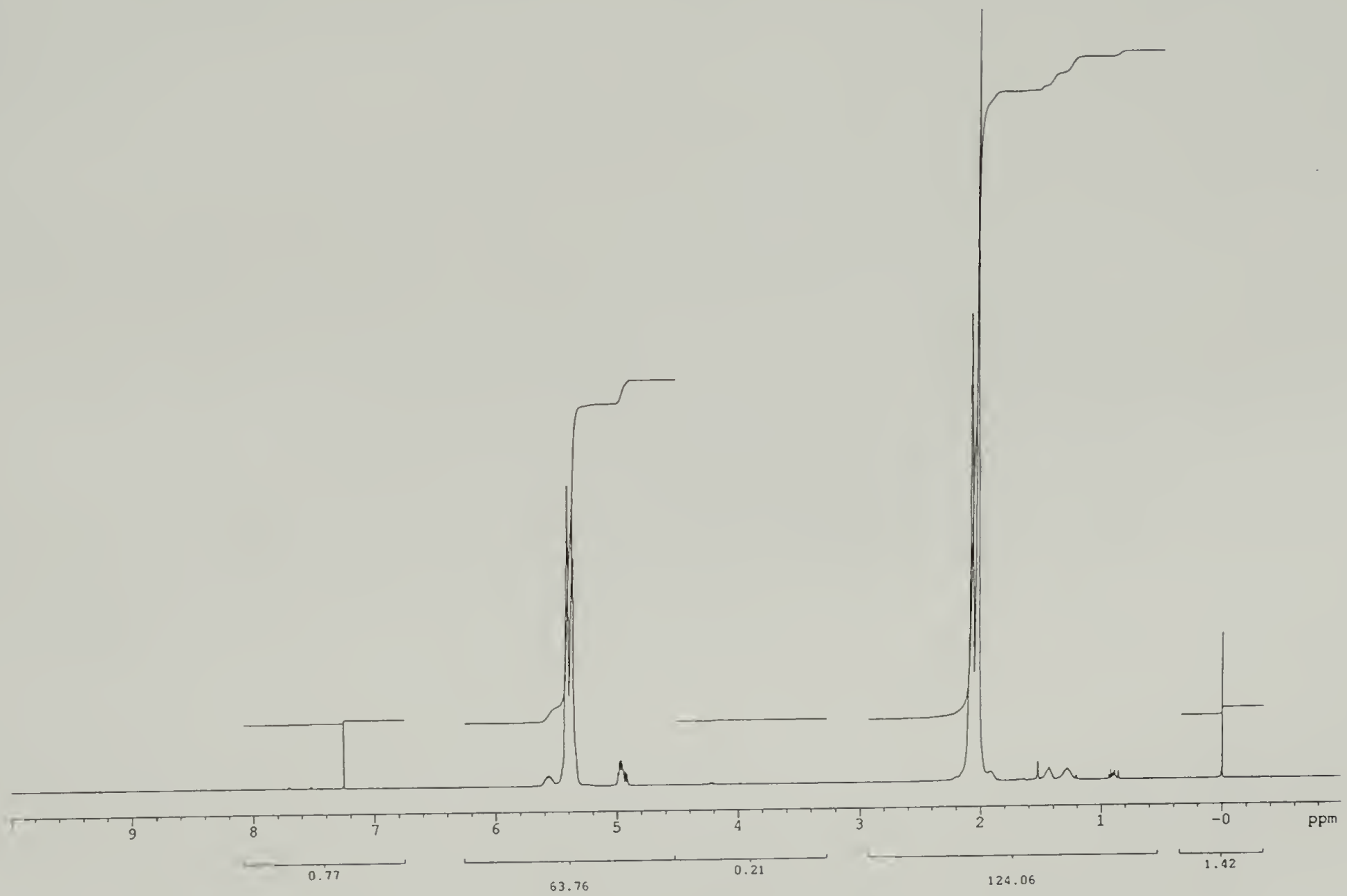

Figure 2.17 ^{1}H NMR Spectrum of PE47.

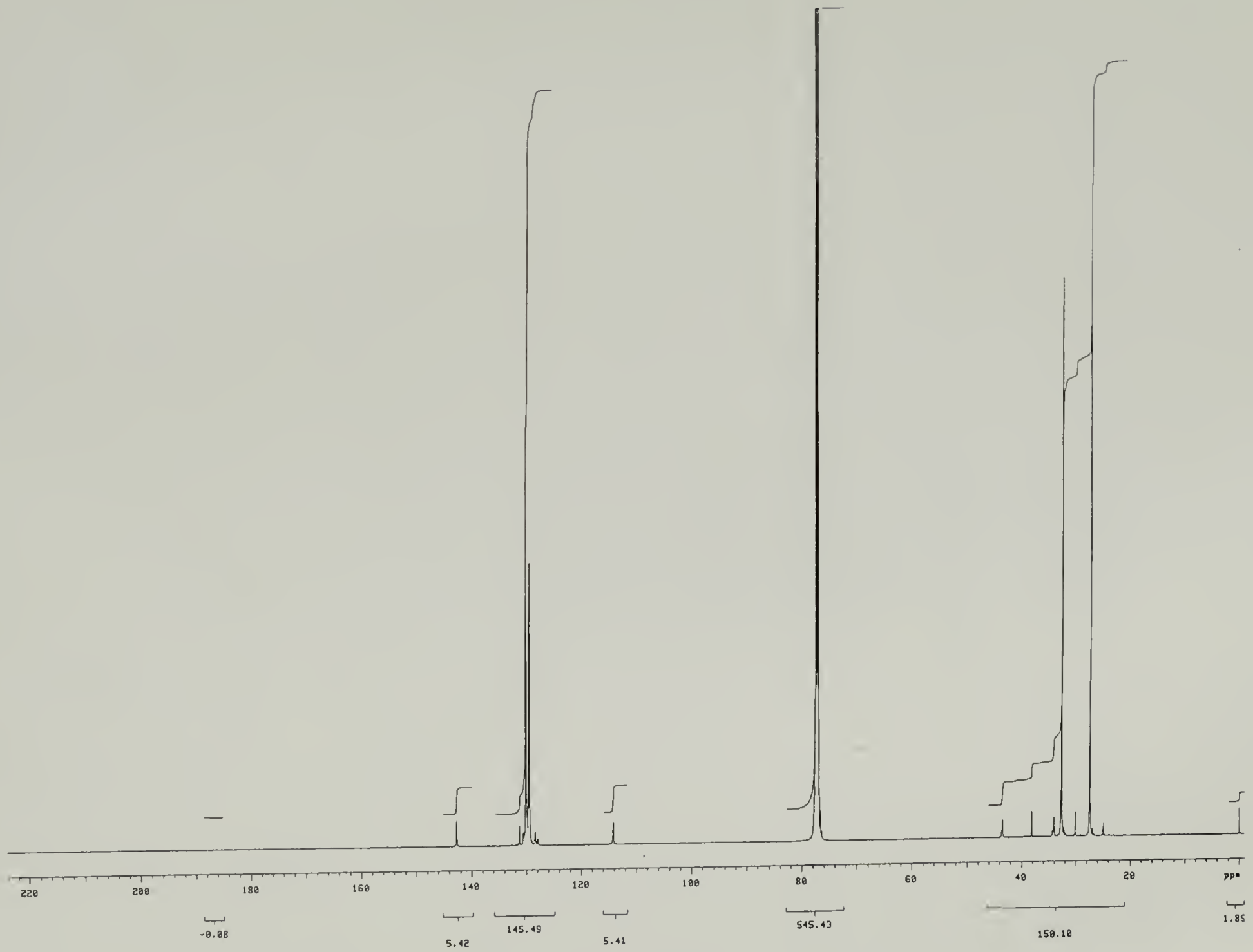

Figure 2.18 ^{13}C NMR Spectrum of PE107.

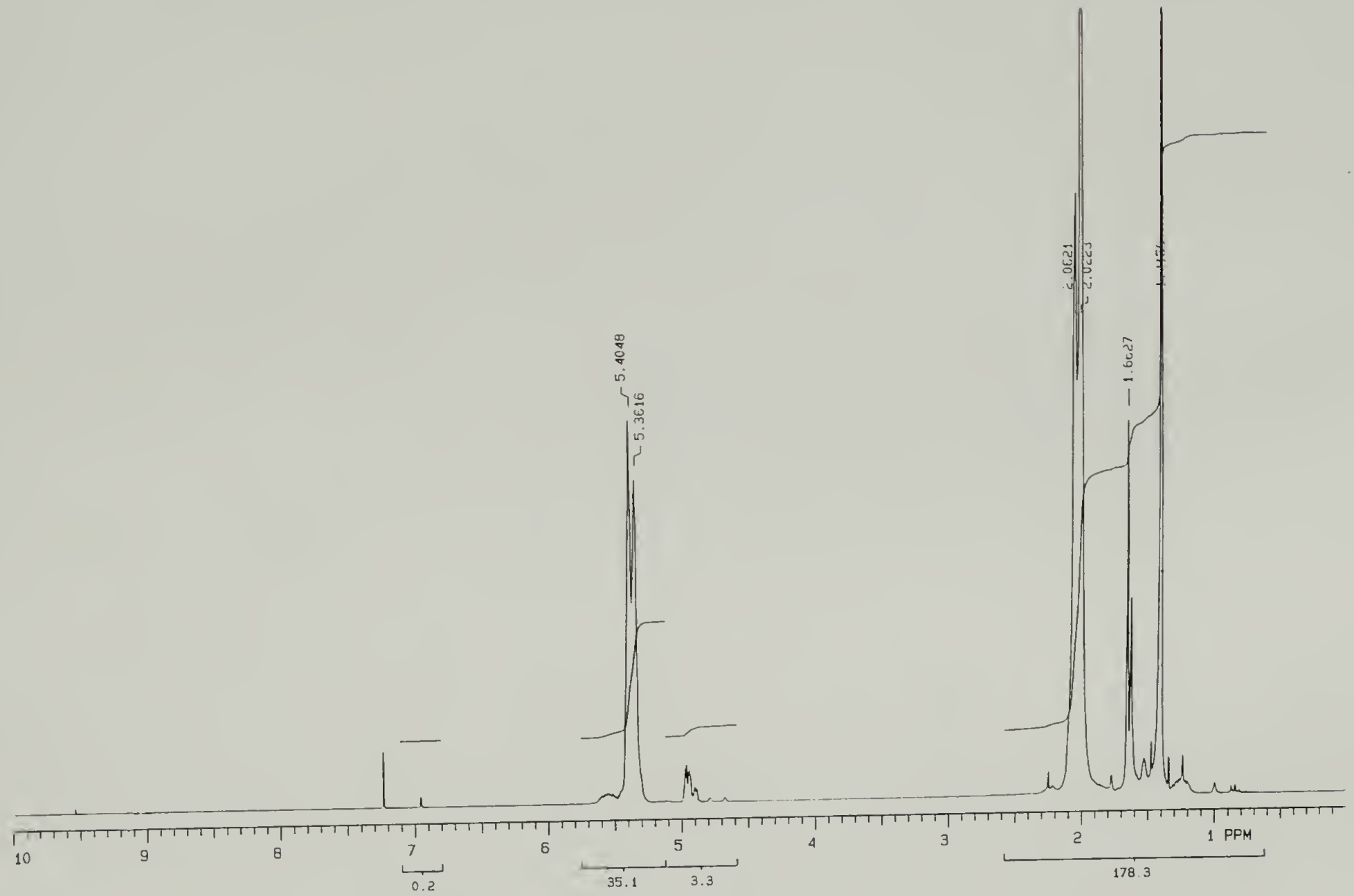

Figure 2.19 ^{1}H NMR Spectrum of a PBD-PDMBD.

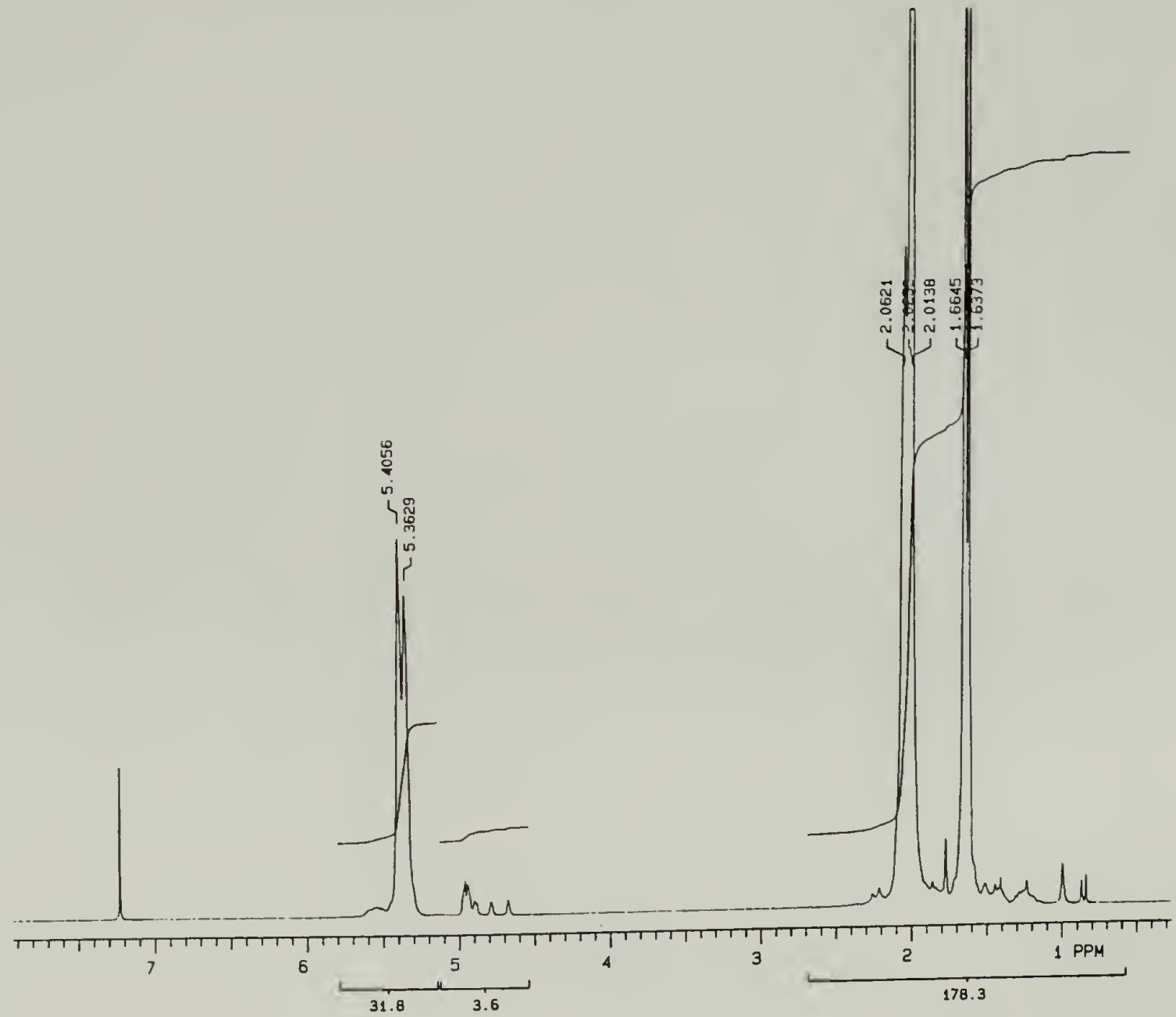

Figure 2.20 ^{1}H NMR Spectrum of a PBD-PDMBD.

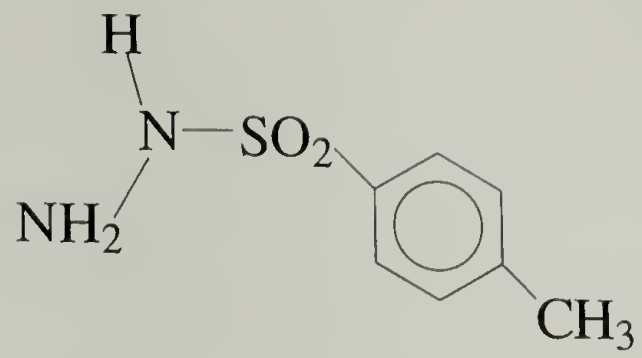

Figure 2.21 Diimide Hydrogenation Catalyst (*p*-Toluene Sulfonyl Hydrazide) Which Was Shown to Cause Fragmentation in PBD Chains.[21]

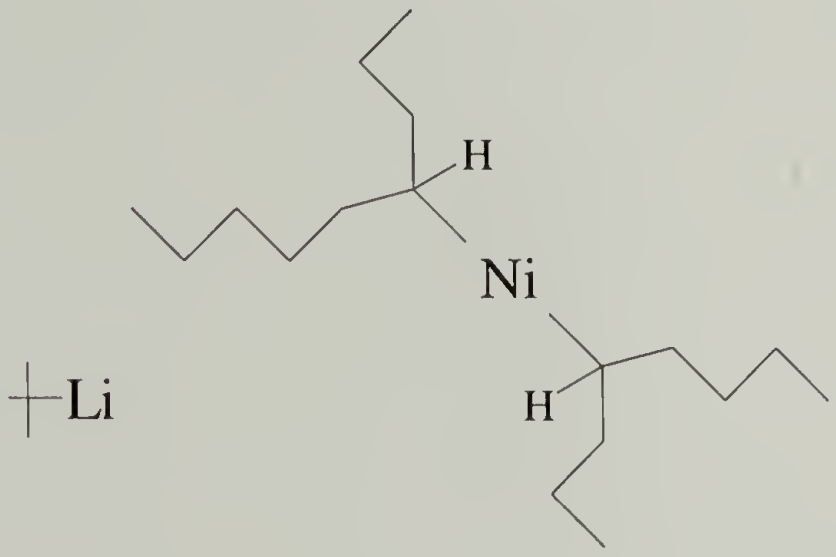

Figure 2.22 Homogeneous Hydrogenation Catalyst (*t*-BuLi/Nickel(II) 2-Ethyl Hexanoate)Which Was Shown to Saturate Incompletely and Bind to PBD Chains.[21]

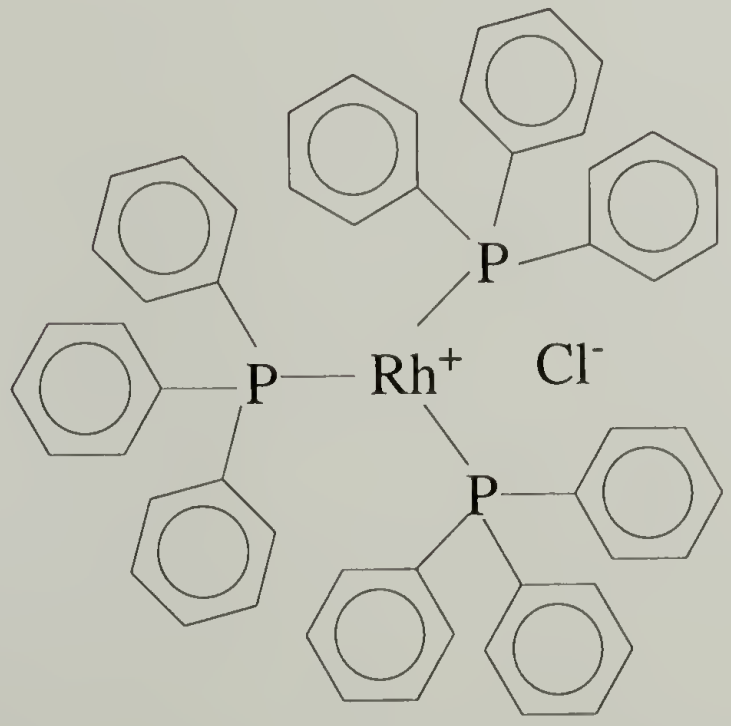

Figure 2.23 Wilkinson's Catalyst (chlorotri(triphenylphosphine)rhodium(I)).

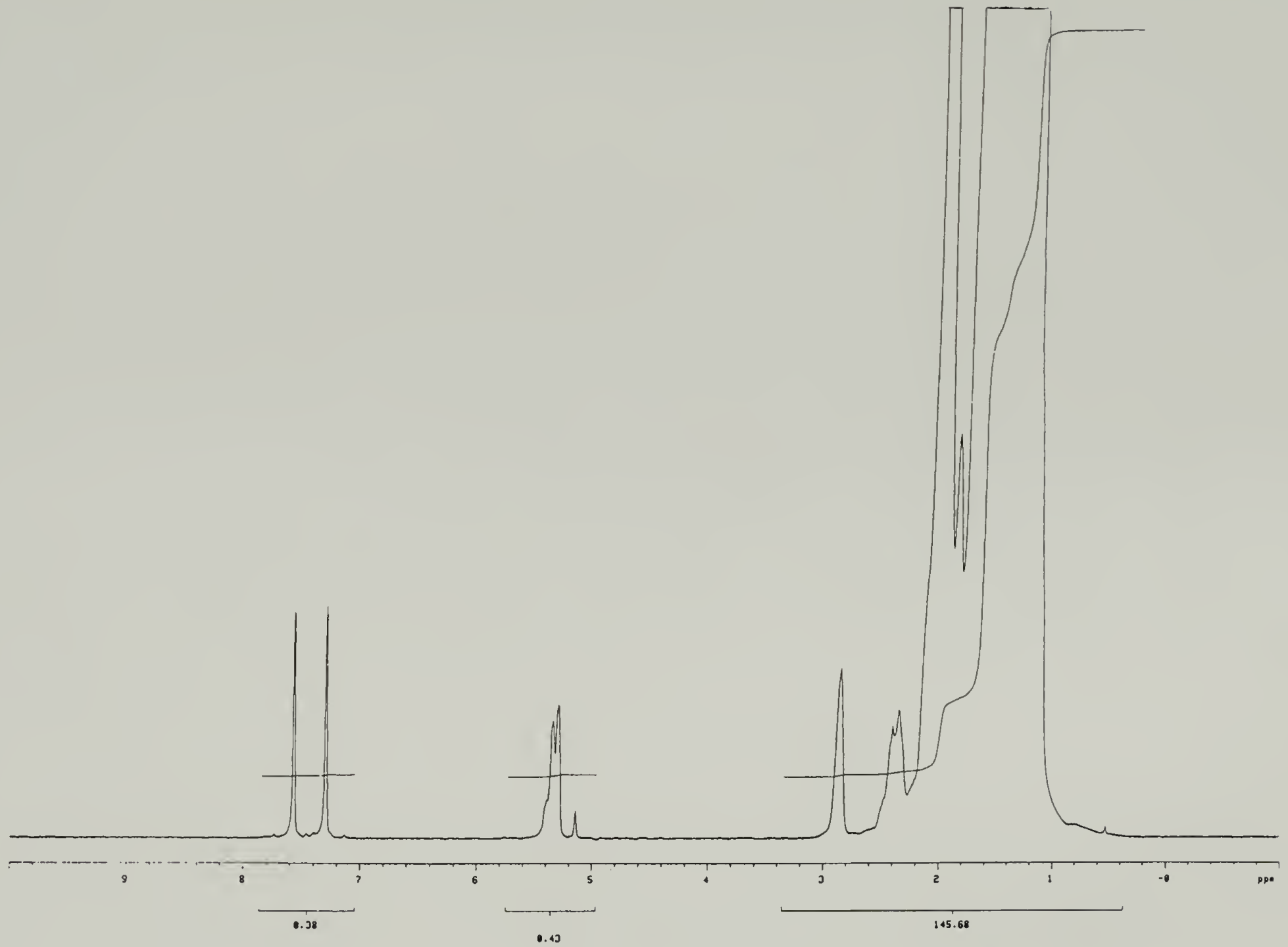

Figure 2.24 ^{1}H NMR Spectrum of DEP100 Showing Residual Unsaturation.

CHAPTER 3

BLENDING

3.1 Introduction

The majority of polymeric materials in everyday life are mixtures of different polymers, additives, etc. Knowledge of the behavior of a blend over a wide range of compositions (and produced by various methods) is important in understanding for which applications that blend may be useful and increases our knowledge of phase behavior and interfacial science.

In this work, two methods of mixing were used to make polymer blends: physical mixing and solution blending. Physical mixing is described first. This technique was only used for comparative purposes by DSC and so the description is brief. A table of blends made by this method is included.

Solution blending is described next. Solution blending is an excellent method to cause mixing of unlike species with similar solubilities to occur on the molecular level, which is why it was the primary method used for making the blends used for this study. Two solution blending techniques were utilized in this research: "stand" casting and "water" casting. All homopolymers and the diblock copolymer were solution cast using the same conditions as the blends for consistency. The techniques are outlined and schematics of the processes are shown.

The results of the blending work are discussed in the following section. This section includes a table on the polymer blends and discusses the advantages and

drawbacks of each. Also, a summary is given concerning the blending work which was performed with comments on any unusual events that occurred during blending.

3.2 Physical Mixing

A series of blends—more appropriately called mixtures—were prepared by physical mixing. This entailed weighing the individual components on a Mettler (Model AE 163) electronic balance, cutting them into small pieces with a razor blade, and mixing the components together with a spatula. After the co-mingling of the components was complete, the sample was reweighed, placed in a DSC pan, and crimped. This method was used for DSC only, as a means for comparing the effectiveness of mixing with the solution-prepared blends. (see Chapter 4 on DSC for more details.)

3.3 Solution Blending

Solution blends were prepared by two routes. The first technique to be explained will be termed "water casting", since it involved driving off the solvent with hot water, while the second will be called "stand casting", since the polymer solution was allowed to stand untouched while the solvent evaporates out of the blend. The former technique was utilized by K. Sakurai for making blends of ethylene-propylene diblock copolymers (DEPs) with atactic-polypropylene (APP).[1] The latter method is used for making diblock copolymer blends of amorphous components.

Both methods involved first cleaning glassware (30ml beakers) and teflon coated stir bars repeatedly with distilled water and rinsing with acetone. Everything was dried overnight in a drying oven at 80°C. Then the beakers and stir bars were cleaned with

boiling toluene for at least 30 minutes. The toluene was drained and the glassware dried overnight in a vacuum oven at 80°C. The following day the heat to the oven was turned off, and the contents of the oven were cooled in the oven via a nitrogen stream using house nitrogen which was attached to the gas outlet on top of the oven.

3.3.1 Water Casting

For the water casting technique, samples were weighed out on an American Scientific Laboratories (Model B1240-3) electronic balance. While the polymers were being weighed, toluene was preheated to 70°C on a Tekmar (Model RCT-S21) hotplate. Polymers were added individually to the solvent to make up a 5% (w/v) solution, and the temperature of the solution was raised to 85-90°C. Solutions were stirred for a minimum of thirty minutes, or fifteen minutes after all signs of undissolved polymer were gone, whichever took longer. A lack of adsorbed polymer on the walls of the beaker when tipped and no polymer particles floating in the solution were used as indications that the polymers were dissolved. Small amounts of fresh toluene were added during the course of the dissolution to maintain the toluene at a constant level. Meanwhile, a larger beaker of distilled, deionized water was heated to 90-95°C on a separate hotplate. When the water was at temperature, a few drops of the solution were added to the surface of the water. After the solvent had completely evaporated from the blend (usually 5 minutes), the process of adding a few drops of polymer solution was repeated until the solution in the 30ml beaker had been exhausted. Once all of the cast film had been collected, the blend was annealed at 150°C for 5 days in a vacuum oven. At the end of this period of

time, the blends were removed from the oven and quenched in liquid nitrogen to preserve the melt morphology.

The water casting route was used only for DSC since it would give results which were directly comparable with those of b-PE-APP/h-APP, but the morphology was anticipated to be quite disturbed and be of too low contrast for electron microscopy. The stand casting technique was used for morphological analysis as well as for thermal analysis as it was expected at the time that this route would result in blends possessing microdomains with a higher degree of long range order than if the blends were made by the water casting route. The schematic of the water casting technique is shown in Figure 3-1.

3.3.2 Stand Casting

The starting portion of the stand casting technique was the same as that for water casting. Polymer components were weighed out on an electronic balance as the toluene was preheated on a hotplate to 85-90°C. The polymers were cut into small pieces with a razor blade and mixed together before adding to the hot toluene. Small amounts of fresh toluene were added during the course of the dissolution to keep the level of solvent constant.

Once it was decided that both components were fully in solution, the solution was taken off the hotplate and the stir bar removed. The degree of mixing was later confirmed by proton NMR of samples taken from the bottom and sides of a typical blend. The solution was allowed to sit under a slightly tipped beaker (200ml) or large crystallization dish (for more than one solution) until it appeared that all of the solvent had evaporated.

This typically took eight (8) days. A lack of change in the physical appearance of the film overnight was used as an indication of residual solvent content. The blends were then dried completely over two (2) days in a vacuum oven at room temperature with an applied vacuum. A schematic of this method is shown in Figure 3-2.

3.4 Results and Discussion

Table 3-1 lists the compositions for the mixtures and blends prepared by physical mixing and solution blending, respectively. Solution blending is typically found only on the laboratory scale to make polymer blends, since an industrial scale process would involve huge quantities of solvent in addition to the long times necessary to dissolve the components in order to form a homogenous mixture, which would be cost-prohibitive. Solution blending can, however, achieve a more homogeneous mixture than many physical processes. Extrusion and ball mills have been shown to generate nearly uniform homopolymer blends, but this is only when using high shear/mixing rates and/or small initial particle sizes.[2]

As was stated in the Introduction, the physical mixtures of the diblock copolymer with the various homopolymers were used as the extreme case of mixing of polymer components on the macroscopic size scale. This resulted in domains of sufficient size to give rise to two melting/crystallization peaks from each of the different crystallizable components, as can be seen from the sample plots of DSC heating and cooling curves in Figures 3-3 and 3-4, respectively. An example of a stand cast solution and of a water cast solution blend of the same composition are shown in Figure 3-5. Both of these heating curves only show one melting peak—indicative of mixing of the two components on the

length scale of individual chains. This comparison will be discussed in more detail in the next chapter on Thermal Analysis (Chapter 4).

The physical appearance of the solution blends were quite different, both from the standpoint of the technique used and the blend composition. For the water casting technique, all films had a "stringy" appearance, but those with higher levels of homopolymer were opaque and whiter than blends containing essentially all diblock. The stand cast blends followed a similar trend for opacity, but since they were allowed to quiescently cool in beakers, they had shapes that ranges from plugs to broken thick films or islands. The pure homopolymers which were cast from this technique were opaque, white, and fragile (so much so that they would fall apart at the slightest touch). A lack of change was noted in the physical appearance of the blend films before and after they were vacuum dried. None of the solution cast blends showed signs of degradation due to heating (i.e. yellowing); however, the blends with PE107 were grayish in color, possibly indicating the presence of some residual $Pd/BaSO_4$ hydrogenation catalyst. This situation would generally be assumed to be deleterious to the polymer chain—causing chain scission at elevated temperatures. The thermal analysis technique, TG, would be able to determine whether this was the case. As will be described later, the degradation behavior of PE107 was observed to be similar as PE20 and PE47, ruling out the possibility of residual catalyst in PE107.

In order to determine the homogeneity of the stand cast solution blends, samples were taken from the sides and the bottom of a beaker containing a typical solution blend (50wt% DEP100/50wt% PE20) after the solvent had been driven off. These samples were dissolved in *d*-ODCB and checked for overall composition by proton NMR (see

Figure 3-6). As can be seen in Table 3-2, the compositions were within 4 wt% of each other, confirming the ability of the stand casting method for producing blends of fairly homogeneous composition.

The rationale for casting the diblock copolymer solutions on hot water was that the hot water would reduce the amount of polymer demixing by both evaporating the solvent at a rapid rate and by suppressing the crystallization of the polyethylene block of copolymer into spherulites prior to melt-annealing. This technique worked very well for the blends which utilized the atactic polypropylene as the homopolymer; however, it was not known whether this route could sufficiently to suppress the additional driving force to crystallize into spherulites when using polyethylene as the homopolymer. Formation of spherulites would especially be problematic if the blend was allowed to cool to room temperature between casting and melt-annealing. The morphology of the blends made in this fashion were quite disordered; and, therefore, orientation of the blends in the melt followed by more melt-annealing would be required to obtain ordered microdomains. For these reasons a change of solution blending methods was made—from the water casting technique to the stand casting technique.

As will be seen later in the chapter on thermal analysis, the stand casting technique yielded changes in the location of the crystallization peak for the blends of the diblock copolymer with the lowest and medium molecular weight polyethylenes, whereas the water casting technique showed only an initial change in the location of the crystallization peak and only for blends with the lowest molecular weight homopolymer upon changing from a pure diblock to a blend system.

An advantage of the stand casting technique in amorphous copolymers and their blends is the orientation of the minority phase parallel to the bottom of the beaker in which it cast. For this system, which includes a crystallizable component, it was found that the stand casting route allowed formation of spherulites due to the slow rate of evaporation of solvent and the low temperature (room temperature) at which the blend was kept for the duration of the process. The spherulites, which can grow to the size of microns in the neat diblock, have been shown to destroy the microdomain structure which was present in the melt.[1] For these blends, the extent of disruption was such that even five days at 150°C in a vacuum oven was insufficient to produce well-ordered morphologies as imaged by TEM.

Therefore an additional step of orientation of the blends in the melt was attempted. The orientation was followed by melt-annealing at 150°C for 5 days in a vacuum oven to increase the long range order in the blends. The orientation was performed using a Carver Model C hydraulic press with heated upper and lower platens and an attached homemade vacuum chamber. The temperature stability of the platens was roughly ±5°C. The stand cast blends were oriented using a PTFE channel die, the details of which may be found elsewhere.[1] A schematic of the orientation process in Figure 3-7. Each blend was loaded into the channel so that the sections laid in the same orientation as they were in the bottom of the beaker. Side sections were placed in the channel of the die in an orientation perpendicular to the way that they were situated in the beaker and were interspersed with the bottom sections in the die. Blends and neat (co-)polymers were allowed to melt and then were compressed to between 1/4 and 1/6 of their original height. The force was removed and the vacuum applied to the environmental

chamber for 15-30 minutes to remove bubbles from the oriented blend. At the end of this time, the vacuum was released, and the sample and die removed from the chamber. The set-up was quenched in liquid nitrogen for several minutes. During the time that the die was in the liquid nitrogen, the insert was first removed from the die and then the oriented blend was removed (to promote more rapid cooling than if the polymer thick film was left in the PTFE die).

In order to expedite melt-annealing of the many blends which were oriented, a "melt-annealing plate" was designed and machined using 6061 aluminum. The annealing plate was made to fit in a standard vacuum oven and contained a series of wells whose dimensions matched those of the PTFE die. Aluminum was used for its high heat conductivity, which would find use when the blends were rapidly cooled with liquid nitrogen. A diagram of this fixture is included in Figure 3-7. The annealing cycle was the same as was used for as-cast blends (under vacuum for 5 days at 150°C). This procedure proved successful as is illustrated by the TEM images in Chapter 5. There was a small amount of discoloration in the blends when they were removed from the vacuum oven. This was most likely due to a seal leak which was exacerbated by a low liquid nitrogen level between the fourth and fifth days of the melt-annealing cycle.

3.5 Summary

A series of physical mixtures and solution blends were prepared. A table of the blend compositions is shown in Table 3-1. The physical mixtures and water-cast solution blends were made without difficulty. Although the solution blends produced using the stand-casting technique proved to be fairly uniform by proton NMR taken from different sections of a typical blend (see Table 3-4 and Figure 3-6), morphological images of as-cast thick films were poorly formed due to the formation of spherulites. From previous evidence[1] it was determined that the creation of spherulites disturbed the microdomain structure to such a degree that long times in the melt alone were insufficient to return the blends to the well-ordered state. Orientation of the stand-cast films in the melt while under vacuum was used to induce order into the blends along which microdomains were formed after melt-annealing for several days, and in doing so was successful in returning the blends to the expected microstructure state (see Chapter 5).

3.6 References

1. Sakurai, K.; MacKnight, W. J.; Lohse, D. J.; Schulz, D. N.; Sissano, J. A.; Lin, J.-S.; Agamalyan, M. *Polymer* **1996**, *37*, 4443.

2. Matthews, G. Polymer Mixing Technology, Applied Science Publishers, Ltd.: Essex, UK; 1982.

Table 3.1 Table of Blends Prepared by Physical and Solution Blending.

Blend Compositions					
DEP100	PE20	DEP100	PE47	DEP100	PE107
Pure DEP100		90	10	90	10
90	10	75	25	75	25
80	20	50	50	50	50
75	25	25	75	25	75
70	30	10	90	10	90
60	40	Pure PE47		Pure PE107	
50	50				
40	60				
30	70				
25	75				
20	80	*All numbers are in weight percent.			
10	90				
Pure PE20					

Note: Water Cast solution blends were prepared using DEP113 and PE25, PE45, and PE99, whereas Stand Cast and Physical blends were prepared using the polymers listed in the above table.

Table 3.2 ^{1}H NMR Comparing Composition of Samples of a 50/50 (wt%) Stand Cast Solution Blend from the Bottom and Sides of the Beaker (DEP100/PE20)].

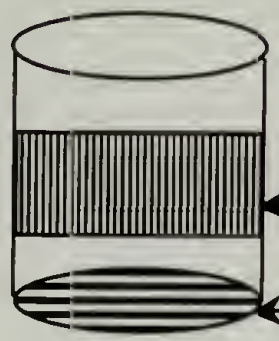

Location	Amount of b-APP	
	Mole %	Weight %
Sides	18.9	25.9
Bottom	15.4	21.4

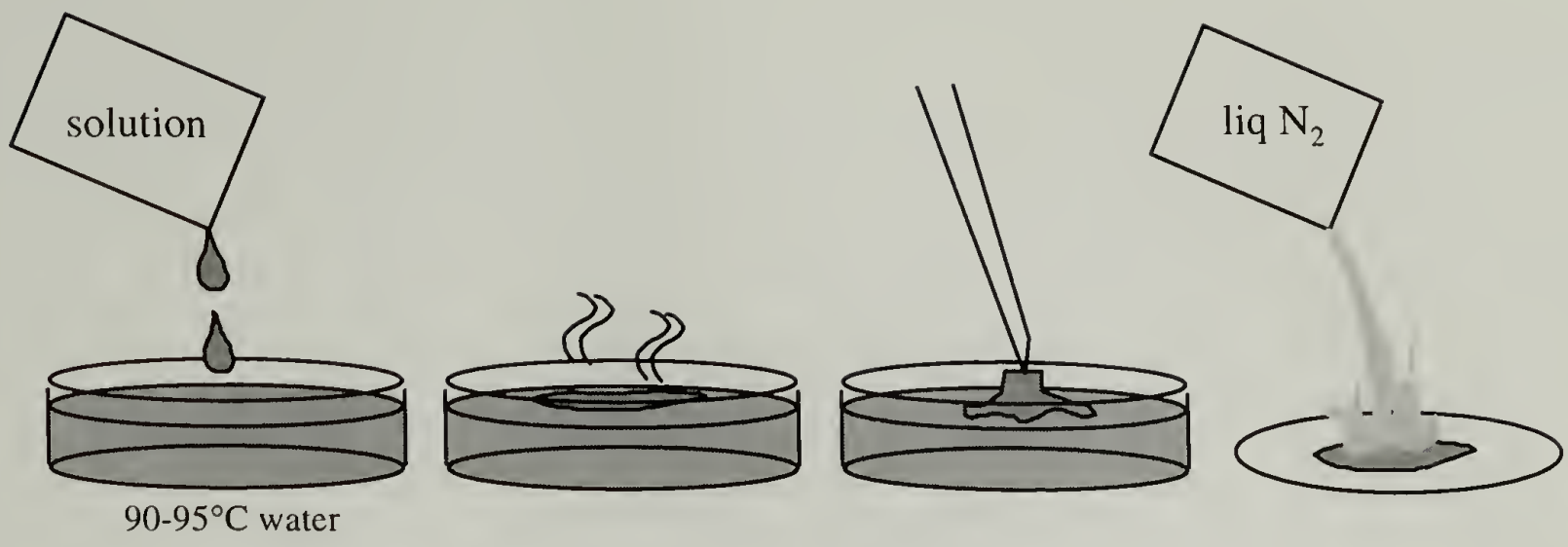

Figure 3.1 Schematic of "Water Casting" Solution Blending Technique.

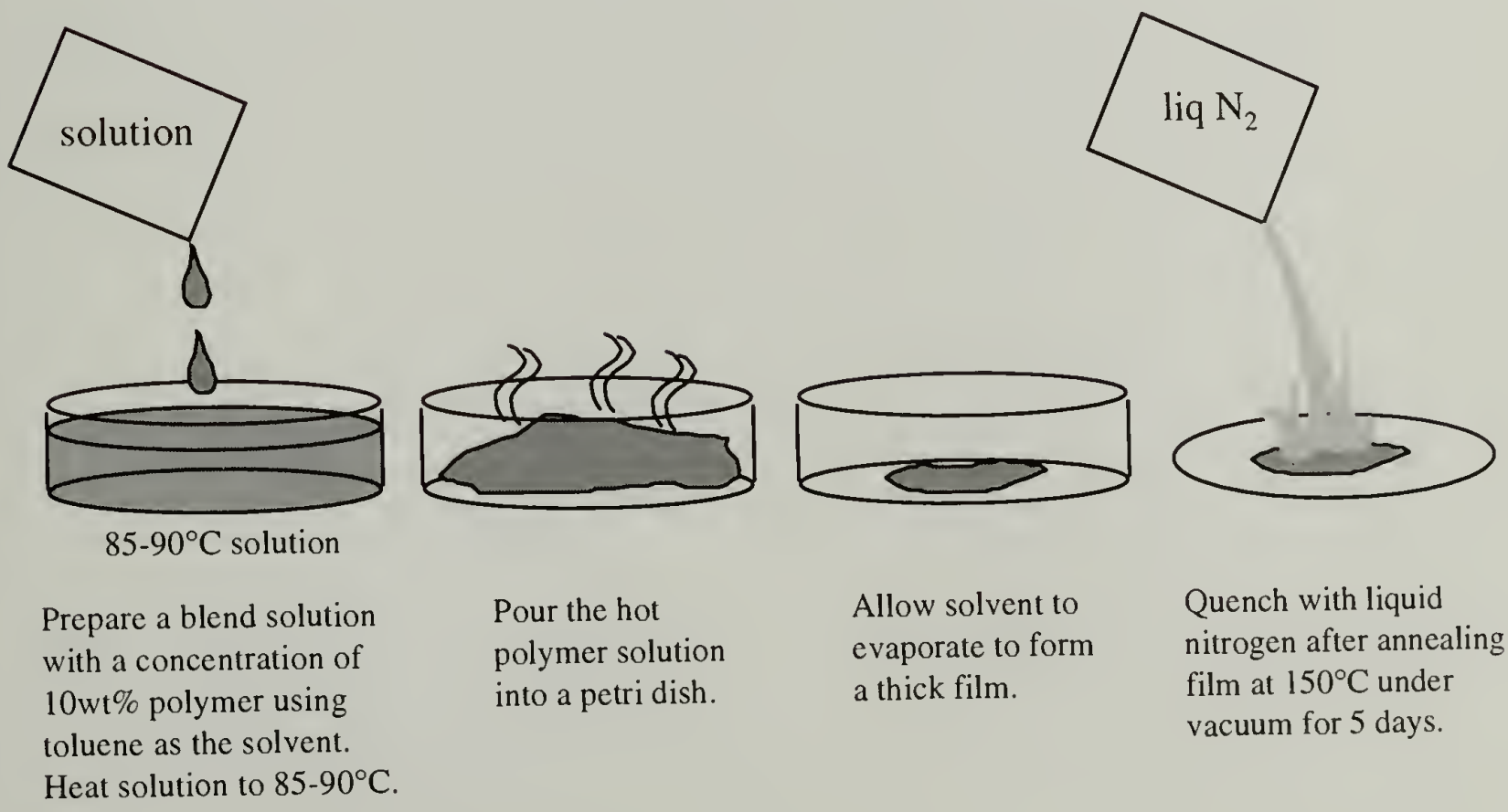

Figure 3.2 Schematic of "Stand Casting" Solution Blending Technique.

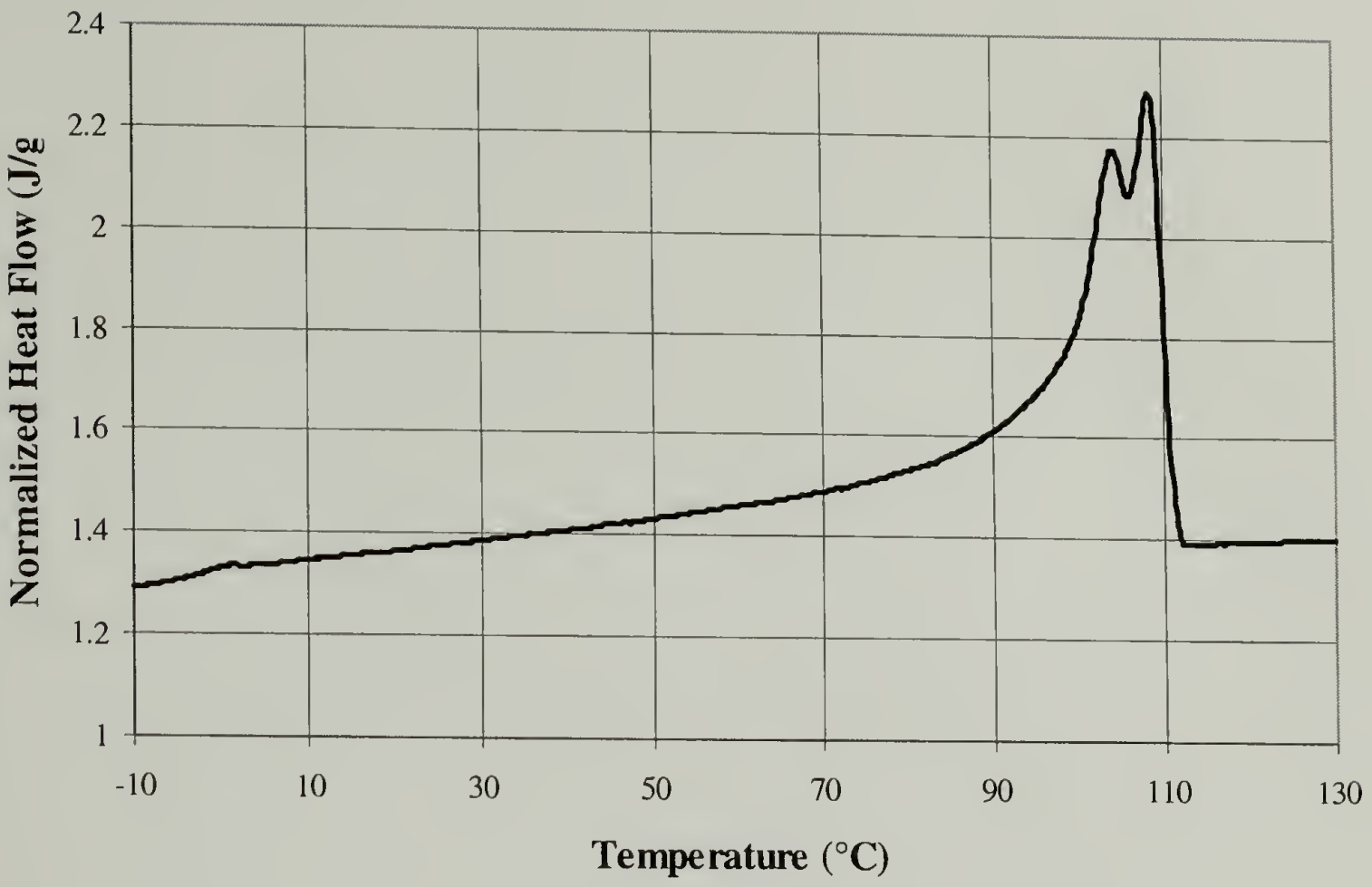

Figure 3.3 DSC Heating Thermogram (10°C/min) of 50/50 (wt%) Physical Mixture (DEP100/PE20).

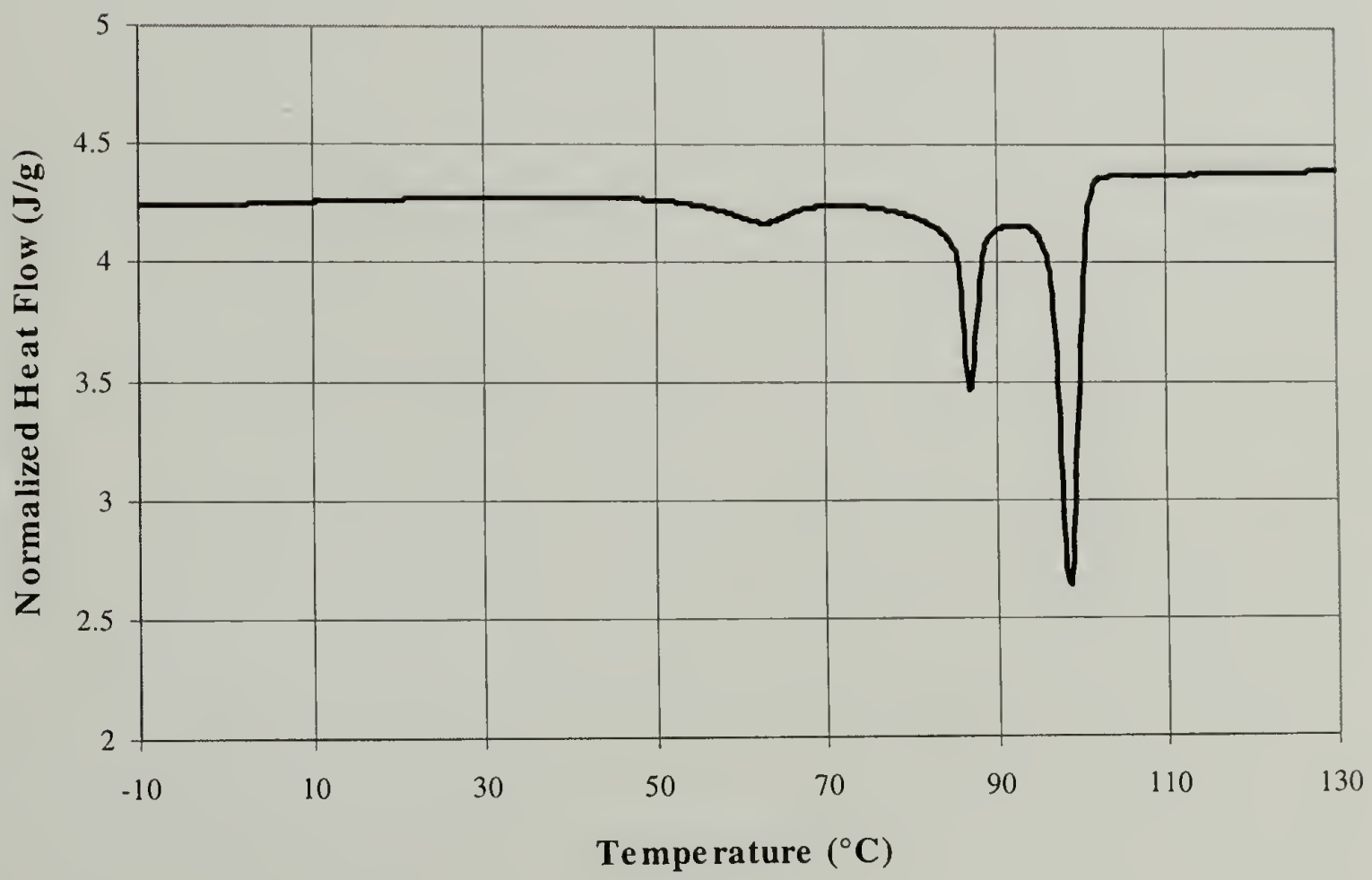

Figure 3.4 DSC Cooling Thermogram (10°C/min) of 50/50 (wt%) Physical Mixture (DEP100/PE20).

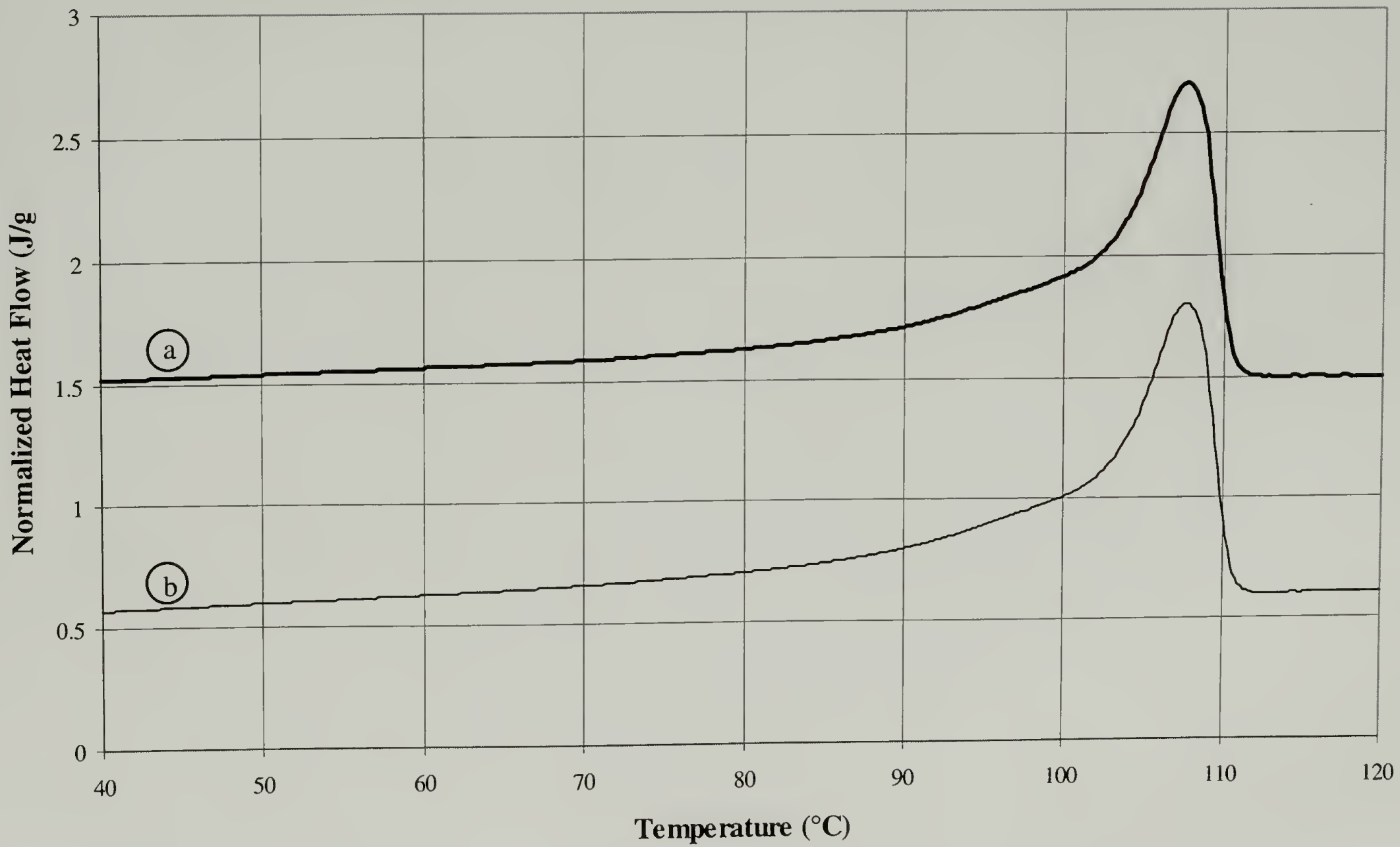

Figure 3.5 DSC Heating Thermograms (10°C/min) of 50/50 (wt%) (**a**) Water and (**b**) Stand Cast Solution Blends (DEP100/PE20).

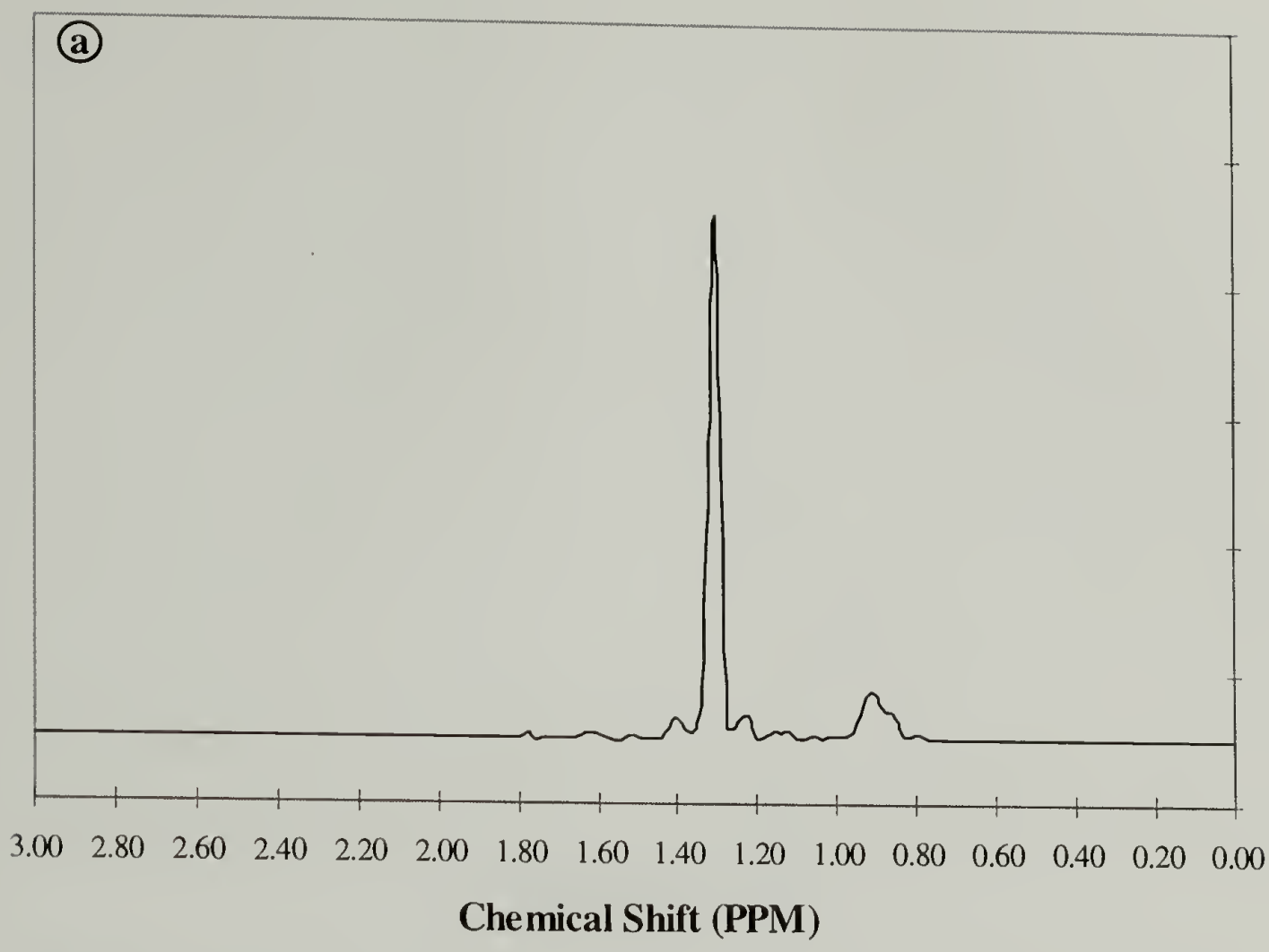

Figure 3.6 ^{1}H NMR of Samples of a 50wt% DEP100/50wt% PE20 Stand Cast Solution Blend Taken from (**a**) Walls and (**b**) Bottom of the Beaker to Determine the Homogeneity of This Technique. (Dissolved in *d*-ODCB at 125°C.)

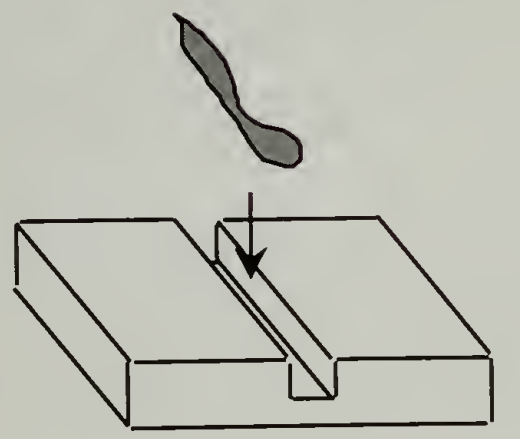

Place polymer blend in shear die and place set-up in Carver press to heat to 120-130°C. Wait until blend appears molten.

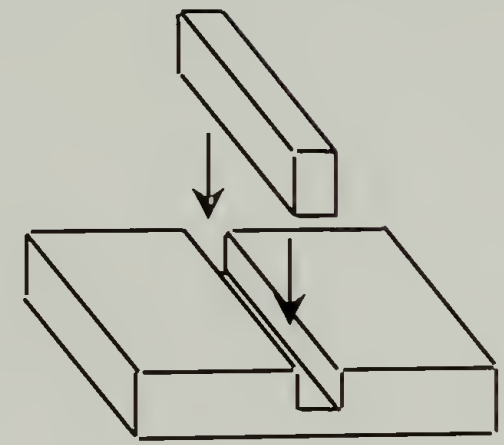

Set preheated PTFE-coated aluminum bar into channel and use press to compress polymer to 1/4 to 1/6 its original thickness.

After allowing 30 min. in vacuum, quench assembly in liquid N_2.

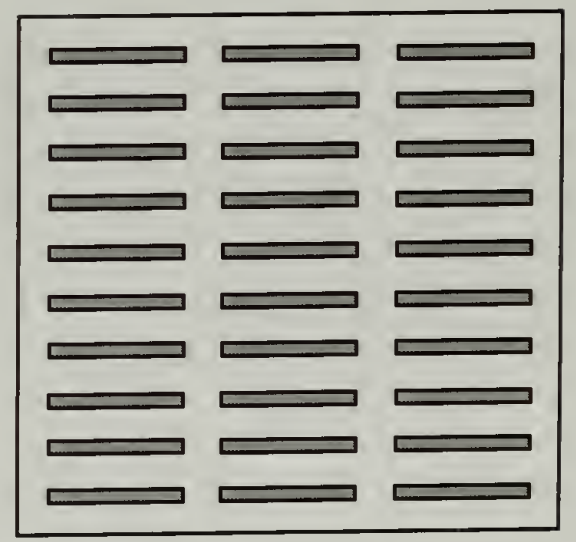

Place oriented blend film into slot of aluminum plate for melt-annealing at 150°C for 5 days.

Quench aluminum plate and polymers in liquid N_2.

Figure 3.7 Schematic of Orientation (Melt Pressing) Technique.

CHAPTER 4

THERMAL STUDIES

4.1 Introduction

Knowledge of the thermal behavior of a polymeric system is important for several reasons. For example, the melting temperature of a semicrystalline thermoplastic polymer (such as HDPE or *i*-PP) is necessary to determine the temperature above which a polymer must be heated before it is able to be formed into usable products. The terms of interest for amorphous polymer systems are the glass transition temperature and change in heat capacity for the polymer(s) involved.

A recent study on hydrogenated polydiene block copolymers[1] found that the additional driving force which occurs as the block symmetry becomes increasingly skewed toward higher PE composition prevents the retention of microdomains in favor of spherulite formation. Further, results indicated that the room temperature morphology (by TEM) was different than the melt morphology (by SAXS). (In this case, cylinders in the melt were transformed by crystallization to lamellae in the solid state.) It would be interesting to compare the results from increasing "block asymmetry" through the addition of low molecular weight homopolymers to a symmetric diblock with the results from neat diblocks containing block asymmetry to determine whether any universality in behavior could be found.

Another recent study investigated the effect of blending an amorphous homopolymer to a crystalline-amorphous diblock copolymer.[2-4] It was found that addition of the low molecular weight amorphous homopolymer allowed the microphase

separated state in the melt to be preserved by rapid cooling to room temperature, with crystallization occurring in the confines of the microdomains. A major finding was that a change in the morphology of the blend (from continuous phases to discrete phases) could be observed by DSC and were related to a change in the crystallization kinetics of the crystallizable component.[5] This change in crystallization kinetics resulted from a change in the continuity of the crystallizable block (from continuous to discontinuous). One of the main objective of the present work has been to determine whether the behavior seen in the previous studies are transferable to this research.

Two major techniques of thermal analysis are thermogravimetry (TG) and differential scanning calorimetry (DSC). These and other methods that are used to investigate how properties and behaviors of polymers change as a function of temperature are explained in detail in References 6-9.

TG was used to examine the degradation behavior of the polymers under study by measuring the mass changes as the temperature was increased according to a controlled program.[6] DSC was performed to measure thermal transitions which occur in the sample as it is being heated or cooled. Physical blends were prepared to serve as an extreme basis for comparison with the results obtained from solution blends. Solution blends made by two casting routes were investigated for differences in heating and cooling behavior. The techniques used to create these blends are covered in the chapter on blending (Ch. 3).

4.2 Experimental

4.2.1 Thermogravimetry (TG)

For this researeh the ehange in mass was reeorded as the temperature was increased from 30°C to 600°C at a ramp rate of 10°C/min using a Perkin-Elmer TGA7 Thermogravimetrie Analyzer with an argon gas flow of 40ce/min. The eurie temperatures of perkalloy (596°C) and alumel (163°C) were used as temperature calibration standards. Samples were prepared from unoriented, melt-annealed solution east blends (5 days at 150°C, *in vacuo*) and eomponent polymers. Sample weights were kept between 12-16mg, but due to the range of forms that these polymer took (from powders to thiek films), some variability was inevitable. Preursor polymers were used in the "as-is" eondition and without thermal treatment. An HDPE sample (Polyseiences) was used to compare behavior with the hydrogenated polybutadienes. A thermogravimetrie measurement of the deuterated dibloek used for NR was also performed to determine its thermal stability as eompared to the hydrogenous dibloek eopolymer, sinee ^{1}H NMR had shown relatively high residual unsaturation (5%). Pyris software (Perkin-Elmer) was used to monitor the degradation of the polymers and to measure the end-points of the eurie transitions for the ealibration metals.

4.2.2 Differential Scanning Calorimetry (DSC)

All DSC studies were performed on Perkin-Elmer DSC7s, and data analysis was aceomplished using Pyris software (Perkin-Elmer) on an attaehed PC. Samples were prepared from unoriented, melt-annealed blends and eomponent polymers, and weights were maintained at 9.0mg to reduee sample-to-sample variability. Indium (T_m =

156.60°C, ΔH_m = 28.45J/g) and mercury (T_m = -38.87°C, ΔH_m = 11.45J/g) were used as calibration standards. The samples were first held at 180°C for 15 minutes, cooled at 10°C/minute to -100°C, heated at 10°C/minute to 180°C, and held at 180°C for 10 minutes. The cooling and heating cycles were repeated. After annealing at 180°C for 15 minutes, samples were also rapidly cooled from 180°C to -100°C at 320°C/minute to simulate quenching. This was followed by heating at 10°C/minute from -100°C to 180°C and the procedure was repeated. Some samples were cooled/heated at 20°C/minute to investigate whether there were differences in transitions due to ramp rate. Results were reported from the second set of scans, since it is believed that all artifacts due to previous thermal/mechanical history in the polymer are fully removed by this point. From the heating curves, the glass transition temperature, T_g, (taken at half ΔC_p), for the atactic polypropylene block of the copolymer, the melting point, T_m (end), and melting enthalpy, ΔH_m, of the polyethylene crystallites were measured using the Pyris software. The heat of fusion, ΔH_f, and crystallization temperature, T_c (onset), for the blends and their components were measured from the cooling curves.

4.3 Results and Discussion

4.3.1 Thermogravimetry (TG)

TG was used to determine thermal stability and to assess the upper limits for melt-annealing and vacuum pressing operations. The temperature which was used as the upper limit (600°C) was chosen since by this temperature essentially all of the polymer should have been pyrolized and only residual catalyst from the hydrogenation procedure which

had not been removed via filtration would remain (as an indication of the thoroughness of this cleaning technique).

A plot of mass percent versus temperature for the saturated diblock copolymer, DEP100, is shown in Figure 4-1. The vertical lines at 150°C and 180°C represent the limits for melt-annealing/pressing and annealing in the DSC, respectively. It can be observed that degradation does not begin until at least 100°C above the melt-annealing/pressing operations and at least 50°C above the melt temperature for the DSC work. Therefore, it was assumed that the temperatures used for these processes would be sufficiently below the start of degradation so that chemical changes in the polymer chains would not occur when thermally treated. A plot comparing the thermograms of a high density polyethylene standard and the saturated versions of the three homopolybutadienes are shown in Figure 4-2. It can be seen that the saturation process yielded polymers with essentially the same decomposition behavior as a "true" polyethylene. (A small caveat to this statement is the slightly lower degradation behavior of PE107, which was later seen to cause a slightly increased amount of coloration during melt-annealing after orientation.) Thus, minimal special care was necessary in handling or preparing blends containing either the saturated diblock or the homopolymers.

Figure 4-3 shows the decomposition curves for the saturated poly(methyl-pentadiene) (APP162) used in the neutron reflectometry studies and a saturated polybutadiene (PE107). The difference on the onset temperatures of degradation is due to the tertiary carbons in the APP, which are less thermally stable than the secondary carbons found in PE. This effect is also shown in Figure 4-4, which compares APP162, DEP100, and PE107.

Another result that should be considered is the difference in degradation behavior between the precursor diblock, PBD-*b*-PMPD, and its saturated version, DEP100 (refer to Figure 4-5). Before running experiments, it was anticipated that the hydrogenated diblock would show at least some increase in thermal stability over the polydiene. However, experimental results did not bear this out. In fact, the precursor copolymer actually showed enhanced thermal stability as compared to the saturated diblock beyond 50-55 weight percent remaining copolymer. This increase in thermal stability would most probably be attributable to the loss of double bonds and the formation of a cross-linked system. Cross-linking is known to increase degradation resistance of a polymer by giving the system a higher activation energy (i.e. more stable) to overcome in order to break up the network. This still left the question of why the onsets of decomposition for both versions of the diblock copolymers were so similar. This is most probably due to the fact that both polymers are hydrocarbons which were decomposed in inert atmospheres, and therefore have degradation mechanisms which are dictated by similar chemical reactions.

An additional feature of the thermograms for the two diblock copolymers in Figure 4-5 is the "knee" that occurs at roughly 50 wt.% residual polymer. A knee indicates that the polymer is not homogeneous (i.e. either contains additives/fillers or is a blend or copolymer). The APP most probably degraded first, followed by the more dense PE. Also note the difference in the curve shapes. The saturated copolymer showed almost continuous degradation, while the precursor showed two more knees. These knees are probably due to some form of cross-linking which was then followed by the breakdown of the network.

Figure 4-6 shows the degradation behavior of the saturated diblock copolymer, DEP100, and a high-density polyethylene from Polysciences. Comparison of the two curves illustrates that the hydrogenation process left few double bonds remaining in the diblock copolymer. If many residual double bonds were in the "saturated copolymer", then one would expect to see more complex degradation behavior as is seen in the precursor copolymer. This behavior would be manifested in the presence of knees and would indicate that crosslinking has occurred, which is an sign that a large number of double bonds existed. As can be seen in Figure 4-6, this is not the case.

At this point, it would be appropriate to discuss the normal mechanisms of degradation of polydienes and polyolefins without additives or fillers.[7,8] The typical order of decomposition for degradation of polydienes is cross-linking followed by chain-scission which is then followed by volatilization. The decomposition pathway for polyolefins is less complex (due to a lack of double bonds) and so only chain-scission and volatilization occur. It should be added that for the system under study, very little carbon ash remained after the temperature ramp to 600°C. Therefore it is assumed that the polymers volatized and were taken up into the argon stream and out of the sample area. (Credence is lent to this idea as some yellow "grease" accumulated on the glass sheathing to the sample chamber, which was probably condensation of the volatile decomposition product on the cool glass surface.)

Thermogravimetry was also performed on the deuterated copolymer used for neutron reflectometry experiments as seen in Figure 4-7. Despite a significantly higher residual level of double bonds after saturation (ca. 5%), the thermal stability was essentially the same as the more fully saturated hydrogenous diblock (which had about

1% residual double bonds). Therefore, no special precautions were necessary besides an inert atmosphere while running the neutron experiments in the melt cell in order to prevent degradation from occurring.

4.3.2 Differential Scanning Calorimetry

The physical properties of the stand cast solution blends measured as functions of heating and cooling at 10°C/minute are presented in Table 4-1. For the values derived from the heating curves, the glass transition temperature of b-APP, T_g, was determined at the half ΔC_p method. The change in heat capacity, ΔC_p, at T_g was measured whenever possible. However, due to the reduction in the fraction of amorphous material in the blends, it was not possible to reliably measure ΔC_p without large errors (over 20%) above a certain concentration of homopolyethylene (roughly 40wt% h-PE) for each set of blends. The melting point, T_m (end), and enthalpy of melting, ΔH_m, of the PE components were also determined from the heating curves. An estimate of the degree of crystallinity is included in Table 4-1 which was based on the amount of the crystallizable polymer present, ΔH_f (or ΔH_m), and the heat of fusion for a perfect PE crystal, 290J/g.[10] From the cooling curves the crystallization temperature, T_c (onset), and the heat of fusion, ΔH_f, for each of the blends were measured. The use of the onset temperature for the stated values of T_c and the end temperature for the stated values of T_m were to keep consistent with results which have been reported for the system DEP/APP.[2-3] Included in Table 4-1 are values for the neat h-PEs, an APP, a HDPE standard (Polysciences), and the pure diblock copolymer of the blending studies.

It was stated in the chapter on blending that physical mixtures were prepared as a source of comparison with the solution cast blends. Since mixing in the physical "blends" was on the macroscopic level, it was assumed that two melting and two crystallization peaks from each of the crystallizable components would be observed, as was indeed the case. (Figures 4-8(a) and 4-9(a)) Included in these figures are blends of the same composition which were prepared by the stand casting solution technique. Clearly the solution blend displays only one melting and one main crystallization peak in the region where the physical mixture shows two of each, indicating that the mixing of the crystallizable polymer chains has occurred on a much smaller length scale, so that co-crystallization of the two types of PE chains could take place. Therefore, it should be concluded that the solution blending route was successful in intimately mixing the two components.

Three cases arise upon blending a symmetric diblock copolymer of amorphous components A and B (b-AB) with amorphous homopolymers of type A (h-A). As was illustrated in the first chapter in Figure 1-5, blending of an h-A with a higher molecular weight than the corresponding block of the diblock copolymer, b-A (Case III), is expected to cause macrophase separation of the polymers upon any addition of the homopolymer. This is the result of the poor miscibility of the homopolymer chains with the like segments of the copolymer. As the length of the h-A chains approach that of the b-A blocks, as in Case II, miscibility of the two chains begin to increase, allowing small additions of the homopolymer to be made to the diblock before macrophase separation occurs. Finally, when the average molecular weight of the h-A chains are lower than that of b-A (Case I), the chains of the homopolymer are able to act as large molecule solvents

and swell the b-A block. This changes the relative volume fraction occupied by b-A and causes order-order transitions to occur with increasing amounts of the low molecular weight h-A. Therefore, miscibility is an important topic when discussing diblock copolymer/homopolymer blends.

The predictions for this research, where crystallization occurs in addition to the issue of miscibility, are as follow. When the molecular weight of the homopolymer is higher than the like block of the copolymer, DEP100 + PE107, the homopolymer chains will be rejected from the diblock copolymer and macrophase separation will occur. This may result in a split crystallization peak if the molecular weight of the homopolymer is substantially larger than the homopolymer (i.e. $M_{h\text{-}A} >> M_{b\text{-}A}$). As one decreases the molecular weight of the homopolymer while keeping the molecular weight of the diblock the same, the h-PE becomes more miscible with the like block of the copolymer. In the limit where the molecular weight of the homopolymer is much lower than the like block in the diblock, as in DEP100 + PE20, the h-PE is able to enter into and mix with the b-PE blocks and affect the morphology of the diblock. Therefore, one would expect that for blends of the diblock copolymer with PE107 that the homopolymer would most likely be excluded from the diblock, whereas for blends of the copolymer with PE20, the opposite should be true and of the blends studied, these are most likely to reside within the DEP100. This should impact the crystallization behavior as well as the melting behavior of the blends as the blends will act increasingly phase separated.

It was determined previously[5] that blending of a high molecular weight symmetric DEP copolymer with APP homopolymers does not affect the melting behavior of polyethylene crystallites in the block copolymer. Because this research involved the

addition of more crystallizable component to the system, it was reasonable to confirm this behavior by performing heating scans on blends of DEP + PE after cooling at 10°C/min. The heating curves at 10°C/min for the blends containing the diblock copolymer, DEP100, and the highest molecular weight homopolyethylene, PE107, are shown in Figure 4-10. The ratio of $M_{h\text{-}PE}/M_{b\text{-}PE}$ for these blends was 2.38. The prominent features of these curves are the glass transition temperature of the APP block of the copolymer at ca. -5°C and the broad crystalline melting transition which peaks from ca. 106-111°C, an example of which is displayed in Figure 4-11. No change was apparent in either the location of the glass transition or the melting peak, but it should be noted that the presence of only one melting peak would indicate the crystallizable segments from the h-PE and the b-PE were able to co-crystallize due to the intimate level of mixing and similar microstructures.

The heating thermograms from the blends containing the medium molecular weight homopolyethylene, PE47, which has an $M_{h\text{-}PE}/M_{b\text{-}PE}$ ratio of 1.04 are shown in Figure 4-12. Similar behavior to that which was seen for the blends of DEP100 + PE107 were also observed for these blends: no shift in T_g or melting peak, a decrease in the amplitude of the T_g due to dilution of the amorphous component, and an increase in the size of the melting transition due to the addition of more crystallizable component. This behavior is consistent with the melting behavior reported for the blends of DEP + APP.[2]

A different melting behavior was observed for blends of DEP100 and PE20 as can be seen in Figure 4-13. For this combination the ratio of $M_{h\text{-}PE}/M_{b\text{-}PE}$ is 0.44, which is the case where the homopolymer chains are short enough to act as a high molecular weight solvent. Therefore, the two crystallizable polymer chain should be miscible with each

other. However, crystallization appears to be affected by the presence of the low molecular weight homopolymer. The most probable explanation for the split in the crystallization peak above 40wt% PE20 is that the h-PE crystallizes slightly ahead of the b-PE, causing the single peak to become two. This may result in an order-order transition which would be consistent with DEP/APP[3], or it may arise from a (macro)phase separation between the two PE components, which is more akin to the behavior observed with the asymmetric diblock copolymers of Ryan et al.[1]

As was seen in the previous blend studies for DEP + APP,[2,3] a sharp crystallization peak and a broad "shoulder" peak were observed for the blends of DEP and PE: one in the range of 85-88°C (which was labeled "Peak I") and a second "shoulder" centered around 61-62°C (which was labeled "Peak II"). An example of this behavior is shown in the cooling thermogram in Figure 4-14. This secondary peak has been reported in LLDPE and was attributed to broad branch length distributions[11] which our polymers do not possess. This behavior can also be attributed to the formation of spherulites, where the main peak in Figure 4-15 is attributed to the highly-ordered crystalline fibrils which make up the arms of the spherulite, while the lower temperature peak arise from the less perfect crystals that fill the space between the arms. The reason why the main peak consisting of fibrils is so sharp is that the crystallites are fairly uniform in size, while the crystallites that form in the spaces in between the fibrils have a distribution of sizes and quality which results in a broad peak.

It would be interesting to anticipate where the shift in crystallization peaks would have occurred in the DEP/PE blends (with the lowest molecular weight h-PE) based on the morphological diagram of Winey et al.[12] and the results of DEP/APP.[3] If one were to

use their morphological diagram as a guide for forecasting composition at which changes in the major peak may occur, for the DEP100/PE20 blends, they would occur between 75vol% and 70vol% h-PE (lamellae to cylinders) and 50vol% to 40vol% h-PE (cylinders to spheres). For the blends of DEP100 + PE47, since the ratio $M_{h\text{-}A}/M_{b\text{-}A}$ = 1.03, the diagram would predict shifts at between 25vol% and 30vol% h-PE since the morphology would be expected to change from microphase separated to macrophase separated—a result of the limited solubility of the h-PE chains in the b-PE domains. For the highest molecular weight homopolymer, PE107, the diagram would predict that if a shift was detectable by DSC, it would occur upon the addition of any h-PE resulting from the inability of the PE107 to mix with the b-PE part of DEP100. (A note should be made for clarity: In the previous work of K. Sakurai,[3] an assumption was made that the volume percent was approximately the same as the weight percent in the melt. This convention will be maintain in this work.)

On the other hand, if one uses the results of DEP/APP as a guide for determining possible changes in the peaks, the shift from Peak I to Peak II would occur between 45vol% and 50vol% h-PE, and this would only occur for the blends with the case where $M_{h\text{-}A}/M_{b\text{-}A} < 1$. As can be seen from the composite cooling plots (at 10°C/min) for the three sets of stand cast blends (Figures 4-16 through 4-18), there is no shift in the dominant crystallization peak, so our blends exhibit different crystallization behavior than was seen for the system DEP/APP.

A composite plot of the cooling curves at 10°C/min for the blends of diblock copolymer, DEP100, with the highest molecular weight h-PE, PE107, is shown in Figure 4-16. Since the ratio of $M_{h\text{-}A}/M_{b\text{-}A}$ = 2.38, it is assumed that any addition of the

homopolymer would result in macrophase separation. As was observed in the heating scans for these blends, the addition of PE107 does not affect the crystallization behavior of DEP100, except to enlarge the peak. This behavior is consistent with both the previous results with h-APP and the morphological diagram discussed above.

The composite plot of the second cooling scans at 10°C/min for the blends DEP100 + PE47 (Figure 4-17) shows another break with the results of DEP/APP due to a slight shift (ca. 2°C) which occurs in the location of the major cooling peak. If this change were to be caused by a change in the morphology from microdomains to essentially pure component domains, then the shift would be considered consistent with the predictions of the morphological diagram.[12] Since this shift is seen in both the stand cast and water cast solution blends, this behavior is probably inherent to the system and not due to preparation technique. The morphological change occurring in these blends is discussed further in the next chapter.

The behavior of the stand cast blends with the lowest molecular weight homopolymer, PE20, (Figure 4-18) is also different than would be expected based on the previous results with DEP/APP. However, in this case the results are likewise inconsistent with the predictions from the morphological diagram because the ratio of molecular weights for the PE components ($M_{h\text{-}A}/M_{b\text{-}A}$ = 0.44) would predict that two shifts in the crystallization peak should occur. In addition, these results differ between the stand cast and water cast solution blending techniques. The cooling curves for water cast blends of DEP113 + PE25 are displayed in Figure 4-19. (PE25 is an h-PE which was synthesized early in this research, and PE20 was synthesized later to have roughly the

same ratio of $M_{h\text{-}PE}/M_{b\text{-}PE}$ as was obtained for DEP113 + PE25.) Since these results appear to indicate a departure from expected behavior, further clarification is required.

In the studies of DEP/APP,[2,3] it was observed that the introduction of the lowest molecular weight h-APP caused a change in the major crystallization peak while cooling at 10°C/min, as seen Figure 4-20. A plot of crystallization temperature versus composition for these blends is shown in Figure 4-21. This change was attributed to a transformation in morphology between 45 and 50wt% added APP15 (the lowest molecular weight homopolymer) from CNC (continuous network cylinders) to discrete cylinders. The cause of the shift in crystallization peaks was due to a change in the polyethylene phase from being a continuous phase to a discontinuous phase. This explanation can be interpreted that in lamellae and CNC, the crystallization growth front was continuous and only a change in direction was necessary in order for the front to continue; but, in discrete cylinders and spheres, "walls" (of the surrounding h-APP) were introduced which frustrated the crystallization growth front so that no change of direction to continue the propagation of the growing crystal was possible. *For this system, because h-PE was added to the diblock, polyethylene was always the continuous phase. Therefore, one would expect to see no large shift in which T_c peak was dominant with increasing homopolymer concentration.*

Because it is possible that spherulites were obtained upon cooling at 10°C/minute, it would be interesting to investigate two related effects: (1) the effect of changing the cooling rate on the morphology of the system (This will be called the "variable cooling rate" study.) and (2) the heating curves after rapidly cooling blends from the melt at 320°C/min. (maximum cooling rate for the DSC7) to compare the melting behavior of a

hopefully now-microphase separated morphology against the heating curves obtained after cooling at the standard 10°C/min.

The purposes of the variable cooling rate study were twofold: first, to investigate different cooling rates in order to determine whether it is possible to see the change in the cooling curves from the spherulitic regime to the microphase separated state using DSC; and second, to use the DSC apparatus as a controlled cooling rate oven to produce samples which would later be microtomed and imaged by TEM (for morphology) and polarized light microscopy (for the presence of spherulites). The latter use was for the investigation of whether an intermediate morphology existed which was not definitely spherulitic nor microphase separated in nature. Drawings of plausible intermediate structures are shown in Figure 4-23.

During the course of running the experiments to determine whether a microdomain/spherulitic transition could be monitored by DSC, it quickly became apparent that this study was not feasible as the slope of the baseline became highly curved at cooling rates over 60°C/min. Therefore, only the second portion of this study was pursued to any degree. This consisted of preparing a series of DSC pans of the pure diblock and a 50/50 blend (by weight) of DEP100/PE20 and cooling the samples at different cooling rates from the melt (180°C). This set of experiments is discussed in the last chapter on future work.

A plot comparing heating scans (at 10°C/min) after cooling at 10°C/min and 320°C/min for a blend of 30% DEP100 and 70% PE20 (by wt) is shown in Figure 4-24 and a composite plot of heating scans after cooling at 320°C/min for selected blends of DEP100 + PE20 is shown in Figure 4-25. It can be observed that the heating scans for

the rapidly quenched blends show two dominant crystallization peaks which increase in distinctness as the composition becomes higher in PE20, consistent with what was seen for the slower cooling rate. Regardless of whether the microphase separation in the melt was preserved in the "quenched" blends, it appears that something has occurred which is different than what was seen for blends of DEP/APP.[5] Proof of whether quenching preserves the microdomain morphology is reserved for the next chapter. Comparing the blends from each of the two cooling studies, it can be seen that the h-PE causes a different melting behavior to occur as opposed to the blending with h-APP. Cooling appears to cause the h-PE to begin to crystallize as it would in the neat homopolymer—at a slightly higher temperature than the b-PE (since the h-PE chains are not inhibited by the amorphous block as are the b-PE chains). This behavior is reflected in the split dominant melting peak. There are two possible molecular mechanisms which may be responsible for this change in melting behavior. The first potential explanation is that the h-PE chains crystallize first, which in turn causes the b-PE segments to crystallize so that layers or grains are formed within the microphase separated structure, but macrophase separation is suppressed. The other possible mechanism is that (partial) demixing occurs between the h-PE and the b-PE because the h-PE is more "perfect" and able to crystallize at a higher temperature that the b-PE chains, which may lead to suppression of phase change (as was seen for asymmetric crystalline-amorphous diblocks)[1] or some degree of phase separation may take place. These hypotheses will be tested in the following chapter on morphology.

Figure 4-26 compares the enthalpies of melting for blends of DEP100 + PE20 after quenching at 320°C/min and slow cooling at 10°C/min. It can be seen that cooling

does not affect the overall crystallinity developed in the system, so a change in the kinetics of the system (which affects crystallinity because crystallization is a path-dependent quantity) is not occurring.

4.4 Summary and Conclusions

Solution cast blends made by the stand casting route were tested by TG. All crystallizable polymers showed onset of decomposition temperatures at least 100°C above the highest temperature to be used in this research. Degradation behavior of the saturated polybutadiene homopolymers was similar to that of a HDPE standard, showing that the hydrogenation process was successful in producing polymers with good thermal stability. The APP homopolymer used for NR showed simple degradation which was ca. 50°C less than that of the PEs as should be found for amorphous versus crystallizable polymers.

Saturation was not found to increase thermal stability as was expected. The most likely reason was because the tests were performed in an inert gas stream, so the chemistry of degradation was dictated by hydrocarbon decomposition chemistry and not the anticipated presence of saturation/unsaturation. Cross-linking is believed to be responsible for the increase in thermal stability of the precursor copolymer at roughly 30wt% remaining polymer over the saturated version. Both the precursor and saturated diblock copolymers showed knees at roughly 50wt% remaining polymer which indicated a change in the type of polymer unit predominantly being degraded.

DSC was completed for heating and cooling of physical blends and solution blends prepared using the stand casting and water casting routes. The physical mixtures showed separate heating and cooling peaks indicative of macrophase separation, whereas both of the solution blends showed only one dominant melting and one dominant crystallization peak at a ramp rate of 10°C/min. Therefore solution blending was successful in intimately mixing the polymer components.

Blending with h-PE affected the melting behavior of solution cast blends. A split in the dominant melting peak with higher amounts of the low molecular weight h-PE (PE20) upon cooling at 10°C/min. Cooling curves (at 10°C/min) for both solution blending techniques of DEP/PE blends showed no change in the dominant crystallization peak, which is quite different than that seen for the system DEP/APP. It was realized that a change in the dominant crystallization peak should not be observed anyway, since the driving force for the shift in crystallization peaks (from Peak I to Peak II) in the system DEP/APP was determined to arise from a change in continuity of the crystallizable phase (b-PE) from CNC to discrete cylinders as seen by TEM.[5] In the present system, the crystallizable phase is always the continuous phase. Therefore, only subtle changes in the crystallization behavior should be observed and not large scale changes as was seen when more of the amorphous component was added. This would be in agreement with the finding of Ryan et al.[1] for pure diblock copolymers.

A small shift was also noted in the 10°C/min cooling curves of DEP100 + PE47, which was thought to be due to a shift in the type of macrophase separation in the melt that later affected the growth of spherulite from bicontinuous to micelles. This will be explored further in the next chapter.

The 10°C/min heating behavior of stand cast blends (DEP100 + PE20) which were cooled at either 10°C/min or 320°C/min to simulate slow cooling and rapid cooling, respectively, was investigated. Enthalpies of melting for the two situations were similar, proving that the cooling rate does not affect the level of crystallinity developed, and a split was observed to develop in the both cases with increasing PE20 content, indicating a consistent crystallization behavior. It was proposed that the split in the melting peak after

cooling could be due to either grain formation (in the context of normal microphase separation) or due to partial phase demixing due to a mismatch in T_c between h-PE and b-PE (in the context of suppressed microphase separation or macrophase development). These ideas will also be put to the test in the next chapter.

4.5 References

1. Ryan, A. J.; Hamley, I. W.; Bras, W.; Bates, F. S. *Macromolecules* **1995**, *28*, 3860.

2. Sakurai, K.; MacKnight, W. J.; Lohse, D. J.; Schulz, D. N.; Sissano, J. A. *Macromolecules*, **1993**, *26*, 3236.

3. Sakurai, K.; MacKnight, W. J.; Lohse, D. J.; Schulz, D. N.; Sissano, J. A. *Macromolecules*, **1994**, *27*, 4941.

4. Sakurai, K.; MacKnight, W. J.; Lohse, D. J.; Schulz, D. N.; Sissano, J. A.; Lin, J.-S.; Agamalyan, M. *Polymer* **1996**, *37*, 4443.

5. Sakurai, K., Ph.D. Thesis, University of Osaka, 1995.

6. Christian, G. D.; J. E. O'Reilly, ed. Instrumental Analysis, Second Ed., Allyn and Bacon, Inc.: Boston, 1986.

7. Wendlandt, W. W. Thermal Analysis, Third Ed., Wiley-Interscience: New York, 1986.

8. Chiu, J., in Thermal Analysis of Fiber and Fiber-Forming Polymers, Schwenker, R. F., ed., Interscience: New York, 1966.

9. Charsley, E. L.; Warrington, S. B., ed. Thermal Analysis—Techniques and Applications, Royal Society of Chemistry: Cambridge, UK, 1992.

10. Quinn, F. A., Jr.; Mandelkern, L. *J. Am. Chem. Soc.* **1958**, *80*, 3178.

11. Mirabella, F. M.; Ford, E. A. *J. Polym. Sci.: Part B: Polym. Phys.* **1987**, *25*, 777.

12. Winey, K. I.; Thomas, E. L.; Fetters, L.J. *Macromolecules* **1992**, *25*, 2645.

Table 4.1 Table of Thermal Properties for Stand Cast Solution Prepared Blends of DEP100 and PE20, PE47, PE107 (Heating/Cooling @ 10°C/minute) (ΔC_p, ΔH_m, ΔH_c, degree of cryst. normalized by respective component.)

		Heating					Cooling		
Sample	wt% PE	Tg, °C	ΔC_p, $Jg^{-1}°C^{-1}$	T_m,°C (end)	ΔH, Jg^{-1}	% Cryst.	T_c, °C (on)	ΔH_c, Jg^{-1}	% Cryst.
HDPE-52k	100	----	----	138.42	209.17	72.13	114.50	214.27	73.89
DEP100	0	-5.67	0.471	106.74	114.04	39.33	88.98	111.98	38.61
PE20	100	----	----	111.08	122.96	42.40	100.57	125.80	43.38
DEP100/PE20	90	----	----	111.10	119.37	41.16	100.15	111.81	38.56
DEP100/PE20	80	----	----	110.86	144.24	49.74	99.10	133.46	46.02
DEP100/PE20	70	----	----	110.43	124.02	42.77	98.59	113.57	35.60
DEP100/PE20	60	----	----	111.06	138.19	47.65	98.43	151.67	52.30
DEP100/PE20	50	----	----	110.45	125.46	43.26	97.70	133.78	46.13
DEP100/PE20	40	-5.09	0.315	110.14	130.90	45.14	96.98	136.92	47.22
DEP100/PE20	30	-3.85	0.158	109.50	119.32	41.14	95.75	116.38	40.13
DEP100/PE20	20	-3.15	0.255	108.99	100.68	34.72	94.06	87.93	30.32
DEP100/PE20	10	-4.73	0.442	109.20	99.98	34.48	92.92	88.84	30.63
PE47	100	----	----	107.87	117.53	40.53	92.53	118.25	40.78
DEP100/PE47	90	----	----	108.72	115.05	39.67	93.54	124.19	42.82
DEP100/PE47	75	----	----	108.10	105.47	36.37	93.76	89.95	31.02
DEP100/PE47	50	----	----	107.71	94.47	32.58	91.46	84.65	29.19
DEP100/PE47	25	-3.17	0.272	108.22	99.46	34.29	91.57	88.66	30.57
DEP100/PE47	10	-2.57	0.222	107.29	92.91	32.04	90.07	83.17	28.68
PE107	100	----	----	106.65	110.35	38.05	92.29	106.04	36.56
DEP100/PE107	90	----	----	106.72	98.05	33.81	91.93	87.25	30.09
DEP100/PE107	75	----	----	106.44	101.81	35.11	91.73	100.86	34.78
DEP100/PE107	50	----	----	107.98	100.95	34.81	92.14	100.73	34.73
DEP100/PE107	25	-2.37	0.225	107.20	92.20	31.79	91.01	84.90	29.28
DEP100/PE107	10	-2.40	0.293	107.42	92.06	31.74	90.86	79.34	27.36

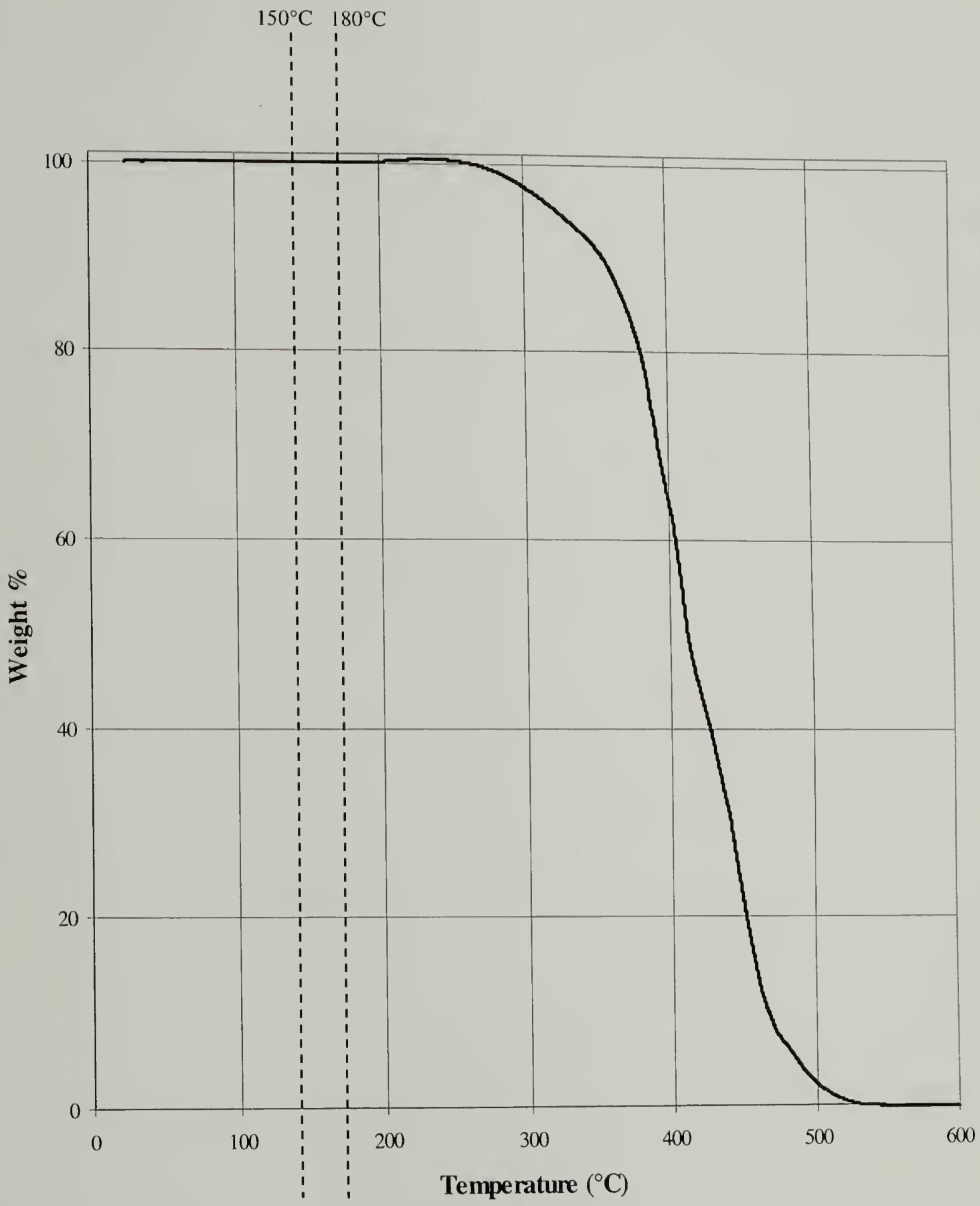

Figure 4.1 TG Plot of DEP100. (Scan rate of 10°C/min)

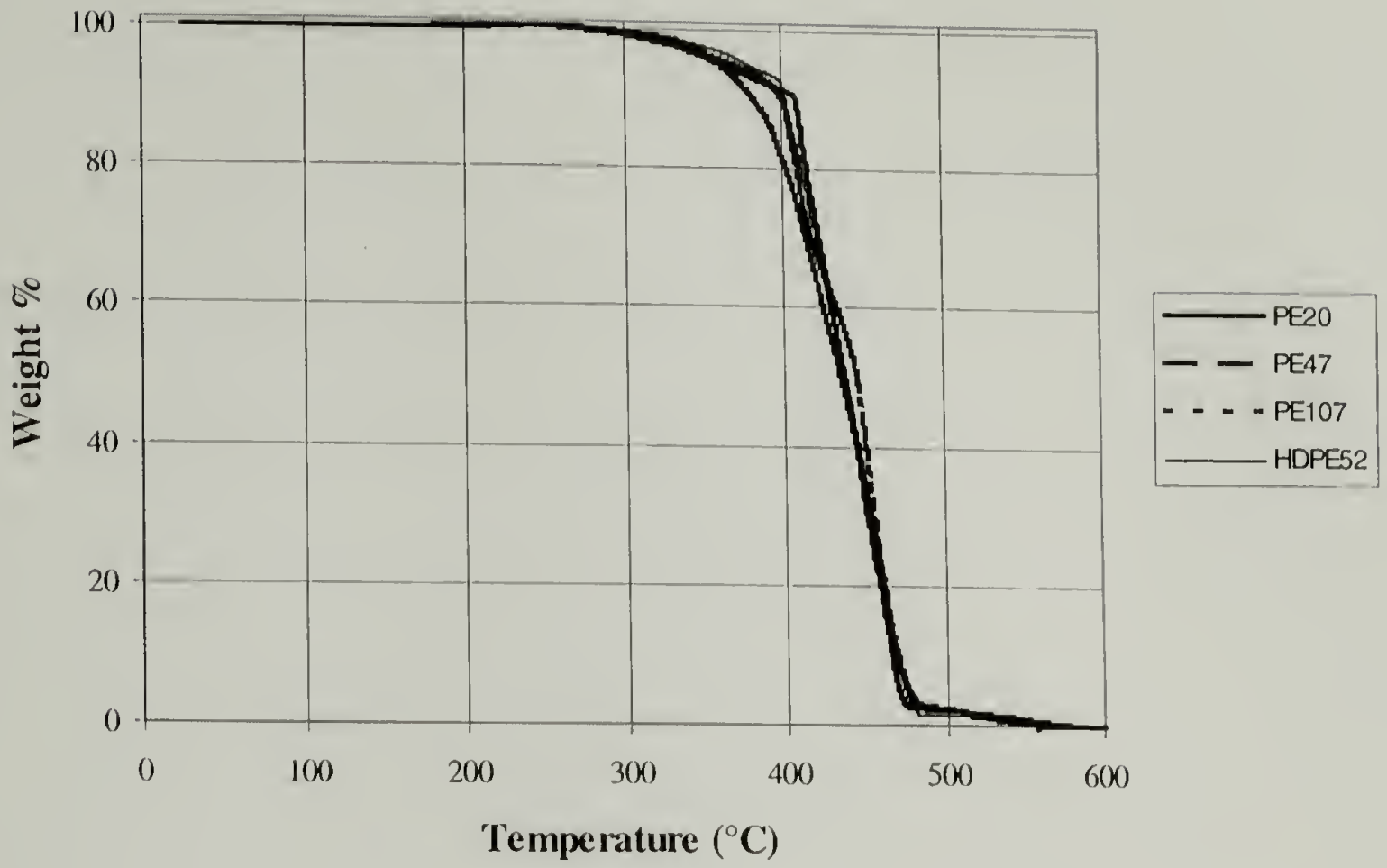

Figure 4.2 TG Plot of h-PEs and HDPE. (Scan rate of 10°C/min)

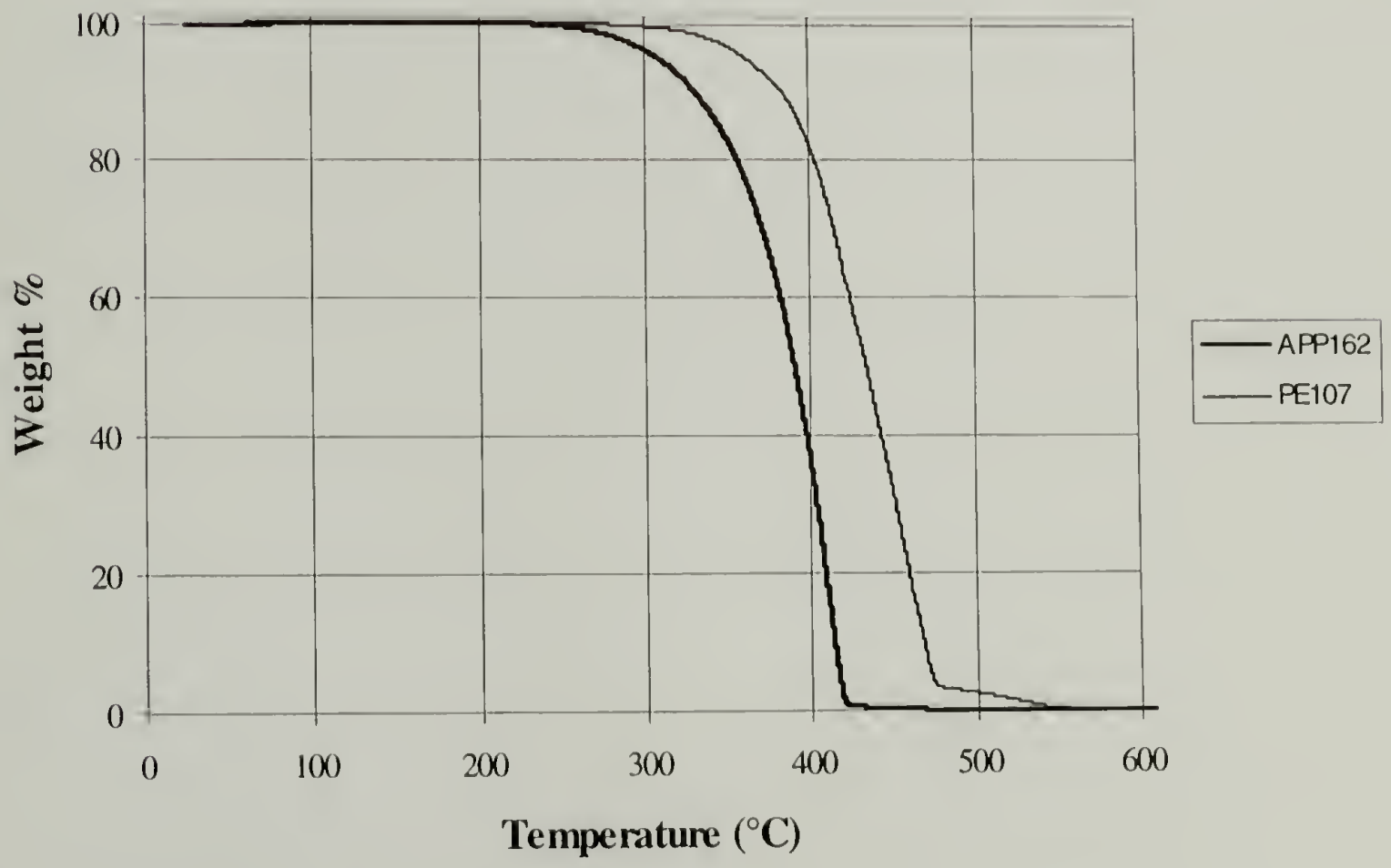

Figure 4.3 TG Plot of APP162 and PE107. (Scan rate of 10°C/min)

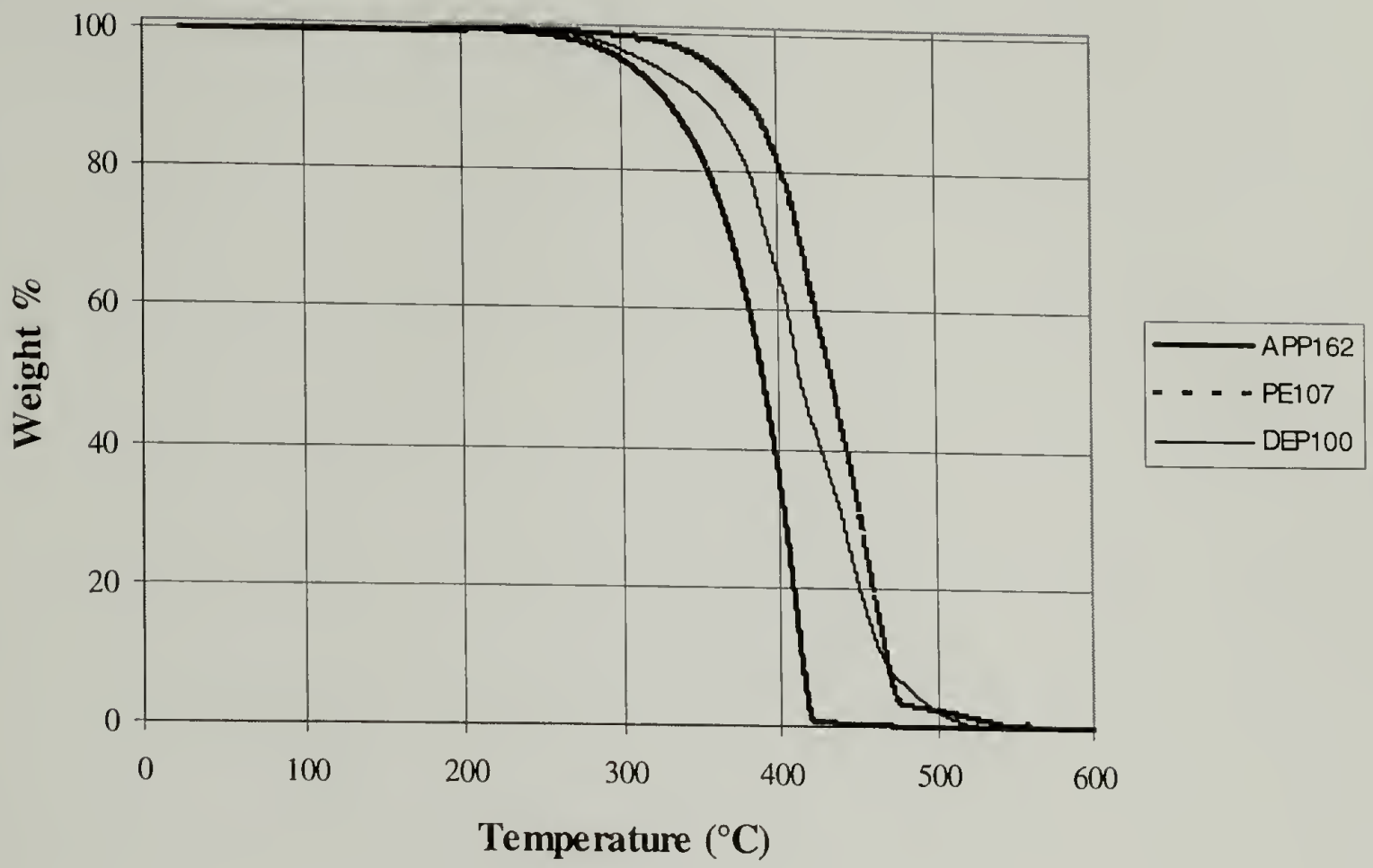

Figure 4.4 TG Plot of APP162, PE107, and DEP100. (Scan rate of 10°C/min)

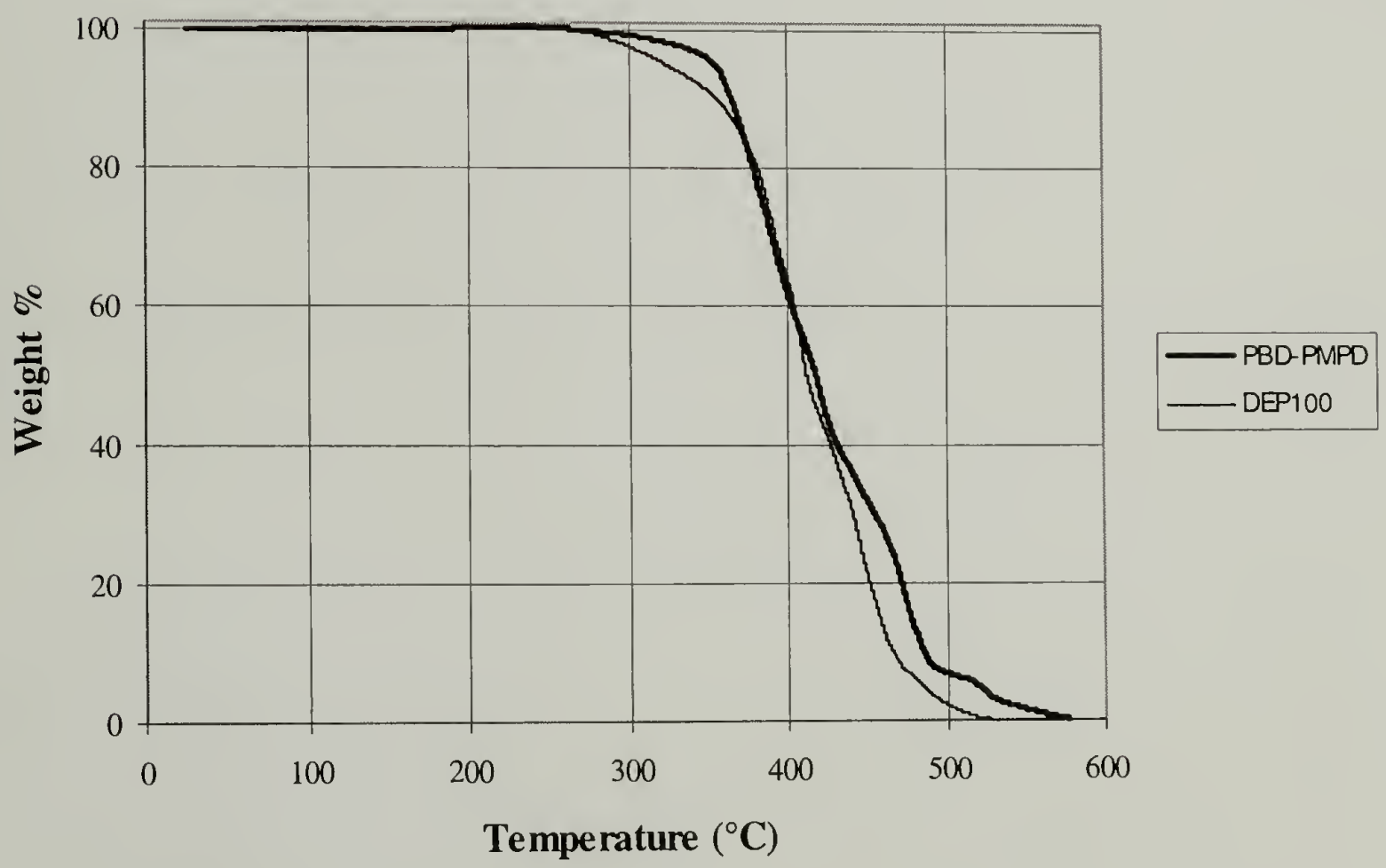

Figure 4.5 TG Plot of PBD-PMPD and DEP100. (Scan rate of 10°C/min)

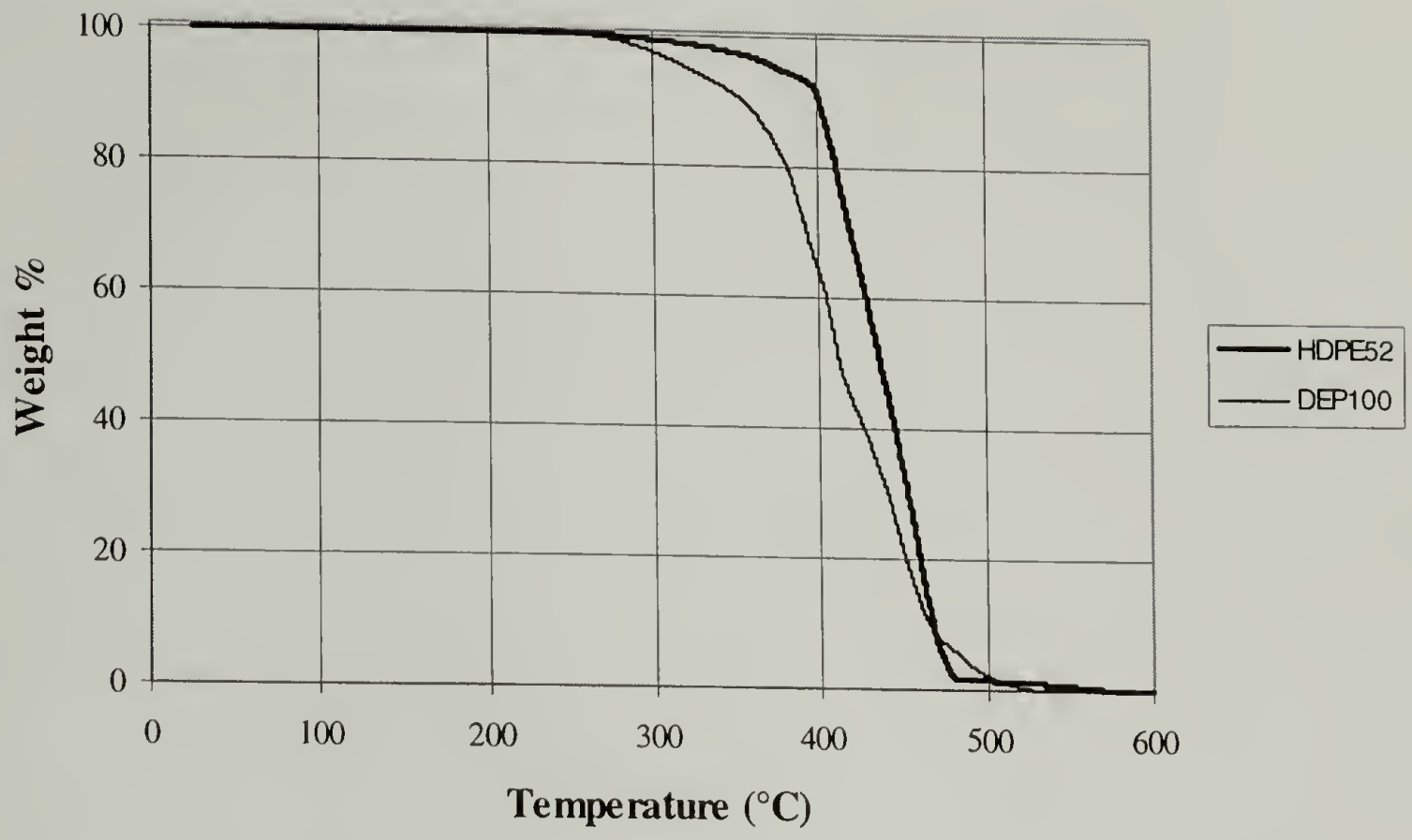

Figure 4.6 TG Plot of HDPE and DEP100. (Scan rate of 10°C/min)

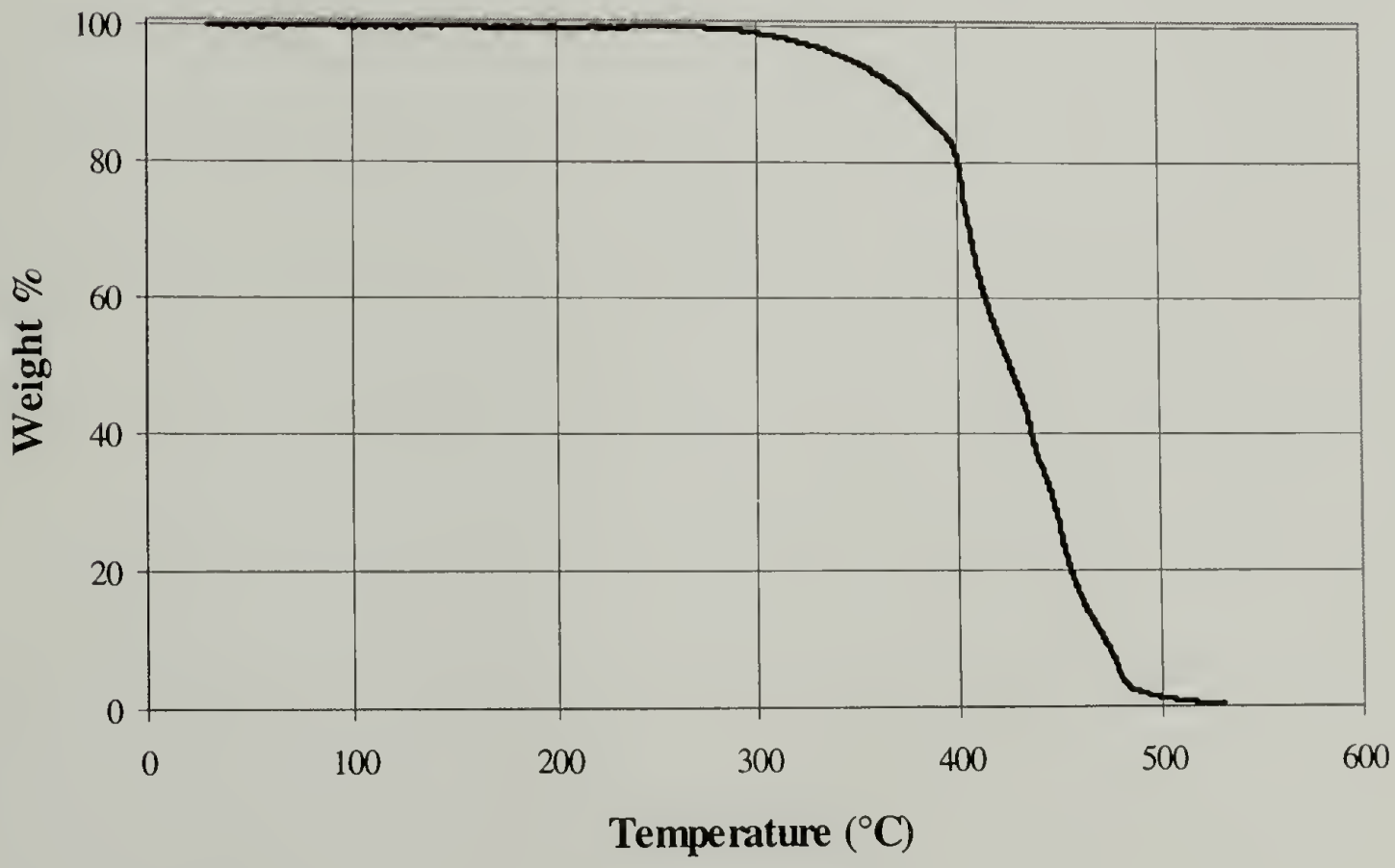

Figure 4.7 TG Plot of *d*-DEP38. (Scan rate of 10°C/min)

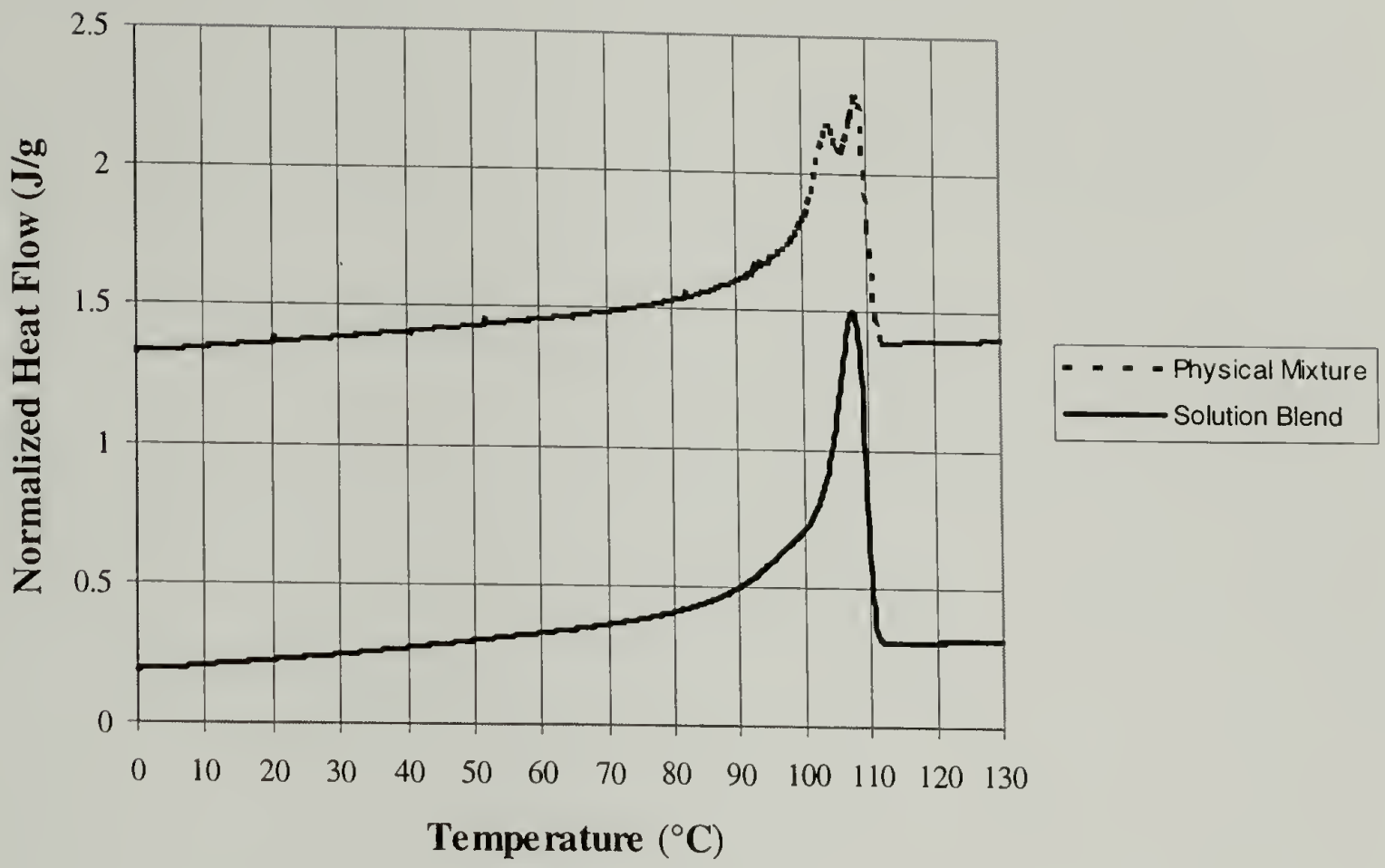

Figure 4.8 DSC Heating Curves (10°C/min) for Physical Mixture and Stand Cast Solution Blend of 50% DEP100/ 50% PE20 (by wt.)

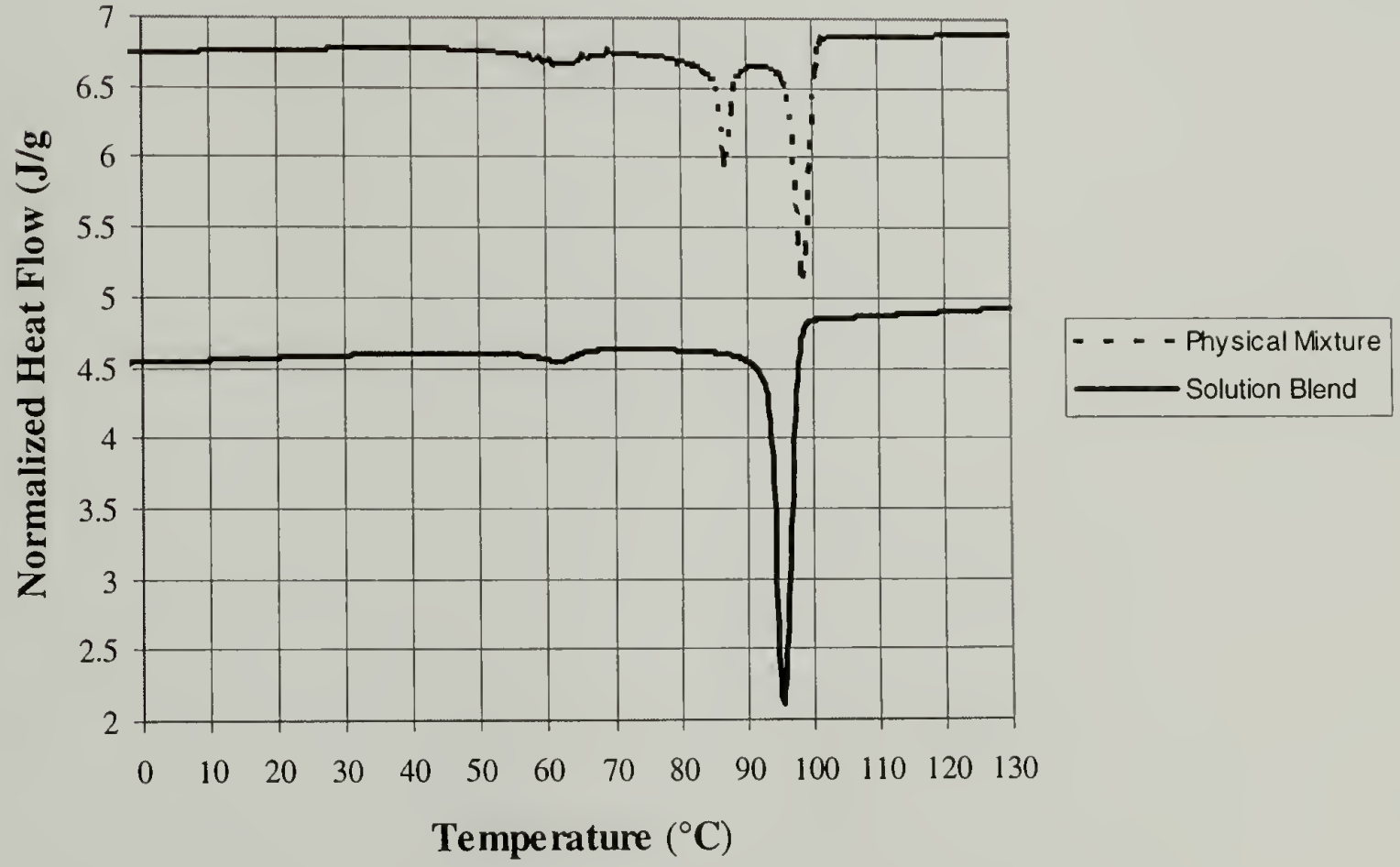

Figure 4.9 DSC Cooling Curves (10°C/min) for Physical Mixture and Stand Cast Solution Blend of 50% DEP100/ 50% PE20 (by wt.)

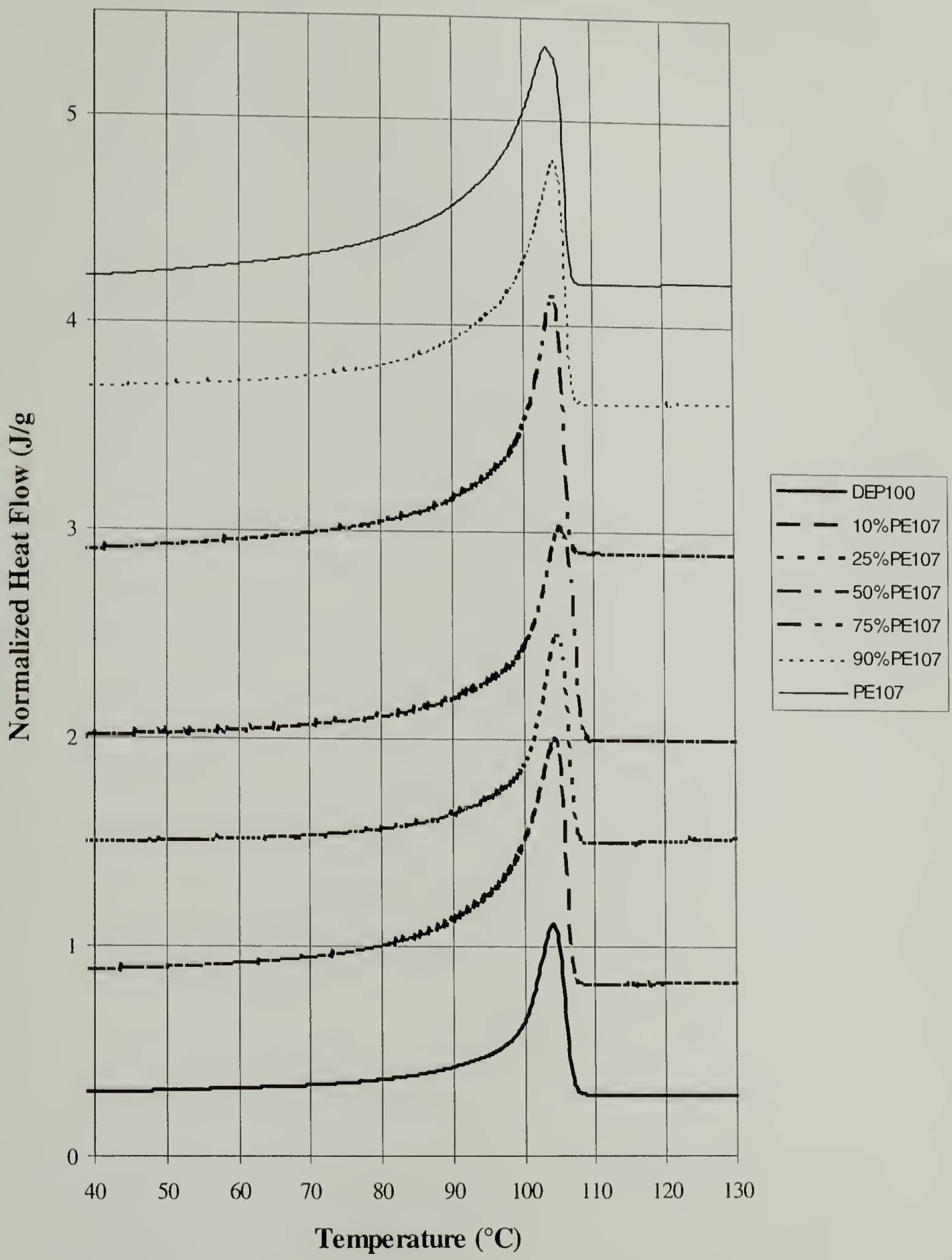

Figure 4.10 Composite Heating Curves for Stand Cast Blends of DEP100/PE107. (Scan rate of 10°C/min)

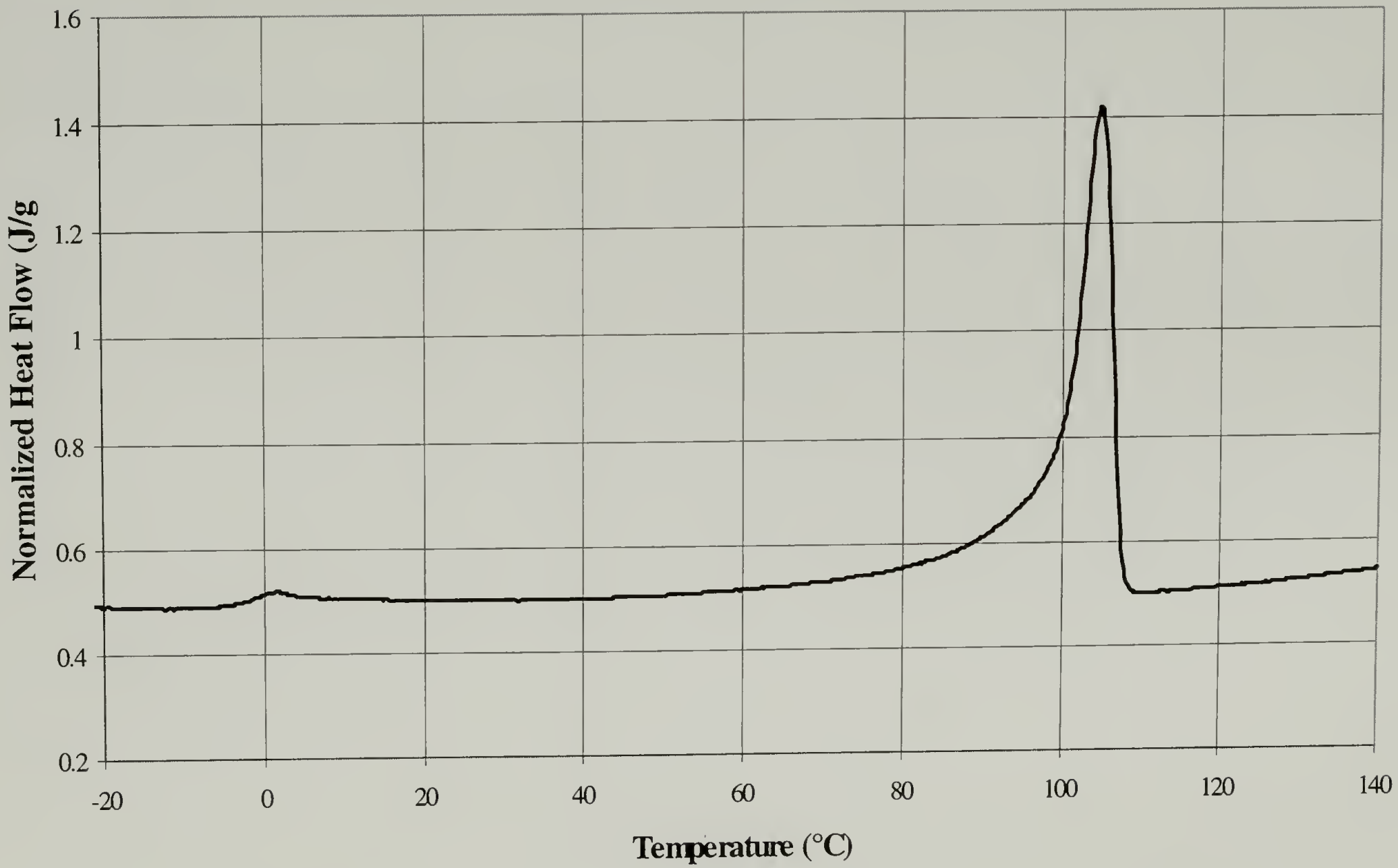

Figure 4.11 DSC Heating Curve (10°C/min) of 90% DEP100/ 10% PE107.

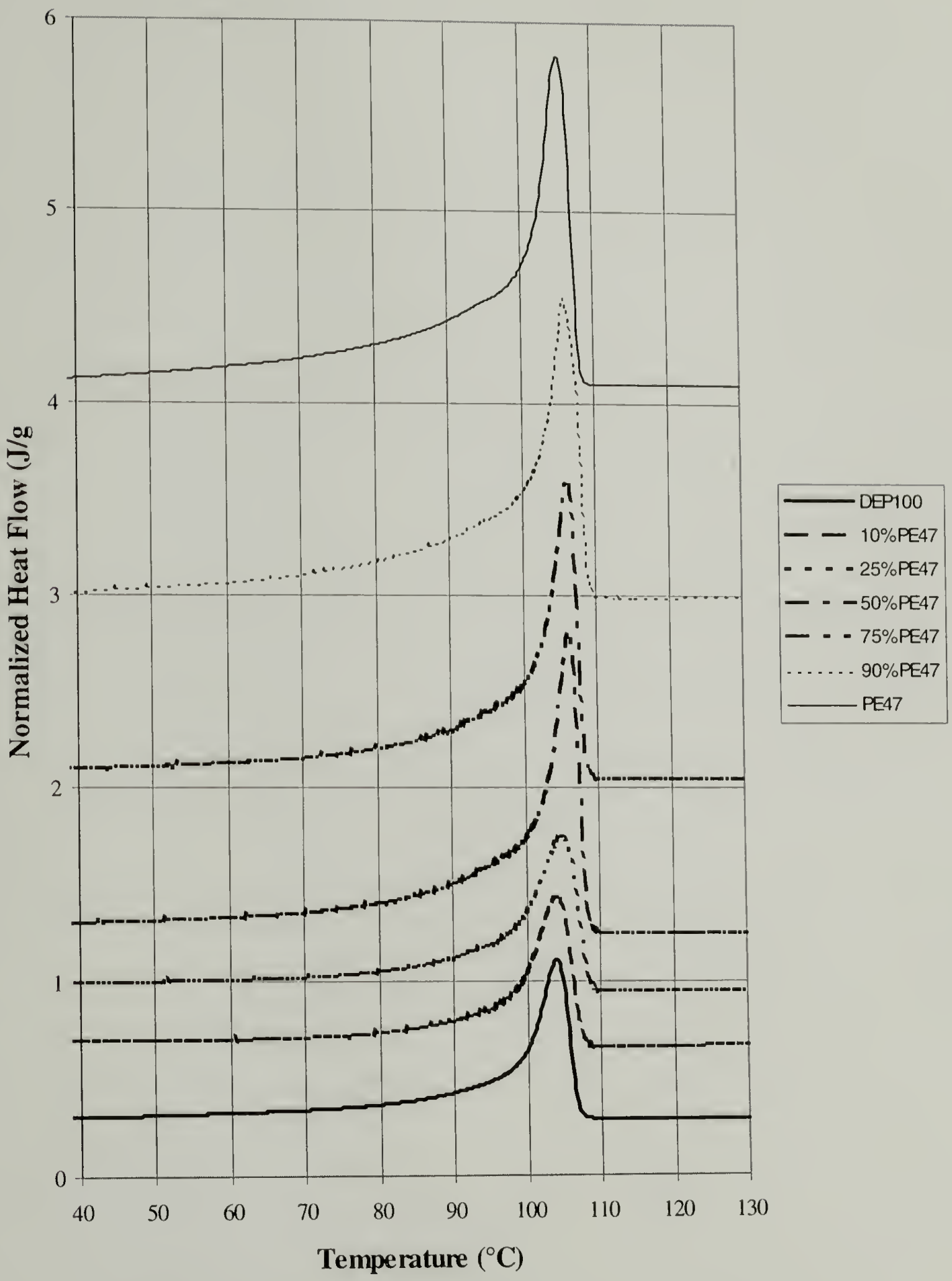

Figure 4.12 Composite Heating Curves for Stand Cast Blends of DEP100/PE47. (Scan rate of 10°C/min)

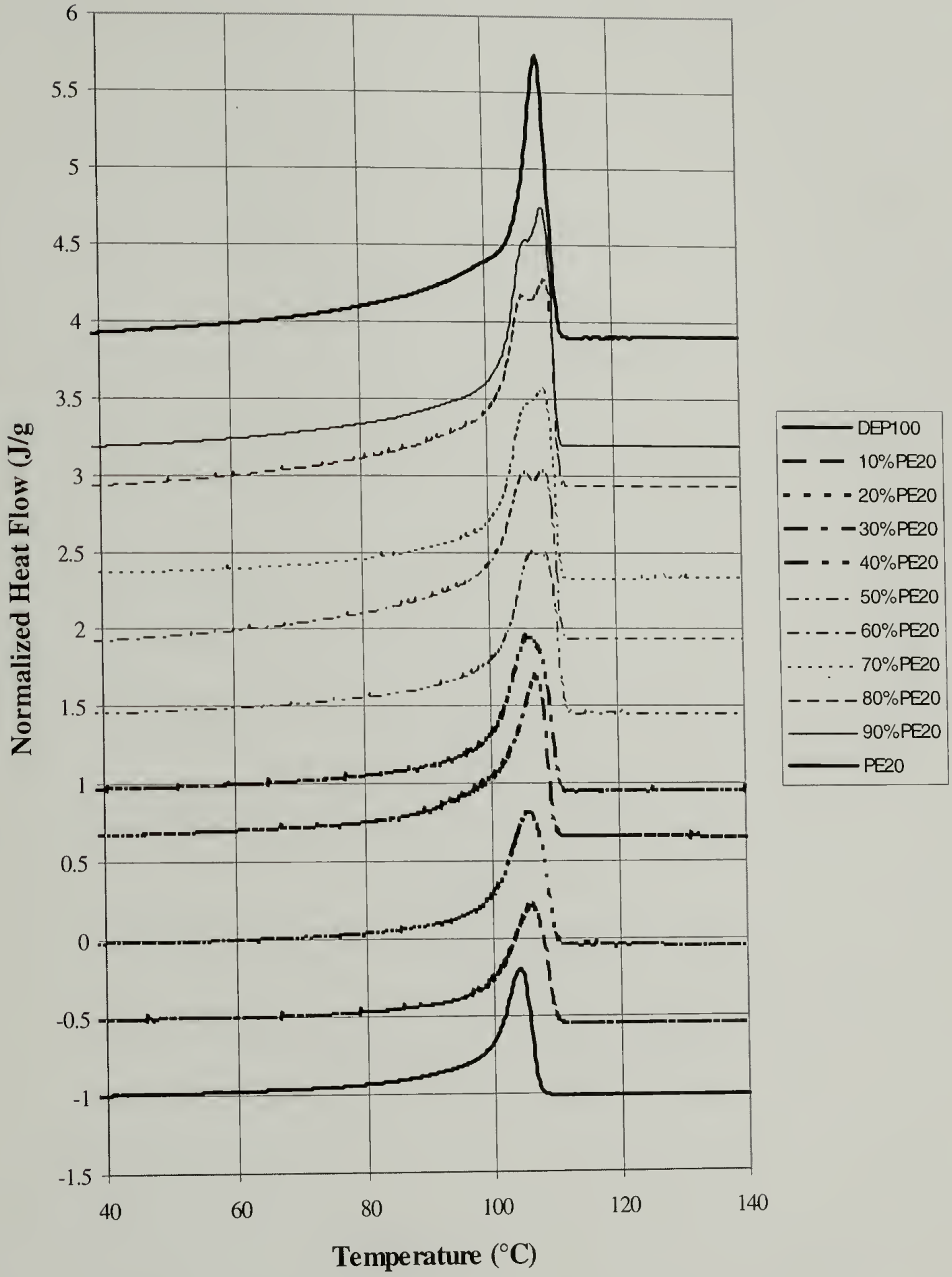

Figure 4.13 Composite Heating Curves for Stand Cast Blends of DEP100/PE20. (Scan rate of 10°C/min)

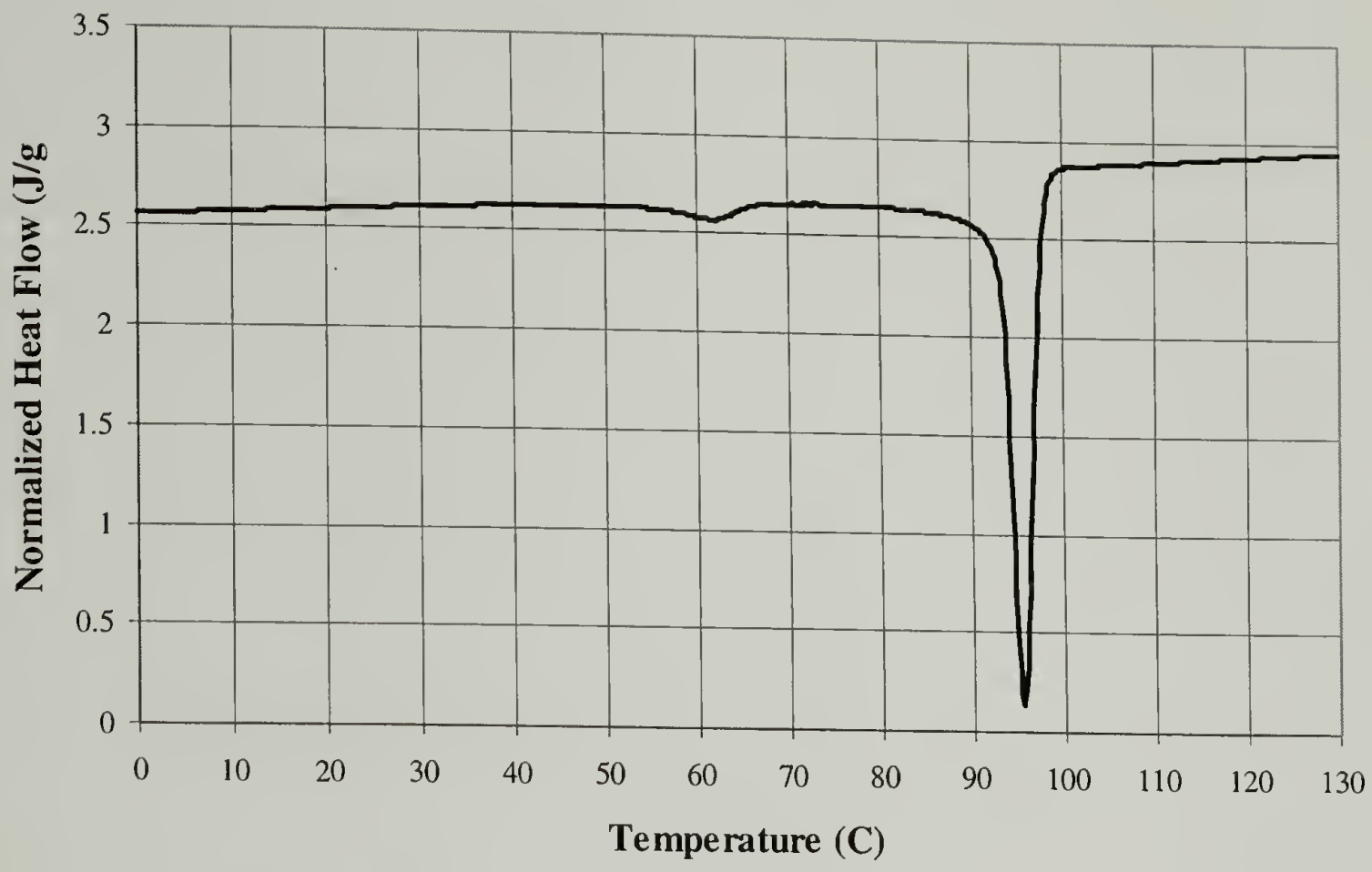

Figure 4.14 DSC Cooling Curve (10°C/min) for Stand Cast 50% DEP100/ 50% PE20 Illustrating Primary and Secondary Crystallization.

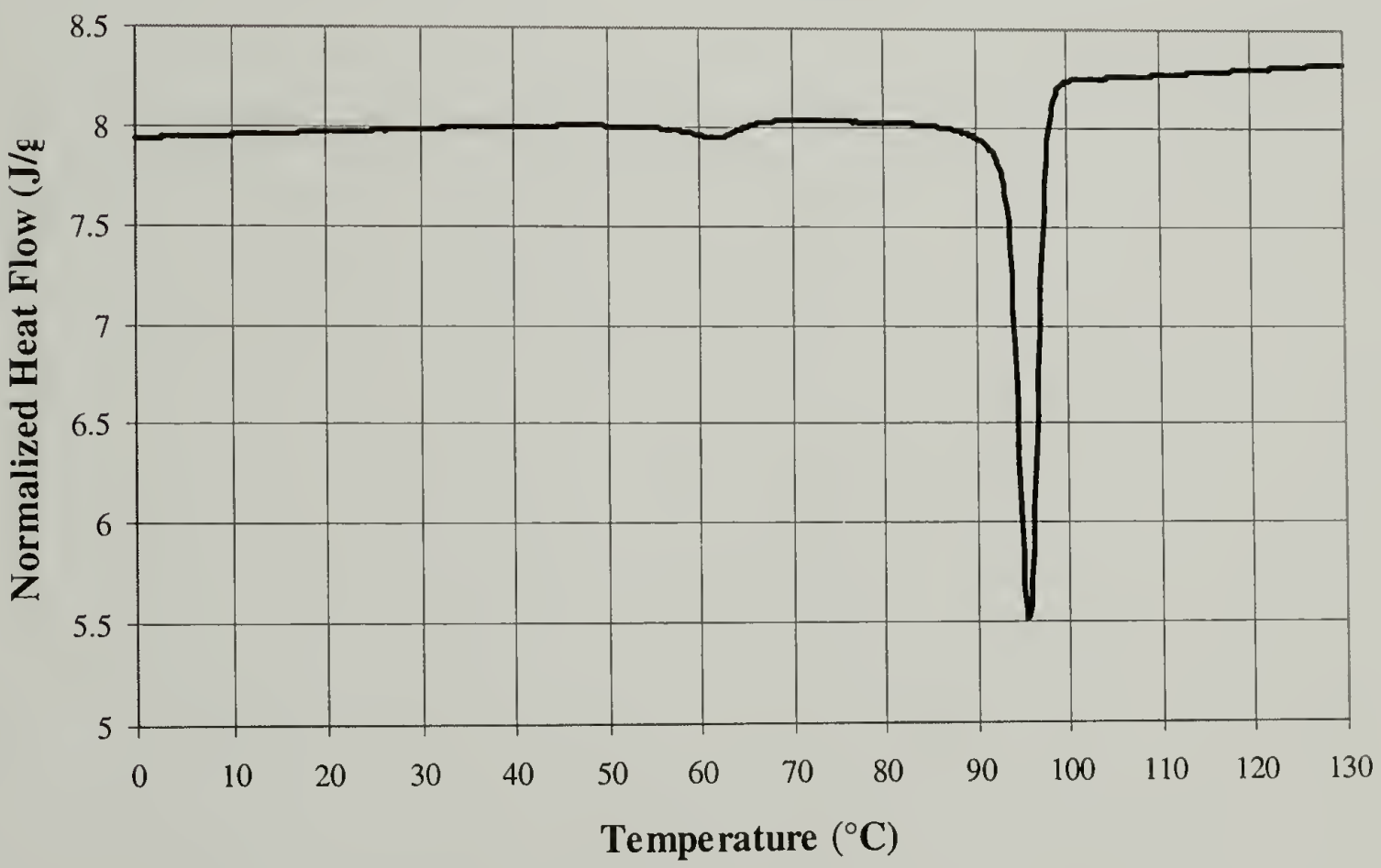

Figure 4.15 DSC Cooling Curve (2°C/min) for Stand Cast 50% DEP100/ 50% PE20 Illustrating Primary and Secondary Crystallization of Spherulites.

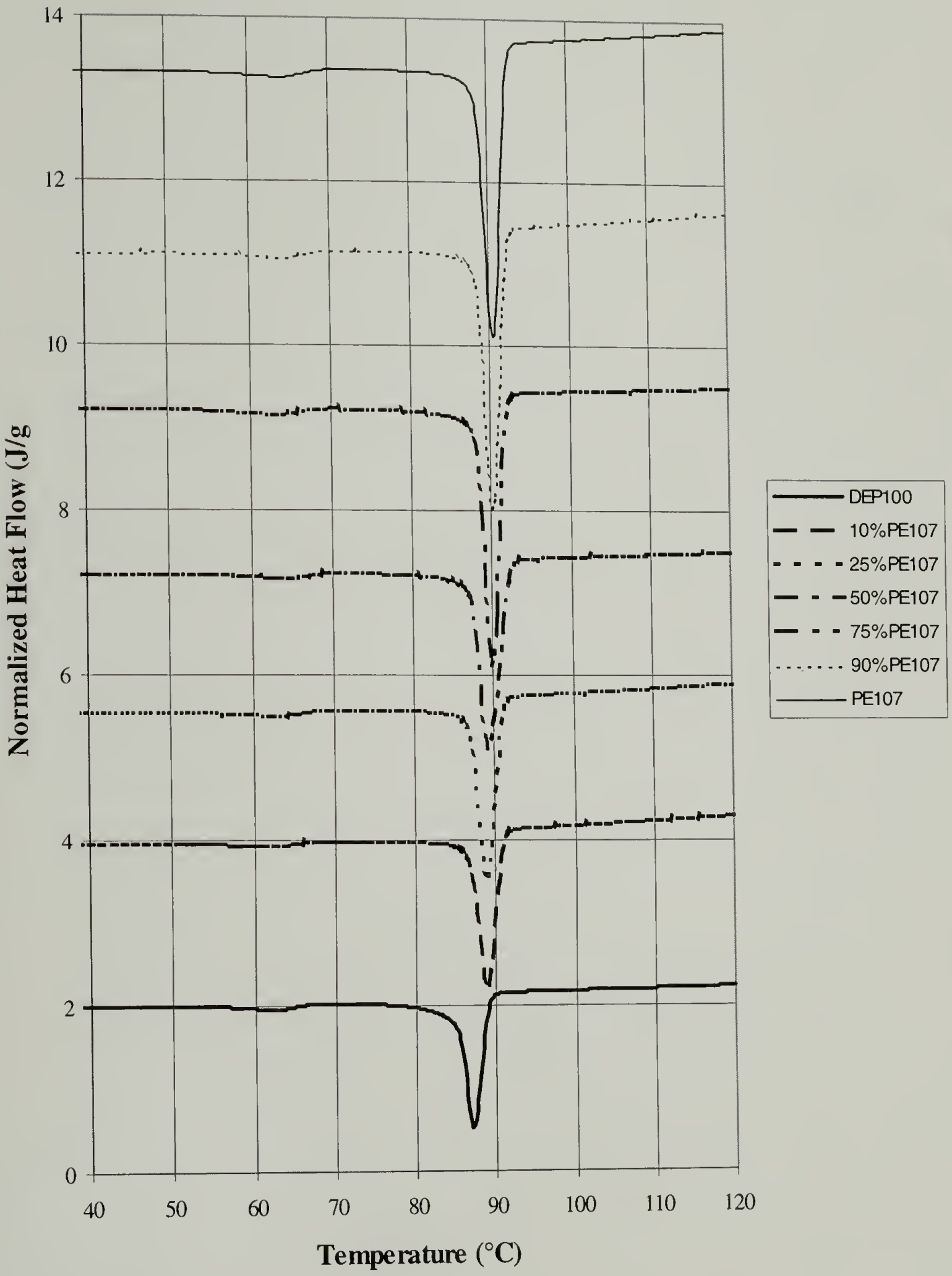

Figure 4.16 Composite Cooling Curves for Stand Cast Blends of DEP100/PE107. (Scan rate of 10°C/min)

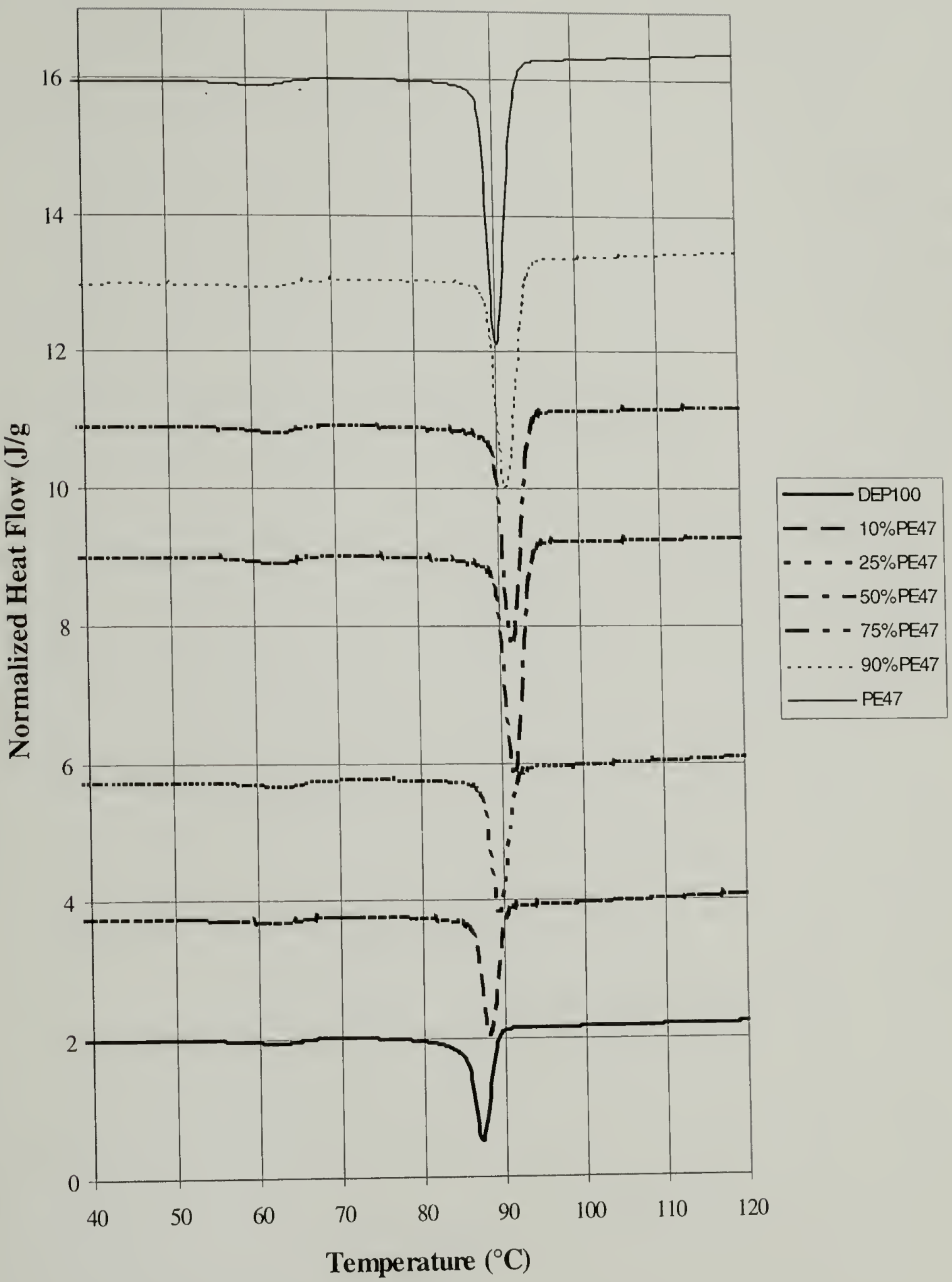

Figure 4.17 Composite Cooling Curves for Stand Cast Blends of DEP100/PE47. (Scan rate of 10°C/min)

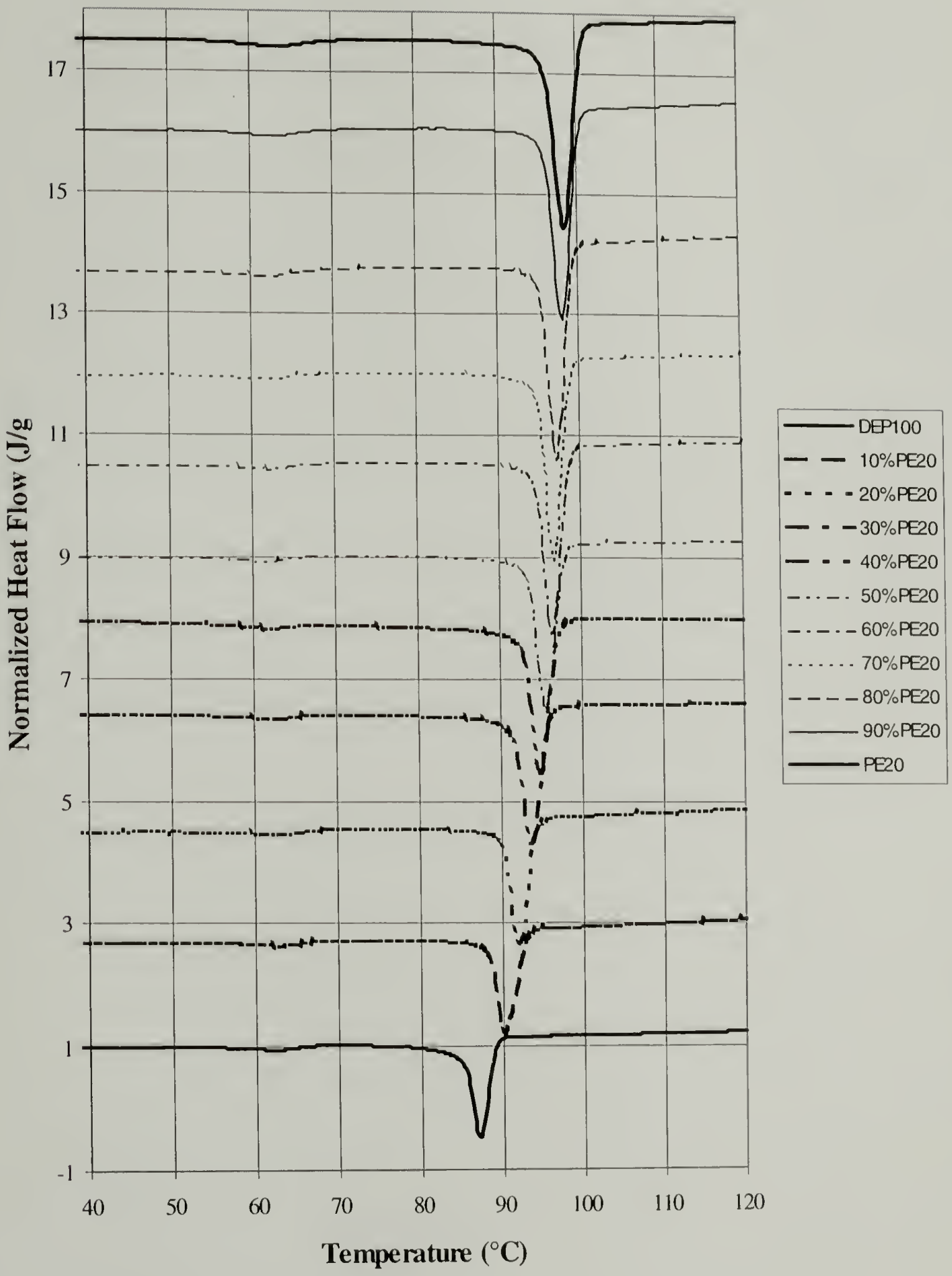

Figure 4.18 Composite Cooling Curves for Stand Cast Blends of DEP100/PE20. (Scan rate of 10°C/min)

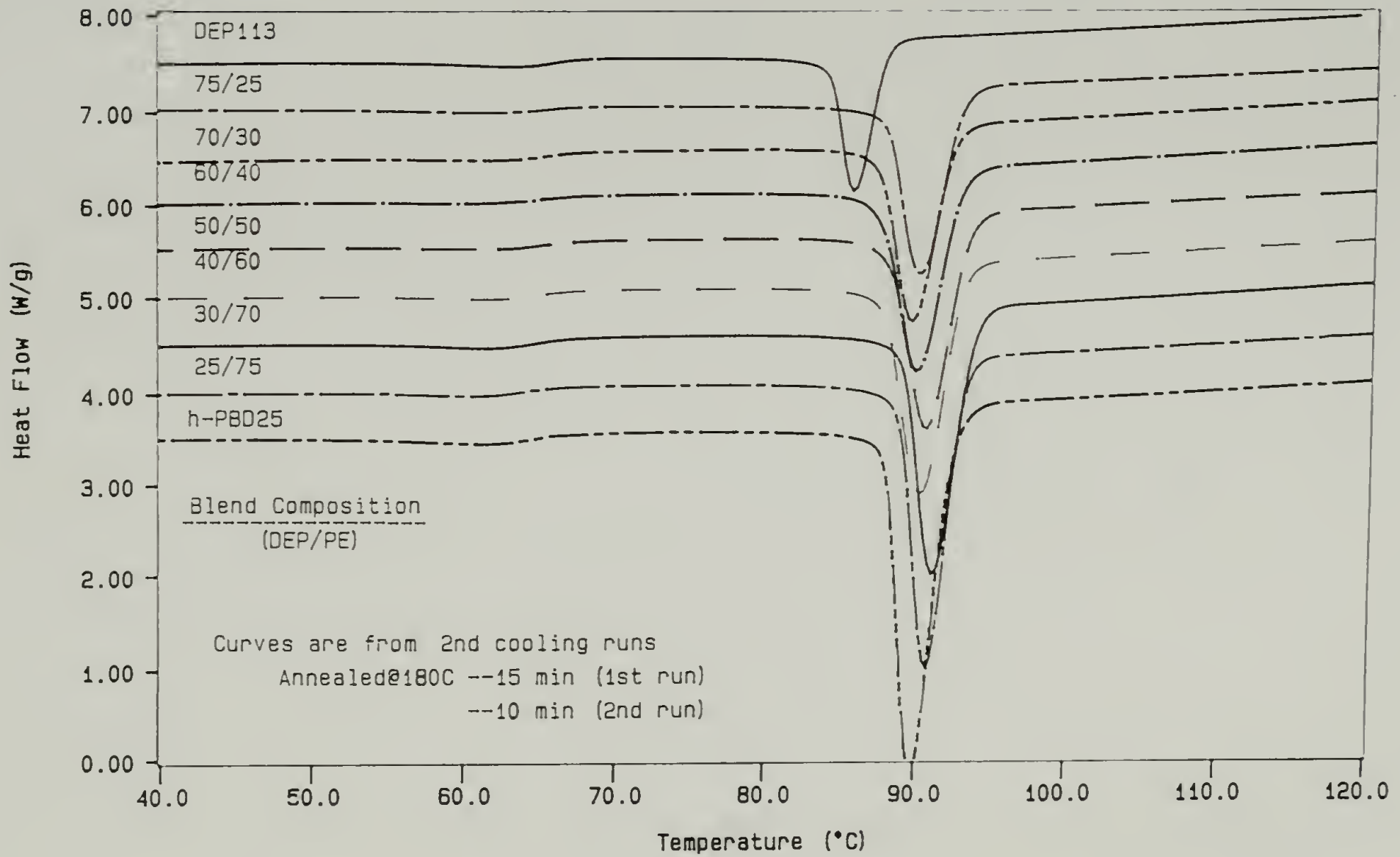

Figure 4.19 Composite Cooling Curves for Water Cast Blends of DEP113/PE25. (Scan rate of 10°C/min)

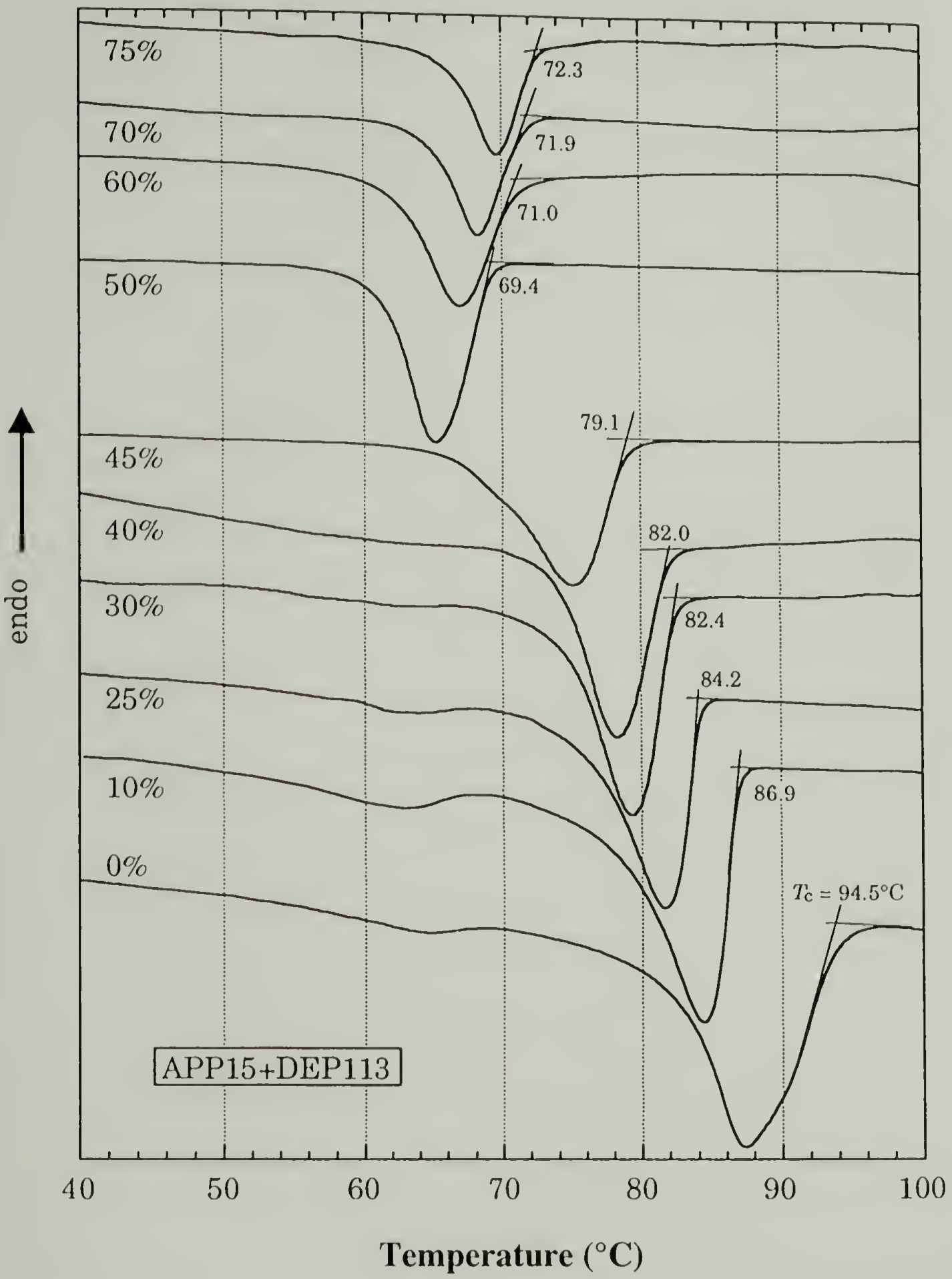

Figure 4.20 Composite Cooling Curves for Water Cast Blends of DEP113/APP15. (Scan rate of 10°C/min)

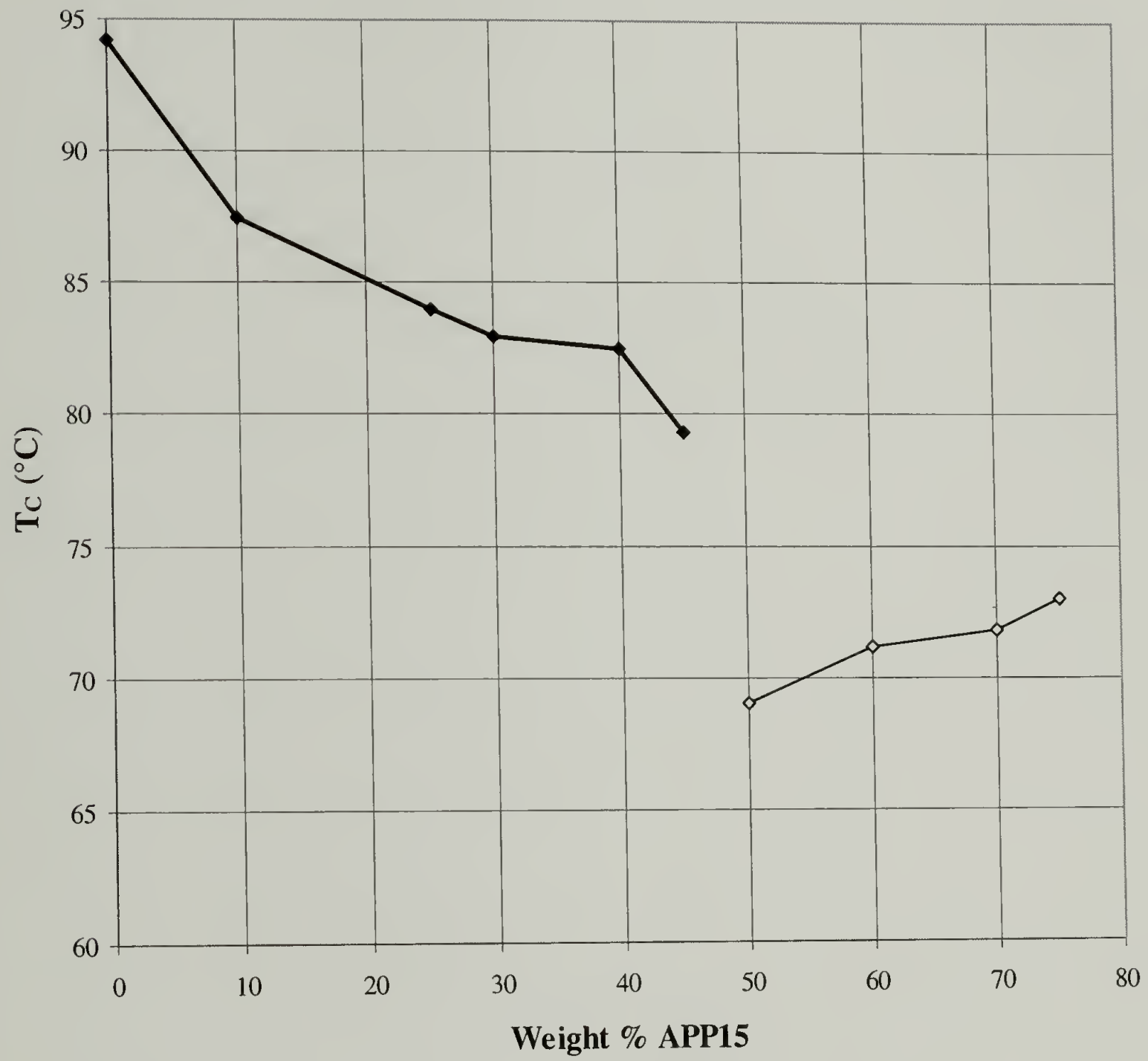

Figure 4.21 Plot of Crystallization Temperature versus Composition for Water Cast Blends of DEP113 with APP15.[3] (Cooling at 10°C/min)

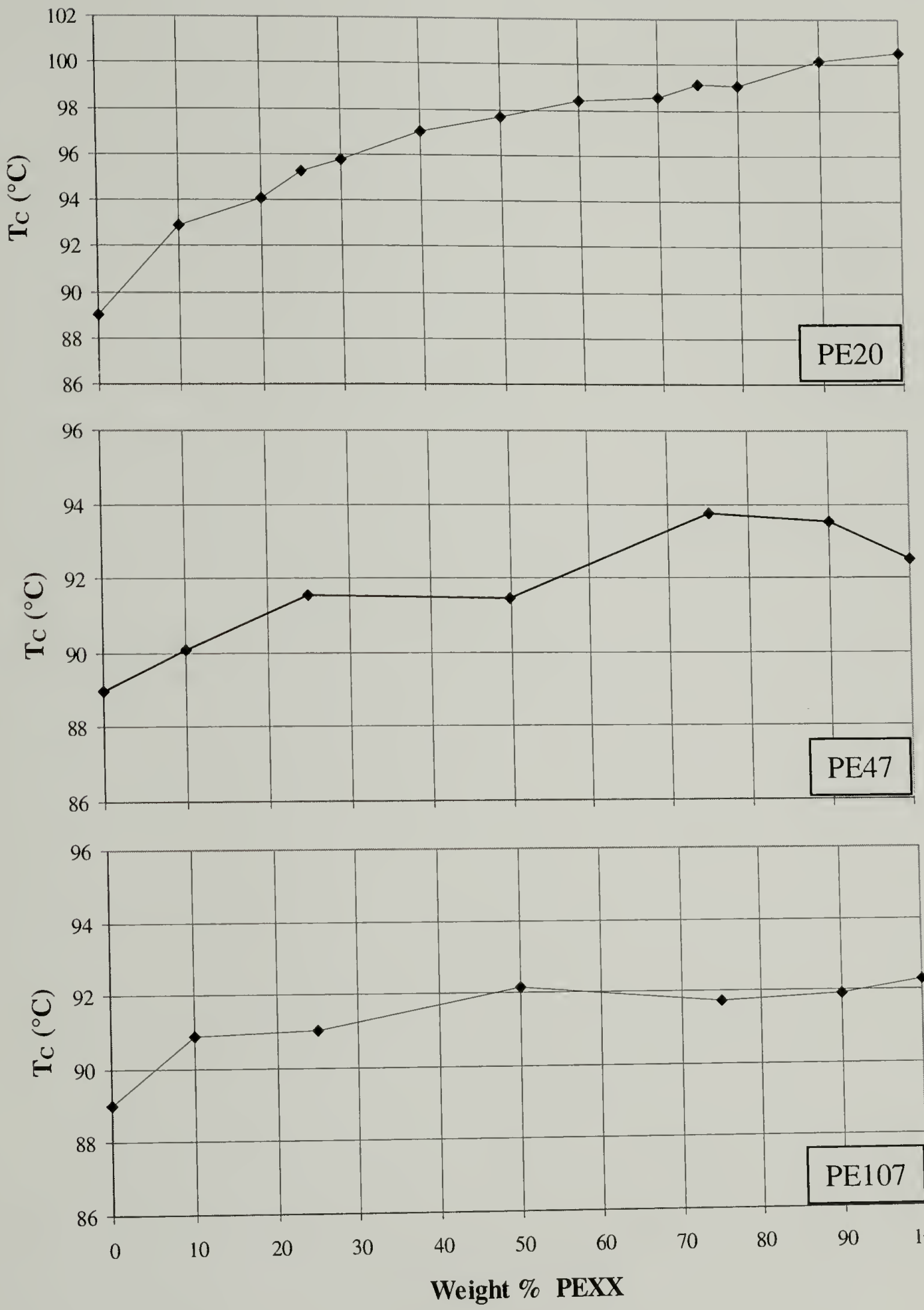

Figure 4.22 Plot of Crystallization Temperature versus Composition for Solution Cast Blends of DEP100 with PE20, PE47, and PE107.

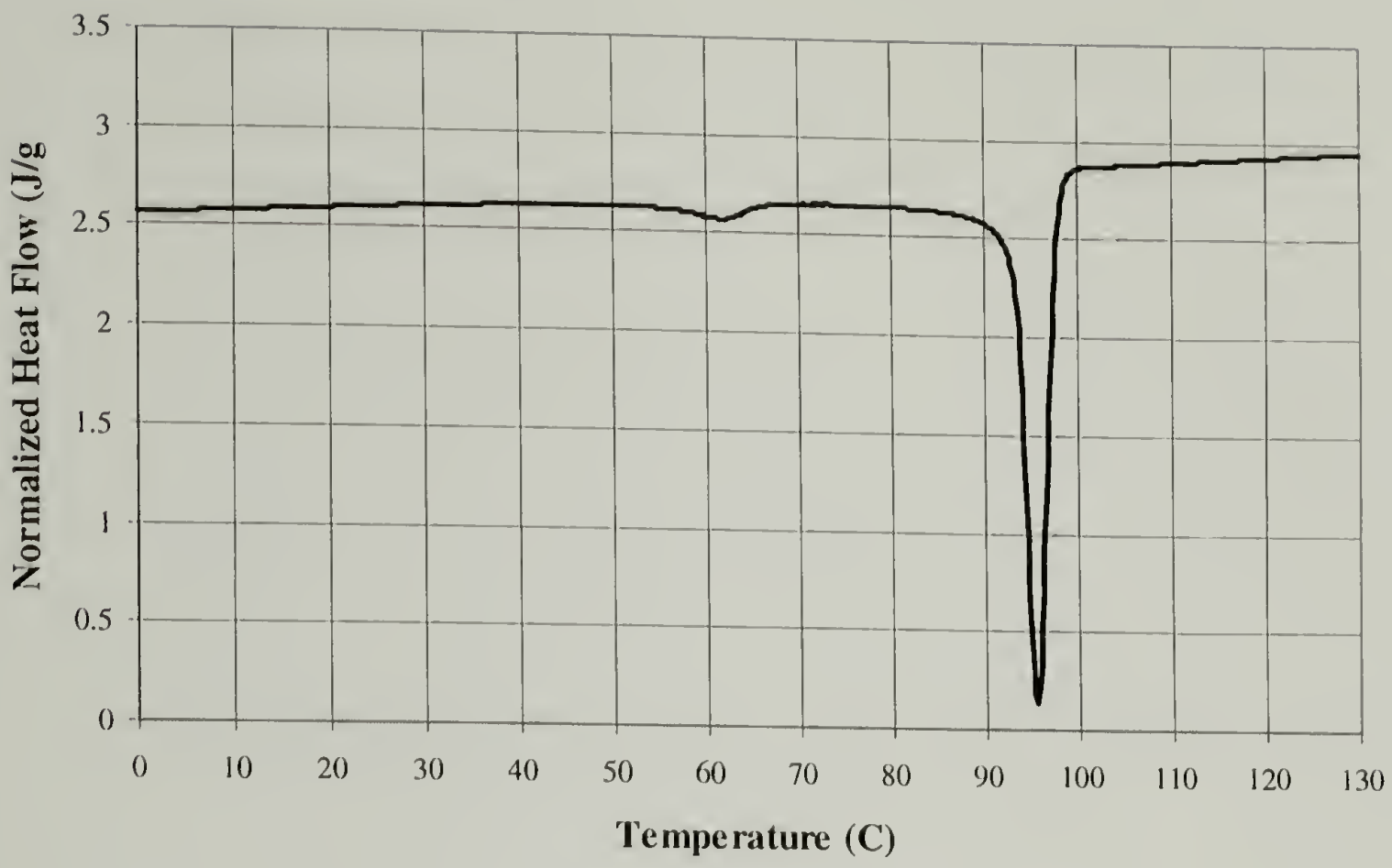

Figure 4.23 DSC Cooling Curve (10°C/min) for Stand Cast Solution Blend of 50% DEP100/ 50% PE20 (by wt.)

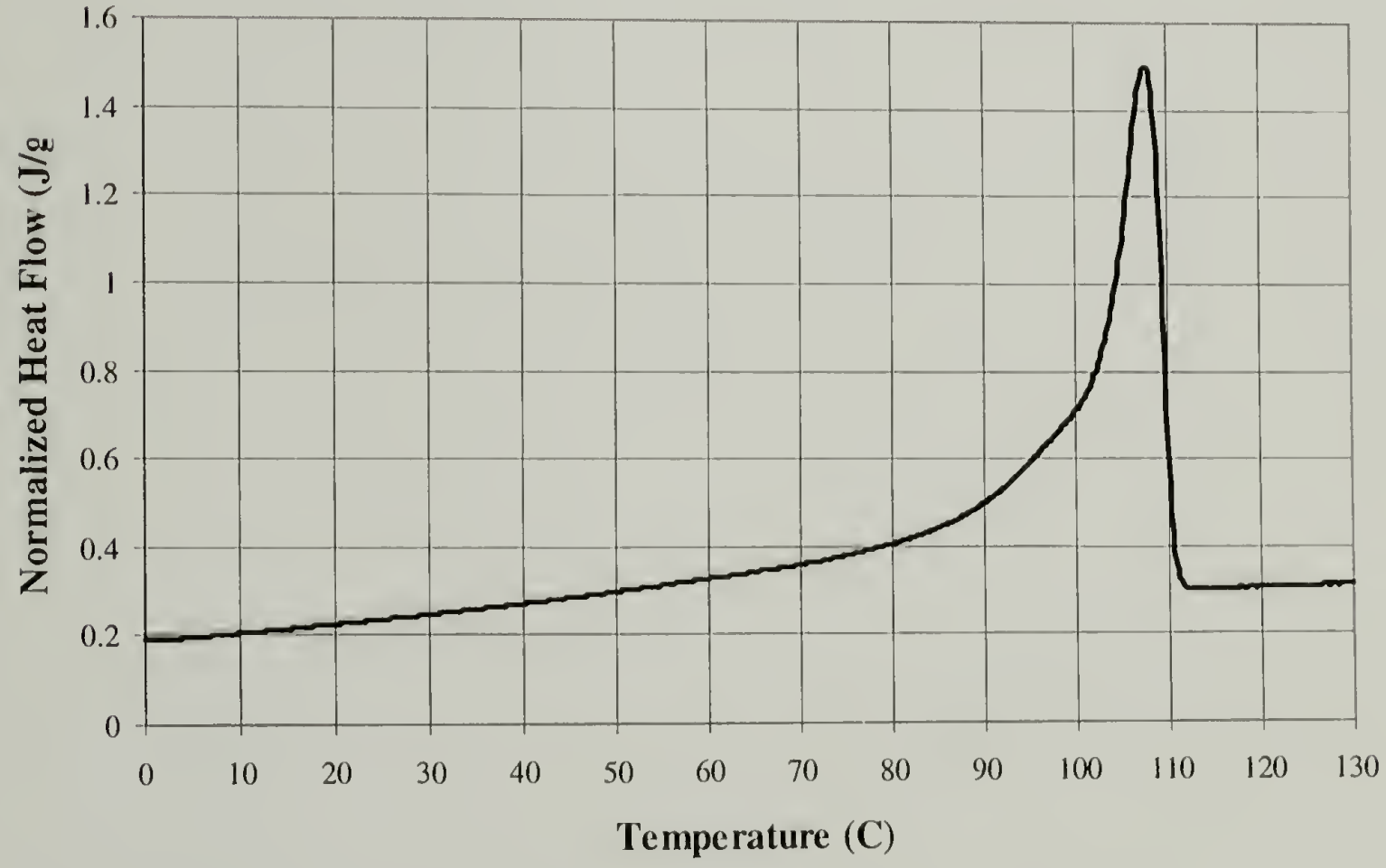

Figure 4.24 DSC Heating Curve (10°C/min) for Stand Cast Solution Blend of 50% DEP100/ 50% PE20 (by wt.)

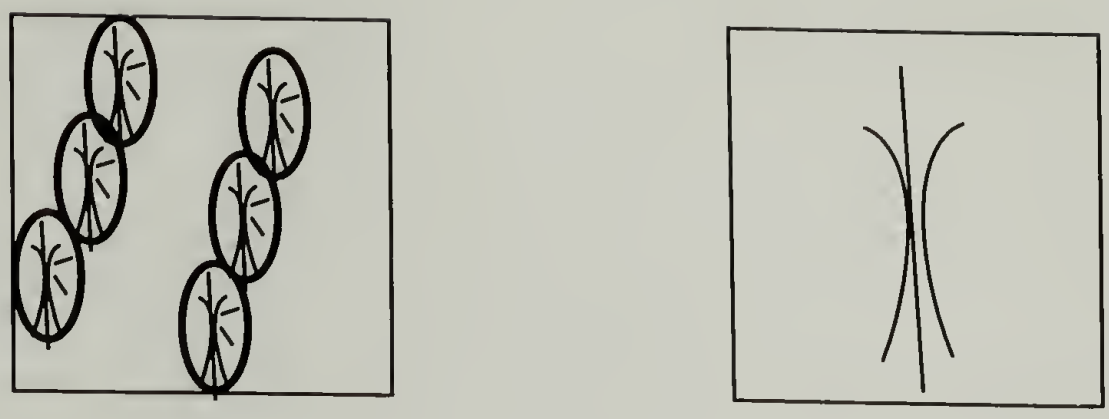

Figure 4.25 Drawing of Plausable Intermediate Structures between Microphase Separated and Spherulitic Morphologies.

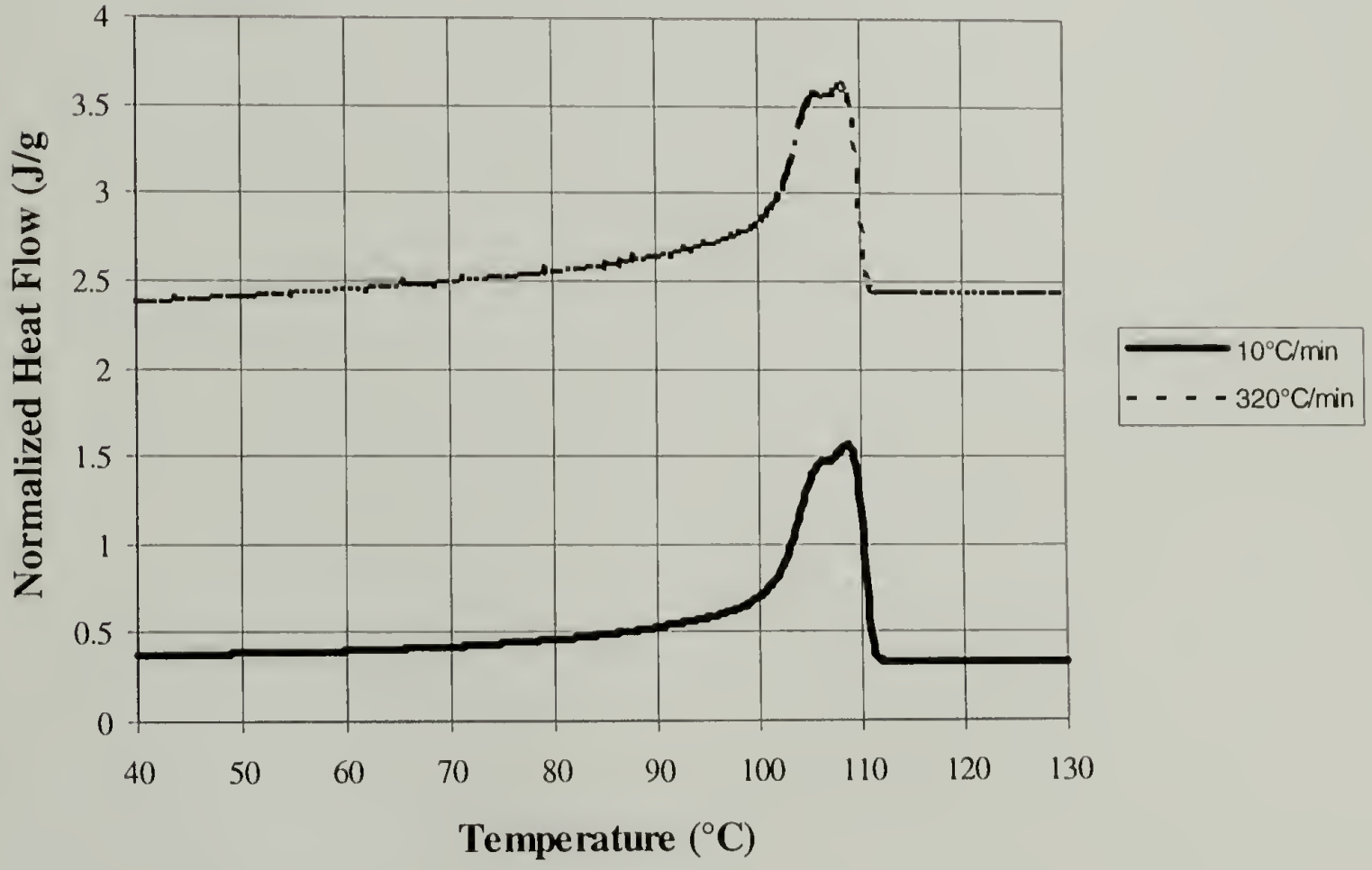

Figure 4.26 DSC Heating Curves for Stand Cast Solution Blend of 60% DEP100 and 40% PE20 (by wt.) After Cooling at 10°C/min and 320°C/min.

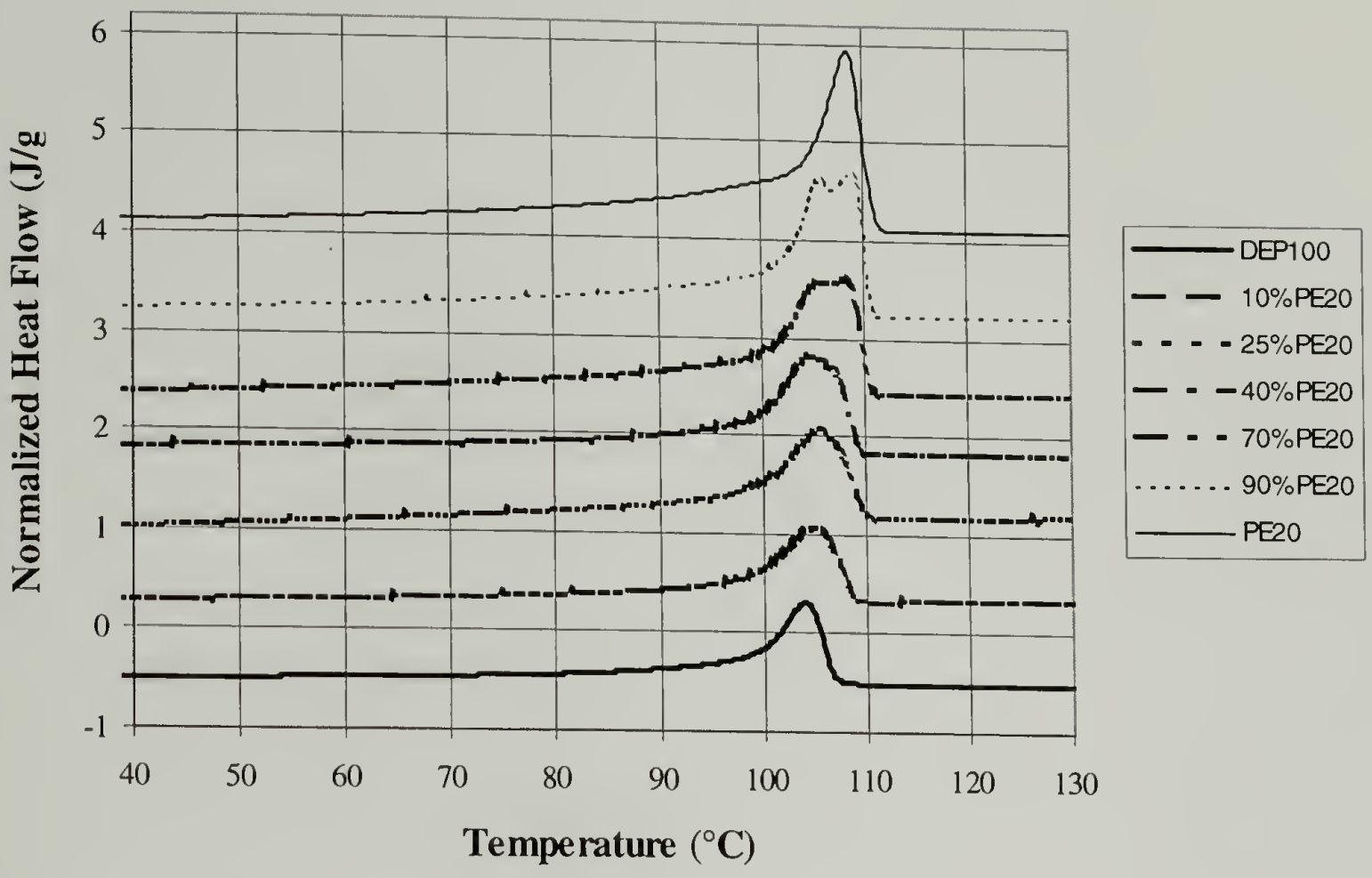

Figure 4.27 Composite Heating Curves for Stand Cast Blends of DEP100/PE20 After Cooling at 320°C/min.

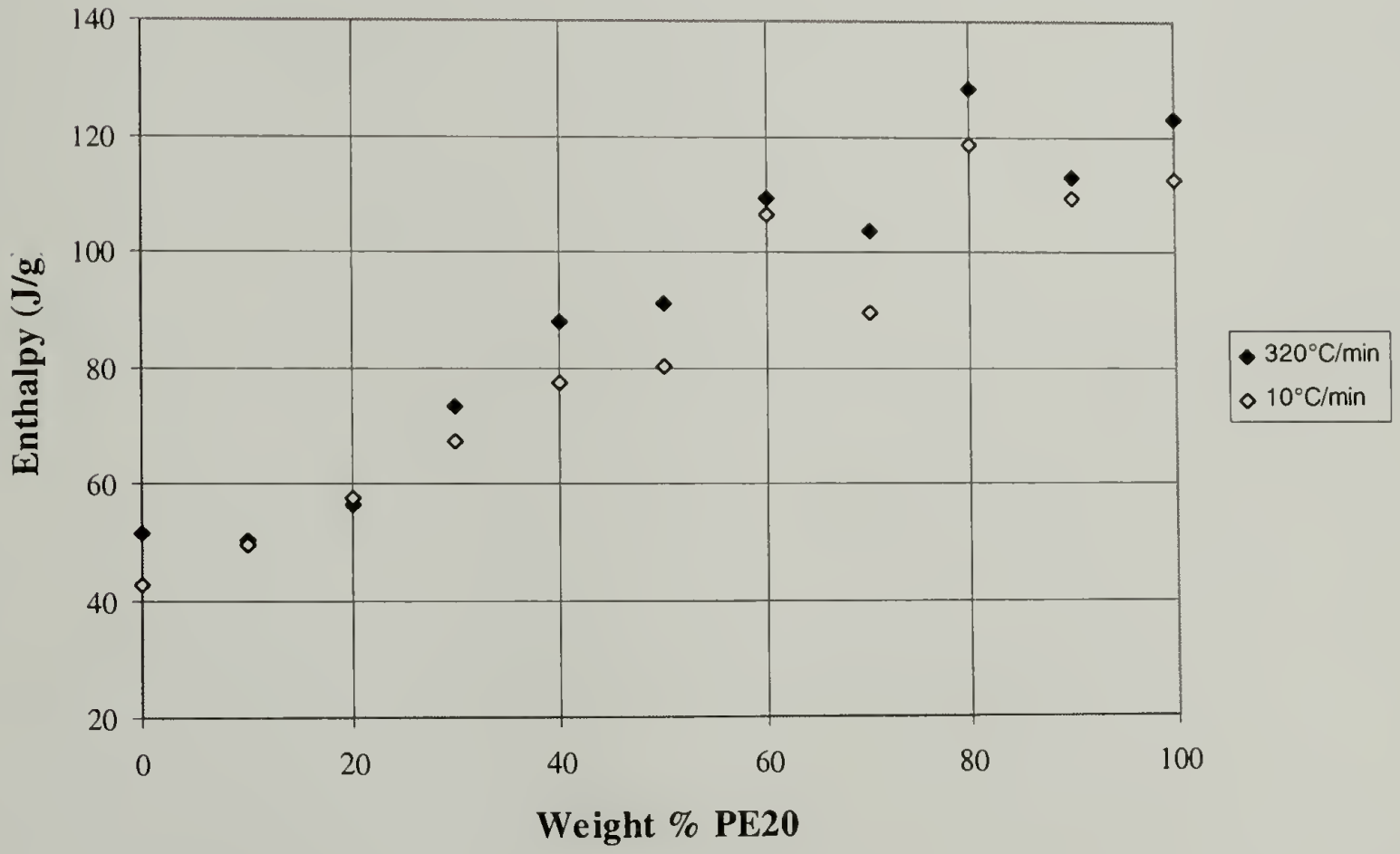

Figure 4.28 Plot of Enthalpies of Melting versus Composition for Blends of DEP100/PE20 after Cooling at 10°C/min (solid diamonds) and 320°C/min (open diamonds).

CHAPTER 5

MORPHOLOGICAL STUDIES

5.1 Introduction

The study of the morphology of diblock copolymers and their blends with homopolymers has been an important part of this field.[1] The ability of diblock copolymers to self-assemble and form periodic structures on the microscopic length scale, and the use of Transmission Electron Microscopy (TEM) to produce striking images of these structures, called microdomains, are the major reasons why this field of study has attracted so much attention.

Other techniques which are used to determine morphology in diblock copolymers and their blends are Scanning Probe/Atomic Force Microscopy (SPM/AFM), Small-angle X-ray Scattering (SAXS), and Small-angle Neutron Scattering (SANS). The research groups of Hashimoto[2] and Bates[3] have extensively used SAXS to investigate diblock morphology, while those of Russell[4], Wignall[5], and Lohse[6] have used SANS. An advantage of SAXS and SANS is the ability to determine the morphology of the microphase separated state in the melt.[7] However, SANS has the distinct disadvantage that it must be carried out at a neutron source, which are limited both in number of sources and in the availability of beam time. AFM has attracted several researchers[8-10] because of its lack of complicated sample preparation and its relative ease of use as compared to TEM.

Recently, the study of the microphase separated state in copolymers has moved to a new level of interest since the understanding of the chemistry of living anionic synthesis

has allowed many novel architectures to be produced. At the forefront of this synthetic work are the groups of J. Mays at University of Alabama-Birmingham and of N. Hadjichristidis at the University of Athens (Greece), who have introduced such architectures as "pi", "H", "mikto-arm" star, and "vergina-star" copolymers.[11-14] (See Figure 5-1 for drawings of these structures.) Some of these structures have produced novel architectures, such as the "randomly oriented worms" and "folded lace" lamellae which are shown in Figure 5-2.[15]

The majority of work to date has centered around the use of entirely amorphous systems.[2-11] Since several commercial polymers are semicrystalline, it would be interesting to study systems that include this important phenomenon. Unfortunately, the driving force of crystallization is quite high and would tend to dominate the microphase separation phenomenon unless special precautions were take to prevent it from doing so. Early studies used SAXS to understand the effect of crystallization on the morphology of neat diblock copolymer of PE-PS,[16] PE-PEB,[17] and Poly(ε-caprolactam-butadiene).[18]

It was previously found for the symmetric crystalline amorphous diblock copolymer, poly(ethylene-*at*-propylene),[19] that annealing of the copolymer in the melt for extended periods of time followed by quenching of the melt in liquid nitrogen prevented the large-scale crystallization of the polyethylene segments and preserved the microphase separated lamellae. It was also found that the polyethylene blocks crystallized in the confines of the lamellar planes. The presence of the crystallites were beneficial for electron microscopy because they provided sufficient mass thickness and diffraction contrast that images could be observed without heavy metal staining. Blending with

additional amorphous component resulted in phase behavior similar to that observed in entirely amorphous systems.

Another study investigated a series of hydrogenated 1,4-polybutadiene/1,4-polyisoprene and 1,4-polybutadiene/1,2-polybutadiene symmetric and asymmetric diblock copolymers in an attempt to understand the effect of crystallization on the morphological and crystallization kinetics behavior of neat diblock copolymers.[20] It was found that as the block asymmetry of the copolymer tended toward a larger PE block, the increased driving force for crystallization outweighed the combination of rapid cooling with liquid nitrogen and microphase separation and forced the morphological diagram (Figure 1-4) to become skewed—requiring more block asymmetry to incur order-order phase transitions than normal. Therefore, copolymer compositions which would normally have a cylindrical morphology (in the melt) were found instead to have lamellae upon rapid cooling to room temperature. Isothermal crystallization was also performed to evaluate the effects of crystallization and asymmetry on the kinetics of crystallization. Using Avrami theory it was found that the crystallization always occurred in the form of nucleation and growth of spherulites (i.e. the Avrami exponent, n, was always equal to three).

A useful method for displaying morphological data of diblock copolymer blends is the morphological diagram.[21] As was explained in the first chapter, the morphological diagram relates the three important variables—composition, molecular weight ratio, and morphology—in a graphical manner. (see Figure 1-4) This utility of plotting blend morphology in this manner is that transitions may be viewed as a function of the ratio of polymer chain lengths, which is desirable for planning experiments.

The objectives of this work were to determine whether a microphase separated morphology could be retained upon quenching from the melt to room temperature, and if so, whether the morphology would follow the trends observed by K. Sakurai for blends of DEP + APP[19] or the behavior seen by A. Ryan for asymmetric crystalline-amorphous diblock copolymers.[20] Because the work of Ryan, et al.[20] indicated that when PE was the majority component, the crystallization kinetics always followed the pathway toward formation of spherulites, isothermal crystallization studies were not performed as part of this research.

In the next section the sample preparation and instrument operating conditions are explained. Then, the results of the TEM study on selected blends at various stages of processing are evaluated and discussed. Finally, the TEM results and the conclusions to the stand casting solution blending work are summarized.

5.2 Experimental

Selected solution-cast blends (for blend preparation, please see Chapter 3) were sectioned by cryomicrotoming at a knife temperature of -125°C and a sample temperature of -110°C using a Leica Model UCT microtome with attached EMFCS cryostat box using liquid nitrogen as the coolant. A schematic relating the various processing techniques which were used to obtain samples is shown in Figure 5-3. Ultrathin slices (30nm) were cut from bulk samples using a diamond knife at a cutting speed of 0.6mm/min. The samples were cut into a well behind the knife edge containing *n*-propanol (J. T. Baker) and were collected on uncoated copper grids (Electron Microscopy Sciences), which were moved to a position under the floating section and slowly raised (so that the thin film

would not float off of the grid along with the displaced *n*-propanol). Grids were allowed to dry overnight at ambient conditions. Samples were used without staining since mass thickness and diffraction contrast were sufficient to obtain good images. Sample grids were initially screened for the quality of the sections on the grid. A 1% (vol/vol) suspension of 102nm polystyrene latex spheres (Electron Microscopy Sciences) in distilled water were added to those possessing reasonably good slices to serve as internal standards during imaging. After adding the suspension the samples were dried in a vacuum oven overnight at room temperature and stored in desiccators prior to examination. TEM was performed on blend samples using a JEOL 100CX electron microscope in the bright field mode with an accelerating voltage of 100kV.

5.3 Results and Discussion

Due to time constraints, only blend compositions which were important in determining whether microdomains were preserved after the orientation/annealing process were sectioned and imaged using TEM. Originally, the neat diblock copolymer which was cast using the stand casting technique exhibited random lamellae, as is shown in Figure 5-4. After the orientation/annealing, lamellae were seen (Figure 5-5) which were well oriented along the shear direction of the orientation die. The orientation die, which was also used for some of the sample in the previous blending study with DEP/APP, is shown in Figure 3-7. The other samples which were microtomed and imaged were 70wt% DEP100/30 wt% PE20, 60wt% DEP100/40wt% PE20, 25wt% DEP100/75% PE20, 75wt% DEP100/25% PE47, and 50wt% DEP100/50wt% PE47. All of the samples were cut perpendicular to the shearing direction. For the blends which

showed macrophase separation, the lack of a preferred orientation indicated that the subsequent melt-annealing removed all traces of the pressing procedure.

The 70/30 blend of DEP100 and PE20 displayed an undulating lamellar morphology (Figure 5-6) which was less oriented than the pure diblock. The blend of 60wt% DEP100 and 40wt% PE20 showed an unusual morphology, as shown in Figure 5-7. This combination is located well within the range of compositions which should exhibit a cylindrical morphology if the blend were amorphous. However, this microstructure possesses a random nature—consisting of both low aspect-ratio cylinders and spheroids. This morphology will be termed the "disordered microphase". Therefore a phase boundary must exist between the stand cast blends consisting of 60wt% and 70wt% DEP100. The 25/75 blend for the same component polymers (Figure 5-8) showed a macrophase separated morphology where spherical domains would normally be predicted. Thus, another phase boundary must be located somewhere between 60wt% and 25wt% DEP100 which defines the microphase-macrophase transition.

For the two blends of DEP100 and PE47 which were sampled, the blend with higher diblock content displayed a network structure as can be observed in Figure 5-9, as was expected for this composition. A TEM image from the second blend is shown in Figure 5-10. This blend was anticipated to have a morphology consisting of light-contrast random micelles (b-APP) against a black matrix of PE. In fact it shows clusters of light colored oval structures which are interpreted as random micelles within the oriented blend. The importance of this observation is that there is a change in morphology for the solution blends containing the medium molecular weight blend (DEP100/PE47) which is reflected in the DSC cooling data (at 10°C/min). Therefore, the shift in the location of

the crystallization peak is due to the formation of large isolated macrodomains from the network structure.

Based on the morphological diagram for amorphous-amorphous systems,[21] (Figure 1-4) it would be anticipated that order-order transitions should occur between 75vol% and 70vol% added h-PE (lamellae to cylinders) and between 50vol% and 40vol% added h-PE (cylinders to spheres). If one were to use the case of asymmetry in neat crystalline-amorphous diblock copolymers as a guide for predicting phase transitions,[20] one would expect morphological transitions to occur roughly between 40vol% and 30vol% added h-PE. From the micrographs of the selected blends sectioned for TEM, there is a transition from lamellae to the disordered microphase state which occurs at a composition between 30vol% and 40vol% PE20. There is also the microphase-macrophase transition which occurs somewhere between 40vol% and 75vol% PE20. For the blends which contained the medium molecular weight h-PE (PE47), the morphologies were more in line with those predicted by the morphological diagram in Figure 1-4. This indicates that our results are more in line with those of Ryan[20] for the blends with the low molecular weight h-PE, while the blends with PE47 exhibits results which are similar to those seen in amorphous systems. Yet neither case is entirely consistent with the behavior previously reported.

When the ratio of the molecular weights of the h-PE to b-PE, $M_{h\text{-}PE}/M_{b\text{-}PE}$, is small, the homopolymer is able mix with the like block of the copolymer and affect the microdomain structure in the melt according to the scheme shown in Figure 1-1. Upon cooling to ambient temperature, the difference in the crystallization temperatures of b-PE and h-PE resulted in the h-PE segments crystallizing slightly before the b-PE segments,

which was later reflected in the DSC heating curves of Figure 4-13. Because the h-PE chains solidified (crystallized) in a melt consisting of b-PE segments, the two PE components became immiscible and the microstructure was likewise affected. This increase in immiscibility upon cooling from the melt was reflected in a shift of the lamellar region to higher amounts of low molecular weight h-PE than would be observed for purely amorphous systems and macrophase separation occurring at a lower volume fraction than was seen for DEP/APP[19] and the asymmetric diblocks.[20] When the length of the h-PE chain is on the same size scale as the like block of the copolymer, miscibility of the h-PE chains is already low and was unable to mix with the b-PE chains to any great extent. Therefore, the effect of the crystallization of the h-PE on the molten microphase separated structure was greatly reduced since the lower miscibility led to macrophase separation at low amounts of h-PE.

5.4 Summary and Conclusions

Stand cast solution blends of the neat diblock copolymer, 70wt% DEP100/30 wt% PE20, 60wt% DEP100/40wt% PE20, 25wt% DEP100/75% PE20, 75wt% DEP100/25% PE47, and 50wt% DEP100/50wt% PE47 were oriented, annealed, and microtomed for TEM. For the blends which showed macrophase separation, the lack of highly elongated b-APP phases indicated that melt-annealing had removed the orientation caused by melt pressing.

The neat diblock and the 70/30 blend of DEP100 and PE20 displayed lamellar morphologies which was less oriented in the blend with h-PE. On the other hand, the 60/40 DEP100/PE20 blend exhibited a disordered microphase separated morphology where a cylindrical morphology would have been expected. The 25/75 blend for the same component polymers showed a highly macrophase separated morphology where spherical domains would be predicted based on amorphous blends.

Two blends of DEP100 and PE47 were microtomed and imaged by TEM. The blend with higher diblock content displayed a network structure. The second blend had a macrophase morphology consisting of light-contrast ovals (b-APP) against a black matrix of PE. Therefore, there was change in the morphology for the solution blends containing the medium molecular weight blend which was reflected in the DSC cooling data (at 10°C/min). The shift in the location of the crystallization peak was thought to arise from the formation of a more macrophase separated structure.

The blends of DEP/PE were determined to be primarily affected by the degree of miscibility of the h-PE chains with those of the block copolymer. It was found that the morphology of the oriented and annealed stand cast solution blends of DEP100 + PE20

followed a trend more similar to that which was seen for highly asymmetric crystalline-amorphous diblock copolymers which were due to the high miscibility of the PE20 chains and the difference in the crystallization temperatures which led to macrophase separation at a much lower composition than would be expected for purely amorphous components. For blends of DEP100 and PE47, because there is low miscibility of the h-PE than for blends with lower molecular weight homopolymers due to reduced miscibility of the h-PE with the b-PE, the difference in crystallization temperatures did not come into play. Further work on the blends with the higher molecular weight homopolymers should shed more light on whether this hypothesis is accurate.

5.5 References

1. Thomas, E. L.; Anderson, D. M.; Henkee, C. S.; Hoffman, D. *Nature* **1988**, *334*, 598.

2. Hashimoto, T.; Nagatoshi, K.; Todo, A.; Hasegawa, H.; Kawai, H. *Macromolecules* **1974**, *7*, 364. Hashimoto, T., Shibayama, M., and Kawai, H. *Macromolecules* **1977**, *10*, 377. Hashimoto, T.; Fujimura, M.; Kawai, H. *Macromolecules* **1980**, *13*, 1237.

3. Bates, F. S.; Cohen, R. E.; Berney, C. V. *Macromolecules*, **1982**, *15*, 589. Almdal, K.; Bates, F. S, *Macromolecules*, **1992**, *25*, 1743.

4. Russell, T. P.; Lin, J. S.; Spooner, S.; Wignall, G. D. *J. Appl. Cryst.* **1988**, *21*, 629. Mayes, A. M.; Russell, T. P.. *Macromolecules*, **1992**, *25*, 6523.

5. Wignall, G. D.; Bates, F. S. *Macromolecules* **1986**, *19*, 32. Chillura-Martino, D.; Triolo, R.; McClain, J. B.; Combes, J. R.; Betts, D. E.; Canelas, D. A.; DeSimone, J. M.; Samulski, E. T.; Cochran, H. D.; Londono, J. D.; Wignall, G. D. *J. Molec. Structure* **1996**, *383*, 3.

6. Lohse, D. J. *Polymer Sci. Eng.* **1986**, *21*, 1500. Lohse, D. J.; Fetters, L. J.; Graessley, W. W. *New Advances in Polyolefins*, **1993**, *8*, 175.

7. Hamley, I. W.; Koppi, K. A.; Rosendale, J. H.; Bates, F. S.; Almdal, K.; Mortensen, K. *Macromolecules* **1993**, *26*, 5959.

8. Stocker, W.; Stadler, R. *Macromolecules*, **1996**, *29*, 7502.

9. Fossum, E. K.; Matyjaszewski, K.; Shieko, S. S.; Möller, M. *Macromolecules* **1997**, *29*, 6076.

10. Karim, A.; Slawecki, T. M.; Kumar, S. K.; Douglas, J. F.; Satija, S. K.; Han, C. C.; Russell, T. P.; Liu, Y.; Overney, R.; Sokolov, J.; Rafailovich, M. H. *Macromolecules* **1998**, *31*, 857.

11. Gido, S. P.; Lee, C.; Pochan, D. J.; Pispas, S.; Mays, J. W.; Hadjichristidis, N. *Macromolecules* **1996**, *29*, 7022.

12. Pispas, S.; Hadjichristidis, N.; Mays, J. W. *Macromolecules* **1996**, *29*, 7378.

13. Beyer, F. L.; Gido, S. P.; Poulos, Y.; Hadjichristidis, N. *Macromolecules* **1997**, *30*, 2373.

14. Hadjichristidis, N.; Iatrou, H.; Behal, S. K.; Chludzinski, J. J.; Disko, M. M.; Gardner, R. T.; Liang, K. S.; Lohse, D. J.; Milner, S. T. *Macromolecules* **1993**, *26*, 5812.

15. Pochan, D. J., Ph. D. Dissertation, University of Massachusetts, 1997.

16. Cohen, R. E.; Cheng, P. L.; Douzinas, K.; Kofinas, P.; Berney, C. *Macromolecules*, **1990**, *23*, 1690.

17. Cohen, R. E.; Wilfong, D. E. *Macromolecules*, **1982**, *15*, 370.

18. Nojima, S.; Kato, K.; Yamamoto, S.; Ashida, T. *Macromolecules*, **1992**, *25*, 2237.

19. Sakurai, K.; MacKnight, W. J.; Lohse, D. J.; Schulz, D. N.; Sissano, J. A.; Lin, J.-S.; Agamalyan, M. *Polymer* **1996**, *37*, 4443.

20. Ryan, A. J.; Hamley, I. W.; Bras, W.; Bates, F. S. *Macromolecules* **1995**, *28*, 3860.

21. Winey, K. I.; Thomas, E. L.; Fetters, L.J. *Macromolecules*, **1992**, *25*, 2645.

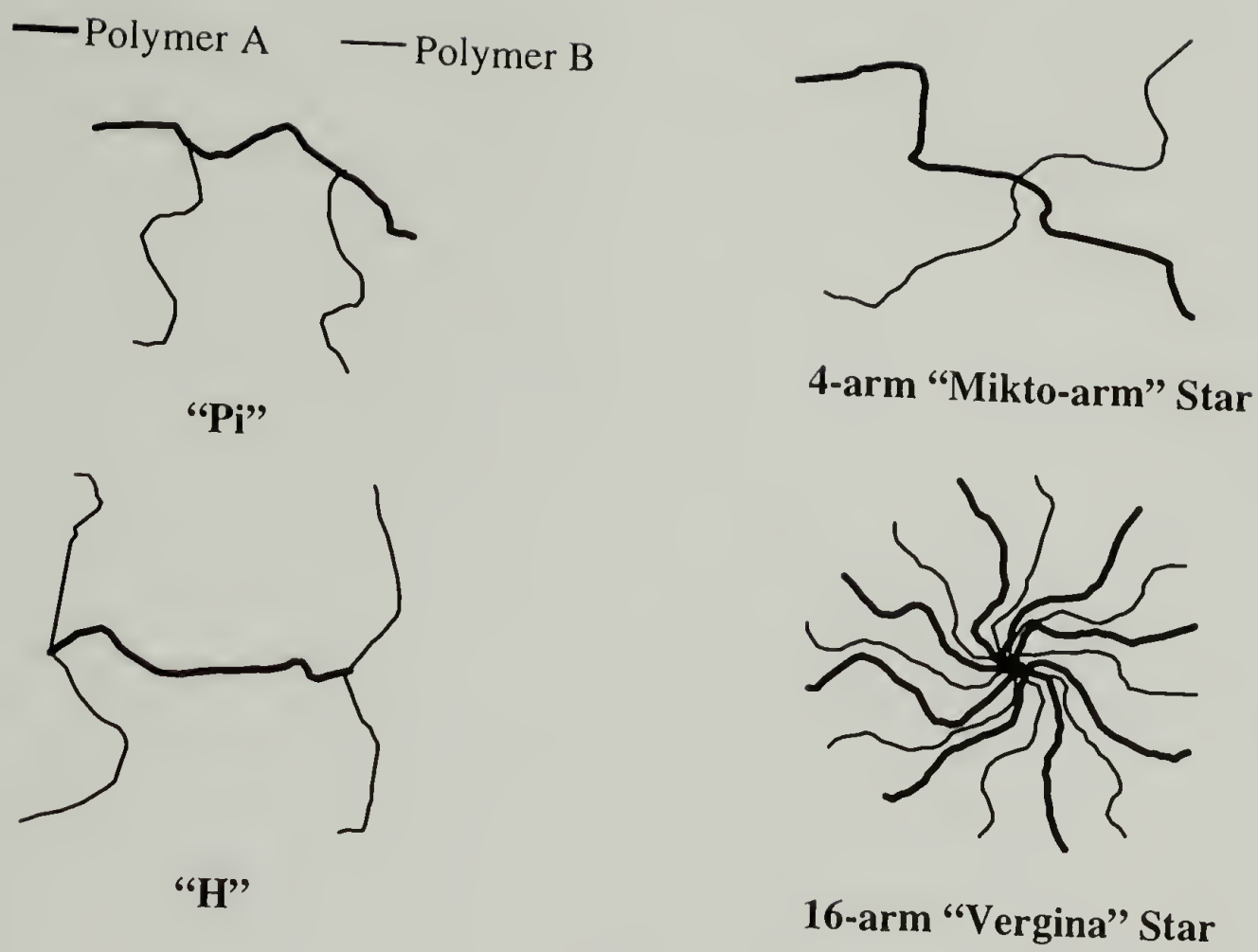

Figure 5.1 Drawings of Novel Architectures Prepared by Living Anionic Synthesis.

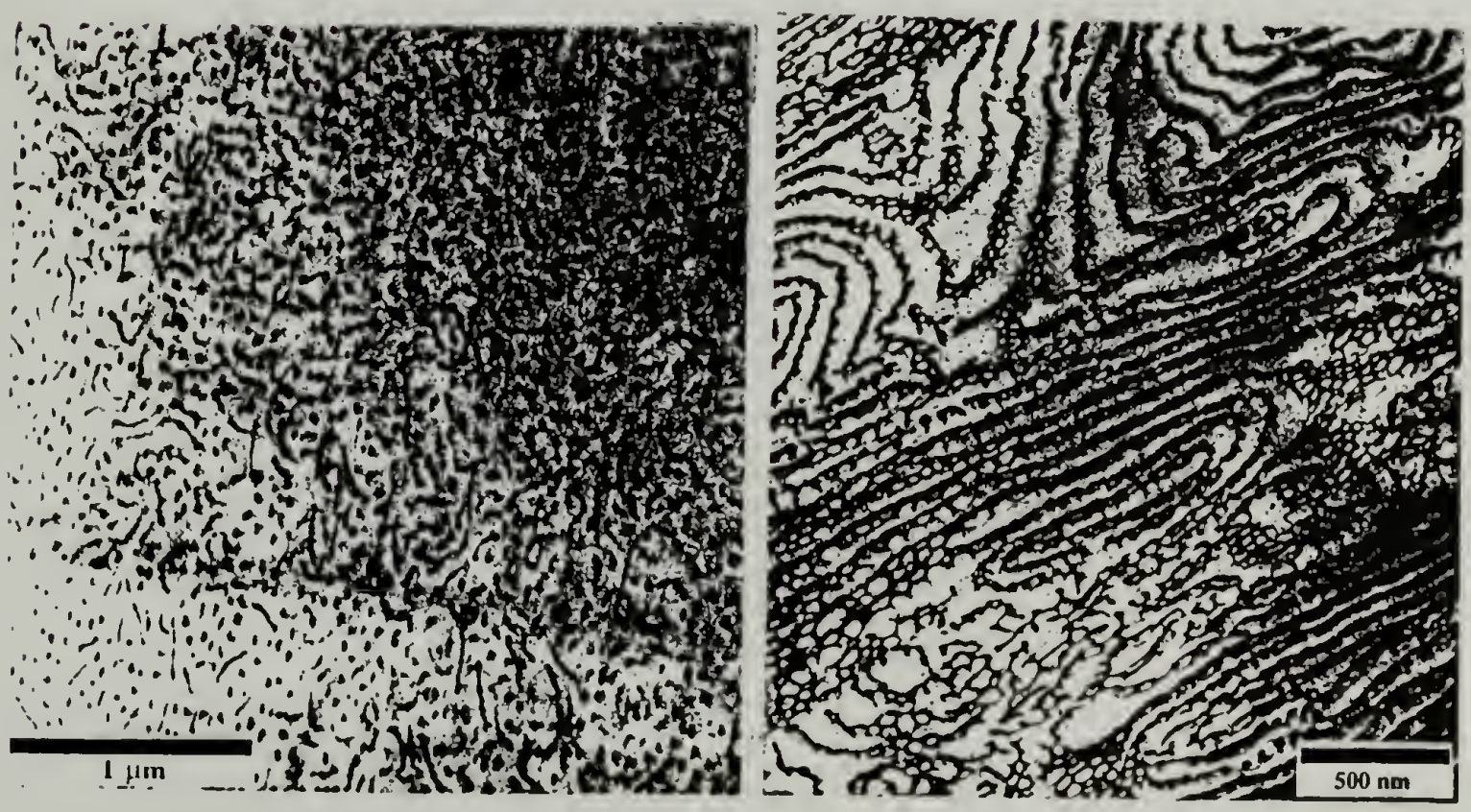

Figure 5.2 Micrographs of "Randomly Oriented Worms" and "Folded Lace".[15]

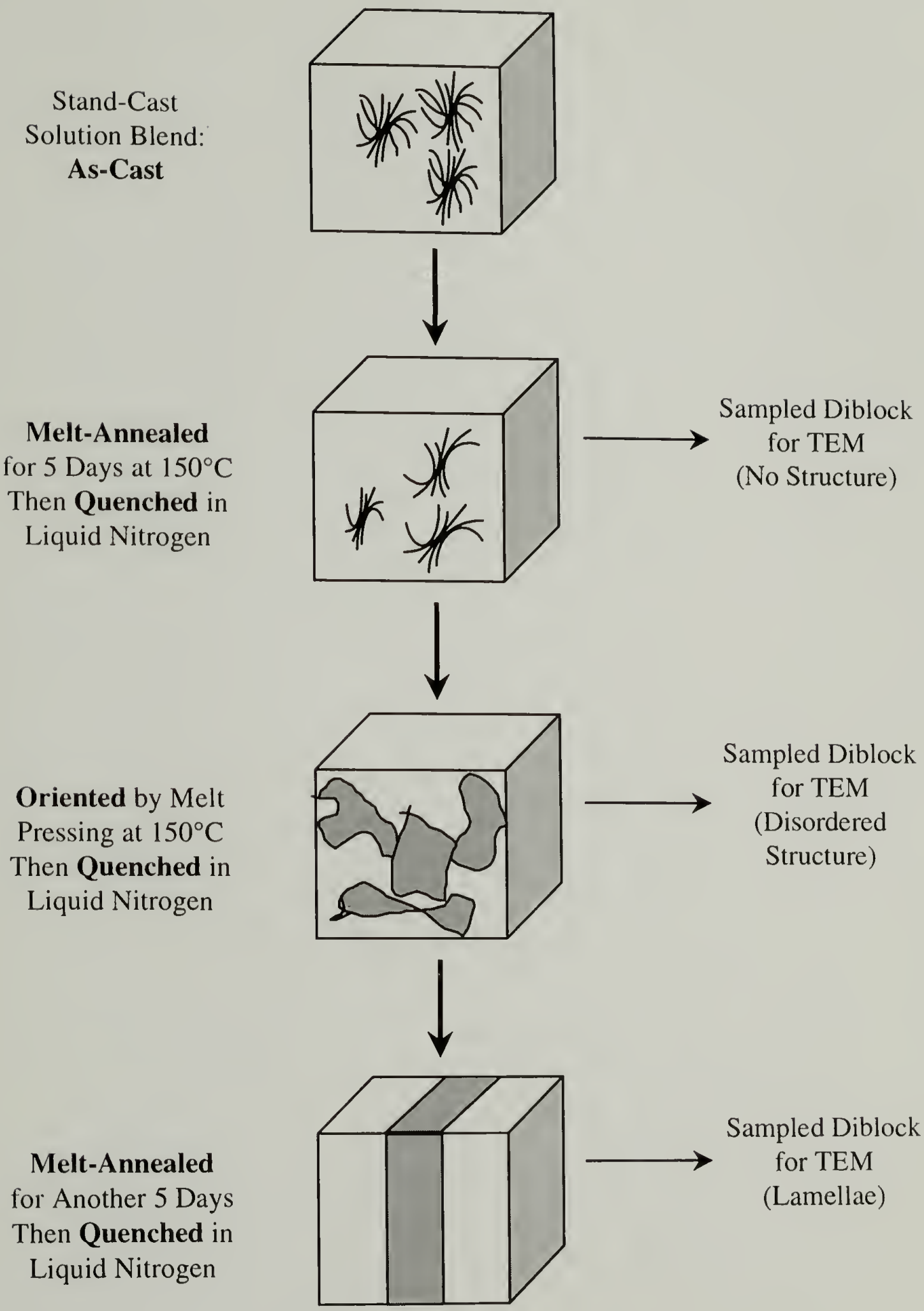

Figure 5.3 Schematic of Sample Preparations for TEM.

Figure 5.4 TEM Micrograph of Solution-Cast DEP100.

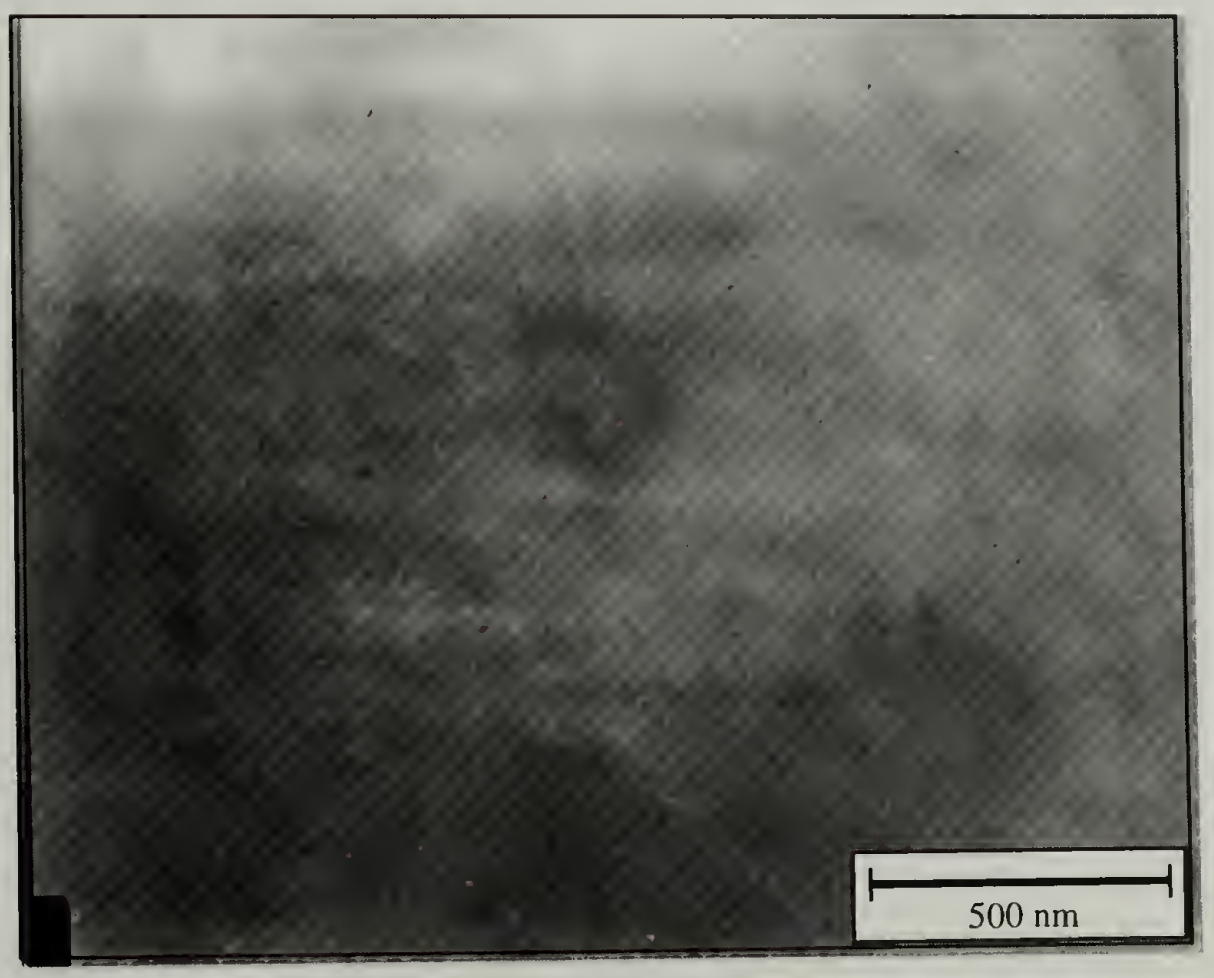

Figure 5.5 TEM Micrograph of Oriented and Annealed Solution-Cast DEP100.

Figure 5.6 TEM Micrograph of Oriented Stand-Cast Solution Blend of 70wt% DEP100 and 30wt% PE20.

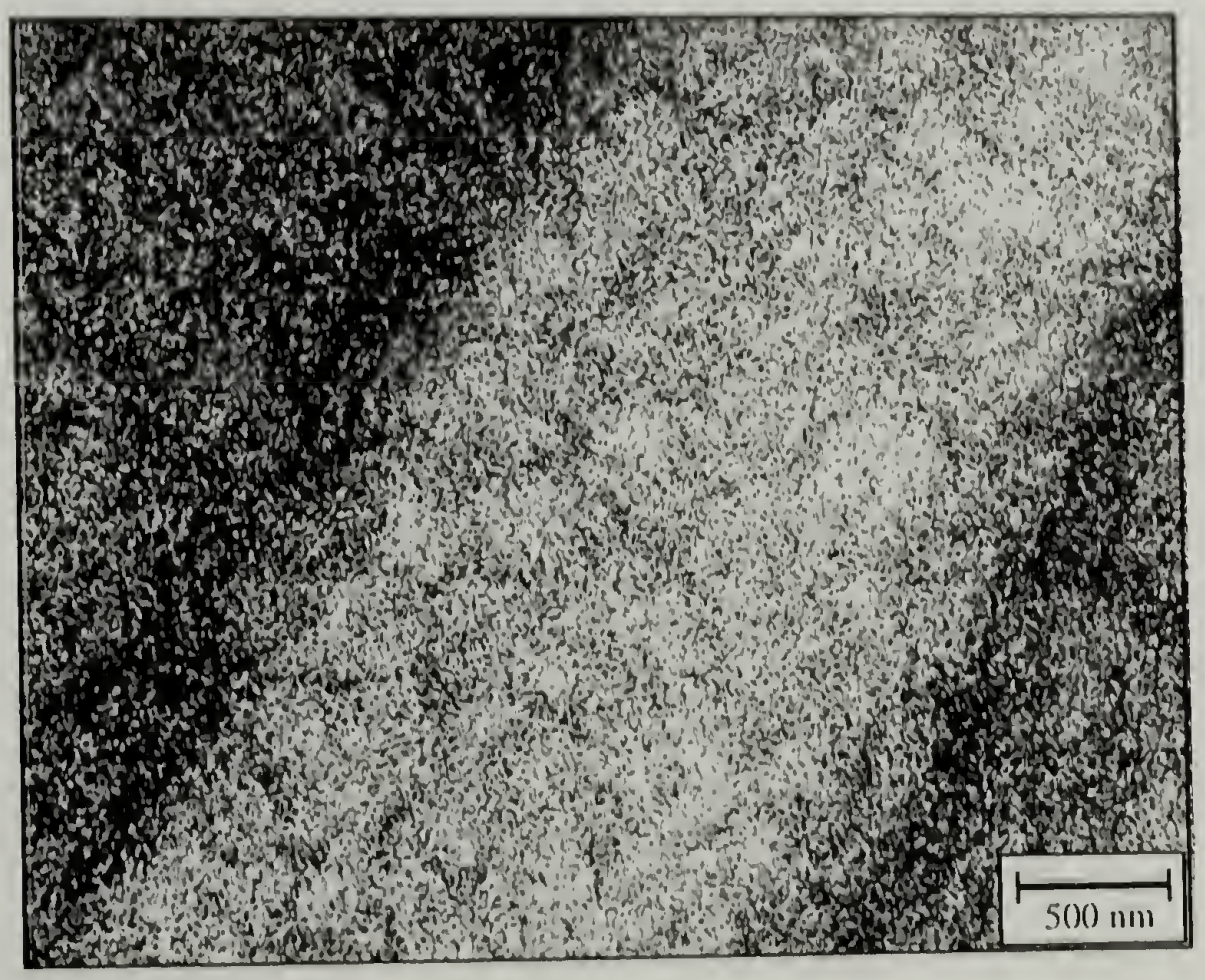

Figure 5.7 TEM Micrograph of Oriented Stand-Cast Solution Blend of 60wt% DEP100 and 40wt% PE20.

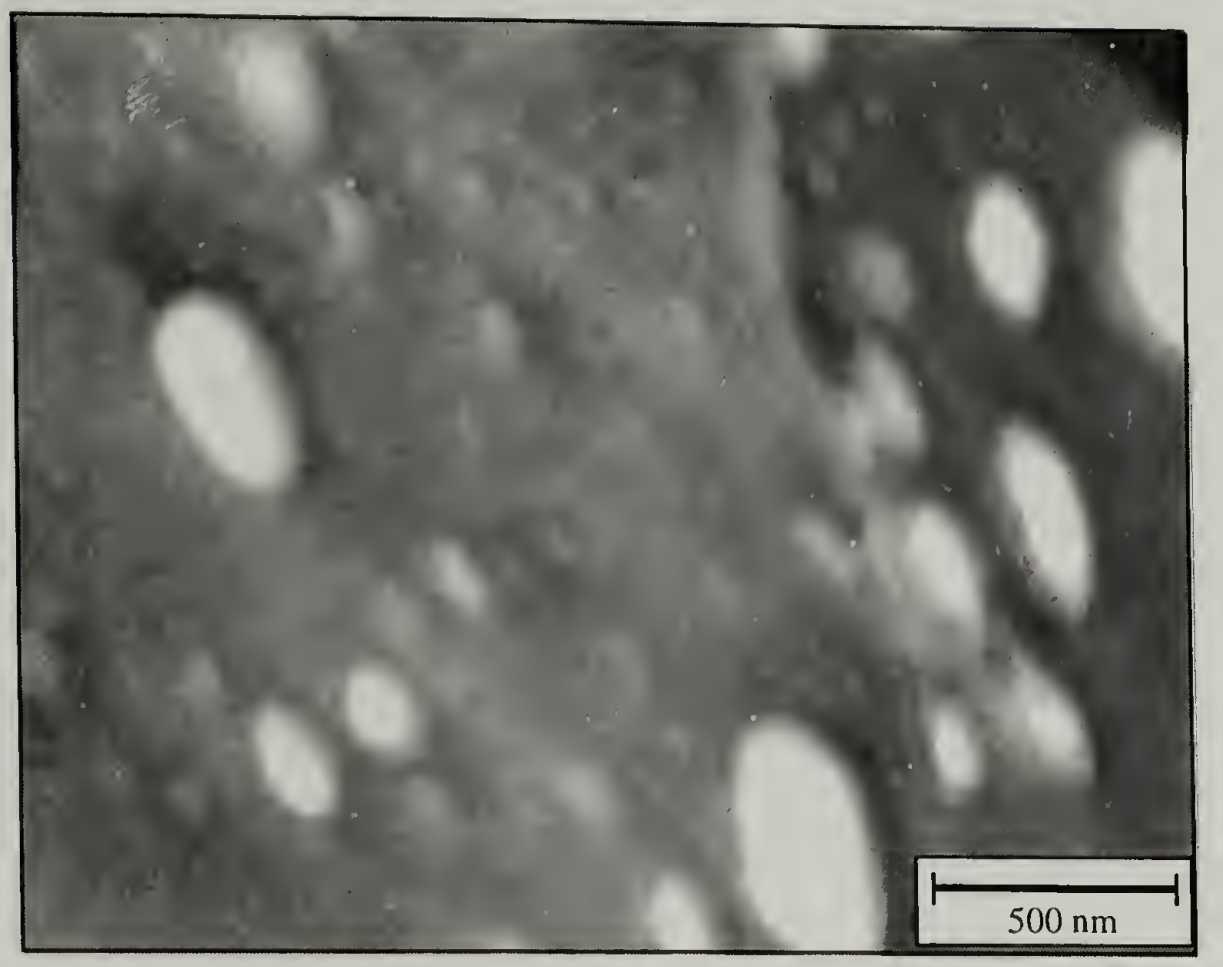

Figure 5.8 TEM Micrograph of Oriented Stand-Cast Solution Blend of 25wt% DEP100 and 75wt% PE20.

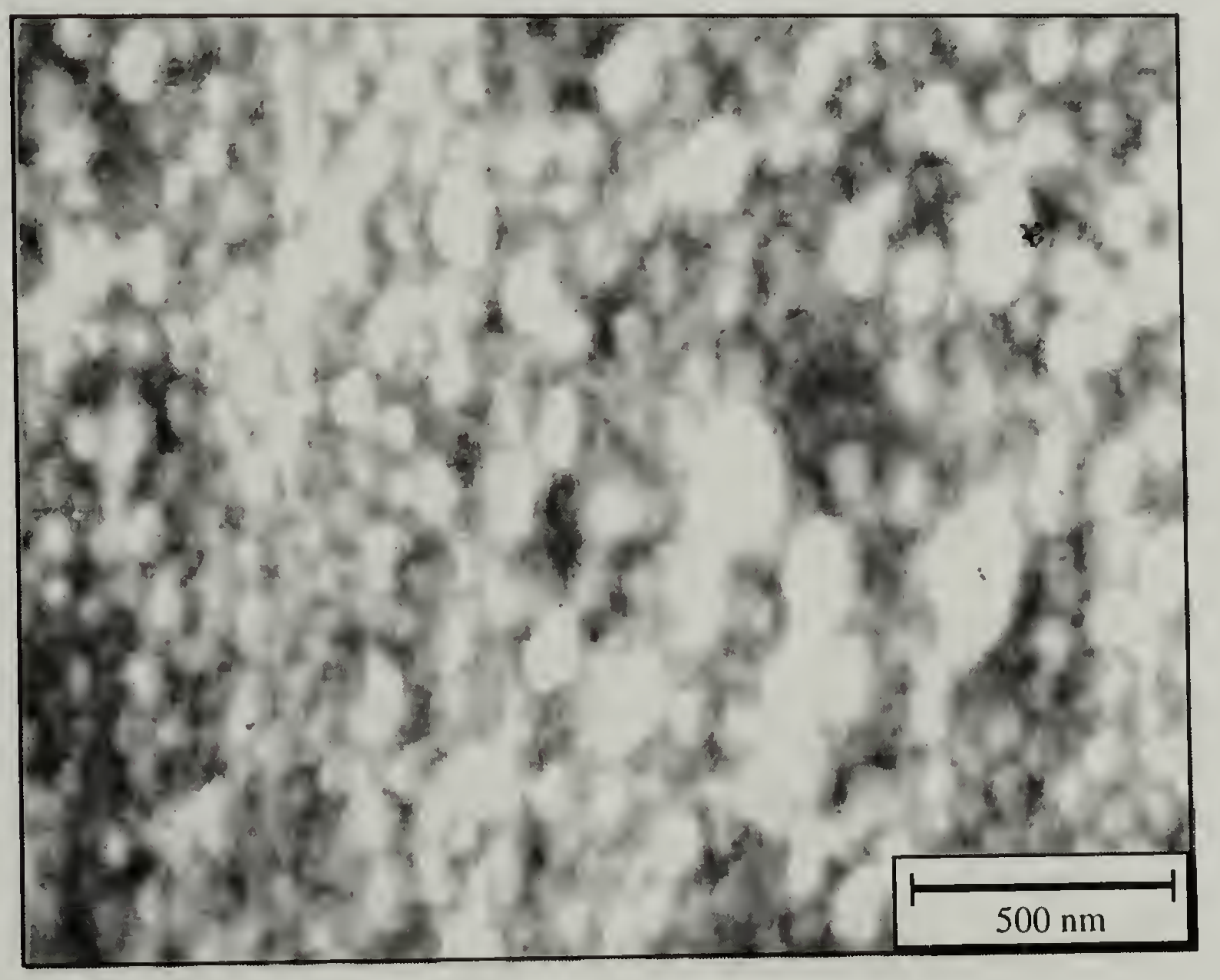

Figure 5.9 TEM Micrograph of Oriented Stand-Cast Solution Blend of 75wt% DEP100 and 25wt% PE47.

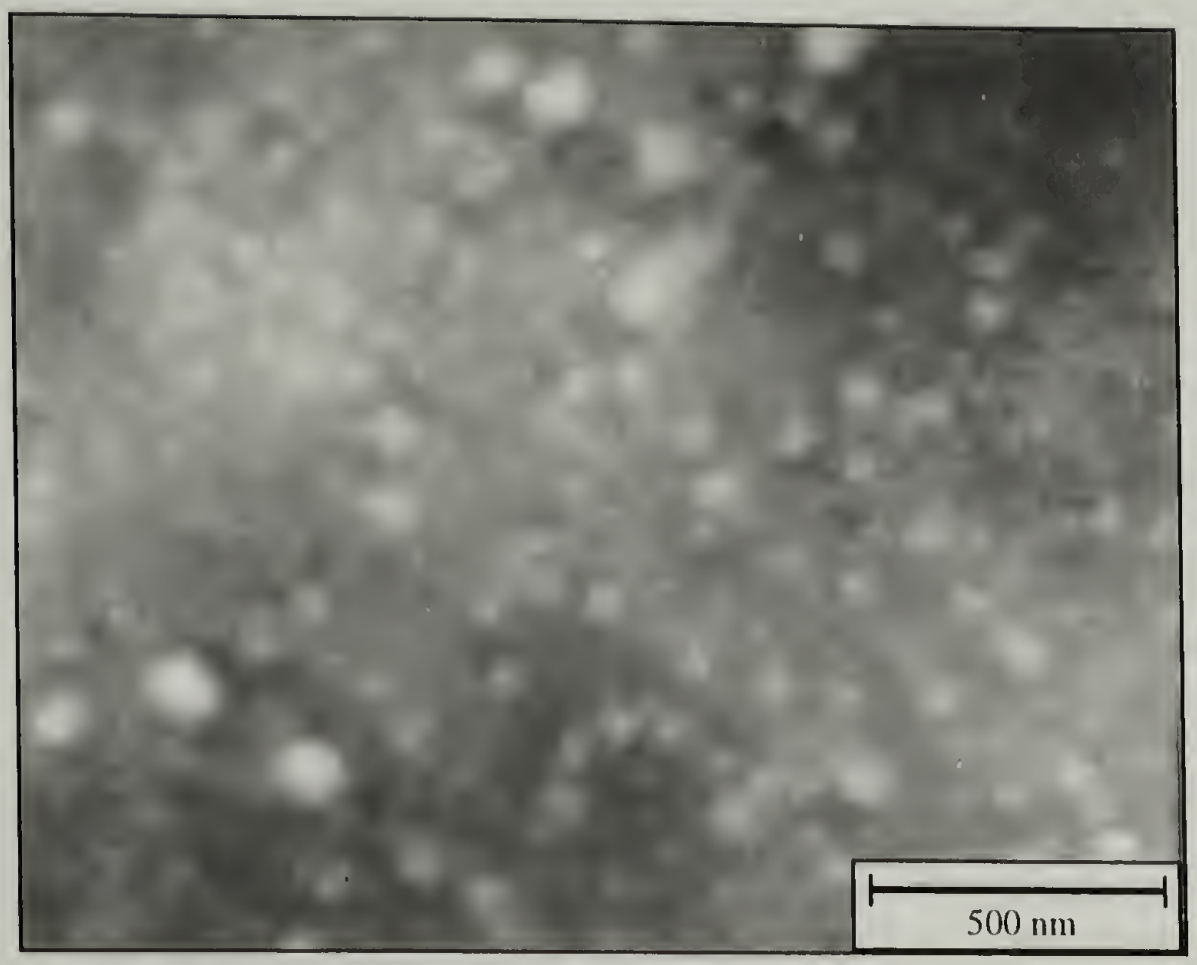

Figure 5.10 TEM Micrograph of Oriented Stand-Cast Solution Blend of 50wt% DEP100 and 50wt% PE47.

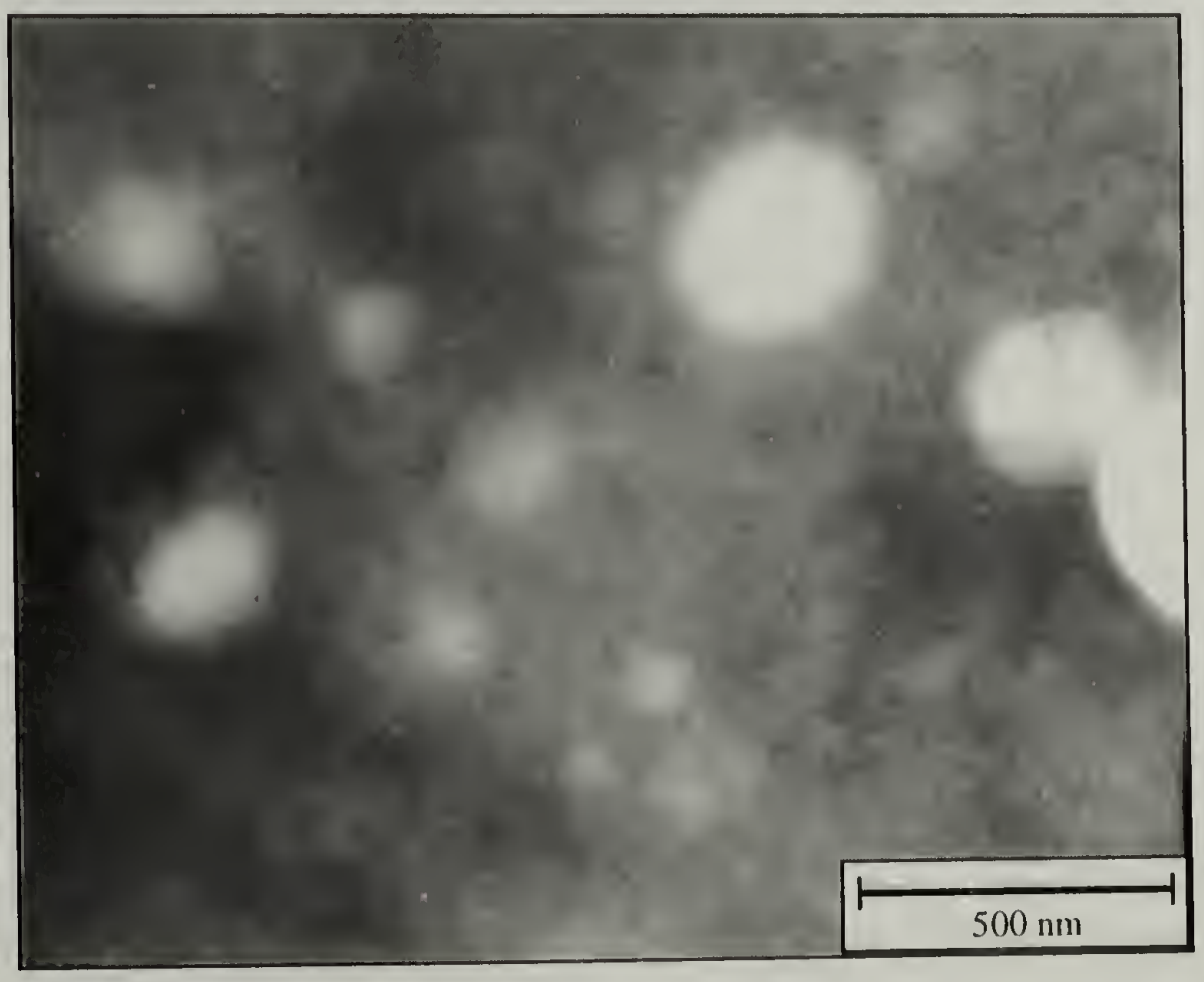

Figure 5.11 TEM Micrograph of Oriented Stand-Cast Solution Blend of 25wt% DEP100 and 75wt% PE47.

CHAPTER 6

INTERFACIAL BEHAVIOR AND MISCIBILITY STUDIES

6.1 Introduction

Neutron reflectometry (NR) uses neutrons to determine the chemical composition profile of a labeled material normal to a polymer surface as shown in Figure 6-1, which may take the form of an interface between a hydrogenous polymer and a deuterated polymer, a gradient across a blend, or a change in the location of the deuterium-labeled chains in a hydrogenous matrix. NR, like small angle neutron scattering (SANS), utilizes the differences in the interaction of neutrons between hydrogen or deuterium to create contrast.

Neutrons reflect from interfaces in much the same way as light. While light is reflected by a smooth surface with a large change in refractive index, neutrons are reflected by smooth interfaces with a large change in scattering length density (the neutron equivalent to the index of refraction). The scattering length density is related to the neutron interaction cross section of the constituent atoms. The reason why deuterium is used as a labeling atom is because it has a high neutron cross section while hydrogen has a low value of the opposite sign—this creates a sort of a "surface" which can be located at a point which is different than the physical surface of the material. Some of the beam may also be refracted with the angle of refraction defined by Snell's Law ($n_i\cos\theta_i = n_j\cos\theta_j$).[1]

The ratio of the refracted beam to the incident beam is called the transmissivity (**T**). For the reflected beam, the ratio of the energy contained in the reflected beam as

compared to the incident beam is called the reflectivity, **R**, of which only the normal component concerns NR. The perpendicular values for **R** are determined using the Fresnel reflection coefficients[2] ($r_{j,j+1}$) for an infinitely sharp interface according to:

$$r_{j,j+1} = \frac{n_j \sin\Theta - n_{j+1} \sin\Theta_{j+1}}{n_j \sin\Theta + n_{j+1} \sin\Theta_{j+1}} \qquad (1)$$

From these values, **R** can be calculated using:

$$\mathbf{R} = r_{j,j+1}\, r^{*}_{j,j+1} = r^{2}_{j,j+1} \qquad (2)$$

The reason why the reflectivity can be simply calculated using $r^2_{j,j+1}$ is because there is no complex conjugate for most materials[2] which also leads to the so-called "phaseless Fourier problem",[3] which is discussed in the next paragraph. Another important quantity is called the critical edge (or critical angle), Θ_c, which occurs at the wavelength that satisfies the relation:

$$\Theta_c = \lambda(Nb/\pi)^{0.5} \qquad (3)$$

where λ is the neutron wavelength and ***Nb*** is the scattering length density of the material.

One advantage of NR is that narrow interfaces can be probed with higher resolution (10 angstroms) than with forward recoil spectroscopy (FRES).[4] Since the composition profile data obtained by NR is in reciprocal space, it would be desirable to invert the data to real space in order to obtain the composition profile. While other techniques such as nuclear reaction analysis (NRA) and dynamic secondary ion mass spectroscopy (DSIMS)[5,6] do give results in real space, their resolution is not as good as NR. A major disadvantage to NR is the fact that the data cannot be directly transformed to obtain the depth profile because there is a loss of phase information—the phaseless Fourier problem—which results from the fact that the reflectivity coefficients (**R**s) must

be squared. Therefore, profile fitting must be performed, which is subject to interpretation if the data is poor. For this reason, additional information on the system from complementary methods such as AFM, CP/MAS NMR[6] and the afore-mentioned techniques listed above is important. An excellent review of the technique of NR was recently published by Bucknall and Higgins[2] and there are well-written books on the subject.[7-9]

The major difference in the instrumentation between a fixed wavelength reactor source and an accelerator source of neutrons is that the reactor produces a (more or less) monochromatic beam of neutrons while the accelerator generates a beam of "white" neutron light containing a range of wavelengths.[2] Therefore, when performing experiments at fixed wavelength sources, the detector must be rotated around the sample in a stepping fashion in order to record the reflection profile. The pulsed source is able to accomplish the same amount of data collection with less motion between the detector and the sample because there are a distribution of wavelengths which satisfy Bragg's law for a range of angles. At the accelerator neutron source, the sample is moved using a computer controlled goniometer, which allows precise alignment of the sample with both the beam and the detector. Schematics of both of these types of instruments are shown in Figure 6-2.[2]

The formation, ordering, or dissolution of an interface between polymers can also be evaluated by NR.[10] Because accelerator sources generate neutrons with a range of wavelengths, the diffusion of species can also be measured in real time, as well as at equilibrium. Therefore, studies evaluating the kinetics of phase mixing/demixing and microphase separation between a labeled and unlabeled component can be investigated.

The only real limitation to time-of-flight measurements is the determination of the acceptable level of error for each data set before taking a new set of measurements. Because advances in component design have improved to the point that both techniques give a comparable quality of data, the choice of neutron source is now based more on convenience and familiarity with equipment than actual experimental concerns.

Previous work in NR has been primarily in the areas of immiscible polymer interfaces, polymer-polymer interdiffusion, and segregation behavior (of which diblock copolymers could be considered a subset.) An important quantity which can be calculated from NR data is the interfacial width, w, which is an indication of the interpenetration of the two polymer chains at their interface and is given by:

$$w = 2l = (2\pi)^{0.5}\sigma \qquad (4)$$

where l is the measured interfacial thickness and σ is the interfacial roughness. Several equations have been used to evaluate the interfacial width which take into account the effects of capillary waves[11,12] and the thickness of the top film.[13] Work relating the ability of diblock copolymers to increase interfacial strength as a function of the interfacial mixing for the system PE-PS has recently been published.[10] This study showed that a broader interphase did not necessarily lead to improved toughness in compatibilized blends.

The objective of the present study was the elucidation of the interfacial behavior and melt miscibility of PE and APP. The majority of work on diblock copolymers using NR has centered on the systems of PS-PMMA[14-16] and PS-PI,[17,18] with the bulk of the published work concerning the former system. Our system is of interest in the academic sense because it deals only with linear and short-branched hydrocarbon molecules. The

investigation of this system has not been widely explored to our knowledge, although it could increase the understanding of the mixing behavior of the commercially important area of polyolefin blends.

The preparation of the polymer films and the configurations for each of the experiments are described in the next section. The results from the various experiments to investigate polyolefin interfacial miscibility are discussed in the following section, with special emphasis placed on the data for the study of the effect of branch content on miscibility and the study investigating the effect of the initial placement of a labeled diblock on its diffusion in homopolymer bilayers. Finally, the work presented in this chapter will be summarized, including conclusions to the results.

6.2 Experimental

The polymers used in these studies were a deuterated diblock copolymer, poly(d_6-butadiene-*b*-methylpentadiene), *d*-DEP, a hydrogenated poly(methylpentadiene), *h*-APP, and a hydrogenated 1,4-polybutadiene, *h*-PE, which were prepared via living anionic polymerizations using a standard high vacuum technique.[19] These polymers were first characterized by GPC and ^{13}C (for the diblock) and ^{1}H (for the homopolymers) NMR, and were then saturated with deuterium or hydrogen using the technique outlined in Chapter 2.[20] Three polymers were generously donated by Exxon Research and Engineering Company for this research: a high-density polyethylene (HDPE) sample and two ethylene-1-butene (E-B) copolymer samples containing roughly 23% and 27% ethyl branches. Table 6-1 lists the important characterization data for these polymers.

Sample preparation was performed in the labs of J. S. Higgins in the Department of Chemical Engineering at Imperial College of Science, Technology, and Medicine in London, UK. NR experiments were performed on the SURF and CRISP instruments using a pulsed neutron (accelerator) source at the Rutherford-Appleton Laboratory (RAL) in Chilton, UK. The neutron source at RAL produces a polychromatic beam with a beam current of roughly 180-200μA out of the accelerator ring and the pulse rate of 50Hz, making it the "brightest" pulsed neutron source currently available.[21] The neutrons were moderated with liquid hydrogen to produce a wavelength range of 0.5 to 6.5Å.

Rectangular silicon wafers (Semiconductor Processing Corp.) were prepared for spin casting by first immersing the wafers in boiling xylene or toluene to eliminate residual polymer film on the silicon surface followed by drying at ambient conditions. The oxide layer on the silicon wafers was then dissolved using a two-step hydrofluoric acid and nitric acid technique.[22] Elimination of the native oxide layer was performed in order to promote adhesion of the hydrophobic polymer film to the hydrophilic silicon surface.

Solutions for polymer films were prepared by first weighing out the polymer into a tared 5ml volumetric flask (with stir bar) using a lab balance and then dissolving the polymer in the appropriate amount of solvent, either toluene or xylene (Aldrich) on a hot plate. Solutions containing APP were prepared by stirring at room temperature, while solutions containing *d*-DEP or PE were prepared by stirring the solution in boiling solvent. Solution concentrations depended on the desired thickness of the spun cast film.

Spinning was performed on an Electron Micro Systems Ltd. spin coater at a rate of 2000 ±5 rpm. For samples which were dissolved in hot solvent, the silicon wafer and

glass pipette were both preheated on the same hot plate as the solution, and the solution was then hot spun. If bilayer samples were to be prepared, the second film was spun onto a glass slide using the same conditions stated previously. These films were then floated off of the glass slides using deionized water in an angled trough and onto the coated silicon wafer by slowly removing the water from the trough. All coated silicon wafers were dried overnight in a vacuum oven at 50°C.

Polymer plugs were prepared in the brass base of the melt cell (see Figure 6-3). The polymers were weighed out and added to the brass base, which was already preheated in a Carver Model C controlled temperature hydraulic press to 175°C. When the polymer had melted, it was compacted manually with a spatula and then compressed between the two plates of the press to 10ksi in air. The polymer and the brass base were kept under pressure for 15 minutes (but the pressure was allowed to relax). At the end of this time, the brass base was removed from the press and allowed to cool to room temperature on an aluminum plate to accelerate cooling. The cooled polymer plug was inspected for bubbles and removed from the brass base so that more plugs could be made. Plugs were used in the "as is" condition without further treatment.

Samples were placed in the melt cell as shown in Figure 6-3. The melt cell was mounted on the goniometer stage of the reflectometer via double-sided tape and then covered with a plexiglass box which was purged with N_2 gas to create an inert atmosphere. After the desired temperature of the melt cell had been reached, either 175°C or 225°C, the sample and the detector were aligned with the neutron beam. Data were recorded at the first angle (0.25°). Once data acquisition was completed for the first

angle, the goniometer was rotated to the second (0.65°), and finally the third angle (1.2°). Total time for each experiment was typically two hours.

6.2.1 Effect of Branch Content on Miscibility at Interface on between *d*-APP and various PEs while in the Melt

d-APP162 was spun cast from solution onto three silicon wafers. Plugs of the HDPE and the two E-B copolymers were prepared by hot pressing. The coated silicon wafers were pressed against each of the polymer plugs in the melt cell and heated to 175°C (or 225°C) at which time data were recorded at 0.25°, 0.65°, and 1.2°.

6.2.2 Ability to Locate Labeled Species Differing Only in Level of Deuteration in Essentially Identical Polymer Configurations in the Melt

h-APP162 was spun cast from solution onto silicon wafers. Thinner films of the 1/4*d*- and 3/4*d*-DEP38 were hot spun onto glass slides and floated onto the coated silicon wafers, forming bilayers. Plugs of *h*-PE150 were prepared in the brass base plates by hot pressing. The silicon wafers coated with bilayer films were pressed against the PE plugs and heated to 225°C. Then data were recorded at 0.25°, 0.65°, and 1.2°.

6.2.3 Effect of Initial Placement of *d*-DEP as a Blend on the Interface of APP/PE in the Melt

A heated solution blend of 5wt% *d*-DEP38 and *h*-APP162 (bal.) were prepared and hot spun onto preheated silicon wafers. Other silicon wafers were spin coated with *h*-APP162 solution. One set of plugs was composed of a solution blend of 5wt% *d*-DEP38

and *h*-PE150 (bal.) precipitated from hot toluene, while a second set was pressed from pure *h*-PE150. The silicon wafers coated with the blend were pressed against the *h*-PE150 plugs, and the *h*-APP162 coated silicon wafers were pressed against the blend plugs in the melt cell. Again, the melt cell was heated to 225°C and then data were recorded at 0.25°, 0.65°, and 1.2°.

6.2.4 Effect of Initial Placement of *d*-DEP as a Film on the Interface of APP/PE in the Melt

h-APP162 and *d*-DEP38 were spun cast from solution onto two sets of silicon wafers. Thinner films of the *h*-APP162 and *d*-DEP38 were hot spun onto glass slides. The thinner films of *h*-APP162 were floated onto the silicon wafers coated with *d*-DEP38, while the thinner films of *d*-DEP38 were floated onto the silicon wafers coated with *h*-APP162. Plugs of *h*-PE150 were prepared in the brass base plates by hot pressing. The silicon wafers coated with bilayer films were pressed against the *h*-PE150 plugs, and when the melt cell had reached 225°C, data were recorded at 0.25°, 0.65°, and 1.2°.

6.2.5 Minimum Deuteration Needed to Obtain Contrast between Labeled Species and Matrix in the Melt

1/4*d*-DEP38 and 3/4*d*-DEP38 were spun cast from hot solutions onto two sets of silicon wafers. Plugs of *h*-PE150 were prepared by hot pressing. The coated silicon wafers were pressed against the PE plugs and heated to 225°C. Then data were recorded at 0.25°, 0.65°, and 1.2°.

6.2.6 Effect of Thermal History on Ability to Detect Labeled Species in the Melt

3/4*d*-DEP38 was hot spun from solution onto silicon wafers. Plugs of the *h*-PE150 were prepared by hot pressing. The coated silicon wafers were pressed against each of the polymer plugs in the melt cell and heated to 175°C. Data were recorded at 0.25°, 0.65°, and 1.2° immediately upon reaching temperature (for one experiment) and also after waiting 3 additional hours while the experiment was held in the melt to investigate the effect time had on the migration of labeled species.

6.3 Data Analysis

Data analysis was performed using Rutherford-Appleton Laboratory's fitting software. After the background had been subtracted from the individual curves, the three curves were combined in a manner analogous to that performed to obtain master curves for dynamic mechanical thermal analysis (DMTA). Some vertical shifting of the finished master curve was necessary if it appeared that a critical edge (which occurs at total reflection when intensity equals unity) existed, but the intensity asymptote was not equal to unity. This can occur due to a misalignment or shift in the melt cell after the calibration had been performed. Once the final reflectivity curve had been produced, curve fitting was accomplished using known parameters as the starting point and allowing all parameters to vary to minimize the deviation of the model fit from the actual data. The parameters which were varied in the fitting program are listed below:

- Background
- Angular Resolution
- Thicknesses of Each Layer
- Roughness between Layers
- Scattering Length Densities of Silicon, Substrate and Each Layer.

Initially, fitting was performed using a single layer profile with more layers added based on the initial configuration of the polymers in the melt cell and the ability to reduce the difference between the fit and the data. If the quality of the data was determined to be poor but not featureless, simulations based on the initial configuration and several probable final depth profiles were performed to examine whether any information could be extracted from the data. The goodness of fit was determined to be reasonable based on the square of standard deviation of the fit, χ^2, the initial configuration/thicknesses of the polymer layers, and the values for the parameters listed above.

6.4 Results and Discussion

An explanation of the difference between good NR data and poor NR data would be helpful to understand these results. Figure 6-4 illustrates excellent data.[23] The peaks and troughs in the data, often called "fringes", are many and well-defined. The data at low values for the momentum transfer, Q, also level off at a reflectance value of unity. This is called the "critical edge", and it is the total reflection off the "surface" of the deuterated material, which can be buried within a multilayered sample. The critical edge is an indicator that sufficiently high contrast exists between the labeled species and the matrix material. The solid line in the figure is the fit to the data, which follows the data quite well. Results like those illustrated in Figure 6-4 occur when: 1.) the level of deuteration in the labeled species is sufficiently high; 2.) the amount of deuterated material is fairly concentrated in a defined region, such as a discrete layer or a fairly narrow gradient close to an interface; 3.) relatively low roughness/good continuity between individual layers exists; and 4.) the thickness of the region containing the labeled

species is not too large to cause multiple scattering of the beam and resulting in few neutrons able to escape from the sample and reach the detector. Therefore, it can be concluded that proper design of the experiment and its various parameters are crucial to obtaining good results.

On the other hand, experiments that have one or more of the following: low deuteration in the labeled species, a highly diffuse concentration of deuterated material, an exceedingly thick layer of deuterated material, poor adhesion/high roughness between layers, or degradation of the labeled species will result in poor data which are either difficult to model or impossible to interpret, as can be seen in Figure 6-5. Low deuteration as well as a highly diffuse layer of deuterated species both cause poor contrast between the labeled material and the matrix and result in few reflected neutrons reaching the detector. These affect the data by reducing the amplitude of the fringes ("washing out" the signal) and causing the curve to fall well below unity at low Q and to not possess a critical edge. The effect of a deuterated layer that is too thick (over 3000Å thick) for the neutron beam results in a washed-out signal also, except that the fringe in this case will be tightly spaced (due to the fact that the data is in reciprocal space). A film which is too thin (under 200Å thick) will yield similar results, except that the washed-out fringes will be widely spaced.

A problem surfaced in the course of these experiments: dewetting of aged films. Coated silicon wafers were prepared for the first set of experiments. Unfortunately, the neutron source went down just before we were scheduled to perform our experiments. Therefore, the coated silicon wafers laid around for several months at ambient conditions. When the next round of experiments occurred, the samples which were already prepared

were utilized for the then-current experiments. All of these samples produced poor reflectivity profiles of the form described above. (see Figure 6-5) The source of the problems was ascribed to dewetting of the hydrophobic polymer films from the hydrophilic oxide layer covering the surface of the silicon wafer. This subject has been reported by Henn, et al. for end-functionalized polystyrene on silicon.[24] In the course of evaluating options to remedy the issue, two potential techniques were identified: the use of a small quantity of an end-functionalized homopolymer to act as an adhesion promoter, or the treatment of the silicon wafer prior to spin coating with hydrogen fluoride (HF) to dissolve the oxide layer to provide a less hydrophilic surface on the silicon wafer.[25] Problems arose with the preparation of an adhesion-promoting polymer (APP-OH) as was discussed in the chapter on synthesis. (Chapter 2) Thus the only real option to decrease the possibility of film dewetting when the polymer layer was heated into the melt was the use of HF to eliminate the native oxide layer on the silicon wafers. The procedure for the HF etching technique was outlined in the Experimental section of this chapter. The HF etch proved to be successful in improving film adhesion to the silicon wafer.

The fitting procedure involved several variables. The background was fit to be at the same level as the background noise (from such sources as specular scattering off rough surfaces), which occurs at high values of Q. Angular resolution is the percentage of spread in the beam that would have to occur to match that which is apparent in the data. Low values (<10%) denote the model to data is good, whereas negative values indicate an incorrect model is being used to fit the data. The initial guess to the thickness of each film layer is based on calibration curves of measured thicknesses (using AFM or SEM) versus solution concentration for the same (or similar) system. The roughnesses

and scattering length densities of the polymer films are derived from experience using similar film casting conditions and calculations based on the additive nature of the scattering length density. The scattering length density for silicon was assumed to be 2.07 x 10-6 ($Å^{-2}$) based on tabular values,[26] but was later determined to change slightly with temperature.[27]

Unfortunately, several of the experiments did not deliver the anticipated results due to poor data. A list of the experiments which showed essentially featureless reflectivity profiles is detailed below.

1.) Half of the experiment investigating the ability to detect the labeled diblock copolymer at different levels of deuteration (Section 6.2.2) which utilized a layer of 1/4*d*-DEP38 between the two homopolymers. This sample exhibited a featureless profile, no doubt because the level of deuteration was too low for the neutron beam to be reflected to any great extent.

2.) The portion of the blend experiment (Section 6.2.3) which added *d*-DEP38 to the plug material (LLDPE) showed no fringes, which was probably the result of the thickness of the deuterated layer being too large. (The molded plugs are roughly 1mm thick, while the neutron beam is unable to deliver meaningful data for layers over 3000Å thick.)

3.) The portion of the bilayer film experiment (Section 6.2.4) which consisted of *h*-APP162 sandwiched between layers of *d*-DEP38 and LLDPE had a featureless reflectivity profile. It is unsure why this part of the experiment gave poor results. Perhaps the film thickness of the *d*-DEP38 was too large or

not well adhered to the *h*-APP162 for the beam to reflect or the layer dissolved into either or both of the homopolymers. (see below)

4.) The whole experiment which examined the level of deuteration in the simple set-up of 1/4*d*- or 3/4*d*-DEP38 against LLDPE (Section 6.2.5) failed. It is believed that the layer thicknesses may have been too thick for the neutron beam to successfully sample the labeled material without substantial signal degradation due to multiple scattering within this layer.

5.) Half of the experiment looking at the annealing of *h*-APP162 sandwiched between layers of *d*-DEP38 and LLDPE as a function of time "failed" in that the reflectivity profile was featureless. However, this experiment occurred during a period of time when the neutron beam was down and necessitated a later experiment in which the experiment took the normal length of time and showed fringes. (This experiment was performed in conjunction with the experiment described in Section 6.2.4. See below for more details and a description of possible sources for this sort of result.)

From these experiments it was determined that the situation where only a portion of the one block of the diblock copolymer was deuterated produces too low of a level of contrast to obtain reasonable results, while blending the labeled species with the plug material creates too much scattering and also causes poor results. It was learned from the above-mentioned results that the concentration of the polymer solutions should be lowered or the spinning rate should be increased to produce thinner films which would decrease the amount of multiple scattering and should give better data.

One of the aims of this work was to look at the effect of short chain branching on polyolefin miscibility in the melt. To this end, three PE samples containing different level of ethyl branching were obtained from Exxon Research & Engineering Co. to be placed in intimate contact with the spun cast film consisting of the *d*-APP162. These polymers were sandwiched in the melt cell and heated to 175°C and 225°C and reflectivity profiles were recorded. These profiles displayed several orders of reflections (Figure 6-6) and each were fit with a two layer model (where the second layer merely created an asymmetric interfacial profile). Flory interaction parameters, χ, were calculated based on the equation $\chi = (v_0/k_BT)(\delta_1-\delta_2)^2$ using reported values for $(\delta_1-\delta_2)$.[28-31] From these χ's were estimated the intrinsic interfacial widths, Δ_0. These values were then compared with the fitted results for the cases of APP/HDPE and APP/E-B.[32] If the intrinsic interfacial widths were too small, the contribution to the interfacial width due to capillary waves, Δ_c, was included to predict the overall interfacial width, w.[33]

$$\Delta_0^2 = a/(3\pi\chi)^{1/2} \tag{5}$$

$$\Delta_c^2 = (k_BT/4\pi\gamma_0)\ln\{(2\pi/\Delta_0)^2/(2\pi/\lambda_c)^2 + (2\pi/a_d)^2\} \tag{6}$$

$$w/(2\pi)^{1/2} = (\Delta_0^2 + \Delta_c^2)^{1/2} \tag{7}$$

The intrinsic width is dependent on the average statistical segment length, a, and the χ parameter. The contribution due to capillary broadening depends on the inplane coherence length of the neutron (λ_c = 20μm), the dispersive capillary length, $a_d = 4\pi\gamma_0 d^4 A^{-1}$, and the interfacial tension, γ_0. (A is the Hamaker constant and d is the layer thickness as determined by AFM.) From the fitted values for the interfacial thickness,

interfacial widths were calculated based on a geometric method as shown in Figure 6-7.[34] The parameters from the fits to data and the calculated interfacial widths are displayed in Table 6-2. The operating assumption at the start of this experiment was that the E-B copolymers would form wider interfaces that the HDPE and that a linear relationship may exist between the degree of branching and the interfacial width. The lower half of Table 6-2 bears this out, with the predicted interfacial width being smallest for *d*-APP/HDPE and largest for *d*-APP/4041 (which contains 27% ethyl branches.) These predicted values also show the rather high contributions due to capillary wave-induced roughness, which are on the same order of magnitude as the intrinsic interfacial width, Δ_0, because the χs are small. It was interesting to discover that the interfacial width between the *d*-APP and the HDPE was broader than the less branched of the two E-B copolymers. It was initially believed that the larger interfacial region between APP and HDPE might have been the result of the potentially high polydispersity which is inherent in HDPE polymers made via Ziegler-Natta catalysis. The reason for this view was the possibility that a very large molecular weight distribution would result in there being a population of relatively short polymer chains, especially because the HDPE had a lower M_w than either of the E-B copolymers. These short chains could act as highly mobile plasticizers (in the melt) and contribute to the interdiffusion between the two homopolymer layers. However, as can be seen in Table 6-1, the polydispersity of the HDPE was only twice that of the E-B copolymers, reducing the possibility that the polydispersity alone could be responsible for the comparatively broad interfacial width. If the HDPE, which was a commercial sample, contained additives, these compounds could act as surfactants that could further add to

mobility at the interface between the HDPE and the *d*-APP. The E-B copolymers were both laboratory samples and would not contain additives, molding agents, etc.

On the other hand, the interface between the *d*-APP with the higher branched E-B copolymer was broader than that with the HDPE which is more in line with expectations. The fact that blending with one E-B copolymer leads to a narrower interface than HDPE, while blending with a slightly more branched E-B copolymer leads to a broader interface is a puzzling result. It is probable that lower molecular weight and broader polydispersity has more of an effect at lower degrees of short chain branching and as the polymer chains become more similar to the APP chains (possibly a crossover at 25% ethyl branches), the effect of branch content dominates and the interface exhibits more "normal" behavior. These results indicate that the situation is not as simple as conceived and warrants further study with more closely matched molecular weight homopolymers.

The experiment which compared the reflection profiles for the bilayers of *h*-APP and *d*-DEP copolymers (differing only in the amount of deuteration) pressed against plugs of *h*-PE and heated into the melt—Section 6.2.2—was intended to investigate the minimum level of labeling which was able to be detected in similar arrangements. The data for this set of experiments are shown in Figure 6-8. As can be seen, only the sample with 3/4*d*-DEP38 showed structure in the reflectivity data, indicating that the more deuterated copolymer must be used in these bilayer configurations in order to obtain usable/interpretable data. Along similar lines of thought was the experiment described in Section 6.2.5, which involved using the different *d*-DEP38 copolymers placed against plugs of *h*-PE and heating the polymers into the melt. Unfortunately, it appeared that

both of these films were too thin, as neither reflections nor critical edges were observed in the data (see Figure 6-9).

The purpose of the experiment utilizing blends of the deuterated diblock copolymer, *d*-DEP38, with either *h*-APP or *h*-PE was to investigate the effect of short chain (methyl) branching on the anticipated diffusion of the diblock to the interface between the two homopolymers. The case where the labeled species was solution blended with the plug *h*-PE showed essentially no features; but the other half of this experiment, where the deuterated diblock was blended with the *h*-APP did exhibit some weak fringes as shown in Figure 6-10. Curve fitting to the latter case was unsuccessful in obtaining a reasonable fit to data, so simulations were performed on several possible resulting outcomes, some of which are shown in Figure 6-11. The process of simulating data is somewhat different than actual curve fitting because iterative regression is not performed in order to find the best fit. Instead, parameters are changed one at a time by the researcher to attempt to find the closest model to the data. When all parameters have been varied, the square of the deviation ("chi-squared") is recorded and the next simulated outcome is tested. Unexpectedly, the simulated final condition with the lowest χ^2 and most reasonable values was not the expected case where the *d*-DEP38 migrated to the interface between the two homopolymers, but instead was the situation where the deuterated diblock copolymer migrated to the "free surface" of the film—namely, the interface between *h*-APP162 and the silicon wafer. The results of the simulations to fit for this and other plausible models are found in Table 6-3 and are shown graphically in Figure 6-11. As can be seen from the table, the other possible final situations gave unrealistic results for various parameters, whereas the most probable model gave a

reasonable layer thickness and scattering length density for the surface layer of deuterated material. From inspection, the potential for this sort of migration (from the bulk blend to the surface layer) could be rationalized as the anticipated response for these particular polymers in this system.

There are several arguments for why this behavior would actually be expected rather than simply a model with a reasonably good fit to the reflectivity profile. The first and foremost explanation would be the result of a surface free energy mismatch between the hydrogenous homopolymer and the deuterated diblock copolymer caused by the presence of deuterium and residual unsaturation in the copolymer, both of which would tend to decrease the surface free energy of the copolymer.[35] A contributing effect would be the lower molecular weight of the diblock copolymer as compared to the homopolymer. As the molecular weight of the polymer becomes lower, the concentration of chain ends per backbone repeat unit as compared to a polymer with a higher molecular weight (longer chain) becomes higher. This would lead to an decrease in the surface free energy as compared to the higher molecular weight polymer. Therefore, the *d*-DEP38 is expected to have a lower surface free energy than the *h*-APP162. An interesting test to prove or disprove whether this surface migration phenomenon was occurring would be to prepare blends of the same polymers as the NR experiments and spin coat silicon wafers or glass (which both contain hydrophilic silanol bonds) with the blends. Atomic force microscopy (AFM) would then be used to image the free surface of "as-prepared" and heat treated samples to simulate the conditions before the sample was placed in the melt cell and after the duration of an average NR test. If migration to the free surface of the blend occurs (This phenomenon is also called "blooming".)[36] then it would be expected

that the *b*-PE in the diblock should attempt to form some sort of spherulitic structure upon cooling from the melt to room temperature as has been observed for LLDPE.[37] (see Figure 6-12) On the other hand, if blooming does not occur upon heating the samples into the melt state for an extended period of time, then the AFM images of the sample before and after heat treatment should look essentially the same, with some possible random surface roughening occurring due to the film being in the melt state. In fact some initial tests using AFM were performed (Figure 6-13) which appear to confirm that migration to the free surface is occurring. In order to verify that these structures are created by the crystallization of the *b*-PE, one would also have to prepare and anneal spun coated samples of the pure component polymers. One would predict that the pure amorphous homopolymer should give a featureless AFM image, while the pure homopolyethylene should produce results similar to Figure 6-13. Because the diblock copolymer contains both amorphous and crystallizable components, the crystallization into spherulites may be prevented to some extent and possibly only the early stages of spherulite formation (i.e. "sheaf-like" structure)[38] may be observed.

The experiments which contained bilayers of the deuterated diblock and the hydrogenous atactic-polypropylene against LLDPE (Sections 6.2.4 and 6.2.6) were intended to investigate the effect of the initial location of the diblock copolymer and the possible migration of the diblock into (a) either homopolymer phase or (b) through the APP to reside at the interface between the two homopolymers. While the "control experiment", the situation in which the labeled diblock copolymer was sandwiched in between the two hydrogenous versions of the homopolymers, had a featureless reflectivity curve, the profile for the case in which the labeled diblock was located on the outside of

the two homopolymers proved more interesting. All coated silicon wafers were dried before the experiments by heating the samples in a vacuum oven at 50°C overnight. As stated above, the initial experiment performed on the situation where the diblock copolymer resided on the outside of the homopolymers was heated to 175°C for four hours. It was assumed that the diblock would prefer to remain at the "free surface" (as was seen above), but the profile was featureless. Therefore, the results were puzzling. Also, a corresponding increase in the scattering length density at the interface between the two homopolymers was not noted. As was stated above, the situation which placed the labeled diblock at the interface also produced a profile without fringes. Thus, it was concluded that one of two phenomena may be occurring: 1.) either the films were too thick (>3000Å) or too thin (<200Å) for the neutron beam to sufficiently reflect off and generate a signal at the detector, or 2.) the diblock was in some way miscible with one or both of the component homopolymers in the melt, and in essence, the copolymer "dissolved" into the homopolymer(s). An experiment to investigate whether solubilization (which would be time dependent) or film thickness was responsible for the poor data was planned.

Therefore, at a later set of experiments another sample which was prepared under the same conditions and using the same polymers, was dried in a room temperature vacuum oven overnight. This sample was placed in the melt cell and brought up to temperature; and reflectivity data was recorded as quickly as possible. As was expected for the first sample, this second sample displayed fringes indicative that at least some of the original *d*-DEP38 film was remaining at the interface between the silicon wafer and the *h*-APP162. Thus, the results would appear to indicate that some time-related

phenomenon must be occurring, such as diffusion of the diblock away from the silicon surface and into the polypropylene homopolymer (as opposed to being a matter of film thickness). A study was published which employed a similar bilayer experiment for the system PS-PMMA.[39] In this work it was reported that the labeled diblock copolymer appeared to migrate away from the silicon/*h*-PS interface in the form of micelles (PS on the outside/ PMMA on the inside) which "peeled" off of that interface in layers. Figure 6-14(a) shows their proposed mechanism. The proof which was cited to confirm this hypothesis was based on the calculation of the critical micelle concentration (cmc) for the diblock in the homopolymer.[40] The results of their calculation indicated that for this combination, the concentration of the diblock was above the cmc, and so they concluded that their hypothesis concerning the manner of transport through the *h*-PS was correct and diffusion occurred in the form of micelles. An interesting experiment to determine the size of the migrating species would be to perform SANS on the current system. If the copolymer migrated through the homopolymer to the interface between the APP in the form of individual chains, then a plot the SANS data would show a maxima where the size scale of the scattering species would be on the order of the radius of gyration for an individual copolymer molecule. On the other hand, if the copolymer did peel off of the silicon in layers to form micelles, then the location of the peak should occur at a size scale which would be much larger that the radius of gyration for a single polymer chain.

From the above results it is concluded that melt miscibility in the system of PE/APP is not as simple as it would seem based on the facts that there are only van der Waals interactions and a lack of specific interactions and the polymers studied differ only in chain length and density of branches. It appears that how the labeled diblock is added

to the system (whether as part of a blend with one of the homopolymers or as a discrete film) has a large impact upon its mobility once the system has been heated into the melt.

6.5 Summary and Conclusions

Several experiments were performed to investigate miscibility and interfacial behavior in the system PE/APP using the technique of Neutron Reflectometry (NR). The investigation of this system has been largely unexplored to our knowledge, although it has the potential to make an impact on the understanding of melt miscibility of the commercially important area of polyolefin blends. To this end experiments were performed which were designed to examine the mixing of labeled species in or against an unlabeled matrix.

The results of the study on the effect of the amount of short chain (ethyl) branching on miscibility at the polyethylene/atactic-polypropylene interface showed that an HDPE sample was found to have a wider interface than did the lower branch content ethylene-1-butene (EB) copolymer. It is believed that a combination of molecular weight, polydispersity, and the presence of additives had more of an effect on miscibility than did branch content. The presence of additives should be investigated in the future using NMR. The more highly branched E-B copolymer possessed a wider interface than did the HPDE/APP sample, possibly indicating that as the PE chain becomes more "PP-like", the more strongly does chain microstructure affect miscibility rather than chain length and chain length distribution.

It appears that how the diblock copolymer is added to the homopolymer(s) has a large effect on its mobility. When placed as blend in the amorphous homopolymer, simulations indicated that migration of the diblock to the free surface occurred, possibly due to surface free energy effects. Substantiation of this interpretation was studied using AFM. When placed as a film, the diblock appeared to dissolve into either one or both of

the homopolymers as micelles or as individual chains. Determination of the form of the migrating copolymer would rely on SANS experiments to determine the size scale of the labeled species.

Cleaning the silicon wafers with an HF etching technique proved successful in minimizing the film detachment problem in spun cast polymer films on the silicon. Since the hydrogenation catalyst could not be remove from the hydroxy-terminated APP polymer, the use of an adhesion-promoting polymer to bridge the hydrophobic/hydrophilic interface was discontinued.

6.6 References and Notes

1. Born, M.; Wolf, E. Principles of Optics, 6th Edition, Permagon Press: Oxford, 1980.

2. Bucknall, D. G. and Higgins, J. S. "Neutron Reflection Studies of Polymer-Polymer Interfaces" CLRC Technical Report No. RAL-TR-97-008, January, 1997.

3. Hong, P. P.; Boerio, F. J.; Smith, S. D. *Macromolecules* **1994**, *27*, 596.

4. Douzinas, K. C.; Cohen, R. E. *Macromolecules* **1992**, *25*, 5030.

5. Jones, R. A. L.; Kramer, E. J.; Rafailovich, M. H.; Sokolov, J.; Schwarz, S. A. *Phys. Rev. Lett.* **1989**, *62*, 280.

6. Zumbulyadis, N.; Landry, M. R.; Russell, T. P. *Macromolecules* **1996**, *29*, 2201.

7. Higgins, J. S.; Benoit, H. C. Polymers and Neutron Scattering, Clarendon Press: Oxford, 1994.

8. Russell, T. P. *Mater. Sci. Rep.* **1990**, *5*, 171.

9. Koester, L., in Neutron Interferometry, Bonse, U. and Rauch, H., eds., Oxford Science Publications: Oxford, 1979.

10. Hermes, H. E.; Higgins, J. S.; Bucknall, D. G. *Polymer* **1997**, *38*, 985.

11. Zhao, W.; Zhao, X.; Rafailovich, M. H.; Sokolov, J.; Mansfield, T.; Stein, R. S.; Composto, R. C.; Kramer, E. J.; Jones, R. A. L.; Sansome, M.; Nelson, M. *Physicsa B* **1991**, *173*, 43.

12. Shull, K. R.; Mayes, A. M.; Russell, T. P. *Macromolecules* **1993**, *26*, 3929.

13. Sferrazza, M.; Xiao, C.; Jones, R. A. L.; Bucknall, D. G.; Penfold, J.; Webster, J. R. P. *Phys. Rev. Lett.* **1997**, *78*, 3693.

14. Russell, T. P. *Physica B* **1996**, *26*, 3929.

15. Walton, D. G.; Kellogg, G. J.; Mayes, A. M.; Lamboody, P.; Russell, T. P. *Macromolecules* **1994**, *27*, 6225.

16. Russell, T. P.; Lamboody, P.; Kellogg, G. J.; Mayes, A. M. *Physica B* **1995**, *213/214*, 22.

17. Jones, R. A. L.; Norton, L. J.; Kramer, E. J.; Composto, R. J.; Stein, R. S.; Russell, T. P.; Mansour, A.; Karim, A.; Felcher, G. P.; Rafailovich, M. H.; Sokolov, J.; Zhao, X.; Schwarz, S. A. *Europhys. Lett.* **1990**, *12*, 41.

18. Hariharan, A.; Kumar, S. K.; Rafailovich, M. H.; Sokolov, J.; Zheng, X.; Duong, D.; Schwarz, S. A.; Russell, T. P. *J. Chem. Phys.* **1993**, *99*, 656.

19. Morton, M.; Fetters, L. J. *J. Rubber Chem. Technol.* **1975**, *48*, 145.

20. Rachapudy, H.; Smith, G. G.; Radu, V. P.; Graessley, W. W. *J. Polym. Sci.; Polym. Phys. Ed.* **1979**, *17*, 1211.

21. The fact that the pulsed source at R. A. L. is currently the most intense source of its kind for neutrons is in no way an indication that this will be continued in the future.

22. S. A. Butler, private communication.

23. Fernandez, M. L.; Higgins, J. S.; Penfold, J.; Shackleton, C.; Walsh, D. J. *Polymer* **1990**, *31*, 2146.

24. Henn, G.; Bucknall, D. G.; Stamm, M,; Vanhoorne, P.; Jerome, R. *Macromolecules* **1996**, *29*, 4305.

25. T. P. Russell, private communication.

26. Sears, V. F. *Neutron News* **1992**, *3*, 26.

27. Bucknall, G. D.; Butler, S. A., unpublished results.

28. Krishnamoorti, R.; Graessley, W. W.; Balsara, N. P.; Lohse, D. J. *Macromolecules* **1994**, *27*, 3073.

29. Graessley, W. W.; Krishnamoorti, R.; Balsara, N. P.; Butera, R. J.; Fetters, L. J.; Schulz, D. N.; Lohse, D. J.; Sissano, J. A. *Macromolecules* **1994**, *27*, 3896.

30. Graessley, W. W.; Krishnamoorti, R.; Reichart, G. C.; Balsara, N. P.; Fetters, L. J.; Lohse, D. J. *Macromolecules* **1995**, *28*, 1260.

31. Krishnamoorti, R.; Graessley, W. W.; Balsara, N. P.; Dee, G. T.; Walsh, D. J.; Fetters, L. J.; Lohse, D. J. *Macromolecules* **1996**, *29*, 367.

32. Bucknall, D. G.; Butler, S. A.; Hermes, H. E.; Higgins, J. S. *PMSE Preprints* **Fall, 1998**, *32*, 292.

33. Sferrazza, M.; Xiao, C.; Jones, R. A. L.; Bucknall, D. G.; Webster, J.; Penfold, J. *Phys. Rev. Lett.* **1997**, *78*, 3693.

34. Calculation related to author through research group of J. S. Higgins, Imperial College. Please see Figure 6-7 for more information.

35. Graessley, W. W.; Kristamoorti, B.; Fetters, L. J.; Lohse, D. J. *Macromolecules* **1993**, *26*, 1137.

36. "Blooming" is a term common to materials science when one component of an alloy or blend preferentially diffuses to the surface, creating a depletion zone behind it.

37. Takagi, S.-Y.; Saito, H.; Chiba, T.; Inoue, T.; Takemura, Y. *Polymer* **1998**, *39*, 1643.

38. Toda, A.; Keller, A. *Colloid & Polymer Sci.* **1993**, *271*, 328.

39. Bucknall, D. G.; Higgins, J. S.; Penfold, J.; Rostami, S. *Polymer* **1993**, *34*, 451.

40. Leibler, L.; Orland, H.; Wheeler, J. C. *J. Phys. Chem.* **1983**, *79*, 3550.

Table 6.1 Molecular Parameters for NR Polymers.

Name	Polymer Type	Mn	Mw	Mw/Mn	% Ethyl	Other
d DEP38	(d/h) PBD-*b*-PMPD	37	38	1.03	7%	40wt% PBD
APP162	(d/h) PMPD	111	162	1.46	---	
PE150	(h) PBD	146	150	1.03	7%	
HDPE	High Density PE	12.5	49	3.9	1%	
E-B 4021	(h) PBD	49.0	90	1.9	23%	
E-B 4041	(h) PBD	52.5	87	1.7	27%	

M(n), M(w), PDI by GPC; PBD standards.
For DEP100, estimated uncouple PBD < 5% (by peak height).
Polymer compositions by ^{13}C NMR and Proton NMR.

Table 6.2 Interfacial Thicknesses and Widths for *d*-APP against Various PEs.
(upper table: Results from Fitting Data.)
(lower table: Predictions based on χ.)

Sample Setup	d-APP/4021	d-APP/4041	d-APP/HDPE
Layer 1			
Layer Thickness (Å)	873.7	879.5	941.4
Interfacial Roughness (Å)	59.36	81.19	99.66
Layer 2 (adds asymmetry)			
Layer Thickness (Å)	13.47	13.32	30.22
Interfacial Roughness (Å)	10.89	23.61	37.69
Interfacial Width (nm)	9.9	12.8	12.1
χ [a]	2.963E-03	1.772E-03	1.807E-03

Sample Setup	d-APP/4021	d-APP/4041	d-APP/HDPE
χ	1.683E-03	1.569E-03	2.447E-03
Intrinsic Width (nm)	5.24	5.43	4.15
Interfacial Width (nm) [b]	9.88	10.05	9.00

a: based on current results and references 28-31.
b: includes intrinsic width and contribution due to capillarity.

Table 6.3 Simulations to Fit for Plausible Models for (h-APP165 + 3/4*d*-DEP38)/LLDPE.

		①	②	③
Sample Setup		***h* -APP + 3/4*d* -DEP / LLDPE**		
Background (Å)		5.80E-06	6.31E-06	5.70E-06
Angular Resolution		7.01%	**-49.69%**	5.00%
N(b)--Silicon ($Å^{-2}$)		2.56E-06	2.07E-06	2.07E-06
N(b)--Substrate ($Å^{-2}$)		-3.10E-07	-2.70E-07	-2.70E-07
Roughness (Å)		12.9	12.5	10.0
(Si / Layer 1)				
Layer 1				
Layer Thickness (Å)		**3180**	1800.0	**180.0**
N(b)--Layer 1 ($Å^{-2}$)		**-3.10E-07**	**-1.30E-07**	2.90E-06
Interfacial Roughness (Å)		164.8	120.0	9.0
(Layer 1 / Layer 2)				
Layer 2			----	
Layer Thickness (Å)		841.2		1420.0
N(b)--Layer 2 ($Å^{-2}$)		6.60E-07		-2.25E-07
Interfacial Roughness (Å)		135.0		90.0
(Layer 2 / Layer 3)				
X^2		1.42	**14.86**	2.179

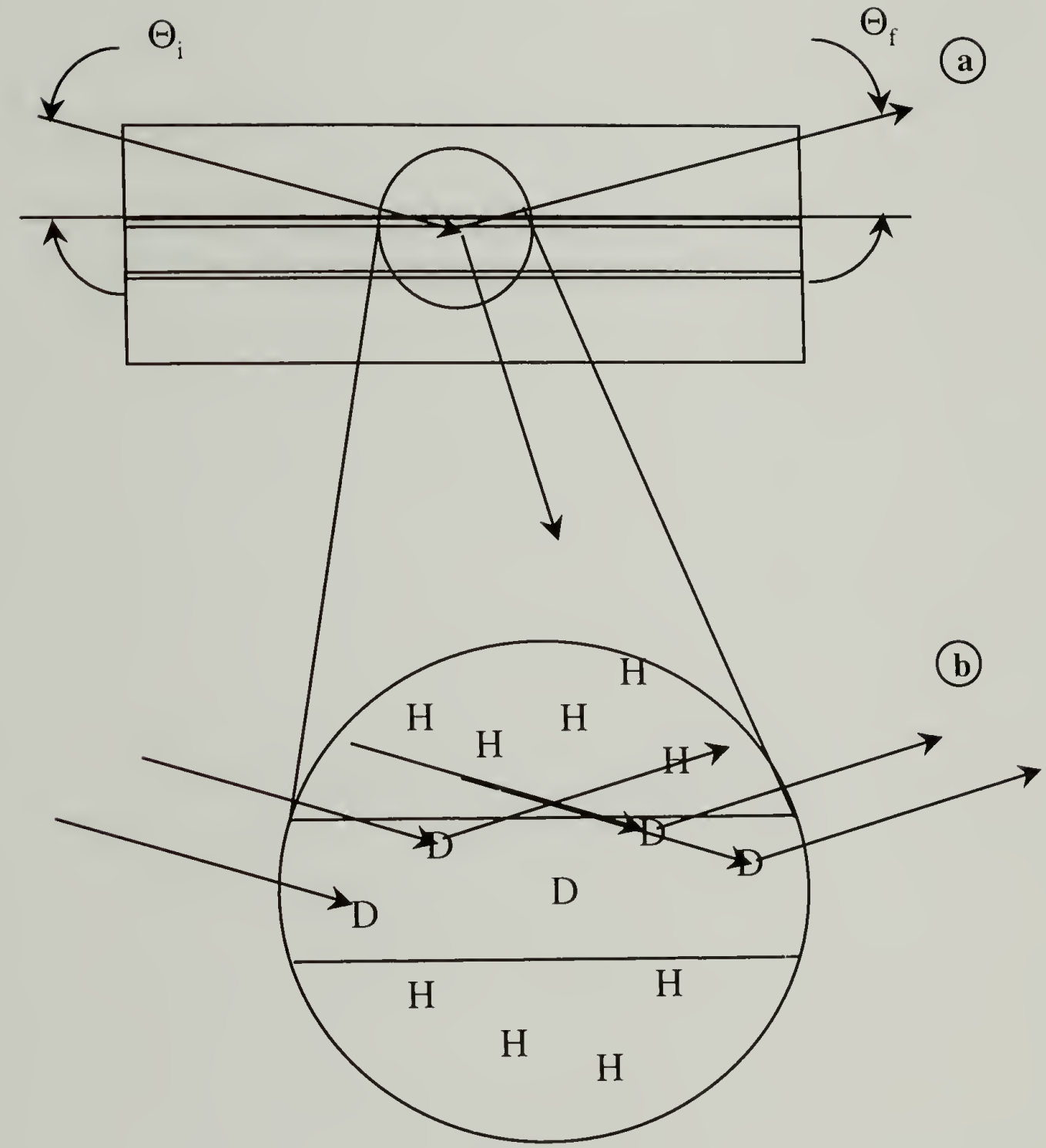

Figure 6.1 (**a**) Schematic of a Neutron Beam Reflecting off a Polymer Containing a "Layer" of Deuterated Material and (**b**) Close-up of Reflection off of Deuterium in Polymer.

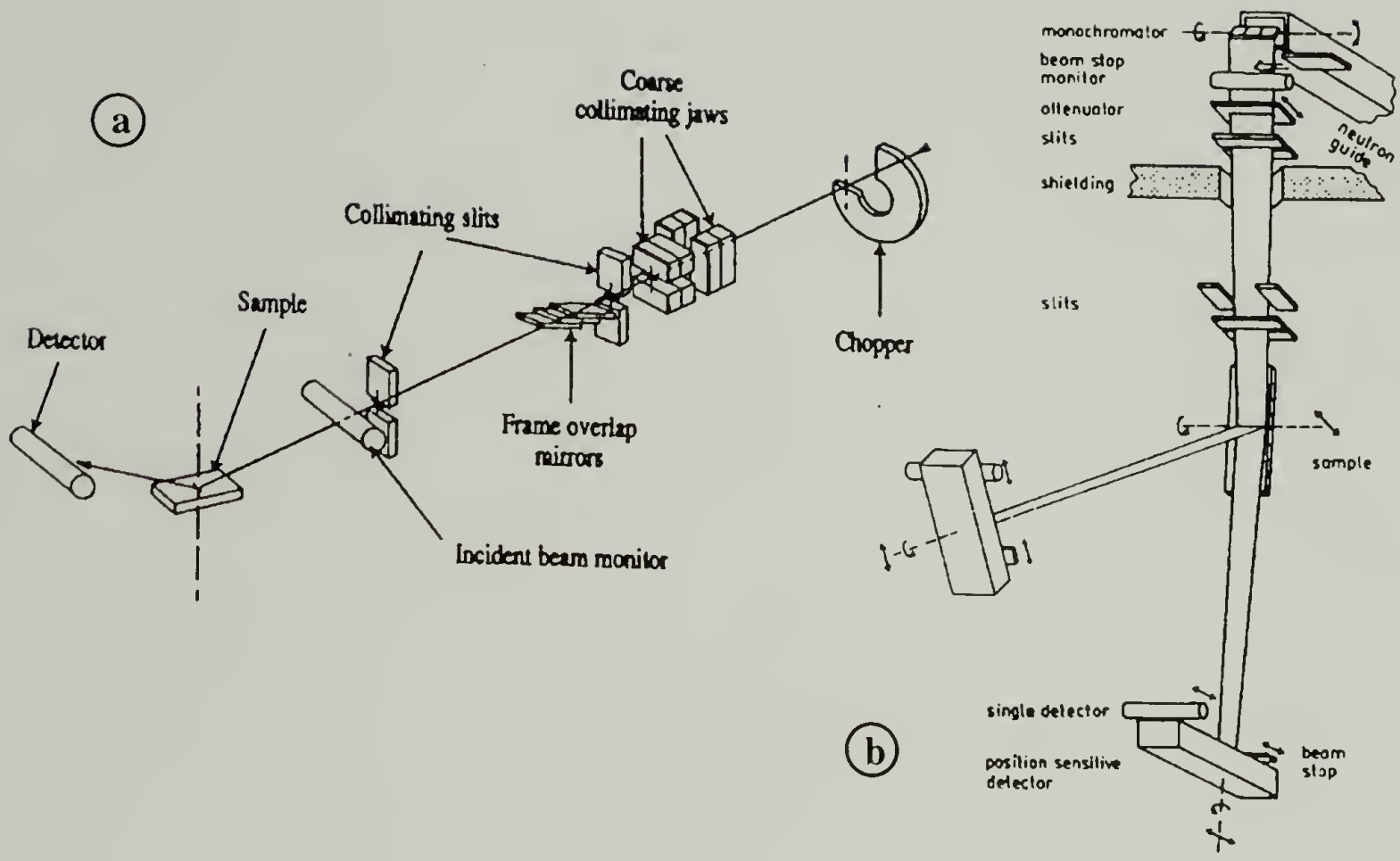

Figure 6.2 Schematics of (**a**) Spallation and (**b**) Reactor-based Neutron Reflection Instruments.[2]

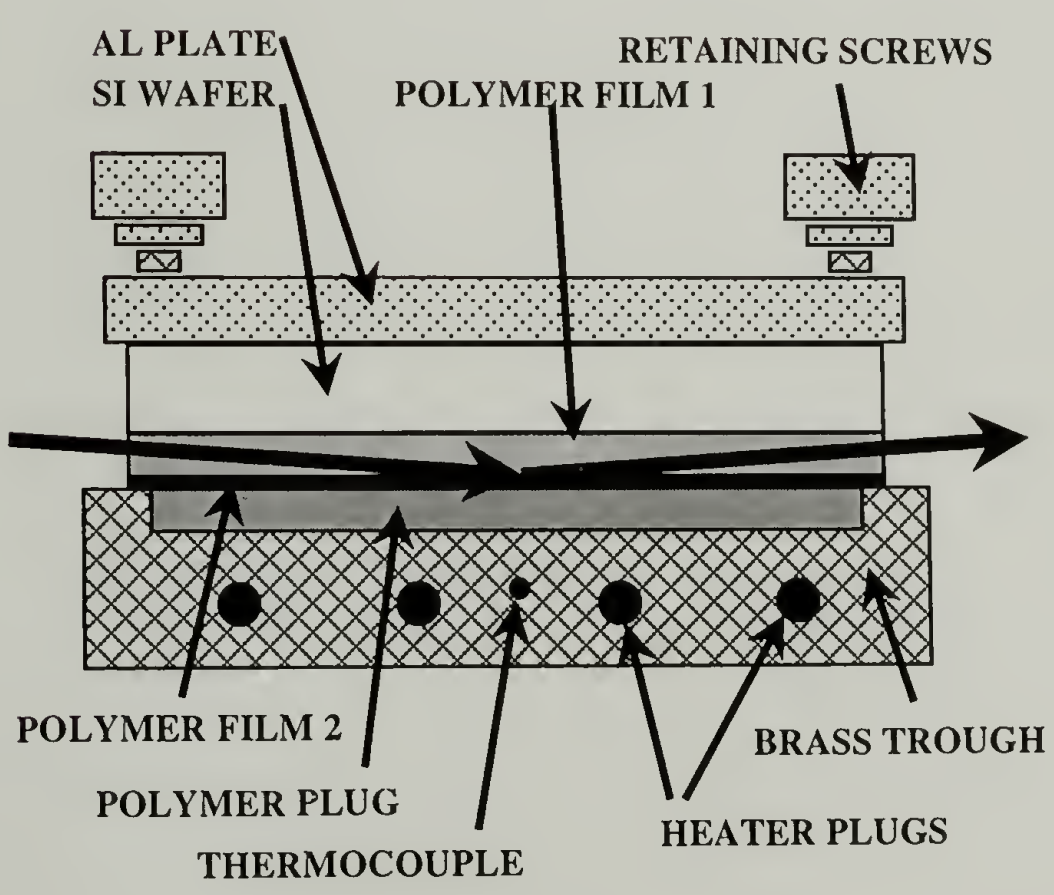

Figure 6.3 Schematic of Melt Cell used for Neutron Reflection Experiments.[10]

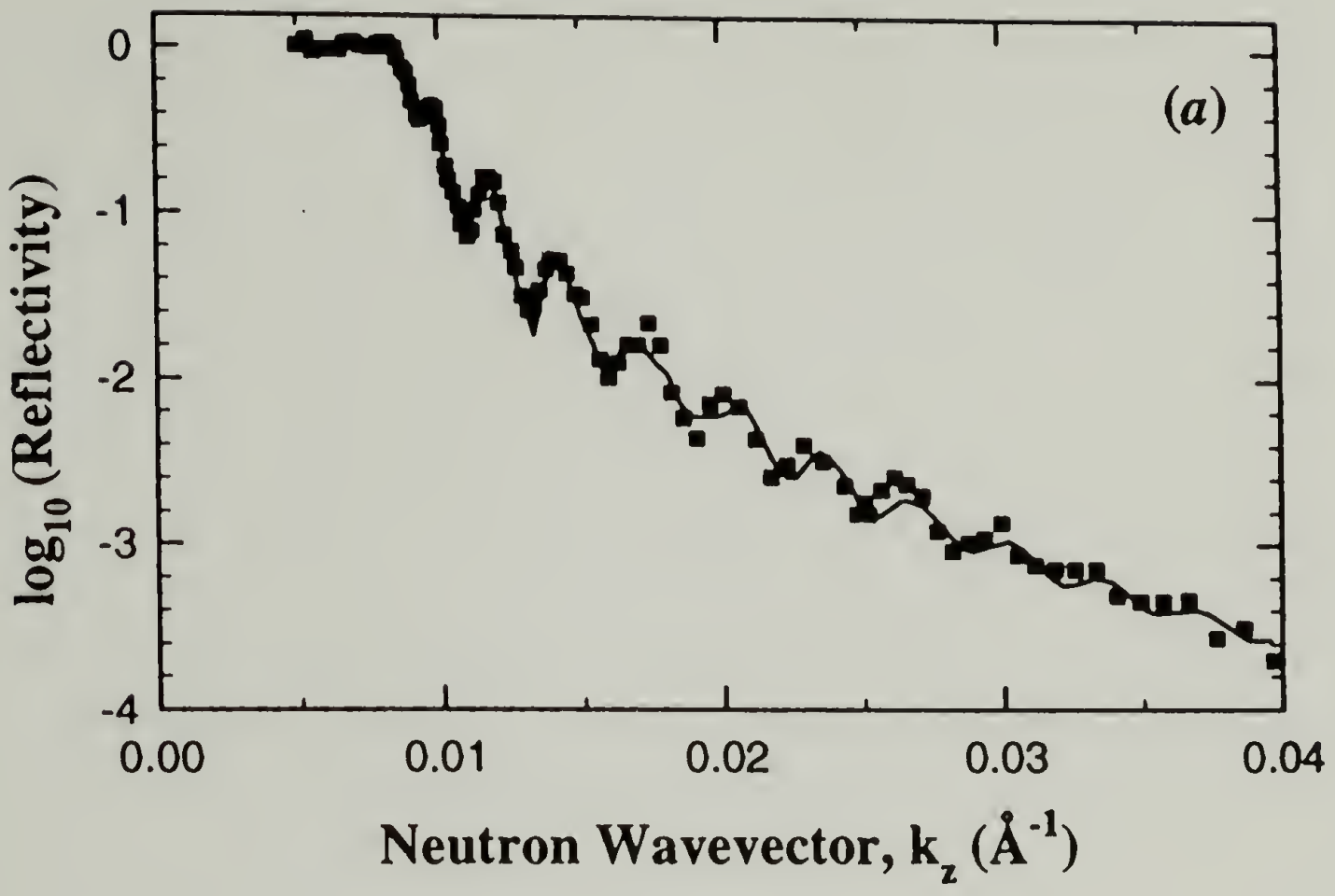

Figure 6.4 Example of "Good Data" (Composition Profile for PS-PMMA).[2]

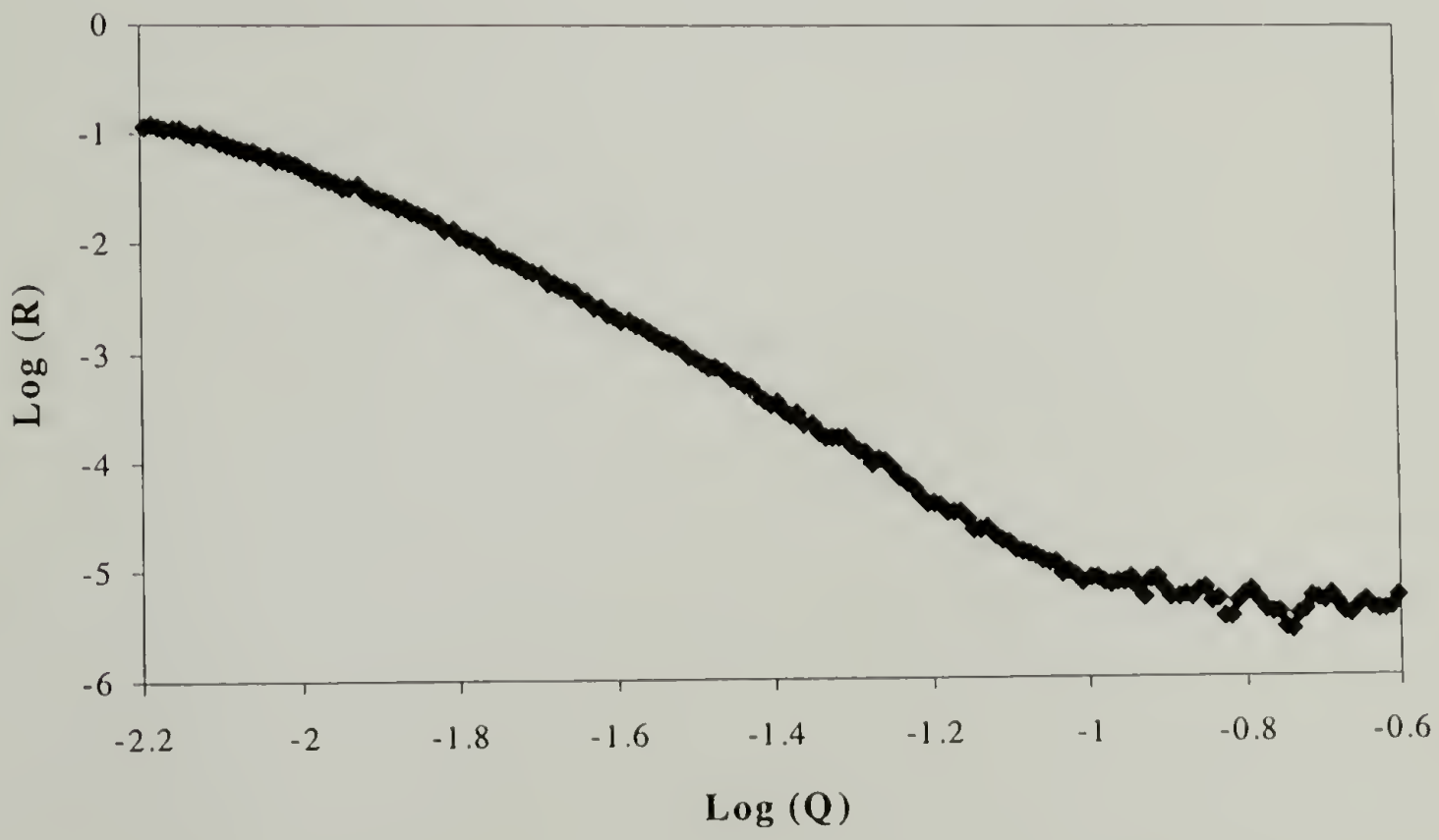

Figure 6.5 Example of "Poor Data" (Composition Profile for 1/4*d*-DEP38/*h*-PE150).

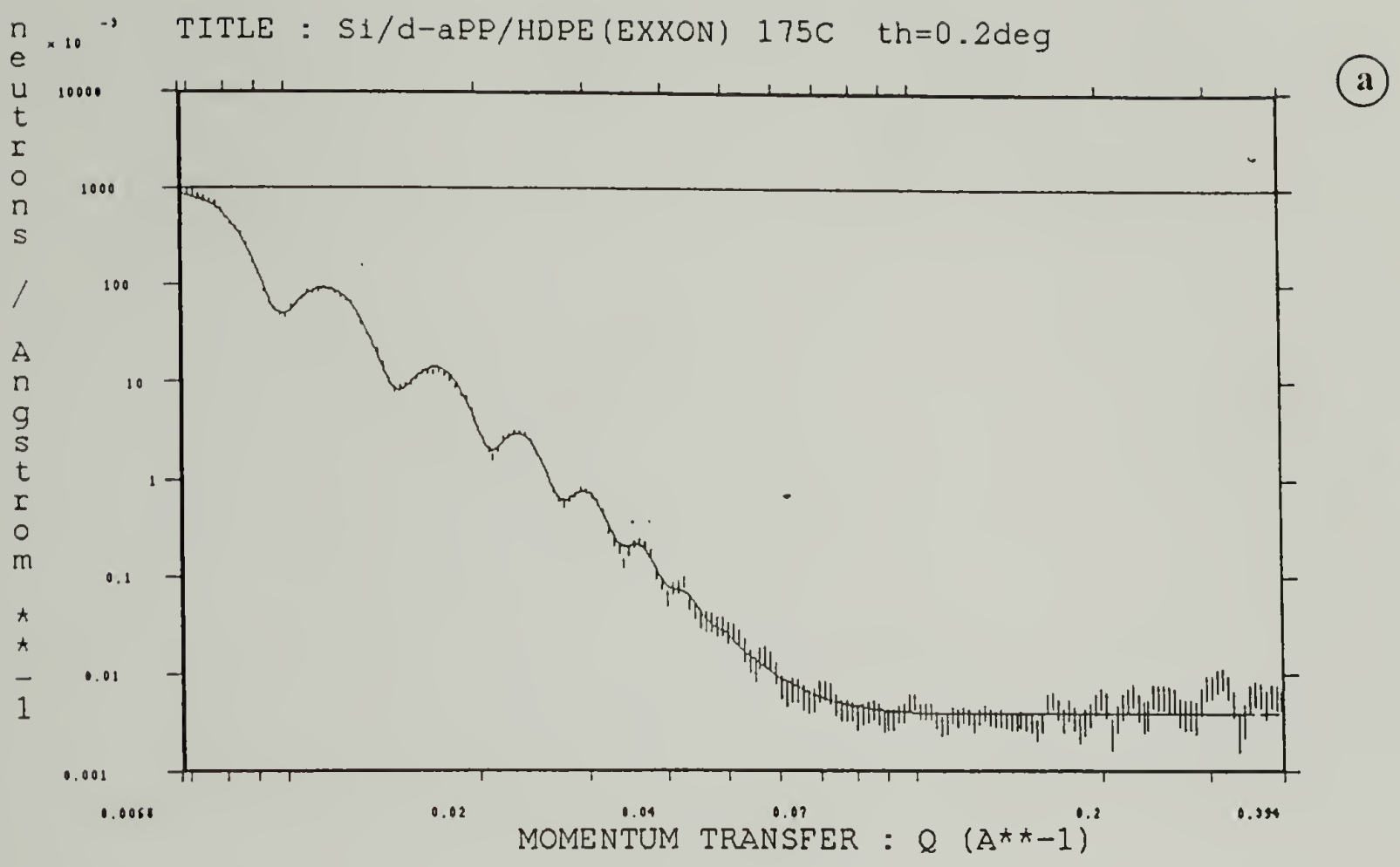

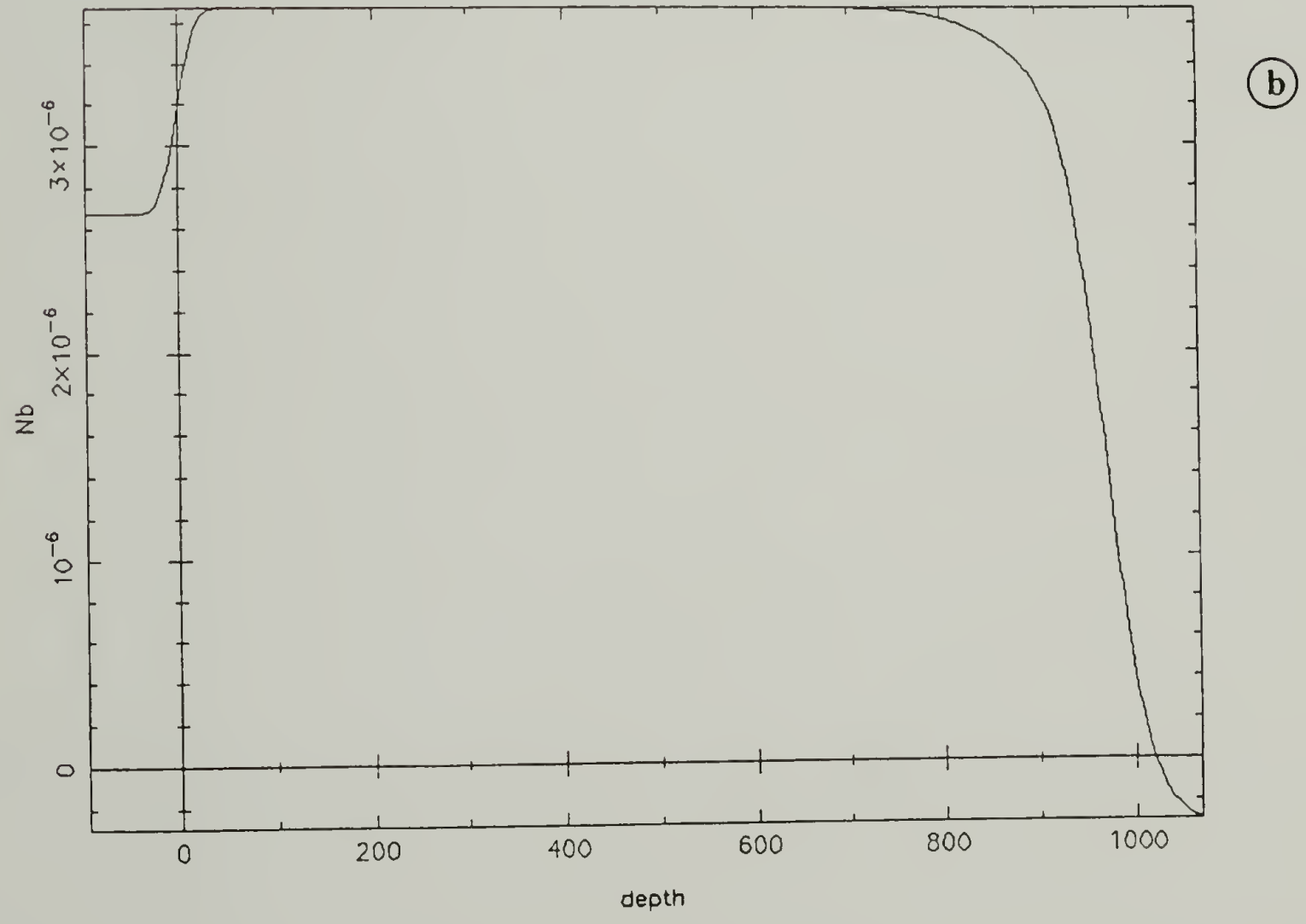

SLD profile

Figure 6.6 Reflectivity Data (**a**) and Fitted Composition Profile (**b**) for *d*-APP165/HDPE.

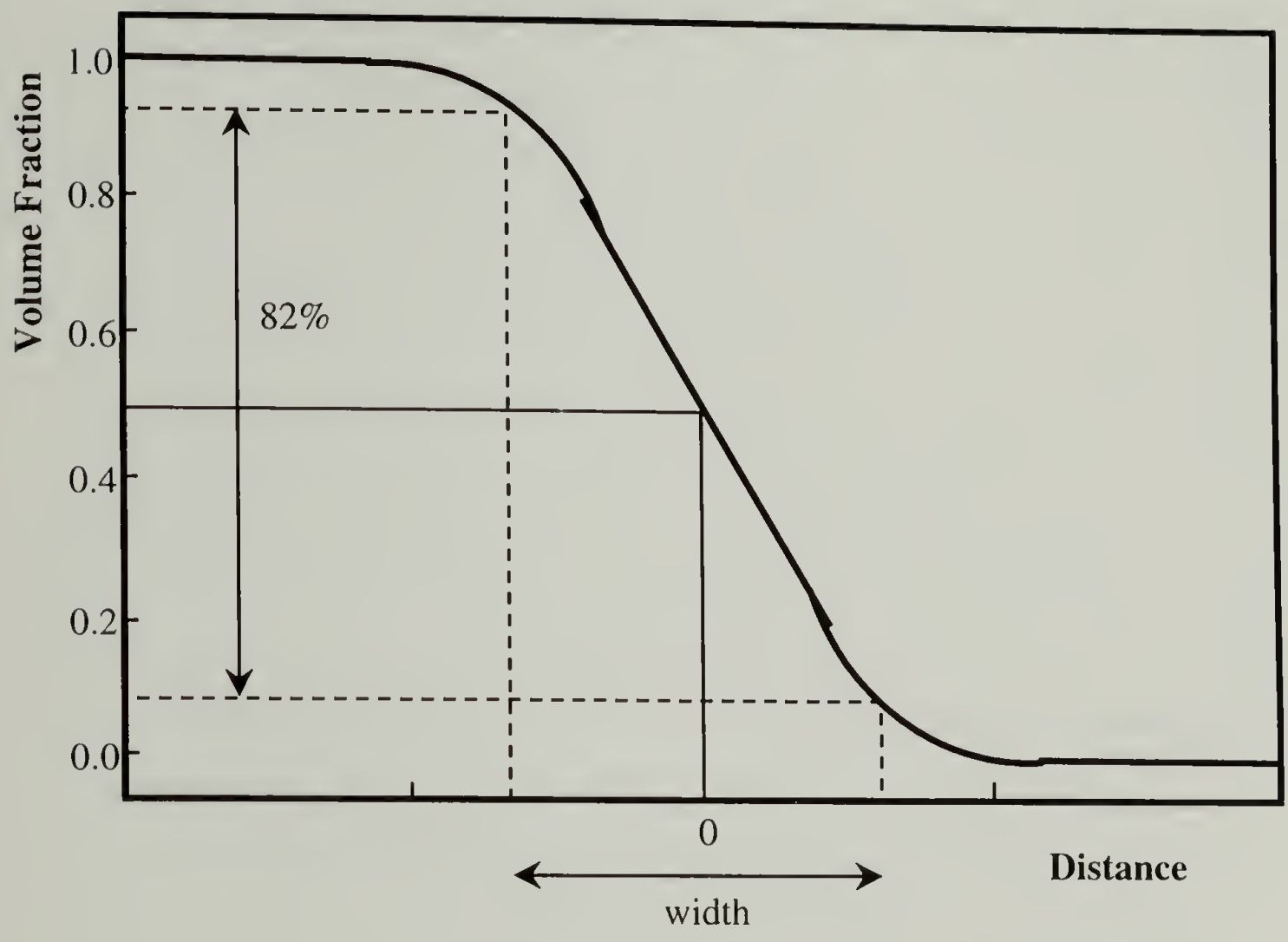

- Assuming a symmetric interfacial profile as shown schematically above, the interfacial width, *w*, is defined as the distance covered by 82% of the total change in volume fraction between the two media, centered around the half height position.

- If the interface is a Gaussian then *w* is defined as $\sigma\sqrt{2\pi}$ where σ is the Gaussian width. This method of calculating the interfacial width is most applicable when using assymetric interfaces that are described simply as a single Gaussian (or tanh) profile.

Figure 6.7 Graphical Method for Determining Interfacial Width from Volume Fraction Profiles.[27]

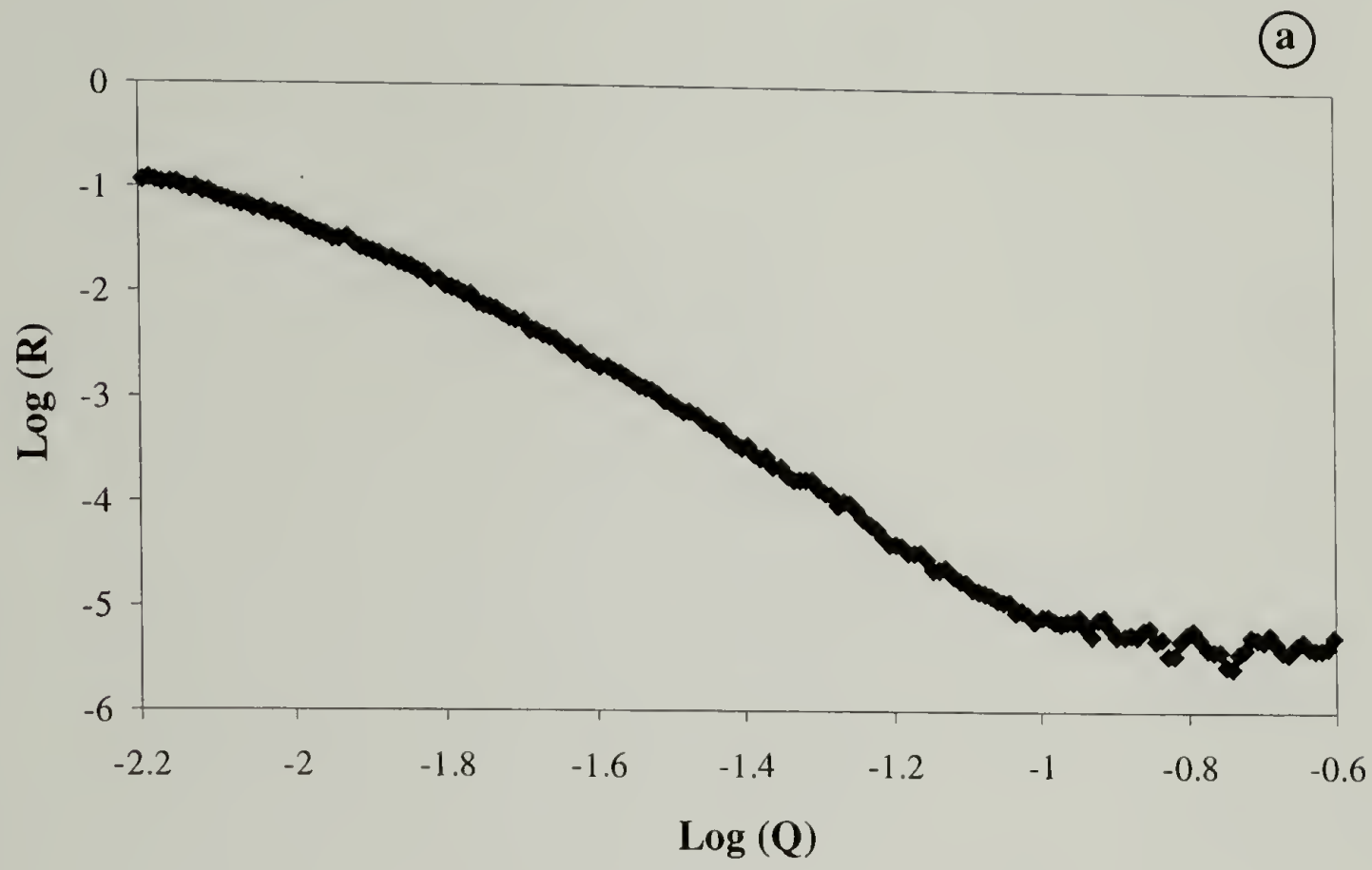

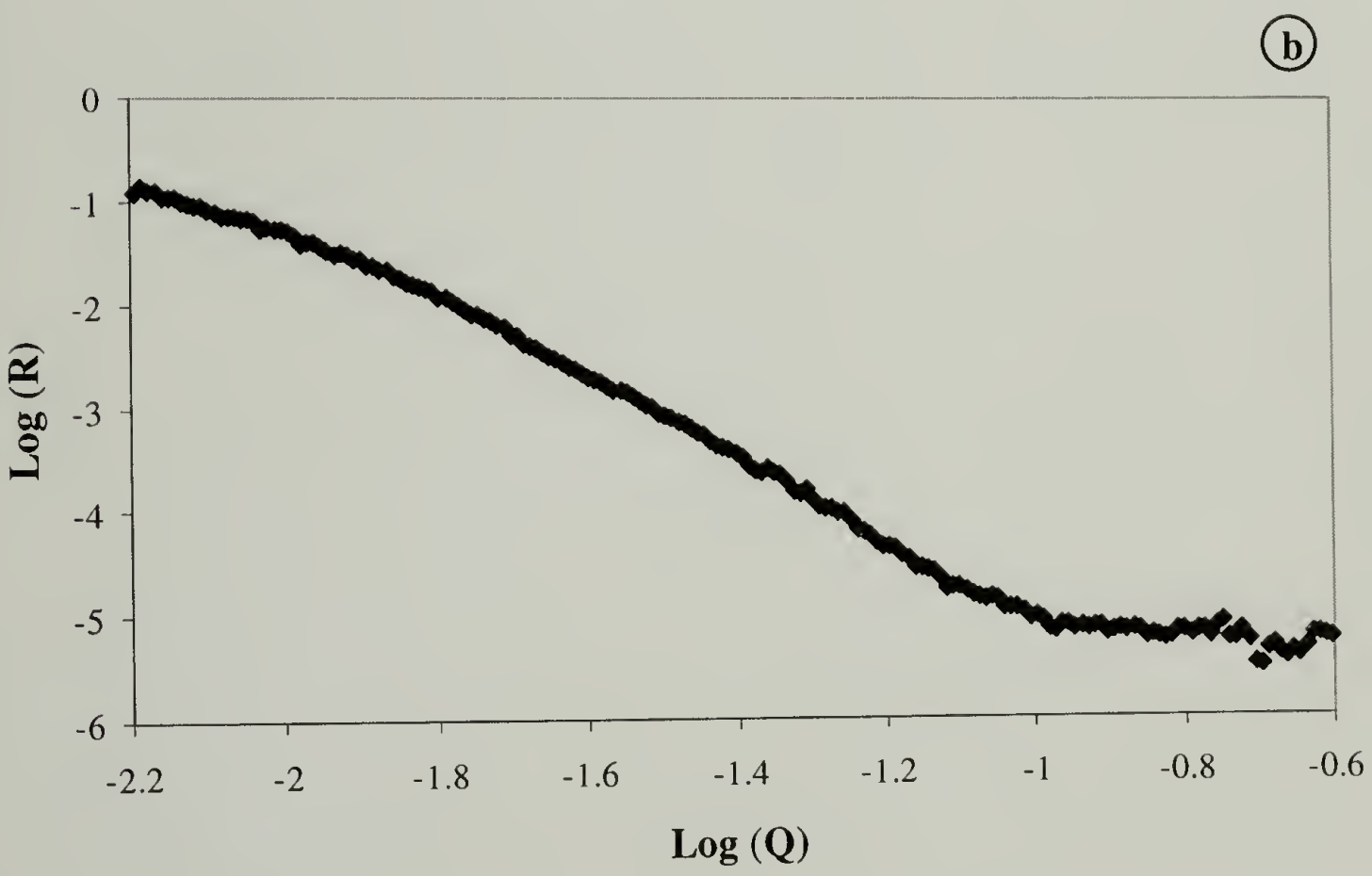

Figure 6.8 Reflectivity Data for (**a**) 1/4*d*-DEP38/LLDPE and (**b**) 3/4*d*-DEP38/LLDPE.

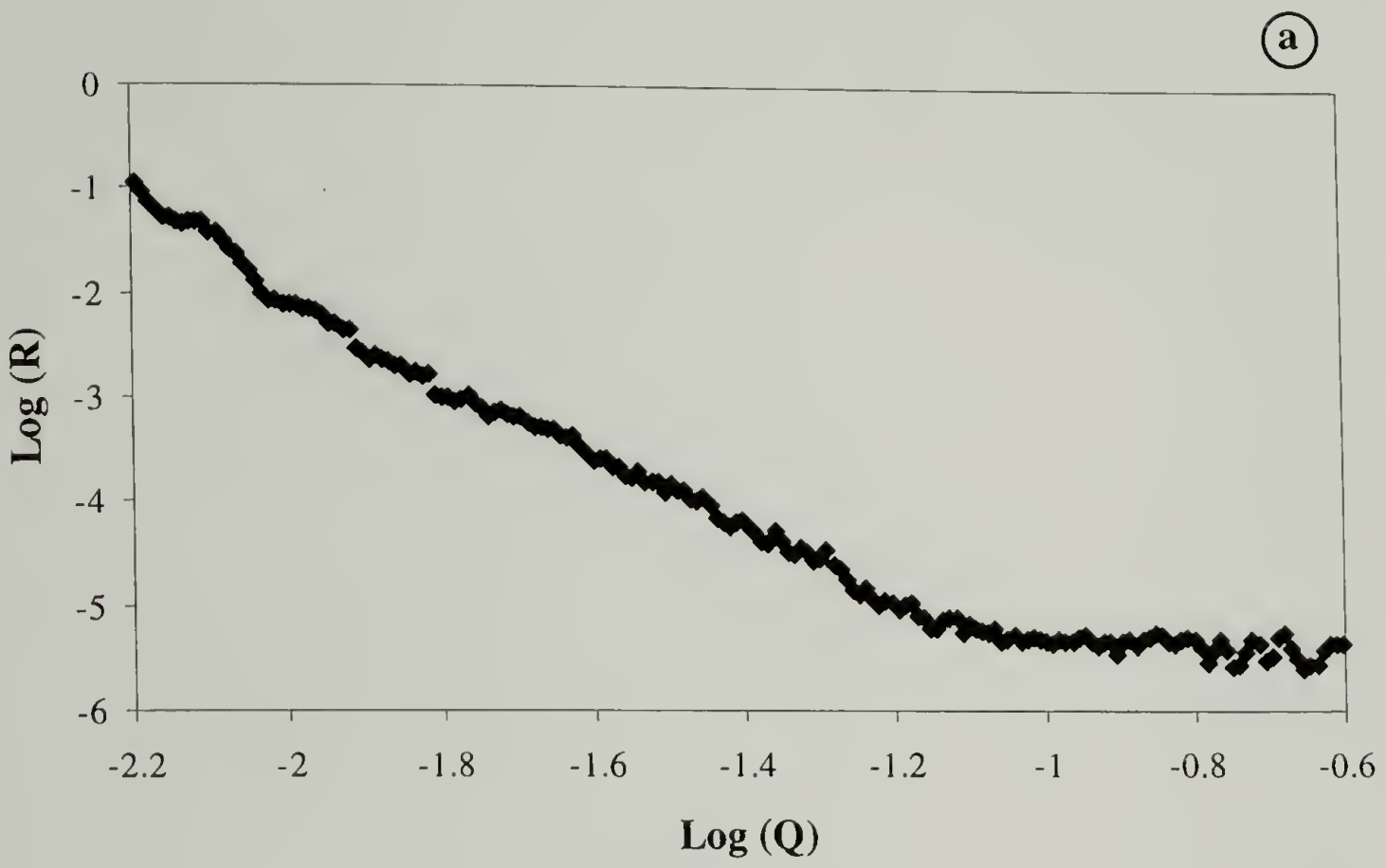

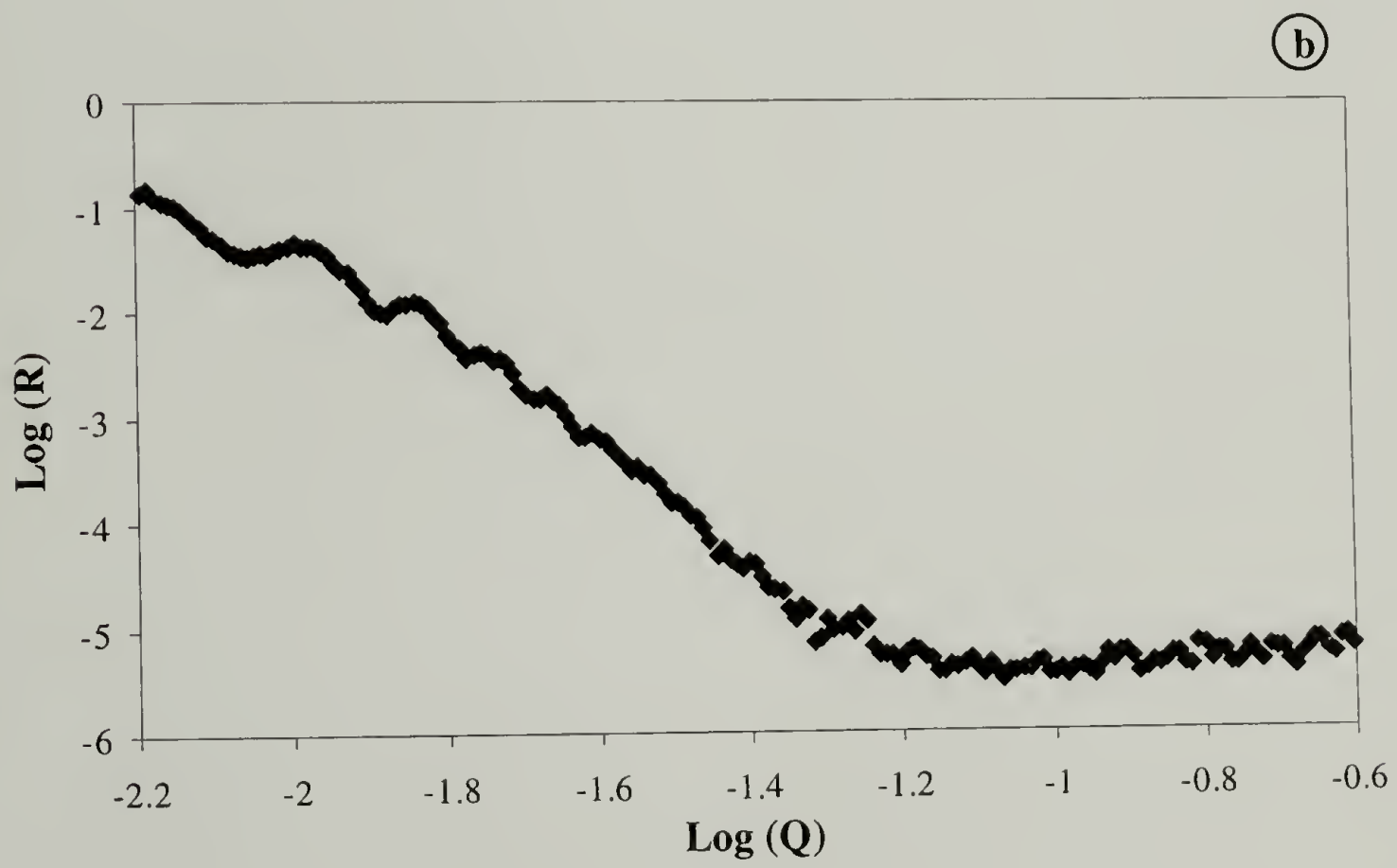

Figure 6.9 Reflectivity Data for (**a**) h-APP165/1/4*d*-DEP38/LLDPE and (**b**) *h*-APP165/3/4*d*-DEP38/LLDPE.

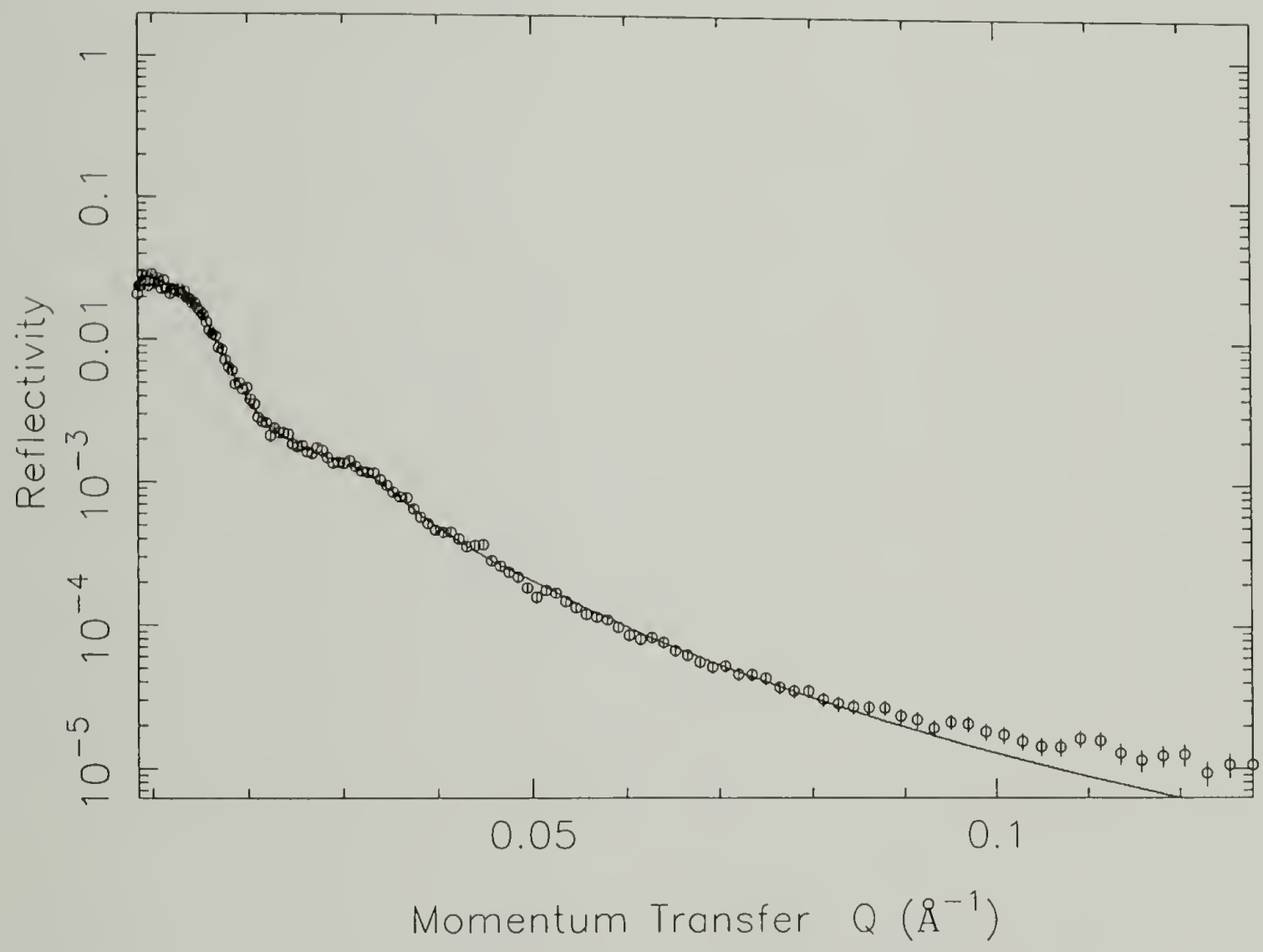

Figure 6.10 Reflectivity Data for 3/4*d*-DEP38+h-APP/LLDPE.

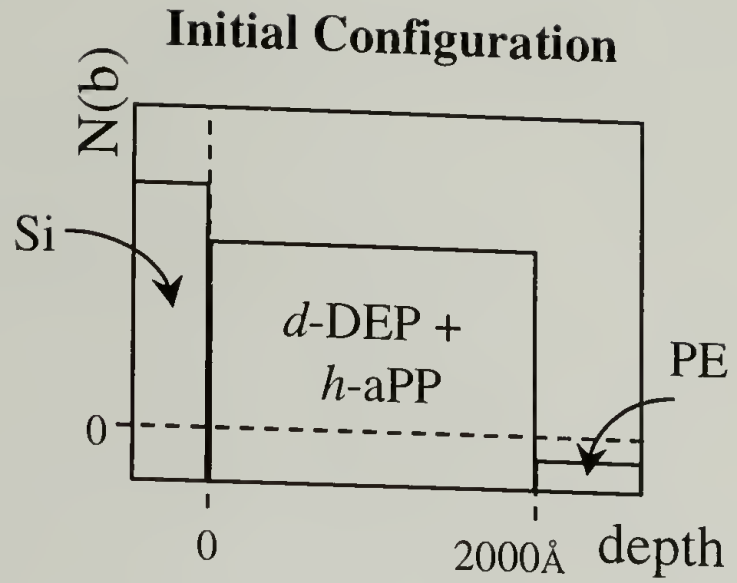

Depth Profiles Simulated

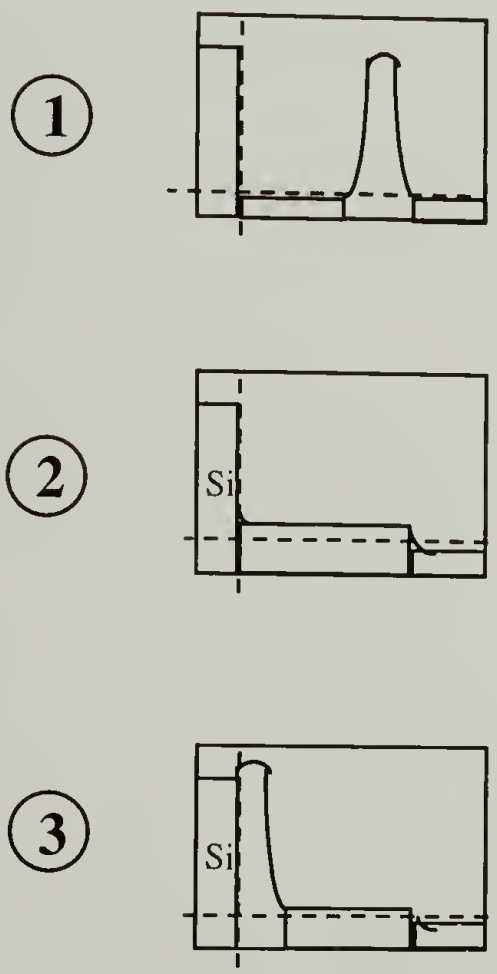

Figure 6.11 Initial Configuration and Final Depth Profiles Simulated for (h-APP165 + 3/4*d*-DEP38)/LLDPE.

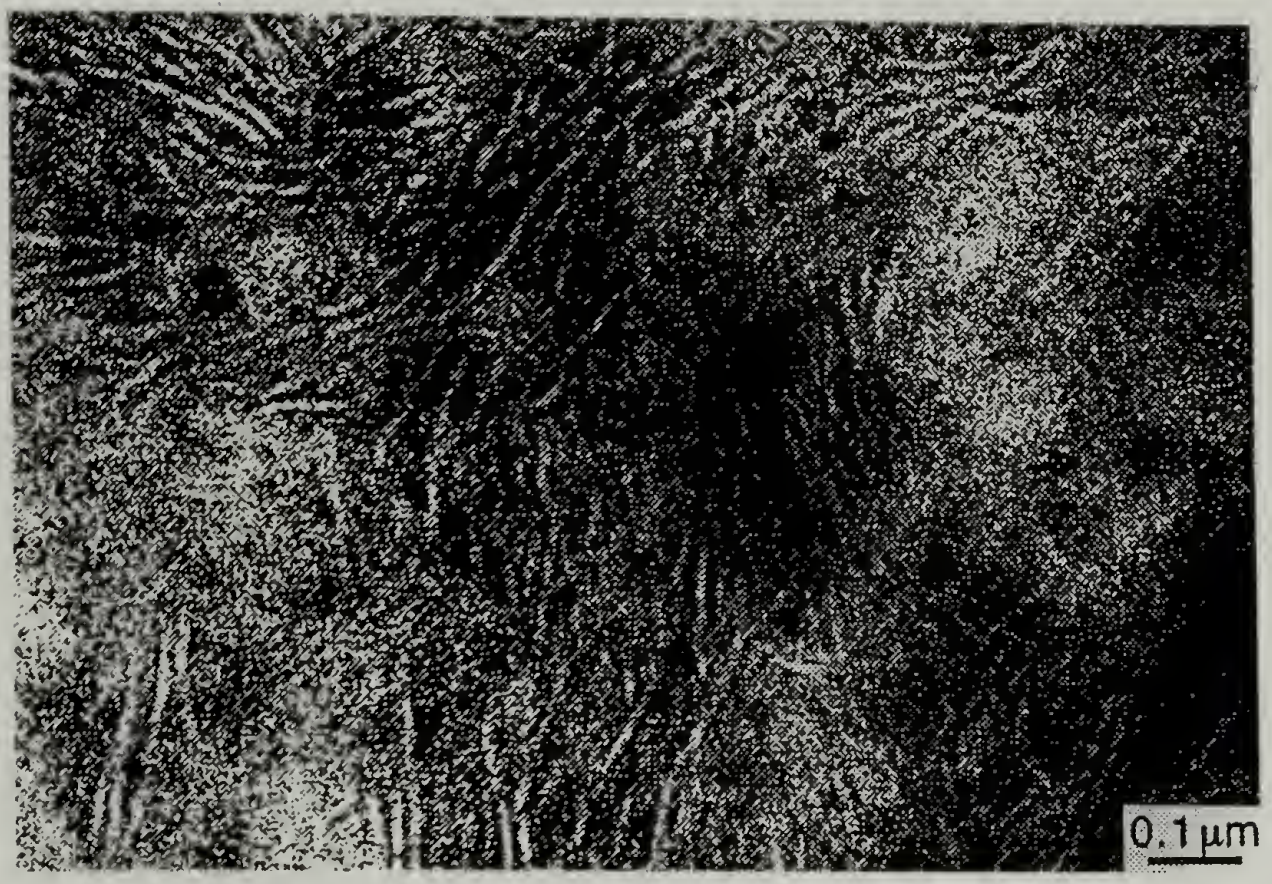

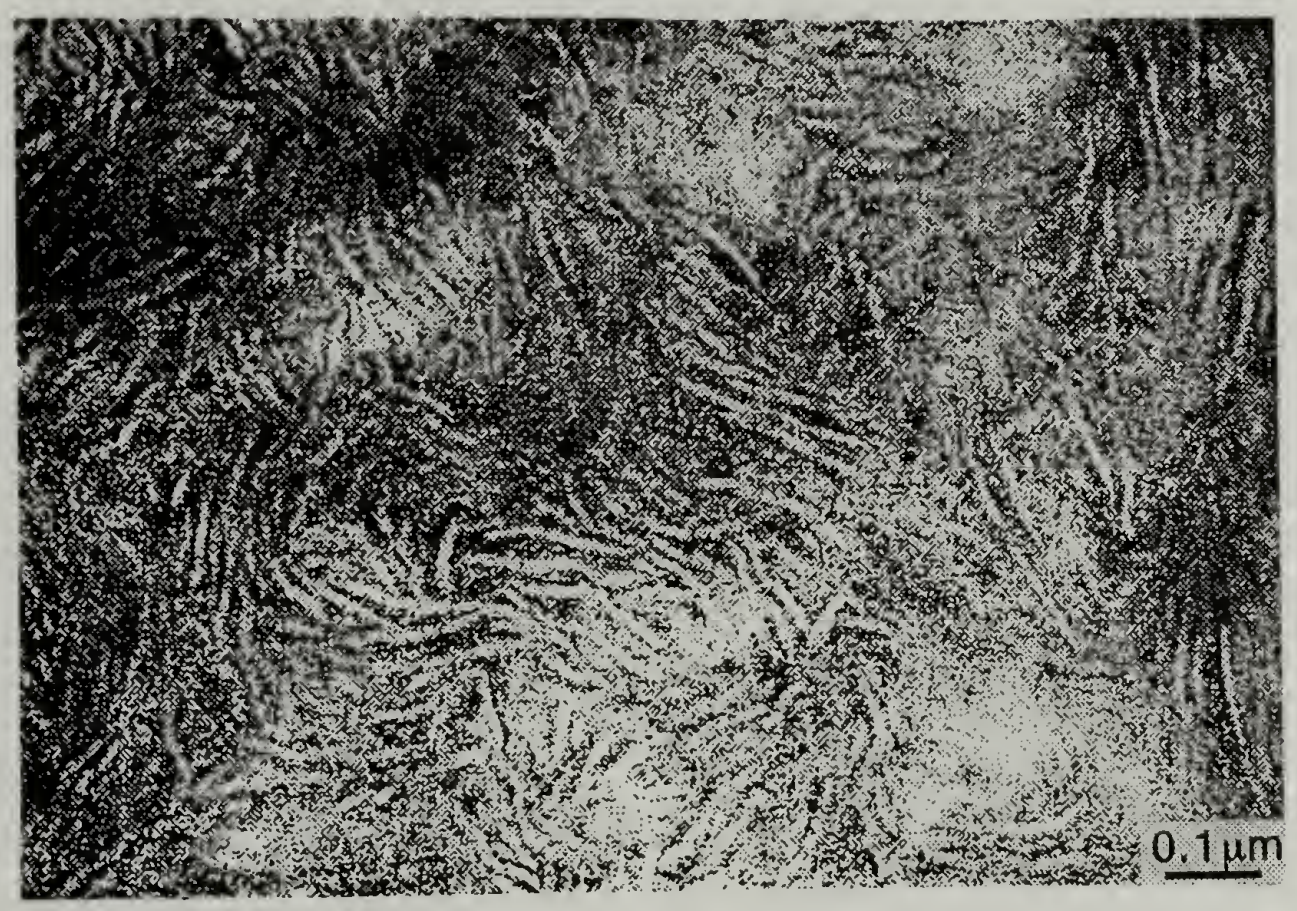

Figure 6.12 TEM Images of LLDPE.[30]

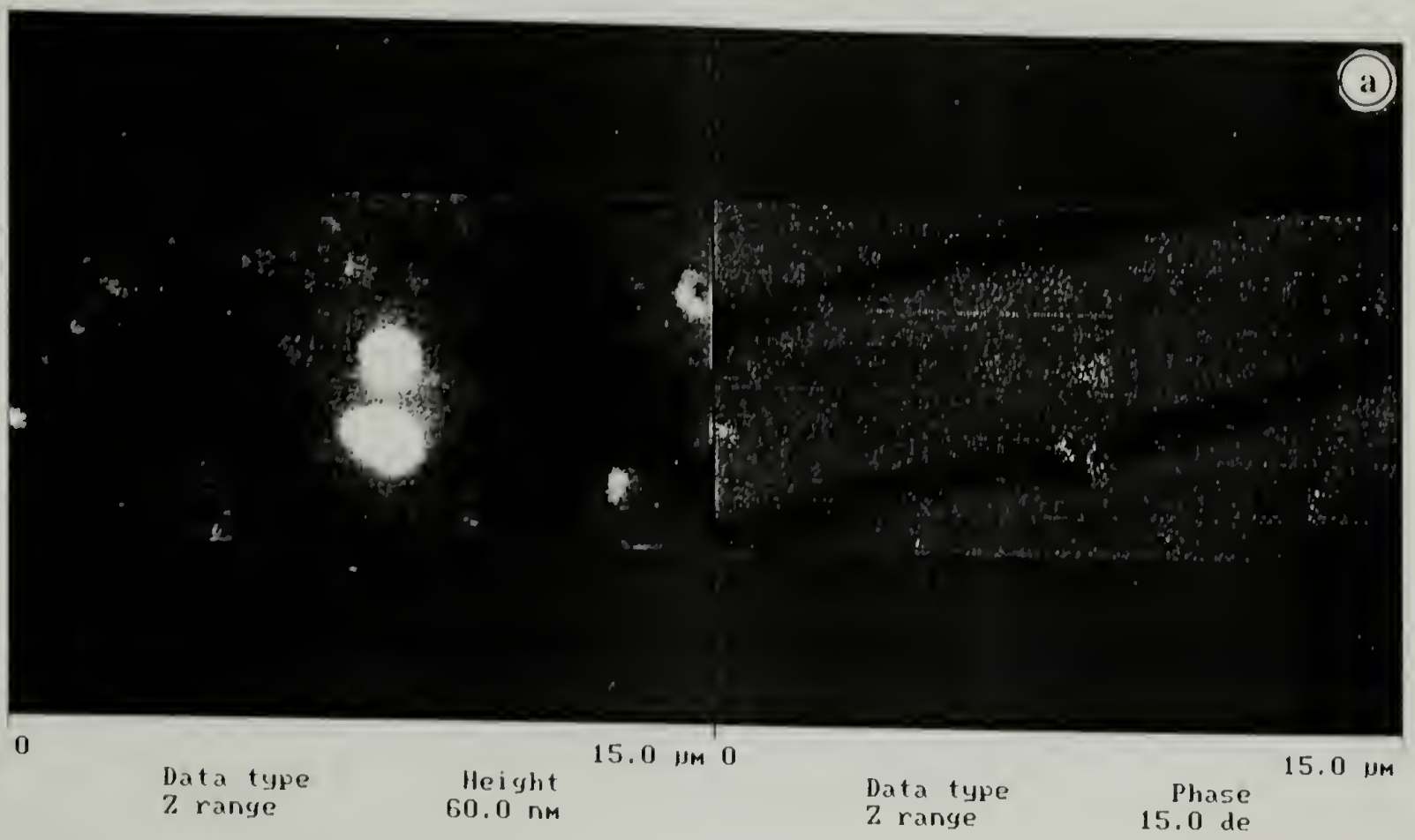

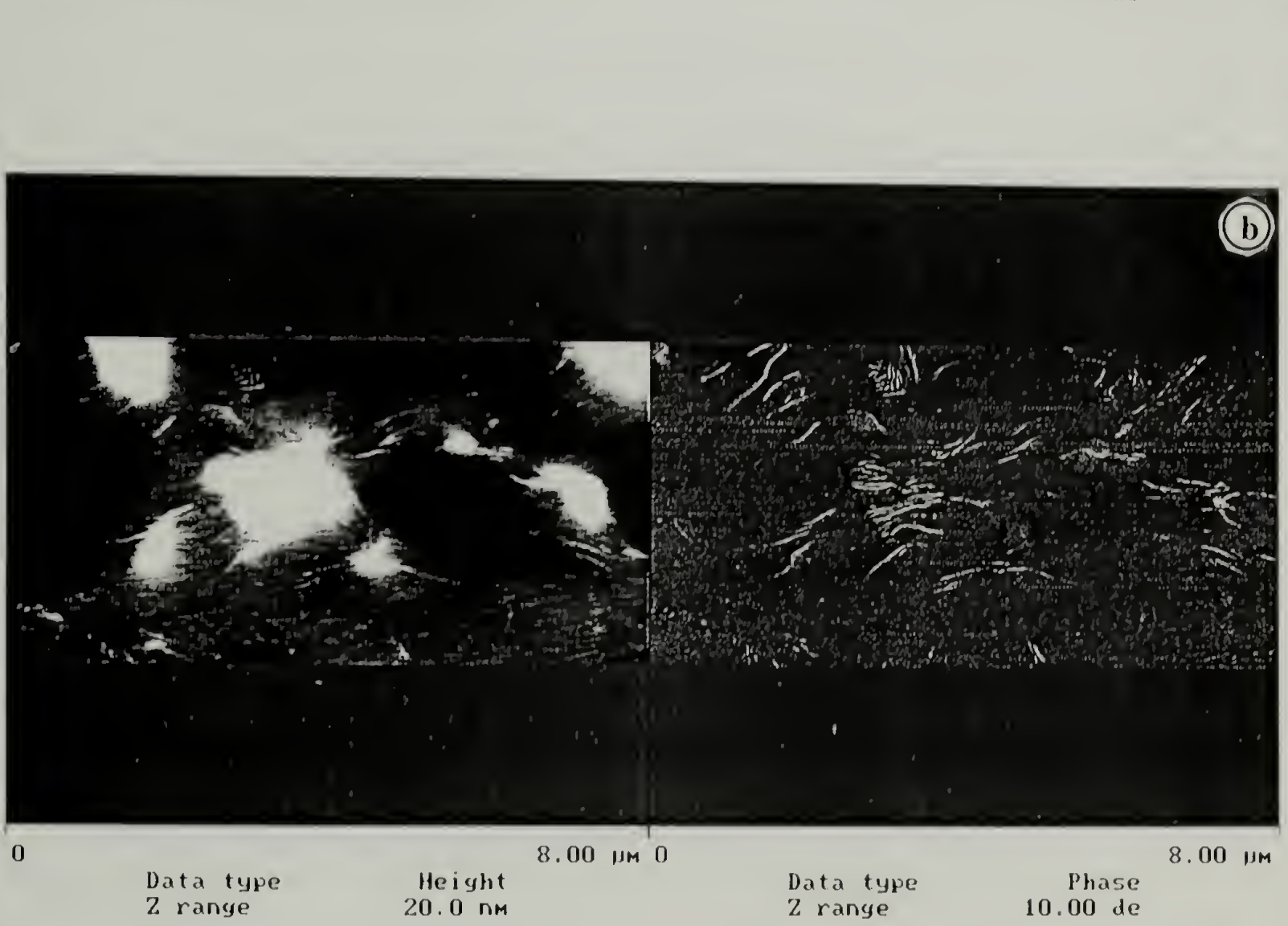

Figure 6.13 AFM Images of 15wt% Blend of 3/4*d*-DEP38 and *h*-APP165 (**a**) Before and (**b**) After Two (2) Hours of Thermal Treatment at 175°C. Believed that Structure in (**b**) is Result of Diblock Migrating to Free Surface and Forming Sheaf-like Structures on Surface.

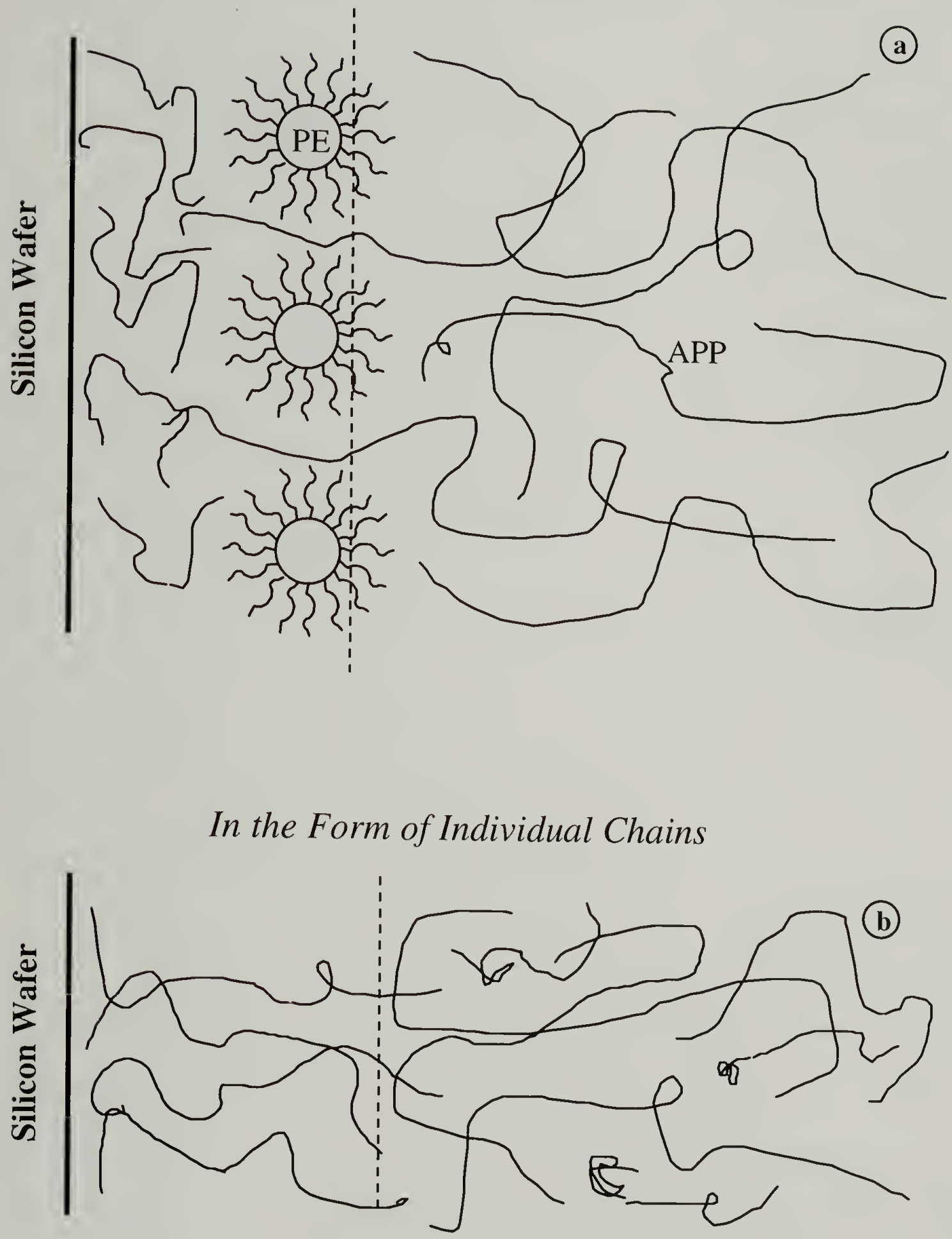

Figure 6.14 Possible Behavior of Diblock Copolymer at "Air"-Homopolymer Interface.[32] (**a**) in the form of micelles and (**b**) as individual chains.

CHAPTER 7

CONCLUSIONS AND PROPOSED FUTURE WORK

7.1 Conclusions

Living anionic polymerizations successfully yielded diblock copolymers and homopolymers based on butadiene and methyl pentadiene. Polymerizations involving DMBD were not successfully fractionated from coupled precursors, and therefore were not used in later work. Changing to MPD reduced the coupling problem and resulted in cleaner polymer samples.

A series of physical mixtures and solution blends were prepared and characterized by TG, DSC, and TEM. Solution cast blends made by the stand casting route were tested by TG. All crystallizable polymers showed onset of decomposition temperatures at least 100°C above the highest temperature to be used in this research. Degradation behavior of the saturated polybutadiene homopolymers was similar to that of a polyethylene standard, showing that the hydrogenation process was successful in producing polymers with good thermal stability. The APP homopolymer used for NR showed simple degradation which was ca. 50°C less than that of the PEs, as was expected since APP contains tertiary carbons which are less stable that secondary carbons.

Saturation was not found to increase thermal stability as was expected. The most likely reason was because the tests were performed in an inert gas stream, so the chemistry of degradation was dictated by hydrocarbon decomposition chemistry and not the anticipated presence of saturation/unsaturation. Cross-linking is believed to be responsible for the increase in thermal stability of the precursor copolymer at roughly

30wt% remaining polymer over the saturated version. Both the precursor and saturated diblock copolymers showed knees at roughly half remaining polymer which indicated a change in the type of polymer unit predominantly being degraded.

DSC was completed for heating and cooling (at 10°C/min) of physical mixtures and solution blends (the latter prepared using stand casting and water casting routes). The physical mixtures showed more resolved individual heating and cooling peaks indicative of macrophase separation, whereas both of the solution blends showed essentially one dominant melting and one dominant crystallization peak over the range of compositions. Thus, solution blending was determined to be successful in intimately mixing the polymer components.

It was realized that no change in the dominant crystallization peak should be observed anyway, since the driving force for the shift in crystallization peaks (from Peak I to Peak II) in the system DEP/APP arose from a change in continuity of the crystallizable phase (b-PE) from CNC to discrete cylinders (as seen by TEM). In the present system, the crystallizable phase is always the continuous phase. Therefore, only subtle changes in the crystallization behavior should be observed and not the large scale changes as was seen when more of the amorphous component was added.

Stand cast blends involving the high molecular weight h-PE, PE107, exhibited no shift in the dominant cooling peak for the 10°C/min cooling data. On the other hand, the cooling curves for DEP100/PE20 showed a gradual shift in the onset temperature of crystallization with increasing h-PE content. This could arise from spherulite formation, where the homopolymer serves to swell the thickness of the lamellar stack. An unusual result occurred upon cooling DEP100/PE47 blends from the melt. A small shift was

were observed for the neat diblock and the stand cast 70/30 blend of DEP100/PE20, while a disordered microphase morphology was found for the 60/40 blend. Macrophase separation was seen in the 25/75 blend of DEP100/PE20 where spheres should be observed, indicating that a microphase/macrophase separation boundary occurs between these two compositions. This behavior shows that the morphological transitions of the DEP100 + PE20 stand cast solution blends are more similar to that seen for highly asymmetric crystalline-amorphous diblock copolymers than to what was observed water cast solution blends of DEP113 + APP15.

The conclusion put forth for this morphological behavior was as follows: When the molecular weight of the h-PE is less than that of the corresponding block of the diblock copolymer (namely, $M_{h\text{-}PE} < M_{b\text{-}PE}$—Case 1 in Figure 1-5), the relatively high miscibility of the homopolymer allows morphological transitions to occur in the melt with increasing additions of the h-PE. But, upon cooling from the melt the difference in the crystallization temperatures of the two PE components causes a reduced miscibility due to the crystallization of the h-PE chains in the still-molten b-PE phase. At h-PE compositions greater that 40wt%, this led to macrophase separation occurring at lower h-PE loadings than would be observed if the system were entirely amorphous. Then, as the molecular weight of the h-PE was increased to be roughly equivalent or higher than the corresponding block of the copolymer ($M_{h\text{-}PE} \geq M_{b\text{-}PE}$—Cases 2 and 3 in Figure 1-5), the reduced miscibility of the h-PE chains in the b-PE while in the melt minimized the effect of the difference in crystallization temperatures because macrophase separation occurred almost immediately as h-PE was added to the diblock. Figure 7-1 shows a schematic of the proposed behavior.

A "ternary morphological diagram" combining the results of the work with DEP + APP[1] and the above results is presented in Figure 7-2. The utility of displaying the obtained information in this fashion is that it aides in visualizing how the complete system behaves in one plot. However, it does not anticipate how the diblock would act if it were placed at the interface between the two homopolymers. It should be read as two individual morphological diagrams, with increasing concentrations of h-APP to the right and increasing concentrations of h-PE to the left. The abscissa is relative molecular weight, with the relevant ratios on either extreme of the diagram. It is quickly seen that the behavior of the system is similar in form to that observed to asymmetric diblocks of PE-APP and PE-PEP. Unlike the pure copolymers, cylinders are not observed for the PE rich side, but instead a disordered microphase is found. To the author's knowledge, this structure is unique to this system, and a physical representation of this structure has not been previously offered.

Neutron Reflectometry was performed to investigate miscibility and interfacial behavior in the system PE/APP. The study of this system using this technique has been not explored to our knowledge, although it has the potential to make an impact in the understanding of the commercially important area of polyolefin blends. To this end experiments were performed which were designed to examine the mixing of labeled species in or against an unlabeled matrix.

The results of the investigation of the effect of the amount of short chain (ethyl) branching on miscibility at the polyethylene/atactic-polypropylene interface indicated that HDPE sample was found to have a wider interface than did the lower branch content ethylene-1-butene (EB) copolymer and that the combination of molecular weight,

polydispersity, and the presence of additives had more of an effect on miscibility than did branch content. The presence of additives should be investigated in the future using NMR.

It appears that the form and placement of the diblock copolymer has a large effect on mobility and diffusional behavior when in the presence of the corresponding homopolymers. When placed as blend in the amorphous homopolymer, simulations indicated that migration of the diblock to the free surface occurred, possibly due to surface free energy effects. Substantiation of this interpretation was studied using AFM. When placed as a film, the diblock appeared to dissolve into either one or both of the homopolymers as micelles or as individual chains. Determination of the form of the migrating copolymer would rely on SANS experiments to determine the size of the labeled species.

Cleaning silicon wafers with an HF etching technique proved successful in minimizing the film detachment problem in spun cast polymer films on the silicon. Since the hydrogenation catalyst could not be remove from the hydroxy-terminated APP polymer, the use of an adhesion-promoting polymer to bridge the hydrophobic/hydrophilic interface was discontinued.

7.2 Future Work

Several interesting studies should be pursued to answer some of the questions arrived at during the course of the research performed for this dissertation.

(1) Complete TEM and polarized light microscopy studies of the pure DEP100 and the 50/50 DEP100/PE20 stand cast blends cooled at various rates using the DSC. (See Table 7-1 for a list of the cooling rates.) This will determine whether intermediate structures may exist.

(2) Complete the TEM study of the morphology of the solution blends made by the stand casting technique to strengthen the conclusions drawn in this work concerning crystallization, relative block lengths, composition, miscibility, and morphology.

(3) Complete the AFM work on the blends of 5wt% *d*-DEP38 and h-APP162 by investigating the changes in surface morphology of the neat diblock, a neat LLDPE, and the neat APP162 before and after the two hour melt annealing cycle to strengthen the assertion that the deuterated diblock is migrating to the free surface upon heating to the melt.

(4) Perform TEM studies on the effect of solution casting technique on the final morphology of blends of DEP100 and on PE20, on PE47, and on PE107 to determine whether differences observed in the crystallization behavior of the blends (by DSC) can be seen by TEM.

(5) Perform Single Crystal studies using the neat diblock copolymer to investigate whether single crystals of the symmetric copolymer can be formed or whether the presence of the amorphous block completely disrupts this phenomenon.

7.3 References

1. Sakurai, K.; MacKnight, W. J.; Lohse, D. J.; Schulz, D. N.; Sissano, J. A.; Lin, J.-S.; Agamalyan, M. *Polymer* **1996**, *37*, 4443.

2. Ryan, A. J.; Hamley, I. W.; Bras, W.; Bates, F. S. *Macromolecules* **1995**, *28*, 3860.

Table 7.1 List of Rates for Variable Cooling Rate Study.

Cooling Rates
Quench in Liq. N_2
320°C/min
300°C/min
250°C/min
200°C/min
175°C/min
150°C/min
125°C/min
100°C/min
80°C/min
60°C/min
40°C/min
30°C/min
20°C/min
10°C/min

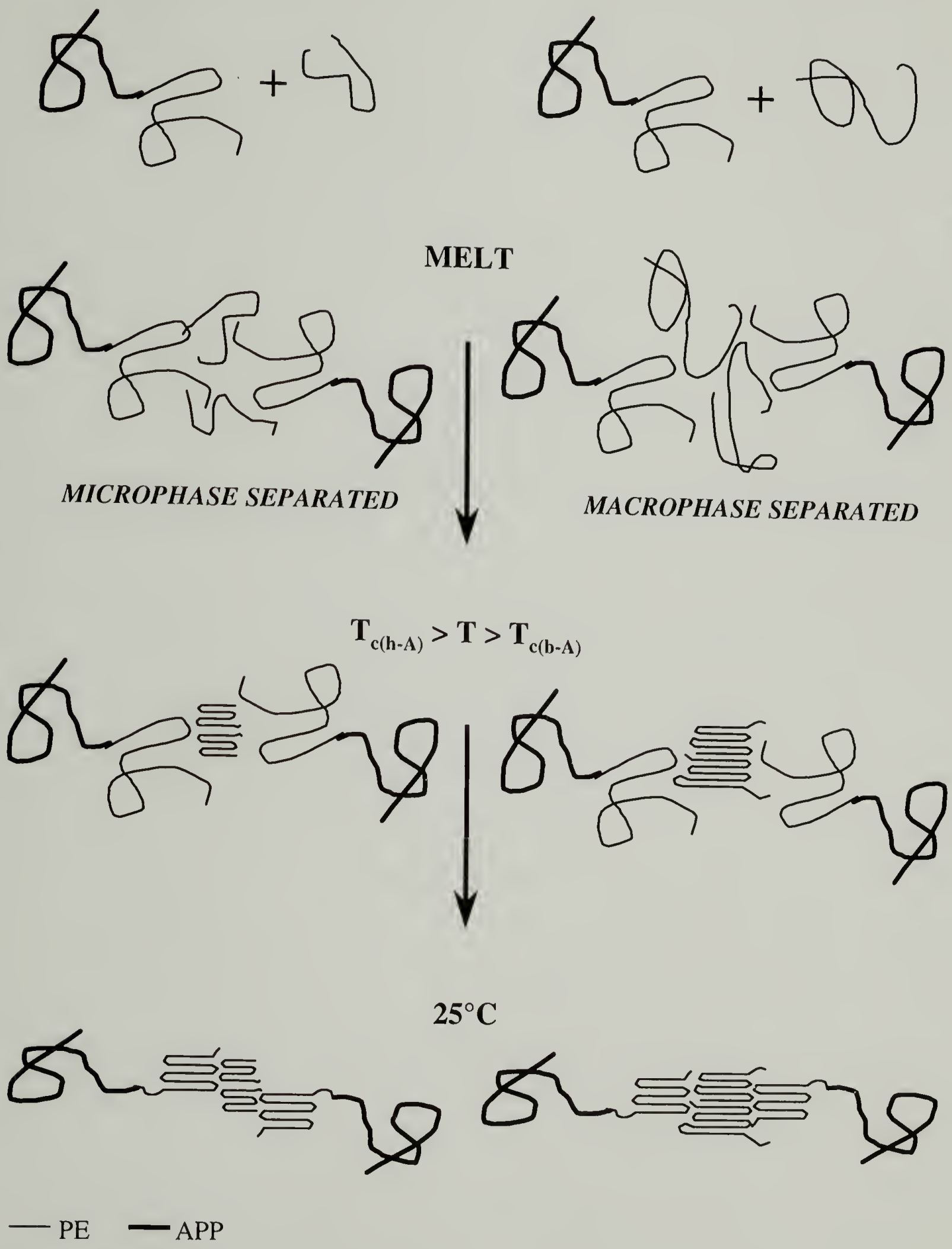

Figure 7.1 Mechanism for System DEP/PE Demonstrating the Effect of Molecular Weight Ratio and Crystallization on Phase Behavior.

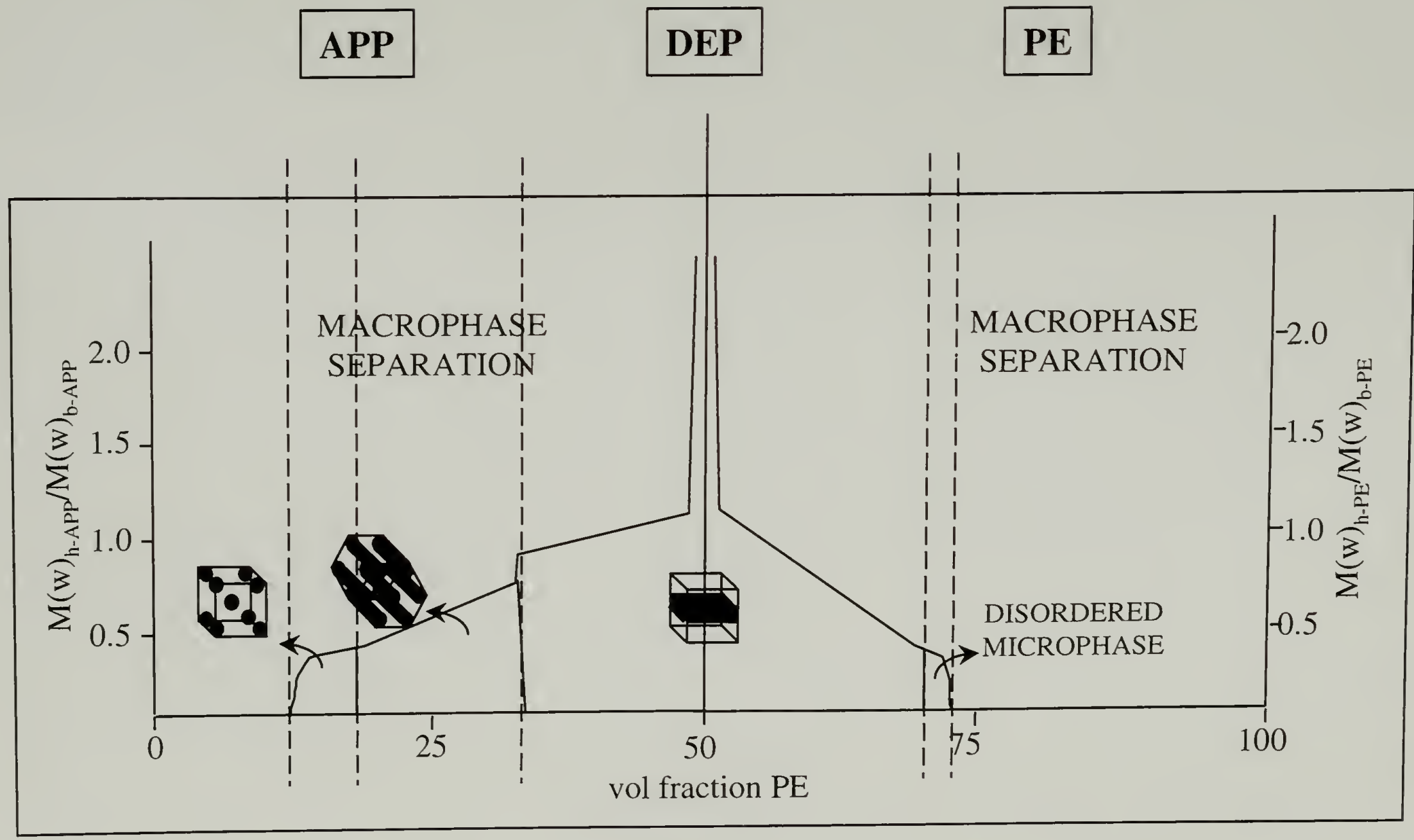

Figure 7.2 Proposed Ternary Morphological Diagram to Predict Blend Behavior.

BIBLIOGRAPHY

Alamo, R. G.; Mandelkern, L. *Macromolecules* **1991** *24*, 6480-93

Alamo, R. G.; Graessley, W. W.; Krishnamoorti, R.; Lohse, D. J.; Mandelkern, L.; Londono, D. L.; Wignall, G. D. *Macromolecules* **1997**, *30*, 561-6.

Allport, D. C.; Barker, C.; Chapman, J. F., in Developments in Block Polymers—1, Goodman, I., ed., Elsevier Applied Science Publishers: London, 1982.

Almdal, K.; Bates, F. S, *Macromolecules*, **1992**, *25*, 1743-51.

Avgeropoulos, A.; Poulos, Y.; Hadjichristidis, N.; Roovers, J. *Macromolecules* **1996**, *29*, 6076-8.

Avrami, M. *J. Chem. Phys.* **1939**, *7*, 1103-12; **1941**, *9*, 177-84.

Balta-Calleja, F. J.,; Vonk, C. G. X-ray scattering of synthetic polymers, Elsevier: London, 1989.

Bates, F. S.; Cohen, R. E.; Berney, C. V. *Macromolecules* **1982**, *15*, 589-92.

Bates, F. S.; Bair, H. E.; Hartney, M. A. *Macromolecules* **1984**, *17*, 2607-13.

Beyer, F. L.; Gido, S. P.; Poulos, Y.; Hadjichristidis, N. *Macromolecules* **1997**, *30*, 2373-6.

Blondin, D.; Regis, J.; Prud'homme, J. *Macromolecules* **1974**, *7*, 187-90.

Born, M.; Wolf, E. Principles of Optics, 6th Edition, Permagon Press: Oxford, 1980.

Bucknall, D. G.; Higgins, J. S.; Penfold, J.; Rostami, S. *Polymer* **1993**, *34*, 451-7.

Bucknall, D. G. and Higgins, J. S. "Neutron Reflection Studies of Polymer-Polymer Interfaces" CLRC Technical Report No. RAL-TR-97-008, January, 1997.

Bucknall, D. G.; Butler, S. A.; Hermes, H. E.; Higgins, J. S. *PMSE Preprints* **Fall, 1998**, *32*, 292-3.

Cahn, J. W.; Hilliard, J. E. *J. Chem. Phys.* **1958**, *28*, 258.67.

Charsley, E. L.; Warrington, S. B., ed. Thermal Analysis—Techniques and Applications, Royal Society of Chemistry: Cambridge, UK, 1992.

Chillura-Martino, D.; Triolo, R.; McClain, J. B.; Combes, J. R.; Betts, D. E.; Canelas, D. A.; DeSimone, J. M.; Samulski, E. T.; Cochran, H. D.; Londono, J. D.; Wignall, G. D. *J. Molec. Structure* **1996**, *383*, 3-10.

Christian, G. D.; J. E. O'Reilly, ed. Instrumental Analysis, Second Ed., Allyn and Bacon, Inc.: Boston, 1986.

Chiu, J., in Thermal Analysis of Fiber and Fiber-Forming Polymers, Schwenker, R. F., ed., Interscience: New York, 1966.

Cohen, R. E.; Wilfong, D. E. *Macromolecules* **1982**, *15*, 370-5.

Cohen, R. E.; Torradas, J. M. *Macromolecules* **1984**, *17*, 1101-2.

Cohen, R. E.; Cheng, P. L.; Douzinas, K.; Kofinas, P.; Berney, C. *Macromolecules*, **1990**, *23*, 1690-5.

Dai, C.-A.; Kramer, E. J.; Washiyama, J.; Hui, C.-Y. *Macromolecules* **1996**, *29*, 7536-43.

Datta, S.; Lohse, D. J. Polymer compatibilizers: uses and benefits in polymer blends, Hanser/Gardner Publications, Inc.: Cincinnati, OH, 1996.

DiMarzio, E. A.; Guttman, C. M.; Hoffman, J. D. *Macromolecules* **1980**, *13*, 1194-8.

Douzinas, K. C.; Cohen, R. E.; Halasa, A. F. *Macromolecules* **1991**, *24*, 4457-9.

Douzinas, K. C.; Cohen, R. E. *Macromolecules* **1992**, *25*, 5030-5.

Ergoz, E.; Fatou, J. G.; Mandelkern, L. *Macromolecules* **1972**, *5*, 147-57.

Fernandez, M. L.; Higgins, J. S.; Penfold, J.; Shackleton, C.; Walsh, D. J. *Polymer* **1988**, *29*, 1923-28.

Ferreira, P. G.; Leibler, L. *J. Chem. Phys.*, **1996**, 105, 9362-70.

Fetters, L. J. *J. Polym. Sci.: Part C* **1969**, *26*, 1-35.

Fetters, L. J.; Balsara, N. P.; Huang, J. S.; Jeon, H. S.; Almdal, K.; Lin, M. Y. *Macromolecules* **1995**, *28*, 4996-5005.

Fossum, E. K.; Matyjaszewski, K.; Shieko, S. S.; Möller, M. *Macromolecules* **1997**, *30*, 1765-7.

Fredrickson, G. H.; Helfand, E. *J. Chem. Phys.* **1987**, *87*, 697-705.

Gido, S. P.; Lee, C.; Pochan, D. J.; Pispas, S.; Mays, J. W.; Hadjichristidis, N. *Macromolecules* **1996**, *29*, 7022-8.

Graessley, W. W.; Kristamoorti, B.; Fetters, L. J.; Lohse, D. J. *Macromolecules* **1993**, *26*, 1137-43.

Graessley, W. W.; Krishnamoorti, R.; Balsara, N. P.; Butera, R. J.; Fetters, L. J.; Schulz, D. N.; Lohse, D. J.; Sissano, J. A. *Macromolecules* **1994**, *27*, 3896-3901.

Graessley, W. W.; Krishnamoorti, R.; Reichart, G. C.; Balsara, N. P.; Fetters, L. J.; Lohse, D. J. *Macromolecules* **1995**, *28*, 1260-7.

Hadjichristidis, N.; Iatrou, H.; Behal, S. K.; Chludzinski, J. J.; Disko, M. M.; Gardner, R. T.; Liang, K. S.; Lohse, D. J.; Milner, S. T. *Macromolecules* **1993**, *26*, 5812-5.

Hamley, I. W.; Koppi, K. A.; Rosendale, J. H.; Bates, F. S.; Almdal, K.; Mortensen, K. *Macromolecules* **1993**, *26*, 5959-70.

Handlin, Jr., D. L.; Thomas, E. L. *Macromolecules* **1983**, *16*, 1514-25.

Hariharan, A.; Kumar, S. K.; Rafailovich, M. H.; Sokolov, J.; Zheng, X.; Duong, D.; Schwarz, S. A.; Russell, T. P. *J. Chem. Phys.* **1993**, *99*, 656-72.

Hashimoto, T.; Nagatoshi, K.; Todo, A.; Hasegawa, H.; Kawai, H. *Macromolecules* **1974**, *7*, 364-73.

Hashimoto, T.; Shibayama, M.; Kawai, H. *Macromolecules* **1977**, *10*, 377-84.

Hashimoto, T.; Fujimura, M.; Kawai, H. *Macromolecules* **1980**, *13*, 1237-47.

Helfand, E.; Tagami, Y. *J. Chem. Phys.* **1972**, *56*, 3592-3601.

Helfand, E.; Lauritzen, J. I., Jr. *Macromolecules* **1973**, *6*, 631-8.

Helfand, E. *Macromolecules* **1975**, *8*, 552-6.

Helfand, E. *J. Chem. Phys.* **1975**, *62*, 999-1005.

Henn, G.; Bucknall, D. G.; Stamm, M,; Vanhoorne, P.; Jerome, R. *Macromolecules* **1996**, *29*, 4305-13.

Hermes, H. E.; Higgins, J. S.; Bucknall, D. G. *Polymer* **1997**, *38*, 985-9.

Higgins, J. S.; Benoit, H. C. Polymers and Neutron Scattering, Clarendon Press: Oxford, 1994.

Hong, K. M.; Noolandi, J. *Macromolecules* **1983**, *16*, 1083-93.

Hong, P. P.; Boerio, F. J.; Smith, S. D. *Macromolecules* **1994**, *27*, 596-9.

Hsieh, H. L.; Quirk, R. P. Anionic Polymerization: Principles and Practical Applications, Marcel Dekker: New York, 1996.

Iatrou, H.; Hadjichristidis, N. *Macromolecules* **1993**, *26*, 2479-84.

Jeon, H. S.; Lee, J. H.; Balsara, N. P. *Macromolecules* **1998**, *31*, 3328-39.

Jones, R. A. L.; Kramer, E. J.; Rafailovich, M. H.; Sokolov, J.; Schwarz, S. A. *Phys. Rev. Lett.* **1989**, *62*, 280-6.

Jones, R. A. L.; Norton, L. J.; Kramer, E. J.; Composto, R. J.; Stein, R. S.; Russell, T. P.; Mansour, A.; Karim, A.; Felcher, G. P.; Rafailovich, M. H.; Sokolov, J.; Zhao, X.; Schwarz, S. A. *Europhys. Lett.* **1990**, *12*, 41-51.

Karim, A.; Slawecki, T. M.; Kumar, S. K.; Douglas, J. F.; Satija, S. K.; Han, C. C.; Russell, T. P.; Liu, Y.; Overney, R.; Sokolov, J.; Rafailovich, M. H. *Macromolecules* **1998**, *31*, 857-62.

Kinning, D. J.; Thomas, E. L.; Fetters, L. J. *J. Chem. Phys.* **1989**, *90*, 5806-25.

Koester, L., in Neutron Interferometry, Bonse, U. and Rauch, H., eds., Oxford Science Publications: Oxford, 1979.

Kofinas, P.; Cohen, R. E. *Macromolecules* **1994**, *27*, 3002-8.

Krishnamoorti, R.; Graessley, W. W.; Balsara, N. P.; Lohse, D. J. *Macromolecules* **1994**, *27*, 3073-81.

Krishnamoorti, R.; Graessley, W. W.; Balsara, N. P.; Dee, G. T.; Walsh, D. J.; Fetters, L. J.; Lohse, D. J. *Macromolecules* **1996**, *29*, 367-76.

Leibler, L. *Macromolecules*, **1980**, *13*, 1602-17.

Leibler, L. *Macromolecules*, **1982**, *15*, 1283-90.

Leibler, L.; Orland, H.; Wheeler, J. C. *J. Phys. Chem.* **1983**, *79*, 3550-9.

Lohse, D. J. *Polymer Sci. Eng.* **1986**, *21*, 1500-9.

Lohse, D. J.; Fetters, L. J.; Graessley, W. W. *New Advances in Polyolefins*, **1993**, *8*, 175-83.

Mastushita, Y.; Naoya, T.; Mogi, Y.; Noda, I.; Han, C. C. *Macromolecules* **1993**, *26*, 6346-9.

Mayes, A. M.; Russell, T. P.. *Macromolecules*, **1992**, *25*, 6523-31.

Meier, D. J. *J. Polym. Sci.; Part C* **1969**, *26*, 81-98.

Mirabella, F. M.; Ford, E. A. *J. Polym. Sci.: Part B: Polym. Phys.* **1987**, *25*, 777-90.

Morton, M.; Helminiak, T. E.; Gadkary, S. D.; Bueche, F. *J. Polym. Sci.* **1962**, *57*, 471-85.

Morton, M.; Fetters, L. J. *Rubber Rev.* **1975**, *48*, 359-71.

Morton, M. Anionic Polymerization: Principles and Practice, Academic Press: New York, 1983.

Nojima, S.; Kato, K.; Yamamoto, S.; Ashida, T. *Macromolecules*, **1992**, *25*, 2237-41.

Pispas, S.; Hadjichristidis, N.; Mays, J. W. *Macromolecules* **1996**, *29*, 7378-85.

Pochan, D. J., Ph.D. Dissertation, University of Massachusetts, Amherst, 1997.

Quinn, F. A., Jr.; Mandelkern, L. *J. Am. Chem. Soc.* **1958**, *80*, 3178-87.

Rachapudy, H.; Smith, G. G.; Radu, V. P.; Graessley, W. W. *J. Polym. Sci.; Polym. Phys. Ed.* **1979**, *17*, 1211-22.

Rangarajan, P.; Register, R. A.; Fetters, L. J. *Macromolecules* **1993**, *26*, 4640-5.

Rangaragan, P.; Register, R. A.; Fetters, L. J. *Macromolecules* **1995**, *28*, 4932-8.

Russell, T. P.; Lin, J. S.; Spooner, S.; Wignall, G. D. *J. Appl. Cryst.* **1988**, *21*, 629-40.

Russell, T. P. *Mater. Sci. Rep.* **1990**, *5*, 171-201.

Russell, T. P.; Lamboody, P.; Kellogg, G. J.; Mayes, A. M. *Physica B* **1995**, *213/214*, 22-30.

Russell, T. P. *Physica B* **1996**, *26*, 3929-34.

Ryan, A. J.; Hamley, I. W.; Bras, W.; Bates, F. S. *Macromolecules* **1995**, *28*, 3860-7.

The Sadtler Standard Spectra of Carbon-13 NMR, Sadtler Research Labs, Inc.; Philadelphia, PA, 1988.

Sakurai, K.; MacKnight, W. J.; Lohse, D. J.; Schulz, D. N.; Sissano, J. A. *Macromolecules* **1993**, *26*, 3236-8.

Sakurai, K.; MacKnight, W. J.; Lohse, D. J.; Schulz, D. N.; Sissano, J. A. *Macromolecules* **1994**, *27*, 4941-51.

Sakurai, K., Ph.D. Thesis, Osaka University, Japan, 1995.

Sakurai, K.; MacKnight, W. J.; Lohse, D. J.; Schulz, D. N.; Sissano, J. A.; Lin, J.-S.; Agamalyan, M. *Polymer* **1996**, *37*, 4443-53.

Sakurai, K.; MacKnight, W. J.; Lohse, D. J.; Schulz, D. N.; Sissano, J. A.; Wedler, W.; Winter, H. H. *Polymer* **1996**, *37*, 5159-67.

Schue, F.; Ortlieb, C.; Maillard, A,; Deluzarche, A. *Bull. Soc. Chim. Fr.* **1965**, *#178*, 982-5.

Sears, V. F. *Neutron News* **1992**, *3*, 26-38.

Semenov, A. N. *Macromolecules* **1993**, *26*, 6617-26.

Sferrazza, M.; Xiao, C.; Jones, R. A. L.; Bucknall, D. G.; Penfold, J.; Webster, J. R. P. *Phys. Rev. Lett.* **1997**, *78*, 3693-6.

Shull, K. R.; Mayes, A. M.; Russell, T. P. *Macromolecules* **1993**, *26*, 3929-40.

Stocker, W.; Stadler, R. *Macromolecules*, **1996**, *29*, 7502-7.

Strobl, G. *Acta Polymerica* **1997**, *48*, 562-70.

Szwarc, M. *Nature* **1956**, *178*, 1108-9.

Szwarc, M.; Levy, M.; and Milkovich, R. *J. Am. Chem. Soc.* **1956**, *78*, 2656-7.

Szwarc, M. *Adv. Polym. Sci.* **1983**, *49*, 1-11.

Takagi, S.-Y.; Saito, H.; Chiba, T.; Inoue, T.; Takemura, Y. *Polymer* **1998**, *39*, 1643-5.

Thomas, E. L.; Anderson, D. M.; Henkee, C. S.; Hoffman, D. *Nature* **1988**, *334*, 598-601.

Thomas, E. L.; Fetters, L. J., in Model Polymers for Materials Science, 1992.

Toda, A.; Keller, A. *Colloid & Polymer Sci.* **1993**, *271*, 328-42.

Walton, D. G.; Kellogg, G. J.; Mayes, A. M.; Lamboody, P.; Russell, T. P. *Macromolecules* **1994**, *27*, 6225-28.

Washiyama, J.; Kramer, E. A.; Hui, C.-Y. *Macromolecules* **1994**, *27*, 6011-15.

Wendlandt, W. W. Thermal Analysis, Third Ed., Wiley-Interscience: New York, 1986.

Whitmore, M. D.; Noolandi, J. *Macromolecules* **1985**, *18*, 657-65.

Whitmore, M. D.; Noolandi, J. *Macromolecules* **1988**, *21*, 1482-96.

Widmaier, J. M.; Meyer, G. C., in Developments in Block Polymers—2, Goodman, I., ed., Elsevier Applied Science Publishers: London, 1985.

Wignall, G. D.; Bates, F. S. *Macromolecules* **1986**, *19*, 32-38.

Winey, K. I.; Thomas, E. L.; and Fetters, L. J. *J. Chem. Phys.* **1991**, *95*, 9367-75.

Winey, K. I.; Thomas, E. L.; Fetters, L.J. *Macromolecules*, **1992**, *25*, 2645-50.

Zeigler, A. *Angew. Chem.* **1936**, *49*, 499-502.

Zhao, W.; Zhao, X.; Rafailovich, M. H.; Sokolov, J.; Mansfield, T.; Stein, R. S.; Composto, R. C.; Kramer, E. J.; Jones, R. A. L.; Sansome, M.; Nelson, M. *Physicsa B* **1991**, *173*, 43-52.

Zhonde, X.; Mays, J.; Xuexin, C.; Hadjichristidis, N.; Schilling, F. C.; Bair, H. E.; Fetters, L. J. *Macromolecules*, **1985**, *18*, 2560-6.

Zumbulyadis, N.; Landry, M. R.; Russell, T. P. *Macromolecules* **1996**, *29*, 2201-4.